The Preserve: Lehigh Library Digital Collections

A study of mercury oxidation and the development of a global predictive kinetic model.

Citation

Agarwal, Hans. *A Study of Mercury Oxidation and the Development of a Global Predictive Kinetic Model.* 2006, https://preserve.lehigh.edu/lehigh-scholarship/graduate-publications-theses-dissertations/theses-dissertations/study-mercury.

Find more at https://preserve.lehigh.edu/

This document is brought to you for free and open access by Lehigh Preserve. It has been accepted for inclusion by an authorized administrator of Lehigh Preserve. For more information, please contact preserve@lehigh.edu.

A Study of Mercury Oxidation and the Development of a Global Predictive Kinetic Model

by

Hans Agarwal

A Dissertation
Presented to the Graduate Committee
of Lehigh University
in Candidacy for the Degree of

Doctor of Philosophy

in

Chemical Engineering

Department of Chemical Engineering
and
Energy Research Center
Lehigh University
Bethlehem, PA 18015

-September 2006-

Reproduced with permission of the copyright owner. Further reproduction prohibited without permission.

UMI Number: 3237489

Copyright 2006 by
Agarwal, Hans

All rights reserved.

INFORMATION TO USERS

The quality of this reproduction is dependent upon the quality of the copy submitted. Broken or indistinct print, colored or poor quality illustrations and photographs, print bleed-through, substandard margins, and improper alignment can adversely affect reproduction.

In the unlikely event that the author did not send a complete manuscript and there are missing pages, these will be noted. Also, if unauthorized copyright material had to be removed, a note will indicate the deletion.

UMI®

UMI Microform 3237489
Copyright 2007 by ProQuest Information and Learning Company.
All rights reserved. This microform edition is protected against unauthorized copying under Title 17, United States Code.

ProQuest Information and Learning Company
300 North Zeeb Road
P.O. Box 1346
Ann Arbor, MI 48106-1346

Reproduced with permission of the copyright owner. Further reproduction prohibited without permission.

CERTIFICATE OF APPROVAL

Approved and recommended for acceptance as a dissertation in partial fulfillment of the requirements for the degree of Doctor of Philosophy.

July 10, 2006
Date

Professor Harvey G. Stenger
Dissertation Advisor

July 10, 2006
Accepted ~~Date~~

Committee Members:

Professor Harvey G. Stenger
Committee Chair
Department of Chemical Engineering

Dr. Carlos E. Romero
Committee Member
Energy Research Center

Professor Hugo S. Caram
Committee Member
Department of Chemical Engineering

Dr. Song Wu
Committee Member
Hitachi Power Systems America, Ltd

Professor Arup K. Sengupta
Committee Member
Department of Environmental Engineering

Dr. Zhen Fan
Committee Member
Foster Wheeler North America Corp.

Reproduced with permission of the copyright owner. Further reproduction prohibited without permission.

© Copyright 2006 by Hans Agarwal

All Rights Reserved

Reproduced with permission of the copyright owner. Further reproduction prohibited without permission.

ACKNOWLEDGEMENTS

First of all, I would like to express my most sincere gratitude and appreciation to my academic advisor, Professor Harvey G. Stenger, for all his guidance during my doctoral study at Lehigh University. His experience, knowledge and thoughtfulness have always helped me in those times when I was bereft of ideas and direction, always pushing me to write and continue doing the right experiments. I would like to thank Sandhya for the discussions we had about the pertinent projects as we wrestled with making the rig operable. I would also like to acknowledge Professor Caram and Sengupta for their interest and help by being on my dissertation committee.

I would like to convey my gratitude to Foster Wheeler for providing the funds to build the project from scratch and continue performing experimental work. Special appreciation goes to Dr Zhen Fan and Dr Song Wu for agreeing to be on my dissertation committee.

In my work at the Energy Research Center, I would like to extend my gratitude to Professor Edward Levy for extending my fellowship, Jodie Johnson and Ursla Levy for putting up with all the purchase orders and business that came with it, John Sale for providing the necessary facilities to perform the experimental work, and Drs. Harun Bilirgen and Nenad Sarunac for their advice and help in the project. I would like to specially mention Dr Carlos Romero for his invaluable help and assistance in writing and direction of the project, and for agreeing to be on my dissertation committee as well.

Reproduced with permission of the copyright owner. Further reproduction prohibited without permission.

Outside the academic world, I would like to thank Reformed University Fellowship of Lehigh University and the spiritual uplifting that I received every Tuesday evening by being a part of the worship ministry. My heartfelt thanks goes to Rev. David Green and family for putting up with me in so many times of difficulties, and for always teaching me the meaning of the word 'discipline'. I would like to also extend my appreciation to members of Ebenezer Bible Fellowship Church and Lehigh Valley Presbyterian Church for their unfailing support in times of need.

My penultimate love and thanks go to my family, my parents in Florida, and my sister in Holland. Thank you for everything that you have done for me thus far. I love you.

Finally, I dedicate this dissertation to my Lord and Savior Jesus Christ for promising to never let me go, even when I falter daily. Without You, I am nothing. I am fearfully and wonderfully made (Psalm 139:14). Teach me Your ways and continue to mold me into the man You want me to be.

Reproduced with permission of the copyright owner. Further reproduction prohibited without permission.

"Those who wait on the Lord
Shall renew their strength;
They shall mount up with wings like eagles,
They shall run and not be weary,
They shall run and not be faint."

Isaiah 40:31 (NKJV)

Henri Ducard:
If you make yourself more than just a man, if you devote yourself to an ideal, and if they can't stop you, you become something else entirely...

Bruce Wayne:
Which is?

Henri Ducard:
Legend, Mr. Wayne.

Batman Begins (2005)

Reproduced with permission of the copyright owner. Further reproduction prohibited without permission.

TABLE OF CONTENTS

Certificate of Approval ii
Acknowledgements iv
List of Tables xi
List of Figures xiv
Abstract 1

Chapter 1: Introduction 2

1.1 A Chemistry Look at Hg 2
1.2 An MSDS Look at Hg 3
1.3 Uses of Hg^0 and Hg Compounds 5
1.4 Hg Contamination and Bioaccumulation 8
1.5 Sources of Hg Emissions 10

1.5.1 Municipal Solid Waste (MSW) 10
1.5.2 Coal Fired Power Plants 12

1.5.2.1 Types of Coal 12
1.5.2.2 Types of Coal Fired Power Plants 15
1.5.2.3 Sections of a Pulverized Coal Fired Power Plant 18

1.6 Current Work Being Done on Hg 21

1.6.1 Hg Regulations 21
1.6.2 Oxidation of Hg with Various Halogenated Compounds 24

1.6.2.1 Current Experimental Research on Hg 26

1.6.3 Other Methods of Capturing Hg 43

1.6.3.1 Using Other Oxidizing Agents 43
1.6.3.2 Hg Capture with Impregnated Fly Ash and Other Sorbents 46

1.6.4 Current Commercial Technology for Hg Removal 48

1.7 Objective of This Project 50

1.7.1 Flue Gas from PRB Coal Combustion 50
1.7.2 "What this Project Aims to Accomplish" 51

Chapter 2: Laboratory Apparatus 53

2.1 Design of the Rig 53
2.2 Objective of Rig 53

2.2.1 First Idea: Pulverizer and Boiler 54

Reproduced with permission of the copyright owner. Further reproduction prohibited without permission.

2.2.2 Second Idea: Propane Combustion 54
2.2.3 Third Idea: Blending Gases 55

2.3 Construction of the Apparatus 55

2.3.1 R1 61

2.3.1.1 Design of R1 61
2.3.1.2 Purchasing Information for R1 67
2.3.1.3 Modifications on R1 72

2.3.2 R2 73

2.3.2.1 Design of R2 75
2.3.2.2 Purchasing Information for R2 78
2.3.2.3 Modifications on R2 80

2.3.3 HX1 80

2.3.3.1 Design of HX1 81
2.3.3.2 Purchasing Information for HX1 83

2.3.4 Air Pre Heater (APH) 84

2.3.4.1 Design and Construction of APH 84
2.3.4.2 Purchasing Information for APH 86
2.3.4.3 Modifications on APH 88

2.3.5 Steam Pre Heater (SPH) 89

2.3.6 Riser and Baghouse 89

2.3.6.1 Design of Riser and Baghouse 91
2.3.6.2 Modifications on Riser and Baghouse 92

2.3.7 Other Modifications 113

2.3.7.1 Measuring Linear Flow of Gas 113
2.3.7.2 Condenser Unit 113
2.3.7.3 Carbon Filter 115
2.3.7.4 Totalizer 117
2.3.7.5 Exhaust Line with Constriction 118

2.3.8 Sample Lines 119

2.3.8.1 Using Teflon for Sampling 121
2.3.8.2 Design of Sample Lines 121
2.3.8.3 Modifications on Sample Lines 121

2.3.9 Gas Blending System 122

2.3.9.1 Using Mass Flow Controllers (MFCs) for All Gases 122
2.3.9.2 Setup for Air Flow 127
2.3.9.3 Using Rotometers for Corrosive Gases 131
2.3.9.4 Combining Gases and Entry Point into R1 135

Reproduced with permission of the copyright owner. Further reproduction prohibited without permission.

2.3.9.4.1 Purchasing Information for Gases 137

2.3.9.5 Setup for Water Flow 138
2.3.9.6 Frame 139

2.4 Continuous Emissions Monitor (CEM) 142

2.4.1 Comparison of PSA to other CEMs 144
2.4.2 Details of the PSA 146

2.4.2.1 Conditioning Unit 147

2.4.2.1.1 Hot Box 148
2.4.2.1.2 Impinger Units 151
2.4.2.1.3 Chiller Unit 154
2.4.2.1.4 Peristaltic Pump 154

2.4.2.2 Stream Selector Box 155
2.4.2.3 Sir Galahad Analyzer 158

2.4.2.3.1 Calibration of Sir Galahad Analyzer 163

2.4.2.4 CAVKIT 166
2.4.2.5 Software 167

2.4.3 Trouble-shooting the PSA 173

2.5 Control Panel 174

2.5.1 Heater Controllers 176
2.5.2 Temperature Readouts 176
2.5.3 Baghouse Control 176

Chapter 3: The Effects of H_2O, SO_2 and NO on Homogeneous Hg oxidation by Cl_2. 177

3.1 Abstract 177
3.2 Introduction 178
3.3 Testing Facility 179
3.4 Results 181

3.4.1 Experiment 1 181
3.4.2 Experiment 2 184
3.4.3 Experiment 3 185

3.5 Discussion 187
3.6 Summary and Conclusions 191

Reproduced with permission of the copyright owner. Further reproduction prohibited without permission.

Chapter 4: Development of a Predictive Kinetic Model for Homogeneous Hg Oxidation Data 192

4.1 Abstract 192
4.2 Introduction 193
4.3 Background on Chemical Engineering Kinetics 195
4.4 Proposing a Reaction Mechanism 198
4.5 MATLAB Program for Predicting Experimental Data 202
4.6 Results and Discussion 210
4.7 Conclusions and Future Work 216

Chapter 5: Comparing and Interpreting laboratory results of Homogeneous Hg Oxidation by a Chlorine Species 217

5.1 Abstract 217
5.2 Introduction 218
5.3 Testing Facility 226
5.4 Results 227

5.4.1 Hg and Cl_2 227
5.4.2 Cl_2, H_2O and Hg 229

5.5 Discussion 230
5.6 Predictive Model 231
5.7 Conclusion 234

Chapter 6: A Global Kinetic Mechanism for the Prediction of Hg Oxidation by a Chlorine Species 235

6.1 Abstract 235
6.2 Introduction 235
6.3 Testing Facility 242
6.4 Numerical Model 242
6.5 Results and Discussion 245
6.6 Conclusions 252

Chapter 7: Conclusions 254

7.1 Introduction 254
7.2 Summary of the Experimental Apparatus constructed 254
7.3 Summary of the Experimental Work 255
7.4 Creating a Global Kinetic Mechanism 255
7.5 Validating the Global Kinetic Mechanism 256

References 257

Appendix: Ph.D. Defense Presentation 275

Vita 310

Reproduced with permission of the copyright owner. Further reproduction prohibited without permission.

LIST OF TABLES

Table 1.1	A list of physical properties of elemental Hg.	2
Table 1.2	Comparison of oral LD_{50} values of mercury compounds in rodent species.	4
Table 1.4	Range of mean mercury concentrations (ppm) for major fish species.	8
Table 1.5.1	Discards (before recovery) of mercury in products in the MSW Stream.	11
Table 1.5.2.1-1	Some typical concentrations of various components of the flue gas stream from coal combustion and household waste incineration.	13
Table 1.5.2.1-2	Distribution of coal present in the United States estimated by DOE/EIA.	14
Table 1.5.2.1-3	List of nationwide quantities of coal and supplemental fuels burned in coal-fired electric utility boilers for the year 1999.	14
Table 1.5.2.1-4	Summary of the 4 main ranks of coal and their content.	15
Table 1.5.2.2-1	Summary of the 5 major coal fired configurations.	16
Table 1.5.2.2-2	Nationwide distribution of electric utility boiler units with respect to coal firing configuration for the year 1999.	17
Table 1.6.1-1	Air Emissions of Mercury and Mercury compounds from electric utilities by State, 2002.	21
Table 1.6.1-2a	Combined estimates of total Hg emissions from various sources in 1994-1995.	22
Table 1.6.1-2b	Estimates of total Hg emissions from Area sources in 1994-1995.	22
Table 1.6.1-2c	Estimates of total Hg emissions from Combustion sources in 1994-1995.	22
Table 1.6.1-2d	Estimates of total Hg emissions from Manufacturing and other miscellaneous sources in 1994-1995.	23
Table 1.6.2.1-1	Gas composition for bench scale tests performed by Laudal et al.	35
Table 1.6.2.1-2	Bench scale results – adapted from Laudal et al.	35
Table 1.6.2.1-3	Composition of simulated flue gas blend (dry basis) used in experimentation by Norton et al.	36

Reproduced with permission of the copyright owner. Further reproduction prohibited without permission.

Table 1.6.2.1-4	Absaloka coal combustion flue gas composition.	40
Table 1.6.3.1-1	Summary of Hg^0 removal results with iodine and bromine solutions.	45
Table 1.6.3.1-2	Summary of Hg^0 removal results with chlorine solutions.	45
Table 1.6.4	Summary of various companies offering technology to capture mercury, and the status of development.	49
Table 1.7.1	Summary of component and respective composition, typical to a PRB coal combustion flue gas.	50
Table 2.3.1.2-1	List of items purchased for R1, with respective vendors and prices.	67
Table 2.3.2.1-1	List of main components in Inconel 625®.	75
Table 2.3.2.2-1	List of items purchased for R2, with respective vendors and prices.	79
Table 2.3.3.2-1	List of items purchased for HX1, with respective vendors and prices.	83
Table 2.3.4.2-1	List of items purchased for APH, with respective vendors and prices.	87
Table 2.3.9.1-1	List of mass flow controllers and the controller boxes purchased for gas flow control.	123
Table 2.3.9.2-1	List of items purchased for air flow delivery system.	128
Table 2.3.9.3-1	Replacement parts (rotometers) for individual gas streams.	131
Table 2.3.9.4.1-1	List of Gases and regulators purchased for individual gases.	137
Table 2.4-1	List of all items purchased for the Continuous Emission Mercury (CEM) Monitor system.	142
Table 2.4.2.5-1	Procedure of the 5 minute cycle for each sample point.	167
Table 3.3-1	Summary of components and composition.	179
Table 3.3-2	Values of temperature versus residence time profiles, and the respective locations on the experimental apparatus.	180
Table 3.4.1	Composition of gas used in each stage of Experiment 1, and Hg^0 oxidation results.	183
Table 3.4.2	Composition of gas used in each stage of Experiment 2, and Hg^0 oxidation results.	184

Reproduced with permission of the copyright owner. Further reproduction prohibited without permission.

Table 3.4.3	Composition of gas used in each stage of Experiment 3, and Hg^0 oxidation results.	186
Table 4.6	Summary of the Reactions used in this work with the corresponding A and E constants for the Arrhenius rate constant.	210
Table 5.2-1	Data adapted from Ghorishi.	219
Table 5.2-2a	Data adapted from Hall et. al.	220
Table 5.2-2b	Data adapted from Hall et. al.	220
Table 5.2-3a	Data adapted from Sliger et. al.	221
Table 5.2-3b	Data adapted from Sliger et. al.	222
Table 5.2-3c	Data adapted from Sliger et. al.	222
Table 5.2-4	Data adapted from Widmer et. al.	223
Table 5.2-5	Data adapted from Mamani-Paco and Helble.	224
Table 5.2-6	Data adapted from Qiu et. al.	225
Table 5.6-1	Constant values of A and Ea for Reactions 1 and 2, and the corresponding reaction rate constants.	233
Table 6.2-1	Summary of data from 11 unique sources.	237
Table 6.5-1	Summary of the values for the pre-exponential factor (A) and activation energy (E) for each of the reactions used in this model.	245

Reproduced with permission of the copyright owner. Further reproduction prohibited without permission.

LIST OF FIGURES

Figure 1.6.2.1-1	Adapted results from experiments performed by Kilgroe et al.	32
Figure 1.6.2.1-2a	Results of various experiments that included Blacksville fly ash at 180°C (Adapted from Norton et al.)	37
Figure 1.6.2.1-2b	Effects of HCl on mercury oxidation in the presence of Blacksville fly ash at 180°C (Adapted from Norton et al.)	37
Figure 1.6.2.1-2c	Effects of NO2 on mercury oxidation in the presence of Blacksville fly ash at 180°C (Adapted from Norton et al.)	38
Figure 1.6.2.1-2d	Effects of NO on mercury oxidation in the presence of Blacksville fly ash at 180°C (Adapted from Norton et al.)	38
Figure 2.3-1	Schematic of Laboratory Apparatus used in this work.	56
Figure 2.3-2	CAD drawing of the rear view of experimental apparatus without condenser unit.	57
Figure 2.3-3	CAD drawing of the front and side view of experimental apparatus without condenser unit.	58
Figure 2.3-4	CAD drawing of the rear view of experimental apparatus with condenser unit.	59
Figure 2.3-5	CAD drawing of the rear view of entire experimental apparatus with condenser unit.	60
Figure 2.3.1.1-A	CAD drawing of R1.	61
Figure 2.3.1-1	Picture of R1, R2 and HX1 as constructed for experimental work.	63
Figure 2.3.1-2	Close-up of insulated R1 and bag-house.	64
Figure 2.3.1-3	Close-up of insulated R1, bag-house and ΔP cell used to send bursts of air into the bag-house.	65
Figure 2.3.1-4	Close-up of insulated R1.	65
Figure 2.3.1.1-1	Close-up of Honeywell control box used to control R1 heaters.	66
Figure 2.3.1.2-1	CAD Drawing of blind flange used on R1.	69
Figure 2.3.1.2-2	CAD Drawing of socket weld flange used on R1.	70
Figure 2.3.1.2-3	CAD Drawing of SS Nuts used to bolt apparatus together.	70
Figure 2.3.1.2-4	CAD Drawing of SS Bolts used to hold apparatus together.	71

Reproduced with permission of the copyright owner. Further reproduction prohibited without permission.

Figure 2.3.1.2-5	CAD Drawing of SS Nuts used to fill R1 to enhance heat transfer and mixing of gases.	71
Figure 2.3.1.2-6	6-channel temperature readout from Omega Engineering.	72
Figure 2.3.2-1	Close-up of R2 and HX1 as constructed for experimental work.	74
Figure 2.3.2.1-A	CAD drawing of R2.	76
Figure 2.3.2.1-1	Flexatellic gasket used between flanges of the apparatus.	77
Figure 2.3.2.1-2	Close-up of the section on top of the riser pipe.	78
Figure 2.3.3-1	Close-up of HX1 as constructed for experimental work.	81
Figure 2.3.3.1-A	CAD drawing of HX1.	82
Figure 2.3.4.1-1	Picture of ceramic heaters used for APH and SPH.	84
Figure 2.3.4.1-2	Picture of APH and SPH as used in experimental work.	85
Figure 2.3.4.1-3	Schematic of APH setup.	86
Figure 2.3.4.2-1	Picture of temperature controller used for SPH and a 6-channel temperature read out used.	88
Figure 2.3.6-1	Picture showing HX1, 180° turn and the riser pipe for sorbent work.	90
Figure 2.3.6-2	Close-up of 180° turn and bottom of the riser pipe used for sorbent work.	91
Figure 2.3.6.1-1	Close-up of riser pipe -- shows flange used to connect riser pieces together.	94
Figure 2.3.6.1-2	Picture of top of riser and Tee-connection of riser to the bag-house.	95
Figure 2.3.6.1-3	Close-up of Tee-junction at the top of the riser.	95
Figure 2.3.6.1-4	Close-up of bag-house.	96
Figure 2.3.6.1-5	Close-up of the ΔP Cell.	96
Figure 2.3.6.1-6	Side view of ΔP Cell and bag-house.	97
Figure 2.3.6.1-7	Close-up of solenoid valves used to control air burst entering bag-house.	98
Figure 2.3.6.1-8	Close-up of the bag-house lid.	99
Figure 2.3.6.1-9	Close-up of bag-house center piece with fabric filter bags attached.	100

Reproduced with permission of the copyright owner. Further reproduction prohibited without permission.

Figure 2.3.6.1-10	Close-up of bag-house body.	101
Figure 2.3.6.1-11	Top view of ash dispenser.	102
Figure 2.3.6.1-12	Controllers for ash dispenser.	103
Figure 2.6.3.1-A	CAD drawing of riser section.	104
Figure 2.6.3.1-B	CAD drawing of flanges on riser section.	105
Figure 2.6.3.1-C	CAD drawing of bag-house body.	106
Figure 2.6.3.1-D	CAD drawing of bag-house body. Basic design.	107
Figure 2.6.3.1-E	CAD drawing of bag-house center piece and bag-house lid.	108
Figure 2.6.3.1-F	CAD drawing of bag-house center piece with "O"-ring grooves.	109
Figure 2.6.3.1-G	CAD drawing of entire bag-house assembly.	110
Figure 2.6.3.1-H	CAD drawing of bag-house fabric filter holders.	111
Figure 2.6.3.1-I	CAD drawing of tube within bag-house. The tube delivered bursts of air.	112
Figure 2.3.7.2-1	Chiller unit used to cool water flowing through condenser unit.	114
Figure 2.3.7.2-2	Water trap to drain condensed water.	115
Figure 2.3.7.3-1	Carbon trap used to remove acid gases and moisture from Flue gas stream before entering totalizer.	116
Figure 2.3.7.4-1	Totalizer used to measure volumetric flow rate of the flue gas in the entire apparatus.	117
Figure 2.3.7.5-1	Constriction before flue gas is vented.	118
Figure 2.3.8-1	Close-up of section between R1 and R2. Injection point of Cl_2.	120
Figure 2.3.8-2	Sample line at the end of HX1 used to collect gas samples for Hg analysis.	120
Figure 2.3.8.2-1	Light dimmer switches used to control heating coils on sample lines.	122
Figure 2.3.9.1-1	Display of MFCs used in this experimental work before being replaced with rotometers.	124
Figure 2.3.9.1-2	Side view of MFC panel to control all gases flowing into experimental apparatus.	125
Figure 2.3.9.1-3	Picture of control panel consisting of temperature read-outs and heater controllers.	126
Figure 2.3.9.1-4	Close-up of 4 channel control box for controlling MFCs.	127

Reproduced with permission of the copyright owner. Further reproduction prohibited without permission.

Figure 2.3.9.2-1	Setup for air flow including air compressor and tank.	128
Figure 2.3.9.2-2	Close-up of the top of air flow setup showing air compressor and the air intake valve.	129
Figure 2.3.9.2-3	Close-up of desiccant – to dry atmospheric air before entering the experimental apparatus.	130
Figure 2.3.9.3-1	Rotometer and ball valve used for SO_2 flow.	132
Figure 2.3.9.3-2	Rotometer used for CO – with built in control valve.	133
Figure 2.3.9.3-3	2 Rotometers attached in series to measure air flowrate.	134
Figure 2.3.9.4-1	Top view of R1 – entry point of all gases.	136
Figure 2.3.9.4-2	Close-up of the top of R1 – entry point of all gases.	136
Figure 2.3.9.4.1-1	Gas cylinders used in the experimental work.	138
Figure 2.3.9.5-1	Water delivery system – consisting of water tank and peristaltic pump.	139
Figure 2.3.9.6-A	CAD drawing of front and side view of frame.	140
Figure 2.3.9.6-B	CAD drawing of the frame with fittings.	141
Figure 2.4.2-1	Picture of entire PSA Hg CEM setup.	147
Figure 2.4.2.1-1	Close-up of conditioning unit of PSA Hg CEM analyzer.	148
Figure 2.4.2.1.1-1	Schematic of Hot Box.	149
Figure 2.4.2.1.1-2	Heating element of the hot box.	150
Figure 2.4.2.1.1-3	Interior of the hot box.	151
Figure 2.4.2.1.2-1	Close-up of impinger unit.	153
Figure 2.4.2.1.4-1	Close-up of peristaltic pump.	154
Figure 2.4.2.2-1	Schematic of interior of Stream Selector Box.	156
Figure 2.4.2.2-2	Schematic of the 3-way valve in Stream Selector Box.	156
Figure 2.4.2.2-3	Close-up of the interior of the Stream Selector Box.	157
Figure 2.4.2.2-4	Interior of Stream Selector Box.	157
Figure 2.4.2.3-1	Rotometer used to control the flow of sample gas into the Sir Galahad Hg analyzer.	159
Figure 2.4.2.3-2	Sir Galahad Hg analyzer.	160

Reproduced with permission of the copyright owner. Further reproduction prohibited without permission.

Figure 2.4.2.3-3	Interior view of Sir Galahad.	161
Figure 2.4.2.3-4	Close-up of gold trap within Sir Galahad.	162
Figure 2.4.2.3-5	Close-up of gold trap.	162
Figure 2.4.2.3.1-1	Mercury contained in a closed container. Used for calibrating Sir Galahad.	164
Figure 2.4.2.3.1-2	Pressure-lock Syringe used to inject Hg samples into Sir Galahad.	165
Figure 2.4.2.4-1	Close-up of CAVKIT.	166
Figure 2.4.2.5-1	PSA Software Page 1.	168
Figure 2.4.2.5-2	PSA Software Page 2.	168
Figure 2.4.2.5-3	PSA Software Page 3.	169
Figure 2.4.2.5-4	PSA Software Page 4.	169
Figure 2.4.2.5-5	PSA Software Page 5.	170
Figure 2.4.2.5-6	PSA Software Page 6.	170
Figure 2.4.2.5-7	PSA Software Page 7.	171
Figure 2.4.2.5-8	PSA Software Page 8.	171
Figure 2.4.2.5-9	PSA Software Page 9.	172
Figure 2.4.2.5-10	PSA Software Page 10.	172
Figure 2.4.2.5-11	PSA Software Page 11.	173
Figure 2.5-1	Control Panel.	175
Figure 3.3-1	Comparing temperature versus residence time profiles of a typical power plant and the experimental apparatus.	180
Figure 3.4.1	Plot of elemental Hg concentration ($\mu g/m^3$) with respect to time for Experiment 1.	182
Figure 3.4.2	Plot of percent Hg oxidation versus concentration of chlorine (ppmv).	185
Figure 3.4.3	Plot of percent Hg oxidation versus stage of Experiment 1 and 3.	186
Figure 3.5	Thermodynamic plot of chlorine species concentration versus temperature.	188
Figure 4.6-1	Plot of Observed % Hg oxidation versus Predicted % Hg oxidation using Reaction 2.	211

Reproduced with permission of the copyright owner. Further reproduction prohibited without permission.

Figure 4.6-2	Plot of Observed % Hg oxidation versus Predicted % Hg oxidation using Reaction 2 and 1.	212
Figure 4.6-3	Plot of Observed % Hg oxidation versus Predicted % Hg oxidation using Reaction 2, 1 and 5.	213
Figure 4.6-4	Plot of Observed % Hg oxidation versus Predicted % Hg oxidation using Reaction 2, 1, 5 and 4.	214
Figure 4.6-5	Plot of Observed % Hg oxidation versus Predicted % Hg oxidation using Reaction 2, 1, 5, 4 and 3.	215
Figure 5.4.1-1	Plot of temperature versus residence time for the apparatus.	227
Figure 5.4.1-2	Comparing percent Hg oxidation versus gas temperature profile.	228
Figure 5.4.2-1	Plot of percent Hg oxidation versus Cl_2 concentration used, with respect to temperature profile of the apparatus.	229
Figure 5.6-1	Plot of observed percent Hg oxidation versus predicted percent Hg oxidation.	233
Figure 6.5-1	Plot of Observed Hg oxidation versus Predicted Hg Oxidation, using Reaction 1.	246
Figure 6.5-2	Plot of Observed Hg oxidation versus Predicted Hg Oxidation, using Reaction 1 and 2.	247
Figure 6.5-3	Plot of Observed Hg oxidation versus Predicted Hg Oxidation, using Reaction 1, 2 and 3.	248
Figure 6.5-4	Plot of Observed Hg oxidation versus Predicted Hg Oxidation, using Reaction 1, 2, 3 and 4.	249
Figure 6.5-5	Plot of Observed Hg oxidation versus Predicted Hg Oxidation, using Reaction 1, 2, 3, 4 and 5.	250
Figure 6.5-6	Plot of Observed Hg oxidation versus Predicted Hg Oxidation, using Reactions 1, 2, 3, 4 and 5. The plot shows the distribution of individual researcher's data.	251

Reproduced with permission of the copyright owner. Further reproduction prohibited without permission.

ABSTRACT

On March 15, 2005, the U.S. Environmental Protection Agency (EPA) issued a federal rule to permanently cap and reduce mercury (Hg) emissions from coal-fired power plants. The rule states that upon complete implementation, Hg emissions are to be reduced by 21% by 2010, and by 70% by 2018. It is therefore imperative to find a means to comply with these regulations.

Experimental work was carried out in a unique laboratory scale apparatus. The apparatus was designed and constructed with the purpose of performing homogeneous and heterogeneous Hg oxidation in a simulated flue gas system. The experimental results presented in this work focus on the oxidation of Hg by chlorine gas (Cl_2) at a variety of temperature ranges.

The flue gas composition was attained by blending and heating of the appropriate gas constituents. The maximum operating temperature used in this work is 540°C. It was found that SO_2 and H_2O severely inhibited the oxidation of Hg by Cl_2. Additionally, NO seemed to inhibit this process, but to a lesser amount. It was also found that the effectiveness of Cl_2 as an oxidizing agent decreased as the temperature increased.

This work also presents a global kinetic model that was developed from the laboratory test results. The model consists of five reactions – two reversible, and three irreversible. The reaction constants for these reactions follow the Arrhenius expression formation and were determined from a set of 35 experiments. A program written in Matlab was used to simulate a non-isothermal plug flow reactor (PFR) system, where a fourth order Runge Kutta routine was used to determine the reaction constants by solving several pertinent ordinary differential equations.

These reaction rate constants were further used to predict experimental data from eleven experimental mercury data sources in the literature. It was found that the predictions from the model correspond very well with the observed published data. Over 90% of the 146 data points were predicted very well.

Reproduced with permission of the copyright owner. Further reproduction prohibited without permission.

CHAPTER 1

Introduction

1.1 A Chemistry Look at Hg

Mercury is a naturally occurring metal. It is a shiny, silver-white, odorless liquid in its elemental form and is the only transition metal in the periodic table that exists in liquid phase at room temperature. Table 1.1 lists the various physical properties of elemental mercury (Hg).

Molecular Weight	200.59 grams per mole
Chemical Formula	Hg
Atomic Number	80
Density	13.55 grams per mL
Boiling Point	356.7°C
Melting Point	-38.87°C
Vapor Pressure	0.0018 mmHg at 25°C

Table 1.1: A list of physical properties of elemental Hg.[1-2]

Hg exists in a number of oxidation states, with Hg^0 and Hg^{2+} being the most abundant and common species. Hg^0, or metallic elemental mercury, is inert and stable under ordinary conditions of use and storage. However, at elevated temperatures, it vaporizes to form toxic fumes. According to the Occupational Safety and Health Administration (OSHA), $0.1 mg/m^3$ is the Permissible Exposure Limits (PEL) of mercury for general industry, construction industry or maritime[3].

An Hg atom has a $5d^{10}6s^2$ closed shell electronic structure which is isoelectronic to He $(1s^2)$[4-6]. Isoelectronic refers to two or more molecular entities, such as atoms, molecules or ions, that have the same number of valence electrons and the same electronic configuration[7]. In this case, elemental Hg is isoelectronic to Helium since they both have the same number of valence electrons, making them very stable. This valence shell configuration results in Hg having an unusual non-reactivity as compared to other metals. Past studies have confirmed this by showing extremely slow or no oxidation in air at high temperatures[8-9].

Reproduced with permission of the copyright owner. Further reproduction prohibited without permission.

1.2 An MSDS Look at Hg

The toxic nature of Hg became apparent during the human poisoning disaster in Minamata, Japan. Since then, mercury has been primarily associated with neurotoxic effects – causing serious neurodevelopmental impairments in the developing fetus, including motor disturbance, seizures, retardation and palsy[10-12]. The Material Safety Data Sheet (MSDS) as provided by J.T. Baker states that the health rating for Hg is 4, implying that it is an extreme poison[13].

There are several modes of Hg poisoning that may occur[14]:

Inhalation is the most common and most toxic mode of entry. It causes severe respiratory tract damage. The symptoms include sore throat, pain, coughing, tightness in chest, shortness of breath and breathing difficulties, headache, anorexia, muscle weakness, gastrointestinal disturbance, liver changes or failure, bronchitis and pneumonitis.

Ingestion of Hg may cause burning of the mouth and pharynx, abdominal pain, vomiting, corrosive ulceration and diarrhea. Death may occur from renal failure.

Eye contact with Hg causes irritation and burns. Symptoms include redness, pain, and blurred vision. Exposure may result in serious and permanent eye damage.

Chronic exposure to Hg by any means can result in damage to the central nervous system. Other symptoms, aside from those mentioned, include memory loss, loosening of teeth, skin rashes, and damage to the brain and kidneys. It is suspected to be a reproductive hazard, causing damage to a developing fetus and decrease fertility in males and females.

Some of the first aid measures are specific to the mode of entry or exposure. Inhalation of Hg will warrant immediate removal to fresh air, and lack of breathing requires artificial

Reproduced with permission of the copyright owner. Further reproduction prohibited without permission.

respiration. In the case of ingestion, vomiting is to be induced. Skin and eye contact with Hg necessitates immediate flushing with copious amounts of water. In all cases, it is essential to get immediate medical attention.

Despite the toxicity of Hg, the United States Environmental Protection Agency (U.S. EPA) has yet to establish a reference concentration (RfC), reference dose (RfD) or a lethal-dose 50 level (LD_{50})[15]. RfC is an estimate of a continuous inhalation exposure of a chemical to the human population[16]. RfD is an estimate of a daily oral exposure of a chemical to the human population[16]. In toxicology studies, LD_{50} is the calculated dose of a chemical administered which kills half the test population[17]. Various sources have reported the LD_{50} values for several Hg compounds. Table 1.2 shows some LD_{50} values published in 1995.

Mercury Compound	Animal Species	LD_{50} (mg/kg)
Mercurous chloride (Hg_2Cl_2)	Rat	166
	Mouse	1500
Mercuric cyanide ($Hg(CN)_2$)	Rat	25
	Mouse	33
Mercurous sulfate (Hg_2SO_4)	Rat	205
	Mouse	152
Mercuric Sulfate ($HgSO_4$)	Rat	57
	Mouse	25

Table 1.2: Comparison of oral LD_{50} values of mercury compounds in rodent species[18].

Other pertinent data is presented by the Risk Assessment Information System[19].

Some pharmacological studies have shown that mercury in humans is not destroyed by metabolism, but rather converted to different forms and oxidation states[19]; the process seems to be similar for animals and humans, and involves an oxidation-reduction cycle[20]. Inhaled Hg vapor is rapidly oxidized to the divalent form in red blood cells[21]. Oxidation of elemental Hg also occurs in the lungs of humans and animals[22-23]. Other tests done on rodents have shown rapid destruction of various organs and a tissue upon exposure to elemental Hg[19]. EPA also presents other health hazard information for elemental Hg, inorganic Hg and methyl mercury[24]. These

Reproduced with permission of the copyright owner. Further reproduction prohibited without permission.

include acute effects, chronic (non-cancerous) effects, reproductive or developmental effects, and cancerous effects.

1.3 Uses of Hg^0 and Hg Compounds

As described earlier, Hg has unique physical and chemical properties. Despite the toxicity of Hg, it is still used in various forms. Common sources of Hg in residential settings, for example, can be separated into two loosely defined categories: materials that contain salts of Hg (either as an intentional additive or an accidental contaminant), and devices that contain free elemental mercury[25]. This section expands on some of the popular uses of Hg.

Latex Paints: Indoor latex paints represent one of the most prominent examples of Hg sources, along with phenylmercuric acetate and other mercury compounds which were common additives through the late 1980s because of their usefulness as fungicides and bactericides[26].

Cleaners and/or household products: Chlorine based cleansers and household products may contain Hg as a contaminant. Even though these products may contain Hg salts, volatile Hg^0 may be formed either during the manufacture of these products or due to the decomposition of the compounds within them[27].

Electric Lighting: In 1989, it was estimated that electric lighting was the second largest source of mercury in municipal solid waste (MSW) [28-30]. This came from two sources:

- Ordinary fluorescent lamps (bulbs) used in residences, offices, and other commercial and institutional buildings
- High intensity lamps (bulbs) used in lighting streets and parking lots.

Fever Thermometers: Mercury is used in a wide variety of medical instruments, most commonly in a fever thermometer. Thermometers were identified as a major source of mercury discarded

Reproduced with permission of the copyright owner. Further reproduction prohibited without permission.

from homes and medical establishments. However, mercury thermometers are being replaced by digital thermometers, especially in medical applications.

Thermostats: The typical thermostat used for temperature control in residential areas and other buildings contains mercury. Thermostats have a long life span, estimated to be 20 years, so there is a long lag time before they are discarded. These thermostats sometimes consist of electrical tilt switches and float controls that help in temperature regulation.

Pigments: It is difficult to quantify the use of mercury in pigments. Most pigments containing mercury were apparently used in plastics, often in combination with cadmium. Other uses could be in paints, printing inks, rubber and textiles. The use of mercury in pigments has been steadily declining.

Dental Uses: Mercury is used in dental amalgams for fillings in teeth. Most of the excess Hg is collected from the dentists' offices for re-refining, but some is discarded. The use of mercury in dental applications has also been declining[20].

Special Paper Coating: A small amount of Hg is used in the coating for special paper used for scanning off a cathode ray tube. This is typically used in hospitals and microfiche printers. In 1989, most companies making this special paper announced plans to phase out the use of mercury, and were projected to be done by 1995.

Film Pack Batteries: Instant cameras use a film pack powered by a battery. These batteries contained mercury until 1988, when the use of mercury was reportedly discontinued.

Several of these devices include a mercury reservoir that is made of glass, which is prone to breaking easily, resulting in mercury being released into the environment. Mercury is

Reproduced with permission of the copyright owner. Further reproduction prohibited without permission.

known to adsorb onto a number of surfaces, and thus prevents complete cleanup and removal[31]. Inorganic mercury was used in laxatives, skin-lightening creams and soaps, and in latex paint. However, the use of mercury in exterior paint was discontinued after 1991 and although most agricultural and pharmaceutical uses of inorganic mercury have also been discontinued, mercuric chloride is still used as a disinfectant and pesticide[32].

The following is a list of uses for various mercury compounds, adapted from a report by EPA in 1989[28].

Mercurous Chloride (HgCl): HgCl is also referred as mercury (I) chloride and calomel. It has been used as a fungicide in cosmetics, in agriculture to control root insects, and on the turf to control molding. It also has a pharmaceutical value as a diuretic and an antiseptic.

Mercuric Chloride ($HgCl_2$): $HgCl_2$ is also known as mercury (II) chloride. It is a corrosive sublimate and is sometimes ammoniated. It was used as an intensifier for black and white photography and was first used as a fungicide in 1891. Currently, it is primarily used in pharmaceuticals or on the turf to control molding.

Mercuric Oxide (HgO): HgO appears as a red or yellow powder. Red HgO was used as pigment coloration for anti-fouling paints. It is also primarily used as a cathode material for mercury batteries. It is also listed as an anti-bacterial chemical for some cosmetics.

Mercuric Sulfide (HgS): HgS is also referred as vermilion and is the most frequently occurring natural form of mercury, mined as cinnabar. It is also used as a red pigment for plastics, linen and paper, and sometimes as an anti-bacterial chemical in pharmaceuticals.

Reproduced with permission of the copyright owner. Further reproduction prohibited without permission.

Phenylmercuric Acetate ($C_6H_5HgCH_3COO$): Usually abbreviated as PMA, it has been used as a bactericide. It was first marketed as a seed treatment for agriculture in 1932. Its use was restricted to control turf diseases such as snow mold.

Mercury Fulminate: Mercury Fulminate is used in many explosives due to its high sensitivity. It served as an initiating detonator for larger chain reaction explosions.

Thimerosal ($C_9H_9HgNaO_2S$): Thimerosal is primarily used as a preservative. It was once used as a seed treatment for agriculture, but now is used in cosmetics and pharmaceuticals.

1.4 Hg Contamination and Bioaccumulation

Most of the common uses for Hg were in residential settings. However, in cases of an accidental spillage, Hg can easily contaminate the environment as well. Mercury can be found in many of the foods we eat, from fish[33-34] to other foods we generally do not expect to contain Hg, such as vegetables[35-36]. In 1999, EPA performed a national survey of mercury concentrations in fish. They found that the average concentration of Hg for bottom feeders (such as channel catfish or common carp) was lower as compared to the Hg concentration in the predators (such as largemouth and smallmouth bass)[37]. Table 1.4 lists the mean mercury concentrations for major fish species in parts per million by weight (ppmw).

Fish Species	Mean Hg concentration (ppm)[a]
Largemouth bass	0.001 – 8.94
Smallmouth bass	0.008 – 3.34
Walleye	0.008 – 3
Northern pike	0.10 – 4.4
Channel catfish	0.001 – 2.57
Bluegill sunfish	0.001 – 1.68
Common carp	0.001 – 1.8
White sucker	0.002 – 1.71
Yellow perch	0.01 – 2.14

Table 1.4: Range of mean mercury concentrations (ppm) for major fish species[37]. The ranges represent fish tissue Hg concentrations on a wet weight and fillet basis.

Reproduced with permission of the copyright owner. Further reproduction prohibited without permission.

There are also reports of a concentration of Hg in soil between 20 and 150 ppb, and in certain areas around the Amazon Basin, plant values of mercury reached between 0.91 and 1.04 μg/g[38].

Mercury is also emitted to the air by human activities, such as manufacturing or burning coal for fuel, and from natural sources such as volcanoes[39]. Slemr et al. measured a global distribution of mercury in the troposphere between 5 and 6 kilotons of total gaseous mercury present[39-40].

Typically, in the gas phase, Hg exists in 3 forms:

i. Hg^0 – elemental mercury which can travel a range of distances and accumulates in the atmosphere, remaining abundant due to the large residence time of 0.5 to 2 years[41-42].

ii. Hg^P – particulate bound mercury, which can fall out of the air over a range of distances, depending on the particle size. Hg^P is used to denote that the mercury is bound to a solid particle[43].

iii. Hg^{2+} – oxidized mercury which is very water soluble[44], and may be deposited at a range of distances.

Hg^{2+} can exist as gaseous or solid inorganic compounds, such as $HgSO_4$, HgO, HgS, $HgCl_2$ and CH_3Hg. Each compound has different thermal stabilities and properties[45]. Upon emission, the fate of Hg is determined by various factors, including form, location of emission source, surrounding terrain and the weather[46]. When Hg falls back to earth in rain or snow, it may flow into water bodies such as lakes and streams. In the presence of bacteria, Hg is converted to methylmercury (CH_3Hg), which is the most toxic form of mercury[47]. It is then taken up by aquatic plants and small organisms. The concentration of methylmercury increases within the bodies of fish, which eat these organisms. It gets more concentrated further up the food chain, as bigger fish and other animals, such as beavers, otters, raccoons and minks eat the smaller fish[48-50]. This process is called bioaccumulation[46]. This is clearly seen when comparing the average Hg concentrations in fish, as presented by the national survey done by EPA – the smaller fish had lower concentrations of Hg, while the larger fish had higher concentrations of Hg[37]. Fish

Reproduced with permission of the copyright owner. Further reproduction prohibited without permission.

consumption is the primary source of exposure to Hg in the general population of the United States and many other countries because of the high bioaccumulation rate of methylmercury in the aquatic food chain[25].

1.5 Sources of Hg Emissions

Based on previous sections, there have been an abundance of uses for mercury. However, the Hg that is released into the environment is undesirable, and there are two major sources of these emissions: Municipal Solid Waste Treatment Plants and Coal Fired Power Plants. This section will expand on these two sources of Hg emissions, but emphasis will be given to the latter, since this project deals with a system derived from a coal fired power plant.

1.5.1 Municipal Solid Waste (MSW)

Mercury has been a primary concern because it has been detected in the emissions from municipal waste combustion facilities and in the ash produced after combustion. It is also an undesirable contaminant when wastes are managed by other methods such as recycling or land filling. According to a recent study done in Florida, six operating landfills were analyzed for Hg emissions and it was found that an estimated 10 to 50 kg per year of Hg was released[51].

In 1992, the EPA submitted a report entitled "Characterization of Products Containing Mercury in Municipal Solid Waste in the United States, 1970 to 2000"[28]. They reported an estimated 709 tons of Hg were discarded in the U.S. in municipal solid waste (MSW) compared to the 1,338 tons reported to be consumed in 1989. Table 1.5.1 lists the discards of mercury in products in that year, as compared to 1970 and 1980.

Reproduced with permission of the copyright owner. Further reproduction prohibited without permission.

Products	1970	1980	1989
Household Batteries	310.8	429.5	621.2
Electric Lighting	19.1	24.3	26.7
Paint Residues	30.2	26.7	18.2
Fever Thermometers	12.2	25.7	16.3
Thermostats	5.3	7.0	11.2
Pigments	32.3	23.0	10.0
Dental Uses	9.3	7.1	4.0
Special Paper Coating	0.1	1.2	1.0
Mercury Light Switches	0.4	0.4	0.4
Film Pack Batteries	2.1	2.6	0.0
Total Discards	421.8	547.5	709.0

Table 1.5.1: Discards (before recovery) of mercury in products in the MSW Stream[28]

As seen, the batteries discarded from households and other sources of MSW are by far the largest source of Hg which accounts for over 85%. It is assumed that discarded batteries containing Hg are mostly of two types:

- Alkaline batteries – usually cylinder-shaped, used in flashlights, radios and other electronics and toys
- Mercury-Zinc batteries – usually button-shaped, used in hearing aids, watches, calculators and cameras. They are also used in some medical applications.

Mercury was used in alkaline batteries to prevent corrosion and reduce hydrogen buildup within the cell, which could lead to the battery rupturing. These batteries accounted for 59% of the discards of mercury in 1989. Despite having low concentrations of Hg, the use of these batteries was extremely high resulting in them being the leading source of Hg in MSW. As a result, the battery industry was under intense pressure to eliminate any amounts of Hg present.

The mercury-zinc batteries differ from the alkaline batteries, in that they contain a relatively high percentage of Hg within them. They contributed over 28% of Hg discards in 1989. Unfortunately, Hg is an integral part of these batteries since mercury oxide is used as the cathode material. As a result, the battery industry was required to decrease the usage of Hg, but not eliminate it completely.

Aside from batteries, all the other sources of mercury, as mentioned in the previous section, contributed to the total amount of Hg released by the MSW treatment plants. Many of

Reproduced with permission of the copyright owner. Further reproduction prohibited without permission.

these uses are from residential settings, and as technology continues to develop, the use of Hg in most of these uses is being phased out, to the point of being completely eliminated.

1.5.2 Coal Fired Power Plants

In contrast to mercury emissions derived from MSW from residential settings, the second major source of Hg emissions comes from coal burning industries, such as coal-fired power plants that generate electricity for human consumption. This section gives an introduction to the various types of coals and compositions, and a generic outline of a coal-fired power plant.

1.5.2.1 Types of Coal

Coal is a major source of the world's energy supply and is an important raw material for several types of heavy industry – predominantly for electricity generation. Of the 3140 billion kWh of electricity consumed in 1997, 1788 billion kWh was generated from coal fired power plants. Coal consumption in the United States that year was approximately 900 million tons[52]. Federal government agency responsible for estimating coal resources in the U.S., projected that the coal reserve in the U.S. is approximately 508 billion tons[53].

In 1997, the United States Environmental Protection Agency (EPA) issued a mercury study to the U.S. Congress, which estimated that 158 tons of Hg was released into the atmosphere in 1994-1995 and this accounts for approximately 3% of the world total emissions[54]. Coal fired combustion contributed 48 tons of emissions[55-57]. Hg is normally present in quantities between 1 and 5 μg/Nm^3 in coal combustion power plants, and around 100-1000 μg/Nm^3 in waste incineration[8]. According to Galbreath et al. Hg concentrations in coal combustion flue gas can range from 1 to 30 μg/Nm^3 – typically concentrations are from 5 to 12 μg/Nm^3 [56]. Some of this variation is accounted for by varying mercury levels in the coal types, but the vapor phase concentration does not always correspond to the Hg content of the coal being burnt. Note that the units of (Nm^3) refers to, in this case, "normal cubic meters". Table 1.5.2.1-1 shows some typical

Reproduced with permission of the copyright owner. Further reproduction prohibited without permission.

concentrations of various components of the flue gas stream as derived from coal combustion and house hold waste incineration.

	Coal Combustion	Waste Incineration
O_2	4-10 %	6-15 %
CO_2	10-16 %	5-14 %
CO	10-100 µL/L	10-100 µL/L
NO	100-1000 µL/L	100-1000 µL/L
NO_2	5-50 µL/L	5-50 µL/L
SO_2	100-2000 µL/L	100-2000 µL/L
HCl	1-100 µL/L	400-1000 µL/L
NH_3	5 µL/L	<1 µL/L
N_2O	5-200 µL/L	<1 µL/L
Hg	1-5 µg/m^3	100-1000 µg/m^3

Table 1.5.2.1-1: Some typical concentrations of various components of the flue gas stream from coal combustion and household waste incineration[8].

By definition, flue gas refers to the gas consisting of the air and pollutants produced and emitted into the atmosphere as a result of a production process or, in this case, combustion of coal. It is also called stack gas[58].

Coal can be classified into four types of coal rank, which is defined as the degree of progressive change from lignite to anthracite, and is based on fixed carbon, volatile matter, heating value and agglomeration (or caking) properties[59]. Classification depends on physical and chemical properties. The classes in increasing coal rank are: lignite, sub-bituminous, bituminous and anthracite[60]. Generally, lower ranking coals have higher concentrations of Hg. The distribution of the coal present in the United States by coal rank is presented in Table 1.5.2.1-2. Table 1.5.2.1-3 is a list of the nationwide quantities of coals and supplemental fuels burned in coal fired electric utility boilers for the year 1999[43].

Reproduced with permission of the copyright owner. Further reproduction prohibited without permission.

Coal Rank	Estimated U.S. Demonstrated Coal Reserves (billion tons)	Percentage of U.S Demonstrated Coal Reserves (%)
Anthracite	8	2
Bituminous	271	53
Sub-bituminous	185	36
Lignite	44	9
Total	508	100

Table 1.5.2.1-2: Distribution of coal present in the United States estimated by DOE/EIA[53].

Fuel Type	Total Tonnage Burned (million tons)	Percentage by weight (%)
Bituminous coal	406	51.7
Sub bituminous coal	287	36.5
Lignite	51	6.5
Bituminous / sub bituminous coal mixture	24	3.0
Bituminous coal / petroleum coke mixture	6	0.7
Waste anthracite coal	5	0.6
Waste bituminous coal	4	0.5
Petroleum coke	2	0.3
Other[a]	1	<0.2
Total	786	100

Table 1.5.2.1-3: List of nationwide quantities of coal and supplemental fuels burned in coal-fired electric utility boilers for the year 1999[43].
[a] Mixes of anthracite, bituminous, and waste bituminous fuel, tires, sub bituminous coal, and petroleum coke, or waste sub bituminous coal.

Lignite is the lowest ranking coal. It ignites easily and releases a smoky flame. In contrast, high ranking coal (anthracite) has a clean flame and difficult ignition. Lignite coal is often called 'soft' or 'brown' coal, with a carbon content of 25-35%. It has a high moisture content of up to 45% by weight and has the least energy value of all the coals. Sub-bituminous coal has a carbon content of 35-45% with a moisture content of 20-30% by weight. Bituminous generally has 70% carbon content with less than 15% moisture by weight, and anthracite has a carbon content of 86-98% with less than 15% moisture[11]. Table 1.5.2.1-4 summarizes this information along with their respective energy content.

Reproduced with permission of the copyright owner. Further reproduction prohibited without permission.

Fuel Type	Color	Carbon content (%)	Moisture Content (%)	Energy (kJ/kg)	Energy (BTUs/lb)
Lignite	Brown/black	25-35	45	15-20K	6.3-8.3K
Sub-Bituminous	Black	35-45	20-30	20-27K	8.3-10.5K
Bituminous	Black	70	<15	27-33K	10.5-14K
Anthracite	Black	86-98	<15	>30K	>12.6K

Table 1.5.2.1-4: Summary of the 4 main ranks of coal and their content[11].

General analysis of coal shows that it consists of carbon (C), hydrogen (H), oxygen (O), sulfur (S) and nitrogen (N). The combustion of coal results in the release of several other hazardous air pollutants such as antimony (Sb), arsenic (As), beryllium (Be), cadmium (Cd), chromium (Cr), cobalt (Co), lead (Pb), manganese (Mn), nickel (Ni) and, of course, mercury (Hg)[46].

1.5.2.2 Types of Coal Fired Power Plants

Coal can be burned in a boiler using three basic techniques: burning coal particles in suspension, burning large coal chunks in a fuel bed, or in a two-step process, where coal is first converted to a synthetic gas, and then fired in the boiler[43]. There are five basic firing configurations that are used to burn coal for electric power generation[43]:

- Pulverized coal fired furnace
- Cyclone furnace
- Fluidized bed combustor
- Stoker fired furnace
- Gasified coal fired combustor

Table 1.5.2.2-1 is taken from the EPA Report No 600/R-01-109, where all five configurations are listed and expounded. Table 1.5.2.2-2 shows a distribution of the 1,143 coal fired electric utility boilers listed in the EPA Information Collection Request (ICR) data by coal configuration. The pulverized coal fired design, by in large, account for over 80% of the configurations and obviously provides the majority of the electric generating capacity of the United States. More information is available in the report by EPA.

Reproduced with permission of the copyright owner. Further reproduction prohibited without permission.

Coal-Firing Configuration	Coal Combustion Process Description	Characteristic Design and Operating Procedure	
Pulverized Coal Fired Furnace	Coal is ground to a fine powder, then fed pneumatically to a burner, where it is mixed with combustion air. The mixture is blown into the furnace and the coal particles burn in suspension in the furnace. Unburned and partially burned coal particles are carried off with the flue gas.	Wall Fired	An array of burners fire into the furnace horizontally. Depending on the design, the burners are positioned on one wall or opposing walls.
		Tangential Fired (Corner Fired)	Multiple burners are positioned in opposite corners of the furnace producing a fireball that moves in a cyclonic motion and expands to fill the furnace.
Cyclone Furnace	Coal is crushed into small pieces and fed through a burner into a cyclone furnace. A portion of the combustion air enters tangentially and creates a cyclonic motion to the incoming coal.	Designed to burn low-ash fusion coals and retain most of the ash in the form of molten slag.	
Fluidized Bed Combustor	Coal is crushed into fine particles, and the particles are suspended in a fluidized bed by upward blowing jets of air. This results in turbulent mixing. The unit can be designed for combustion within the bed to occur at atmospheric or elevated pressures. Typically, coal is mixed with an inert material, such as sand, silica, or alumina, and a sorbent such as limestone for SO_2 emission control.	Bubbling Fluidized Bed	Consists of coarse bed size particles and operates at relatively low gas stream velocities. Air is in excess and passes through the bed in form of bubbles
		Circulating Fluidized Bed	Consists of finer bed size particles and operates at higher gas stream velocities. No defined bed surface. Recirculation of entrained solid particles in flue gas required to maintain the bed and achieve high combustion efficiency.
Stoker Fired Furnace	Coal is crushed into large lumps and burned on a moving, vibrating, or stationary grate. Coal is pushed, dropped, or thrown onto the grate by a mechanical device called a "stoker".	Spreader Stoker	A flipping mechanism throws the coal into the furnace above the grate. Fine coal particles burn in suspension. Heavier coal lumps fall to grate and burn in a fuel bed.
		Underfeed	Coal is fed by pushing lumps along in a feed through underneath the grate.

Reproduced with permission of the copyright owner. Further reproduction prohibited without permission.

		Traveling grate	Coal is fed by gravity onto a moving grate and leveled by a stationary bar at furnace entrance.
Gasified Coal Fired Combustor	Synthetic combustible gas from an onsite coal gasification process is burned in a gas turbine combustor. Hot combustion gases turn the gas turbine blades mounted on a shaft to drive the electric generator. Hot exhaust gases from gas turbine pass through a waste heat boiler to produce steam to drive a steam turbine unit.	Burning of gaseous fuel instead of solid coal makes this configuration unique as compared to other coal firing configurations.	

Table 1.5.2.2-1: Summary of the 5 major coal fired configurations[43]. Adapted from EPA Report No 600/R-01-109

Coal Firing Configuration	Nationwide Total Number of Units	Percent of Nationwide Total (%)	Percent of Nationwide Electricity Generating Capacity (%)
Pulverized Coal Fired Furnace	979	85.6	90.1
Cyclone Furnace	87	7.6	7.6
Fluidized Bed Combustor	42	3.7	1.3
Stoker Fired Furnace	32	2.8	1.0
Gasified Coal Fired Combustor	3	0.3	<0.1
Nationwide Total	1,143	100	100

Table 1.5.2.2-2: Nationwide distribution of electric utility boiler units with respect to coal firing configuration for the year 1999[43]. Adapted from EPA Report No 600/R-01-109.

Reproduced with permission of the copyright owner. Further reproduction prohibited without permission.

1.5.2.3 Sections of a Pulverized Coal Fired Power Plant

Due to the fact that pulverized coal fired furnaces account for the majority of coal fired configurations, it is important to briefly describe the various components in a pulverized coal fired steam generator power plant. This thesis focuses on research done on flue gas derived from such a system.

Coal is transported via various means, usually over land or sea, from the mines to the power plant where it is carried by conveyor belts to the pulverizer.

Pulverizer: The pulverizer consists of a mill which prepares the coal for burning by grinding it into a fine powder to the consistency of talcum powder, where at least 70% of the particles will pass through a 200-mesh sieve. The pulverized coal is then entrained in air, dried and mixed well, making it an efficient fuel for combustion. This coal powder and air mixture is then injected into the burner.

Burner: The coal is injected into the burner or furnace via a nozzle device, which is typically located near the bottom of the boiler. A controlled amount of air is added to burn the fuel efficiently and also to control the amount of NO_x and CO production and subsequent emission. The furnaces are classified either as dry or wet bottom, depending on the ash removal technique. Further classification of pulverized coal fired furnaces is with regard to firing position of the burners. Wall fired boilers are characterized by rows of burners on one or more walls of the furnace – the two basic forms being either single wall (having burners on one wall) or opposed (having burners that face each other)[43].

Boiler: The boiler is also known as the steam generator. It is a large vessel that contains pipes of water which is heated to steam to drive the turbines in the generator. Temperatures in the boiler can reach well beyond 1700°C.

Reproduced with permission of the copyright owner. Further reproduction prohibited without permission.

There is usually a NO_x control device at the top of the boiler which helps monitor the amount of NO_x production, and hence helps to control the amount of air added to burn the coal in the burner.

At the bottom of the boiler is a means of collecting any un-burnt coal which typically collects on the walls of the boiler and falls to the bottom. This material, called bottom-ash, is a ceramic-like material, and has a variety of uses, or is disposed accordingly.

Economizer: The steam that was run through the turbine is reheated by the heat from the gas leaving the power plant. This is done so that the steam can cycle around and be reused to power the turbine, while using the energy within the gas flow. It also allows the gas flow to drop down to the required temperature range for the selective catalytic reactor (SCR).

Selective Catalytic Reactor (SCR): The SCR contains a catalyst that causes either the sulfur or the mercury within the flue gas to react with the other materials in the gas stream, and thus creating a less harmful compound. This compound is usually soluble in the liquid section of the scrubber and is easily removed. The exact reaction that occurs depends on the type of catalyst used in the SCR, hence the fact that it is selective. This varies from plant to plant, depending on the local market prices and design of the plant itself.

Air Pre-heater (APH): In the APH, ambient air is heated by the gas system from the SCR. This allows the air entering the boiler to be warmer, causing more heat in the boiler to go into the steam, instead of having to heat up the air. At the same time, air from the SCR is cooled down, allowing the electrostatic precipitator (ESP) to function better.

Baghouse: The baghouse is also known as a precipitator and helps trap any particulate matter, including fly-ash. Fly-ash is different from bottom-ash in the sense that fly-ash is a light gray or tan powder and is the largest byproduct of un-burnt coal. Typically, it gets entrained within the hot

Reproduced with permission of the copyright owner. Further reproduction prohibited without permission.

exhaust (flue) gases. It has uses similar to bottom-ash, which include making asphalt, concrete, aggregate and insulation, just to name a few. The flue gas then exits the baghouse and passes through a scrubber.

Electrostatic Precipitator (ESP): Some power plants do not have the design of a baghouse. Instead, they have an ESP which functions similar to a baghouse. The ESP unit causes the particles in the gas stream to become polarized – they now carry either a positive or negative charge. The particles then pass electrically charged plates and the charged particles are attracted to the side with the opposite charge. Eventually, the particles slide down the side of the unit and are collected at the bottom. Most power plants have a combination of an ESP and a baghouse – the ESP polarizes the particles, and these particles get attached to the bags within the baghouse, which then fall by gravity and are collected at the bottom.

Scrubber: The scrubber is a device that is specially used to remove SO_2 from the boiler exhaust. One of the main reasons SO_2 control is necessary is because it forms H_2SO_4 in the atmosphere, which falls as acid rain and causes a wide range of problems.

Stack: Upon exiting the scrubber, the flue gas exits the system via a chimney or stack, and the hot gases are dispersed.

Generator: The generator consists of turbines, which is a device consisting of fan-like blades attached to a shaft. The kinetic energy of the expanding steam is converted to mechanical energy as the turbines spin. The mechanical energy is then converted into electric energy via a transformer. Also, all the steam is then condensed back to water in a condenser.

Condenser: The condenser is essentially a cooling device which converts the steam back to water and transports it back to the boiler to be reheated and used again.

Reproduced with permission of the copyright owner. Further reproduction prohibited without permission.

Transformer: A transformer is an electromagnetic device that reduces the current, or amperage, by increasing the output voltage of the generator. This makes the transmission of electricity more efficient.

1.6 Current Work Being Done on Hg

1.6.1 Hg Regulations

The U.S. EPA has designated 189 substances as hazardous air pollutants. Mercury (Hg) in particular has attracted significant attention because of its increasing concentration levels in the environment[46]. As mentioned earlier, a study submitted by EPA to Congress stated that an estimated 158 tons of Hg were released into the environment in 1994-1995, where 51.8 tons were from coal fired power plants[56]. Table 1.6.1-1 shows the air emissions of Hg and Hg compounds from electric utilities by state, as of 2002.

Rank	State	Hg Emissions (lbs)
1	Texas	9,840.01
2	Ohio	7,358.24
3	Pennsylvania	7,002.18
4	Indiana	4,926.55
5	Illinois	4,318.07
6	Alabama	3,931.35
7	West Virginia	3,680.30
8	Kentucky	3,539.80
9	North Carolina	3,434.17
10	Missouri	3,084.29

Table 1.6.1-1: Air Emissions of Mercury and Mercury compounds from electric utilities by State, 2002[61].

Table 1.6.1-2a-d are tables from the EPA report to Congress that summarizes other significant sources of Hg emissions in that same year of 1994-1995, thus accounting for the total of 158 tons of Hg emissions in that year[56].

Reproduced with permission of the copyright owner. Further reproduction prohibited without permission.

Sources	1994-1995 (tons/year)	% of Total Emissions
Area Sources	3.4	2.2
Combustion Sources	137.7	86.9
Manufacturing Sources	15.6	10.0
Miscellaneous Sources	1.4	0.9

Table 1.6.1-2a: Combined estimates of total Hg emissions from various sources in 1994-1995[56].

	Source	1994-1995 (tons/year)	% of Total Emissions
Area Sources	Lamp breakage	3.1	2.2
	General laboratory use	1.1	0.7
	Dental preparations	0.7	0.4
	Landfills	0.08	0.1
	TOTAL	3.4	2.2

Table 1.6.1-2b: Estimates of total Hg emissions from Area sources in 1994-1995[56].

	Source	Sub-source	1994-1995 (tons/year)	% of Total Emissions
Combustion Sources	Utility boilers	Coal	51.8	32.8
		Oil	0.2	0.1
		Natural gas	<0.1	0.0
	MWC[a]	--	29.6	18.7
	Commercial/ industrial boilers	Coal	20.7	13.1
		Oil	7.7	4.9
	MWI[b]	--	16.0	10.1
	HWC[c]	--	7.1	4.4
	Residential boilers	Coal	0.5	0.3
		Oil	3.2	2.0
	SSI[d]	--	1.0	0.6
	Wood-fired boilers	--	0.2	0.1
	Crematories	--	<0.1	0.0
	TOTAL	--	154.7	86.9

Table 1.6.1-2c: Estimates of total Hg emissions from Combustion sources in 1994-1995[56].

[a] MWC: Municipal Waste Combustors

[b] MWI: Medical Waste Incinerators

[c] HWC: Hazardous Waste Combustors

[d] SSI: Sewage Sludge Incinerators

Reproduced with permission of the copyright owner. Further reproduction prohibited without permission.

	Source	1994-1995 (tons/year)	% of Total Emissions
Manufacturing and other Miscellaneous Sources	Chlor-alkali	7.1	4.5
	Portland cement	4.8	3.1
	Pulp and paper manufacturing	1.9	1.2
	Instruments manufacturing	0.5	0.3
	Secondary Hg production	0.4	0.3
	Electrical apparatus	0.3	0.2
	Carbon black	0.3	0.2
	Lime manufacturing	0.1	0.1
	Primary lead	0.1	0.1
	Geothermal power	1.4	0.9
	TOTAL	17.0	10.9

Table 1.6.1-2d: Estimates of total Hg emissions from Manufacturing and other miscellaneous sources in 1994-1995[56].

On March 10, 2005, EPA issued the Clean Air Interstate Rule (CAIR), a rule to achieve the largest reduction in air pollution in more than a decade. CAIR will ensure that the air is to be made cleaner by considerably reducing air pollution, and by 2015, providing health and environmental benefits valued at more than 25 times the cost of compliance[62]. In short, CAIR will permanently reduce emissions of sulfur dioxide (SO_2) from 15.7 million tons to 3.5 million tons, which corresponds to over 75% removal, and nitrogen oxides (NO_x) from 6.7 million tons to 2.2 million tons, which corresponds to over 65% removal[62].

On March 15, 2005, EPA issued the first ever federal rule to permanently cap and reduce mercury emissions from coal-fired power plants. The Clean Air Mercury Rule (CAMR) will build on EPA's CAIR to significantly reduce these emissions. When fully implemented, it will reduce Hg emissions from 48 tons a year to 15 tons, a reduction of nearly 70%. This will occur in two distinct phases: The first phase due by 2010 will reduce Hg to 38 tons (21% reduction). The second phase will reduce Hg emissions by 33 tons (69%) to 15 tons when fully implemented in 2018[63].

Four states have established Hg emissions limits that are more aggressive than the federal rules[64]:

Reproduced with permission of the copyright owner. Further reproduction prohibited without permission.

Connecticut: An emissions rate comparable to a 90% reduction in Hg emissions by 2008.

Massachusetts: The first attainment level is a facility average total Hg removal efficiency of at least 85% by October 1, 2006. The second attainment level is a facility average total Hg removal efficiency of at least 95% by October 1, 2012.

New Jersey: Require the state's 10 coal-fired power plants to reduce Hg emissions by 90% by December 15, 2007.

Wisconsin: Approved an Hg rule in June 2004 that places a cap on Hg emissions from major electric utilities as of January 8, 2008. The rule requires major electric utilities to reduce Hg emission by 40% beginning January 1, 2010, and by 80% beginning January 1, 2015.

Other states, such as Indiana, Maryland, New Hampshire, Texas, Virginia and Pennsylvania are considering or currently have bills in legislation.

1.6.2 Oxidation of Hg with Various Halogenated Compounds

As mentioned in section 1.4, there are three major forms of Hg: elemental Hg (Hg^0), oxidized Hg (Hg^{2+}) and particulate Hg (Hg^P). Hg^0 is extremely difficult to remove since it is volatile, very inert and virtually insoluble in water. In contrast, the Hg^{2+} species, especially $HgCl_2$, condenses easily, is very soluble in water and adsorbs easily onto sorbents, thus making it more easily removed from the gas phase. Therefore, to most efficiently remove Hg from a flue gas stream, it would be effective to convert Hg from the elemental state to the oxidized state, and allow for various means of removal. The following lists some of the physical properties of various Hg^{2+} compounds – this would help in finding the best means of removing the Hg species from the flue gas stream:

Reproduced with permission of the copyright owner. Further reproduction prohibited without permission.

Mercuric Chloride ($HgCl_2$): $HgCl_2$ has a relative molecular mass of 271.52 grams per mole, a melting point of 277°C, and a boiling point of 302°C. It has an appearance as white crystals, granules or crystals. It has a vapor pressure of 0.1 kPa at 136.2°C and a water solubility of 28.6 grams per liter, which increases to 47.6 grams per liter in boiling water[65-67].

Mercuric Sulfide (HgS): HgS has a relative molecular mass of 232.68 grams per mole. It occurs as hexagonal crystals, which are red. Upon heating to 386°C, the sulfide transitions from red to black. The black sulfide sublimes at 446°C and is insoluble in water. The red sulfide sublimes at 583°C and has a solubility of 10^{-5} grams per liter of water[68].

Mercuric Sulfate ($HgSO_4$): $HgSO_4$ has a relative molecular mass of 296.7 grams per mole. It has a melting point of 450°C. It decomposes under the influence of light and upon heating above 450°C, decomposes to produce mercury and sulfur oxide fumes. It has a similar effect upon contact with water[69].

Mercuric Oxide (HgO): HgO has a relative molecular mass of 216.6 grams per mole. It has an appearance as yellow, orange-yellow or red powder. It decomposes upon exposure to light and decomposes at temperatures above 100°C, and does not have a known solubility in water[70-71].

One of the earlier works on this subject of Hg oxidation is presented by Hilgen et al. in a patent that describes a process for removing Hg from an Hg containing gas system by the addition of chlorine gas (Cl_2), and then passing the mixture through a gas-permeable bed of a non-porous solid material to collect the chloride compound[70].

The idea of Hg chlorination seems to be first patented by Knepper and Hoeckele in 1965[73]. The patent describes a process and apparatus for recovering $HgCl_2$ from catalysts containing Hg. The process was carried out at sub-atmospheric pressure, between 100 and 500 mm of water. They claim that excess amounts of chlorine in the gas stream reacted with the Hg in

Reproduced with permission of the copyright owner. Further reproduction prohibited without permission.

the catalyst and resulted in the formation of hydrogen chloride and mercury (II) chloride at elevated temperatures (above 350°C). This process was used to regenerate the catalyst in their system. They also found that $HgCl_2$ was easily scrubbed out in condensed water within their experimental apparatus.

Another patent, by Lutz et al. introduced the idea of chlorinating Hg and subsequently scrubbing it out by mixing the gas mixture with water vapor. The water vapor with $HgCl_2$ dissolved in it would condense at lower temperatures and be subsequently removed[74]. These patents clearly state that Hg is readily oxidized by chlorine in the gas stream, and at elevated temperatures. Since these patents, there has been much research that has taken place with regard to oxidation and removal of Hg from gases, especially in light of the hazardous and toxic nature of Hg, and the amount that is released from coal fired power plants.

1.6.2.1 Current Experimental Research on Hg

In 2001, Liu et al. published a paper that discussed the oxidation of elemental Hg in a fluidized bed combustion (FBC) system[75]. The objective of the project was to study the reduction of Hg emissions from coal fired combustors by making use of the hydrogen chloride (HCl) provided by high chlorine coals. According to the patents mentioned earlier, the chlorine species in the gas phase would oxidize Hg to $HgCl_2$ and enhance removal.

Their investigation indicated that the combustion temperature and secondary/primary air ratio were two major factors that influenced mercury emissions in a fluidized bed combustion (FBC) system. The majority of the experiments were done at temperatures ranging from 500 to 600°C. The typical concentration of gas phase Hg in FBC flue gas that they detected ranged from 1.5 -3.0 $\mu g/Nm^3$. Similar analysis was done for chlorine content, and the overall concentration derived from the coal samples was estimated to range from 26 to 420 parts per million by volume (ppmv) of flue gas. They also stated that the presence of fly ash resulted in a decrease in total gas phase Hg, and this suggests that the oxidized Hg adsorbed onto the fly ash particles, forming Hg^P. Generally, the adsorption rate increases as the temperature in the flue gas decreases. For

Reproduced with permission of the copyright owner. Further reproduction prohibited without permission.

example, of the mercury found in the solid phase, almost none was found in the bed ash because of the high surrounding temperature of 850°C. Most of the particulate Hg was found in fly ash, which was entrained in the baghouse. Generally, baghouse temperatures rarely exceed 300°C.

The first sample tested had 0.026% chlorine content and up to 64.3% of the initial total Hg present in the flue gas remained. The second sample had 0.21% chlorine content and 54.3% of the total Hg initially present in the flue gas remained. The ratio of elemental to oxidized mercury was reduced from 0.704 for the first sample to 0.153 for the second sample. The data shows that as chlorine concentrations in the flue gas increased, the amount of Hg oxidized increased. Consequently, the amount of oxidized Hg that adsorbed onto fly ash increased, resulting in a higher elemental than oxidized Hg concentration present in the gas phase.

Their system also consists of SO_2 in the flue gas, at concentrations ranging from 53 to 282 ppmv. The moisture content remained below 7.3% in all cases, and there is no mention of the presence of NO. The researchers do not discuss the effects that any of these components may have on the oxidation of Hg. They are, however, able to prove the effectiveness of Hg oxidation by chlorine.

Much research has been performed on the laboratory scale, bench scale and full scale, and most have concluded that the chlorine species, either HCl or Cl_2, has a primary role in Hg oxidation[76-84]. Upon combustion of coal, most researchers agree that chlorine entrained in the coal is released as chlorine radical, and gets converted to HCl. Many researches speculate that HCl, as opposed to Cl_2, is really responsible for the oxidation of Hg. They postulate that a reaction takes place that converts HCl to Cl_2. Therefore, it is important to discuss the significance of this process, also known as the Deacon Process, and this will be done in a later section.

More recent publications by Western Kentucky University (WKU) have presented various data and ideas that have been obtained either by consultation projects at power plants or by testing done in their own facility.

In particular, WKU has given some evidence that the Hg oxidation process in the combustion process is kinetically limited, although the oxidation process is thermodynamically

Reproduced with permission of the copyright owner. Further reproduction prohibited without permission.

favored[85]. Chlorine is emitted from coal upon combustion at high temperatures, and is initially emitted primarily as atomic chlorine, which then forms HCl or molecular Cl_2, as shown in the following reactions[85-86]:

$$Cl^* + H^* \rightarrow HCl \quad (1)$$

$$2\ Cl^* \rightarrow Cl_2 \quad (2)$$

$$4\ Cl^* + 2\ H_2O \rightarrow 4\ HCl + O_2 \quad (3)$$

$$4\ HCl + O_2 \rightarrow 2\ Cl_2 + 2\ H_2O \quad (4)$$

Elemental Hg from the coal reacts with the chlorine species to form oxidized Hg as shown in the following reactions:

$$Hg + Cl^* \rightarrow HgCl \quad (5)$$

$$HgCl + Cl_2 \rightarrow HgCl_2 + Cl^* \quad (6)$$

$$Hg + Cl_2 \rightarrow HgCl_2 \quad (7)$$

$$2\ Hg + 4\ HCl + O_2 \rightarrow 2\ HgCl_2 + 2\ H_2O \quad (8)$$

Thermodynamic analysis and calculations predict that in a typical combustion environment, almost all elemental Hg should be converted to oxidized Hg at temperatures of less than 450°C. However, based on previous studies, elemental Hg still exists at the stack with temperatures of below 120°C[87].The authors believe that reaction 5 is the initial step of the Hg oxidation process because of its fast rate. The slower reactions, represented by reactions 6-8 seem to dominate the overall oxidation process[88].

But it is not possible to detect the presence of chlorine radicals in a flue gas system. One could speculate the existence of chlorine radicals at high temperatures, for example at the exit of a boiler where temperatures are above 1700°C, but as the system cools, the presence of chlorine radicals decreases rapidly. Therefore, reactions 5 and 6 probably do not take place as expected,

Reproduced with permission of the copyright owner. Further reproduction prohibited without permission.

at temperatures below 1300°C or so since the lifespan of chlorine radicals becomes increasingly shorter. Instead, reaction 7 or 8 is the dominant oxidation reaction for mercury.

The chlorine species is well known to dominate the Hg oxidation process. However, other flue gas components, such as SO_2, NO, and H_2O, may also affect Hg oxidation. The role of sulfur and chlorine, and their involvement in the fate of Hg in flue gas, has long been a subject of research. Researchers from WKU have shown an interesting trend: chlorine has a tendency to encourage the removal of mercury from flue gas, regardless of speciation, by promoting the chemisorption of Hg onto fly ash[89]. Sulfur has a tendency to encourage the oxidation of flue gas Hg, but apparently inhibits the adsorption of oxidized Hg onto the fly ash. Further experimental results suggest that both HCl and SO_2 may directly affect the mercury oxidation mechanism.

Regardless of oxidation state, the total amount of vapor phase Hg seemed to decrease in response to increased coal chlorine content and increased HCl concentration in the flue gas. In this case, between 66 and 359 ppmv of HCl was measured in the gas stream, and they assumed that this was responsible for most of the Hg oxidation taking place. However, oxidized Hg (Hg^{2+}) was observed to decrease only in response to coal chlorine content, not the HCl content of the flue gas. In contrast, elemental Hg in the gas phase was observed to decrease in response to the HCl content in the gas phase, suggesting that HCl may be an active species in the oxidation of mercury as shown in reaction 8.

The concentration of SO_2 in their flue gas system ranged from 481 to 1328 ppmv; NO concentrations ranged from 221 to 384 ppmv; HCl concentrations ranged from 66 to 359 ppmv. The analytical values of mercury content within the coal on a dry basis were found to be between 0.06 and 0.24 parts per million by weight (ppmw). The conclusions were similar to that by Liu et al. where an increase in the concentration of chlorine in the coal led to a decrease in the level of gaseous Hg, since there was a higher amount of Hg oxidation, and more adsorption of the species onto particles. Additionally, an increase in the level of HCl in the flue gas led to a decrease in the level of total gaseous mercury. As a result, sulfur was also shown to be a major factor in the oxidation of elemental mercury, but inhibited the adsorption of Hg onto fly ash.

Reproduced with permission of the copyright owner. Further reproduction prohibited without permission.

However, the overall amount of Hg oxidation taking place in the flue gas in the presence of Cl_2, HCl and/or SO_2 remains unclear as no clear data was reported.

Frandsen et al. have proposed that Hg oxidation may involve both sulfur and chlorine, as shown in reactions 9 and 10[90]:

$$HgO + SO_2 + ½\ O_2 \rightarrow HgSO_4 \qquad (9)$$

$$HgCl_2 + SO_2 + O_2 \rightarrow HgSO_4 + Cl_2 \qquad (10)$$

They claim that if the sulfur oxidizes Hg via these reactions, then the supply of chlorine would be continuously regenerated. Therefore, elemental Hg would not vary directly with chlorine levels, but rather with HCl concentration in the flue gas[89]. Additionally, the Frandsen model predicts that $HgCl_2$ will be the major oxidized species at temperatures above 425°C, and $HgSO_4$ being the major species at temperatures below 320°C.

The modeling results presented show that at a temperature of 570°C, approximately 49% of the Hg species is $HgCl_2$, 49% is elemental Hg, 2% is HgO and $HgSO_4$ is undetected. This is a system consisting of flue gas derived from sub-bituminous coal, with a dry weight Hg concentration of 0.2 ppmw and chlorine concentration of 300 ppmw. Additionally, the composition of the bulk gas stream was assumed to be 78.5% (mole/mole) N_2, 20.5% (mole/mole) O_2 and 1% (mole by mole) H_2O.

It is known that HgO, the species responsible for reaction 9 to occur, decomposes at temperatures above 100°C[70]. Further, according to the MSDS of $HgSO_4$, the substance is very unstable and upon contact with water, decomposes rapidly into a yellow insoluble solids and sulfuric acid[139]. It is unclear how Frandsen resolves this issue within his model.

In summary, Frandsen et al. show that chlorine is again responsible for Hg oxidation. They suggest that the presence of SO_2 encourages the oxidation of Hg by forming $HgSO_4$. In the presence of chlorine and at temperatures above 550°F, $HgSO_4$ and HgO exist in trace amounts. Conversely, in the absence of chlorine, $HgSO_4$ is the dominant Hg species, while HgO

Reproduced with permission of the copyright owner. Further reproduction prohibited without permission.

concentrations remain below 10%. The results presented are a result of modeling work, with very little experimental data to support their work.

In contrast, other researchers have suggested that SO_2 inhibits the oxidation of Hg. An increase in the sulfur content results in an increase in the gaseous elemental Hg present in the flue gas, indicating that conversion of elemental Hg to oxidized Hg was inhibited[85]. Lindbauer et al. and Griffin independently reported an important reaction as follows[91-92]:

$$SO_2 + Cl_2 + H_2O \rightarrow SO_3 + 2\,HCl \qquad (11)$$

This suggests that the concentration of Cl_2 is reduced in the flue gas and HCl is formed instead. The same researchers conclude that HCl has limited abilities to oxidize Hg. The presence of SO_2 causes the formation of HCl which does not oxidize Hg effectively. Also, by reaction 11, since Cl_2 reacts with SO_2, the concentration of Cl_2 would be reduced, and this would result in a decreased amount of Hg oxidation[93].

The oxidation of SO_2 to sulfur trioxide (SO_3) in coal combustion flue gas does not proceed at a fast enough rate below 1,230°C[94-96]. However, at temperatures below 630°C, SO_3 would be the dominant species at chemical equilibrium. In contrast, Romero et al. suggest that at high quenching rates, flue gas measurements from coal combustion indicate that only 1 to 3 percent of sulfur is converted to SO_3[97].

Kilgroe et al. also report similar findings where gas-phase Hg oxidation is inhibited by the presence of SO_2 and water vapor[43]. Experiments were carried out in a simulated flue gas stream, containing a base composition of 40 ppmv Hg^0, 5 mole % CO_2, 2 mole % O_2, and a balance of N_2. The temperature was 754°C, and the effects of SO_2, water vapor and HCl were studied.

HCl was added to the gas stream at three concentrations typical of coal combustion flue gas – 50, 100 and 200 ppmv. In this first test, which was in the absence of SO_2 and water vapor, as the concentration of HCl increased, the percent of Hg oxidation increased – 7.5%, 15% and 27.5% respectively.

Reproduced with permission of the copyright owner. Further reproduction prohibited without permission.

The second test was done with the same gas composition as the first experiment and the three HCl concentrations, but also in the presence of 500 ppmv SO_2. As the concentration of HCl increased, the percent of Hg oxidation was approximately 3%, 6% and 17.5% respectively.

The third test done was the same as the second test, but the gas stream included 1.7 mole % water vapor. As the concentration of HCl increased, the percent of Hg oxidation was approximately 1%, 5% and 15%. These results are shown in Figure 1.6.2.1-1.

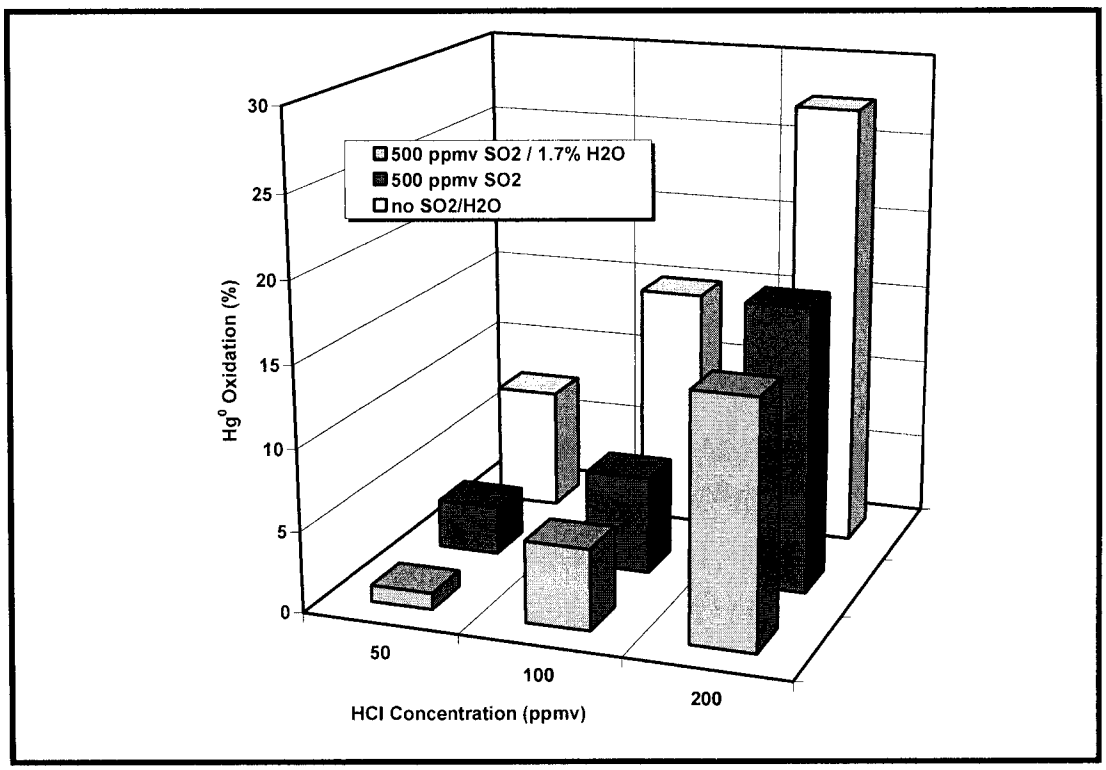

Figure 1.6.2.1-1: Adapted results from experiments performed by Kilgroe et al.[43]

As seen from the results, it is clear that increasing the concentration of HCl results in an increase in the amount of Hg oxidation. The presence of SO_2 reduces the percent of Hg oxidation, and the addition of water further reduces the percent of Hg oxidation. But the researchers still doubt that HCl reacts directly with elemental Hg to cause oxidation, which calls

Reproduced with permission of the copyright owner. Further reproduction prohibited without permission.

into question the results obtained from the first experiment where HCl was added in the absence of water or SO_2. They believe that a separate chlorinating agent such as atomic chlorine (usually present only at very high temperatures) or Cl_2 is required, where Cl_2 is produced by the Deacon Reaction in the presence of water. It is speculated that SO_2 and water vapor scavenge the chlorinating agent and hinder Hg oxidation.

A report by Romero et al. provides a simulation that predicts Hg oxidation under various conditions. The impact of different flue gas components was studied under specified flue gas conditions for circular fluidized bed (CFB) boilers. He shows that Hg oxidation is relatively unaffected by the concentrations of O_2, SO_3, CO_2, CO, NO_2 and NO[97]. The potential effect of these species needs to be explored in terms of the most appropriate operating conditions, which includes a variety of quenching rates. Quenching rates essentially refers to the rate at which the temperatures drop from a higher temperature to a lower temperature, within a power plant gas system. Additional simulations done show that increasing SO_2 and water concentrations inhibits Hg oxidation. As expected, increasing the concentration of HCl increases Hg oxidation[97]. These results agree with those presented by Kilgroe et al..

As stated earlier, it is uncertain whether HCl or Cl_2 is primarily responsible for elemental Hg oxidation. The Deacon Reaction was proposed where Cl_2 is produced by passing a stream of HCl acid gas and atmospheric air over a mixture of copper and manganese oxides[98]:

$$2\ HCl + \tfrac{1}{2}\ O_2 \leftrightarrow Cl_2 + H_2O \qquad (12)$$

In his patents, Deacon varied the temperature from 400 to 850°F. He found that at higher temperatures, the copper compounds volatilized. At lower temperatures, the decomposition of HCl became less active to the point of ceasing completely due to saturation of the catalyst[98-101]. Deacon reported that HCl and O_2 reacted within these catalysts, and Cl_2 and H_2O were released. It is unknown if any experiments were performed without the use of the oxide catalysts. Deacon stated that the reaction is thermodynamically favored between 400 and 850°F, but the

Reproduced with permission of the copyright owner. Further reproduction prohibited without permission.

transformation is kinetically slow, hence requiring a catalyst such that the reaction continues efficiently[102]. In terms of catalysts used, Deacon preferred to use sulfates of copper for his experiments, and several researchers today have quantified the use of these catalysts and other adsorbents that have been inlaid with sulfates – and claim the facilitation of Hg oxidation and removal from flue gas by being adsorbed within the pores[103-105].

Almost all researchers have agreed that the chlorine species is very effective in oxidizing Hg^0 and that the predominant mercury compound present is $HgCl_2$. Additionally, measurements of the concentration of the mercury species taken in the stacks of pilot and full scale coal combustion systems show that more than half of the vapor phase mercury is in the oxidized form, which is likely to be $HgCl_2$[106-108]. However, the debate continues whether HCl or Cl_2 is the species that is responsible for this conversion. A later chapter in this thesis discusses some of the kinetic and thermodynamic issues pertaining to the reaction of elemental mercury with HCl and/or Cl_2, and simulation results are presented to show how temperature affects these reactions.

In a bench scale study using simulated flue gas and the Ontario Hydro Method, Laudal and co-workers carried out experiments to determine the effects of various flue gas components on mercury oxidation and speciation. Table 1.6.2.1-1 summarizes the gas composition used for bench scale tests. Table 1.6.2.1-2 shows some results obtained from bench scale experimentation.

Reproduced with permission of the copyright owner. Further reproduction prohibited without permission.

	Concentration
Main gases	
O_2	4%
CO_2	15%
H_2O	10%
N_2	Balance
Variable gases	
SO_2	0 or 1500ppmv
HCl	0 or 50 ppmv
NO/NO_2	0 or 600/30 ppmv
Cl_2	0 or 10 ppmv
Hg^0	20 μg/Nm^3
$HgCl_2$	20 μg/Nm^3

Table 1.6.2.1-1: Gas composition for bench scale tests performed by Laudal et al.[76]

Test No.	Variable gas composition (ppmv)	Oxidized Hg (%)	Elemental Hg (%)
1	Cl_2	84.8	15.2
3	SO_2	0.7	99.3
5	HCl	0.3	99.7
7	SO_2, HCl, Cl_2	1.9	98.1
9	NO/NO_2	2.1	97.9
11	SO_2, NO/NO_2, Cl_2	0.5	99.5
13	HCl, NO/NO_2, Cl_2	78.7	21.3
15	SO_2, NO/NO_2, HCl	0.1	99.9

Table 1.6.2.1-2: Bench scale results – adapted from Laudal et al.[76]

As seen from Table 1.6.2.1-2, they found that the addition of only Cl_2 resulted in elemental Hg oxidation of up to 84.8%. The addition of only SO_2 resulted in 0.7% oxidation. HCl did not have much of an effect either – only 0.3% Hg oxidation was observed. Similarly, the addition of NO/NO_2 resulted in approximately 2.1% Hg oxidation.

The combined effects of the various components are significant as well. In test 7, they found that SO_2 almost completely eliminates the effect of Cl_2. Since 1500 ppmv of SO_2 was added, apparently SO_2 would almost entirely scrub out both the 50 ppmv of HCl and 10 ppmv of Cl_2. It would have been interesting to see the results of an experiment done where both Cl_2 and HCl were added and the results compared with tests 1 and 5. Comparing tests 1 and 13, it would seem that the presence of NO/NO_2 causes a slight inhibition of Hg oxidation – the amount of Hg

Reproduced with permission of the copyright owner. Further reproduction prohibited without permission.

oxidized reduced from 84.8% to 78.7%, suggesting that HCl has no effect in this process. This idea of NO/NO_2 inhibiting Hg oxidation is further confirmed by comparing tests 7 and 11, where in the presence of SO_2 alone, Hg oxidation reaches 1.9%, whereas in the presence of SO_2 and NO/NO_2, Hg oxidation barely reaches 0.5% - again assuming that HCl has minimal effect on Hg oxidation.

According to the researchers, the results obtained suggest the following:

1. Cl_2 is very effective in oxidizing elemental Hg,
2. HCl oxidizes elemental Hg very poorly,
3. SO_2 inhibits the effect of Cl_2, and potentially scrubs out the chlorine species,
4. NO/NO_2 potentially reduce the effectiveness of Cl_2 as well, but to a much lesser degree than SO_2,
5. The combined effect of SO_2 and NO/NO_2 results in almost complete elimination of Hg oxidation by a chlorine species.

Norton et al. performed similar experiments as Laudal et al. to show the effects of SO_2, NO and NO_2 in a simulated flue gas system injected with HCl[77]. They did not study the effects of Cl_2. Further, most of the experiments were done at a gas temperature of 180°C in the presence of Blacksville fly ash. Table 1.6.2.1-3 lists the composition of the simulated flue gas used in experimentation. Note, that their gas blend system did not include water vapor.

	Concentration
Main gases	
O_2	6%
CO_2	12%
N_2	Balance
Variable gases	
SO_2	0 or 1600ppmv
HCl	0 or 50 ppmv
NO_2	0 or 20 ppmv
NO	0 or 300 ppmv
CO	100 ppmv
Hg^0	12 μg/Nm^3

Table 1.6.2.1-3: Composition of simulated flue gas blend (dry basis) used in experimentation by Norton et al.[77]

Reproduced with permission of the copyright owner. Further reproduction prohibited without permission.

These experiments were done to determine the heterogeneous oxidation of mercury in simulated post combustion conditions. Despite the presence of fly ash, the basic results and effects of the various components contribute to the general understanding of oxidation that takes place in a gas stream. The next four figures summarize the results obtained.

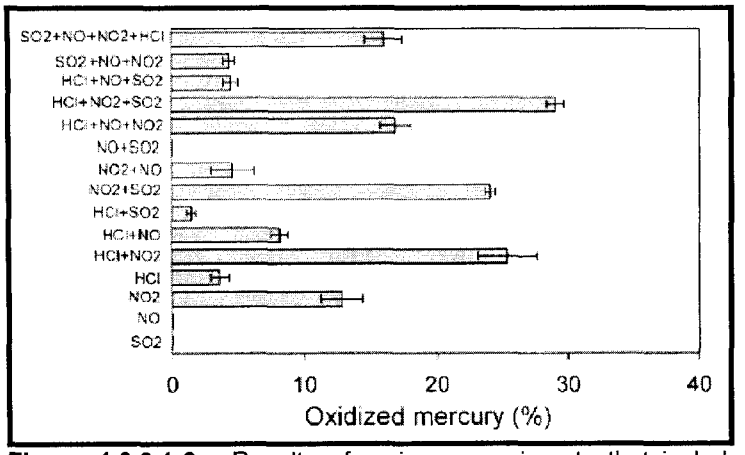

Figure 1.6.2.1-2a: Results of various experiments that included Blacksville fly ash at 180°C (Adapted from Norton et al.)[77]

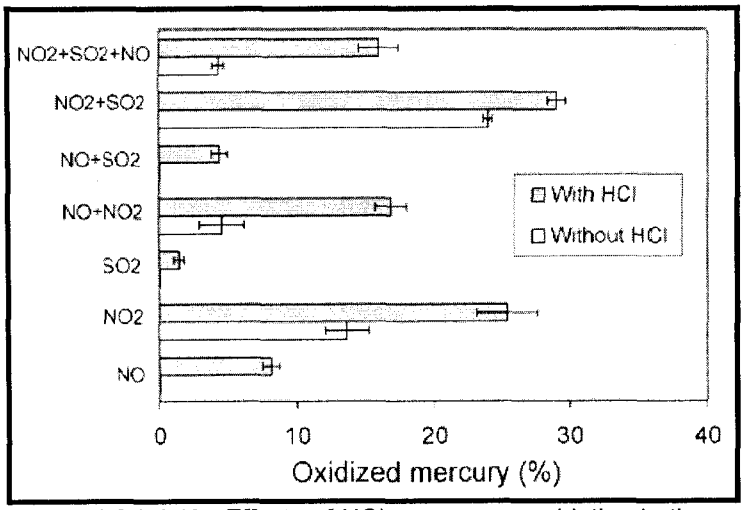

Figure 1.6.2.1-2b: Effects of HCl on mercury oxidation in the presence of Blacksville fly ash at 180°C (Adapted from Norton et al.)[77]

Reproduced with permission of the copyright owner. Further reproduction prohibited without permission.

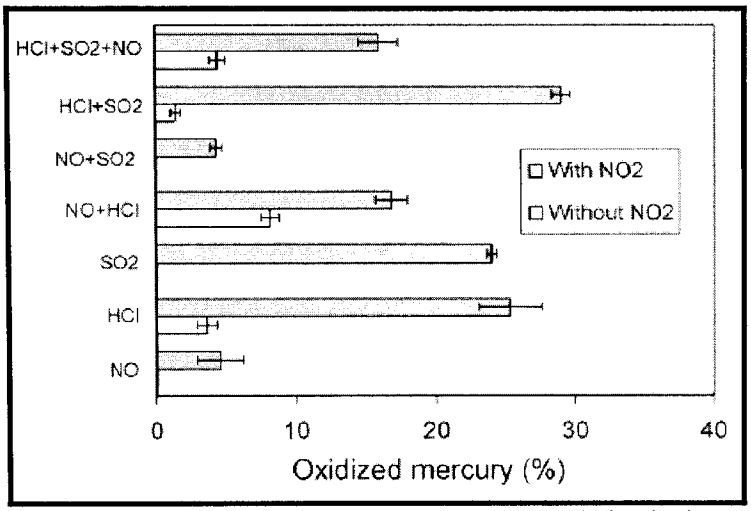

Figure 1.6.2.1-2c: Effects of NO2 on mercury oxidation in the presence of Blacksville fly ash at 180°C (Adapted from Norton et al.)[77]

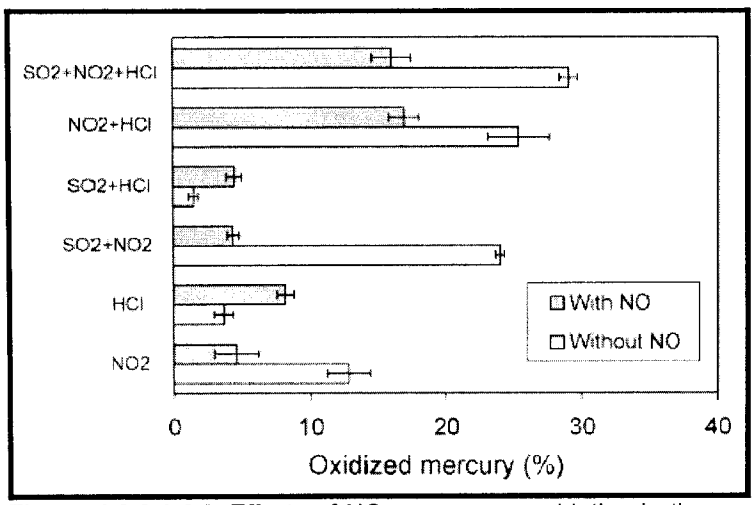

Figure 1.6.2.1-2d: Effects of NO on mercury oxidation in the presence of Blacksville fly ash at 180°C (Adapted from Norton et al.)[77]

The results presented in Figure 1.6.2.1-2a show that HCl is able to slightly oxidize elemental Hg at lower post combustion temperatures (180°C) – up to approximately 4%. NO_2 apparently is a stronger oxidizing agent than HCl, as they found that it is capable of oxidizing an additional 20% of elemental Hg. Neither NO nor SO_2, nor their combination, seem to have any effect on the oxidation of Hg. It is interesting to note that the presence of HCl in the system containing NO and NO_2 seemed to enhance the oxidation of Hg taking place. Similarly, in the presence of NO_2 and SO_2, Hg oxidation reaches above 25%, up to 30% when HCl is added.

Reproduced with permission of the copyright owner. Further reproduction prohibited without permission.

Figure 1.6.2.1-2b displays the effects of HCl on Hg oxidation. NO_2 alone seems to oxidize Hg very well, up to 13% or so. The addition of SO_2 to NO_2 seems to enhance Hg oxidation, while the further addition of NO seems to inhibit Hg oxidation. These results appear to contradict the results presented by Laudal et al., who stated that SO_2 inhibits Hg oxidation, and that NO or NO_2 do not have an affect on Hg oxidation.

Figure 1.6.2.1-2c displays the effects of NO_2 on Hg oxidation. In the absence of NO_2, the other components (SO_2 and NO) do not oxidize Hg, while HCl addition results in less than 5% Hg oxidation. In the presence of NO_2, the Hg oxidation is significantly higher; the combined effect of SO_2 and HCl (in the presence of NO_2) results in Hg oxidation of up to 30%.

Finally, Figure 1.6.2.1-2d displays the effects of NO on Hg oxidation. In all but 2 cases, the presence of NO seems to inhibit the oxidation of Hg as made possible by the presence of NO_2, SO_2, HCl or a combination thereof.

Some conclusions drawn from these experimental results are as follows:

1. Note that there is no water present in the system, the temperature is in a post combustion environment (180°C), and all experiments were done with Blacksville fly ash in the system – resulting in a heterogeneous Hg oxidation scheme.
2. NO_2, HCl and SO_2 seemed to promote mercury oxidation, with NO_2 being the most important factor in doing so.
3. NO seemed to have an inhibitory effect on mercury oxidation.
4. Mercury oxidation mechanisms in the presence of fly ash are very complex.

Galbreath and Zygarlicke also tested for the effects of injecting mercury and a chlorine species, in this case HCl, into a simple gas system consisting of 91.5 mole% N_2 and 8.5 mole% O_2 [56]. They maintained an Hg concentration of 10 $\mu g/Nm^3$ and injected 100 ppmv of HCl. The main furnace temperature remained at a maximum of 1400°C. HCl was injected at 1255°C, and samples were taken from three locations. Most of their gas streams included fly ash, which, similar to Norton et al., results in heterogeneous Hg transformations.

Reproduced with permission of the copyright owner. Further reproduction prohibited without permission.

Upon the addition of 100 ppmv of HCl, they found that the presence of certain metallic compounds, such as Al_2O_3, catalyzed the reaction converting 10% of the injected HCl to Cl_2. They also measured an average of only 35% of the initial amount of total mercury injected. 77% of this remaining amount was in oxidized form, while the remaining 23% was in elemental form.

In another test involved the combustion of Absaloka coal, which is a Powder River Basin (PRB) sub-bituminous coal. The composition of the flue gas obtained is given in Table 1.6.2.1-4.

Component	Concentration
O_2	8.48 mole%
CO_2	10.6 mole%
CO	390 ppmv
SO_2	410 ppmv
NOx	960 ppmv
HCl	3 ppmv

Table 1.6.2.1-4: Absaloka coal combustion flue gas composition[56].

This gas stream also contains an unspecified amount of water and the balance is N_2. It also consisted of fly ash. Before the addition of HCl, the total mercury present consisted of 41% Hg^P, 40% Hg^0 and 19% Hg^{2+}. The addition of 100 ppmv of HCl resulted in approximately 25% total mercury loss, and the speculation is that $HgCl_2$ was formed and adsorbed onto insulating components of the combustor. The remaining 75% of total mercury was divided up as 14% Hg^P, 57% Hg^0 and 29% Hg^{2+}.

They concluded that the low recoveries of mercury during the 100 ppmv HCl injections into a simple gas mixture and the Powder River Basin (PRB) sub-bituminous coal combustion flue gas suggest that $HgCl_2$ was formed and adsorbed onto insulating components of the combustor. They further postulate that a reaction involving elemental Hg and O_2, catalyzed by Al_2O_3 and/or TiO_2 present in the refractory-lined section of the combustion chamber, resulted in the formation of HgO, although mercury nitrite or nitrate could be an intermediate.

Aside from publications, several patents and patent applications have stated the need and use of chlorine, in various forms, to oxidize the elemental mercury in a gas system, and thus enhance its potential removal.

Reproduced with permission of the copyright owner. Further reproduction prohibited without permission.

A patent filed by deJong et al. made use of activated carbon containing a chlorine content of 5% to 12% by weight[109]. The process was set up such that the gas mixture contained 15 to 25 atoms of chlorine per atom of mercury, and as the gas passed through the 5 cm bed of activated carbon; the bed was continuously or periodically replenished with chlorine. This was done by adding a calculated amount of chlorine to the gas stream in an amount such that the carbon itself would absorb a certain amount of chlorine which would equal the quantity that is consumed during the adsorption of mercury. They claim to achieve over 85% mercury removal – by the fact that chlorine would oxidize the elemental mercury, and the oxidized form would adsorb onto the activated carbon. However, experiments were performed at room temperature, and the gas composition in its entirety is unknown.

A patent filed by Felsvang et al. claim that the chloride content within the coal combustion flue gas is insufficient to convert elemental Hg vapor into $HgCl_2$. In order to alleviate this problem, an aqueous suspension of a basic absorbent is atomized to fine droplets and injected into the hot flue gas. This evaporates the water to form dry fine basic absorbent particles, which when passed through the particle collector, comes in contact with the flue gas and results in sorption of various noxious compounds, including sulfur oxides, hydrogen halides, nitrogen oxides, and mercury[110]. They claim a 90-99% Hg removal rate, upon increasing the chloride content of the gas from 20 to 150 ppm by weight. However, the temperature of operation remains below 170°C, which is similar to the inlet temperature of a bag-house, or the stack temperature, depending on various power plant profiles. They also do not provide the composition of the flue gas, which, for a power river basin (PRB) coal system, consists of SO_2, NO, CO and a water content of up to 15%.

A patent by McIntyre et al. describe a process where chlorine is injected in the form of a gaseous liquid or solution into a gas stream that is at temperatures greater than 100°C[111]. This is done for the purpose of oxidizing undesired components in the gas stream, such as but not restricted to, SO_2 and NO_x. The oxidized form of these components is more readily removed. Caldwell et al. then modified this procedure to include elemental Hg as one of the components that can be removed in the same process as SO_2 and NO_x, where elemental Hg is oxidized and

Reproduced with permission of the copyright owner. Further reproduction prohibited without permission.

readily removed from the flue gas stream by water absorption[112]. He claims that a sufficient amount of chlorine in gaseous form, liquid form, or a water solution form is injected and the reaction is allowed to proceed for a sufficient time to enable a significant amount of oxidation of pollutants to occur. However, he gives no concentration profile of the flue gas, no concentration of the amount of chloride injected, no amounts of Hg oxidized and captured, and no experimental results.

U.S. Patent No. 4,443,417 describes a method and apparatus by which elemental mercury can be removed from a gas stream using chlorine as an oxidant[113]. The process takes place at a temperature of 60 to 70°C, and the gas stream is saturated with water. The concentration of mercury used ranges from 0.1 to 300 mmole/L. However, this process uses an acidic liquid containing sulfuric acid (H_2SO_4), hydrochloric acid (HCl) and hydrogen fluoride (HF) in a concentration of about 1% by weight. These chemicals are extremely dangerous and corrosive – injecting such into a power plant system is unfeasible and may result in damage to the internal structure of the power plant.

A patent application by Nolan et al. describes a method for controlling or almost completely eliminating both oxidized and elemental mercury emissions in flue gas[114]. They add molecular chlorine and/or an aqueous species of chlorine, such as hypochlorous acid salts, to the flue gas entering the wet scrubbing zone. As a result of this pre-treatment, subsequent treatment of the pre-chlorinated flue gas to remove oxidized Hg via any known means will allow a removal efficiency approaching 100%[114]. However, they do not seem to give any laboratory data that supports this claim, despite the infrastructure built to perform these experiments.

A novel idea introduced by Lissianski et al. describes a method of blending various coal ranks – where a low-rank coal, consisting of low chlorine content, is mixed with Eastern or Western U.S. bituminous coal, which is a high-rank coal and contains high chlorine content[115]. The low-rank coal has less than 100 ppm of chlorine while the high-rank coal, such as Eastern bituminous coal, has chlorine content greater than 800 ppm by weight. They have performed several tests that incorporate various blends of the different rank coals, and speculate that the

Reproduced with permission of the copyright owner. Further reproduction prohibited without permission.

coals that produce higher amounts of fly ash would enhance the removal of oxidized Hg. The combustion of this blend resulted in up to 60% Hg removal from the gas stream, and since bituminous coal contains high chlorine content, they concluded that $HgCl_2$ was formed and was adsorbed onto the fly ash. Most of this blend is combusted at a temperature in excess of 2000°C.

Ide et al. describe the conversion of mercury into mercuric chloride via the addition of HCl. This technique, though successful, requires large quantities of HCl injection into the mercury containing flue gas, at levels of 500 to1500 ppmv[116]. This could result in excessive corrosion of the coal fired power plant steel components. Further, a considerable amount of alkali within the wet gas desulphurization system (FGD), which is responsible for SO_2 removal, will be consumed due to the high HCl content, and this is not commercially viable.

1.6.3 Other Methods of Capturing Hg

Apart from work being done on mercury oxidation enhanced by chlorine compounds, several researchers are also working on using other halogenated compounds to get similar results. Others have been experimenting with various sorbents to capture the oxidized Hg species. This section will briefly introduce and discuss some of these research topics.

1.6.3.1 Using Other Oxidizing Agents

Breen et al. describes a system which has a temperature profile similar to the one being studied in this work[117]. He uses carbon monoxide and ammonia. He claims that chlorine radicals are present at 660°C, and the concentration of these radicals increases as the chlorine content in the coal increases. These chlorine radicals are responsible for oxidizing elemental Hg, but compete for hydrogen radicals that are available from either water or ammonia. He claims that the concentration of chlorine radicals decreases as the concentration of ammonia and water increases. Carbon monoxide (CO), on the other hand, seems to encourage the formation of chlorine radicals. He measured the concentration of Hg at the inlet and outlet of the electrostatic precipitator (ESP) and found that there was over 95% Hg removal efficiency, and most of the Hg

Reproduced with permission of the copyright owner. Further reproduction prohibited without permission.

was found in particulate form. However, the measurement of chlorine radicals is not possible and the reaction that takes place is most likely with HCl which readily forms at temperatures below 750°C – resulting in the formation of $HgCl_2$ which is well known to adsorb onto fly ash and form particulate Hg.

Meichen et al. describe the use of a noble metal or a mixture thereof in their process to control Hg emissions[118]. The noble metals used include gold, silver, palladium, platinum, copper and various mixtures. The metal is then used to coat a substrate such as silicon oxides, ceramics, glasses, zeolites, organic polymers, resins and various mixtures. The metal coated substrate is then saturated in the presence of dilute HCl or Cl_2 gas. Dilute concentrations of elemental Hg present in a combustion exhaust gas is found to be catalytically converted to $HgCl_2$. This process is limited to a flue gas temperature of below 300°C due to the undesirable loss of gold as volatile gold trichloride. The technique also requires substantial expensive capital equipment and the use of expensive precious metal catalysts.

Biswas and Wu describe a process where elemental Hg is oxidized with the use of ultra-violet (UV) light[119]. They make use of a sorbent particle such as titanium dioxide (TiO_2) which is doped with a material such as silicon, phosphorus, germanium, boron, tin, niobium, chromium, silver, gold, palladium, aluminum or a mixture thereof. UV radiation, with a wavelength of between 170 nm and 500 nm, is used to form a sorbent metal complex. Also in the presence of UV radiation, the complex then induces catalytic photo-oxidation of Hg (and other heavy metal species) to forms that are easily adsorbed onto solid particles. This technique again requires a substantial capital investment and the use of expensive consumable metal catalysts.

Mendelsohn et al. describes a system where elemental mercury is contacted with oxidizing solutions of halogens to effectively capture mercury in the form of mercuric halides[120]. The halogen solutions used were iodine, bromine and chlorine. The gas stream consisted of up to 250 ppmv of NO_x and 1000 ppmv of SO_2, and no water. Table 1.6.3.1-1 and 1.6.3.1-2 show the results obtained for various gas compositions.

Reproduced with permission of the copyright owner. Further reproduction prohibited without permission.

	Hg^0 Removal (%)	
Feed-Gas Composition	I (12.7 ppm)	Br (250 ppm)
$O_2 + N_2 + Hg^0$	41.4	71.1
$O_2 + N_2 + Hg^0 + NO + CO_2$	34.9	50.9, 41.6
$O_2 + N_2 + Hg^0 + NO + CO_2 + SO_2$	---	11.8

Table 1.6.3.1-1: Summary of Hg^0 removal results with iodine and bromine solutions[120].

	Chlorine Concentration (ppm)				
	2.5	250	1000	2500	5000
Feed-Gas Composition	Hg^0 Removal (%)				
$O_2 + N_2 + Hg^0$	11.6	14.4, 13.3	---	9.3	14.3
$O_2 + N_2 + Hg^0 + NO + CO_2$	19.0	20.6	35.4, 28.1	37	44.5
$O_2 + N_2 + Hg^0 + NO + CO_2 + SO_2$	0.5	13.8	35.1, 34	35.4, 41	52.2

Table 1.6.3.1-2: Summary of Hg^0 removal results with chlorine solutions[120].

The amount of chlorine injected reached 5000 ppm, which is very high, and would most likely result in corrosion of the power plant steel, and cause the wet FGD system to be consumed. Also, it is surprising that Hg oxidation barely exceeded 50% even with 5000 ppm of chlorine addition. However, the results seem to follow the trend that suggest in the presence of NO, Hg oxidation increases, while in the presence of SO_2, Hg oxidation is inhibited.

Oehr claims to have a means of treating flue gas with a molecular halogen or thermolabile alkali metal hypohalite, such as calcium hypochlorite, which is able to rapidly convert mercury to mercuric chloride[121]. He reports approximately 34% of the total mercury present in the gas stream is oxidized, while the remainder is either elemental or particulate Hg. The presence of calcium maybe beneficial in capturing SO_2 in the gas stream, but in the power plant, calcium can result in a variety of problems, including fouling, which essentially means the deposition of calcium compounds. This can result in massive amounts of damage to the power plant infrastructure, especially near the air pre-heaters.

Vosteen et al. describe a process of removing mercury by feeding a bromine compound at temperatures between 500°C and 800°C[122]. The combustion is carried out in the presence of SO_2. In order to achieve mercury oxidation as complete as possible, the bromine compound was added in a mass ratio of bromine to mercury in the range from 10^2 to 10^4. They claim that the addition of the bromine compound in such access does not have a detrimental effect on the

Reproduced with permission of the copyright owner. Further reproduction prohibited without permission.

process, but could prove to be expensive. However, in a power plant, bromine is capable of being very corrosive, especially in such high concentrations. Additionally, some experiments were also performed with a combination of chlorine, bromine and iodine compounds. The results seem promising but tend to focus more on waste incineration plants, which have high sulfur and low water content. However, a comprehensive gas composition is not provided, so the concentration of SO_2, NO or H_2O in the gas stream is unknown.

Balabanov et al. provide calculations based on reaction enthalpies to show the viability of using Cl_2, Br_2, BrCl, ClO and BrO to oxidize elemental mercury into $HgCl_2$, $HgBr_2$, HgBrCl, HgClO and HgBrO[123]. However, no experimental data is used to support these claims.

1.6.3.2 Hg Capture with Impregnated Fly Ash and Other Sorbents

Several studies have reported various mercury capture methodologies. Since vapor phase elemental mercury is difficult to capture, it is important to find means to first transform elemental mercury in its oxidized form, and thus enhance the capture efficiency.

Laudal et al. studied the effects of various flue gas constituents on mercury speciation[76]. They found that there seemed to be significant interactions between fly ash and NO_x that greatly impacted mercury speciation. Apparently, the fly ash used was able to catalyze the oxidation of elemental mercury, and these results were confirmed in pilot scale tests. More details on this work are found in an earlier section.

Kellie et al. concluded from their research that chlorine promoted the chemisorption of mercury onto fly ash. However, in spite of the fact that sulfur was shown to be a major factor in the oxidation of mercury, it actually inhibited the adsorption of mercury onto the fly ash[89]. In contrast, it has been suggested that sulfur may promote the absorption of mercury onto fly ash. In a study by Behra et al., ≡S-Hg-OH and ≡S-Hg-Cl complexes were detected[124]. However, work done by Rio and Delebarre were unable to find any Hg-S bonds in X-ray diffraction (XRD) examinations when an aqueous solution of mercury was filtered using fly ash[125]. Further, sulfur is known to produce an acid gas that interferes with the trapping of Hg by activated carbon. The

Reproduced with permission of the copyright owner. Further reproduction prohibited without permission.

formation of H_2SO_4 has been shown to release previously trapped mercury. Serre and Silcox proposed that SO_2 may compete with mercury for binding basic sites on fly ash[126]. Under such conditions, the significant amounts of sulfur already present within these sites would serve as an oxidizing agent for elemental Hg. This would explain why oxidation of elemental Hg is seemingly promoted in the presence of SO_2 and yet adsorption of oxidized Hg does not occur.

Fujiwara et al. reported that coals with excessive chlorine generated an abundance of oxidized mercury species. Extents of mercury oxidation did not increase for progressively longer residence times in the exhaust system, but were affected by the level of unburned carbon in the system. They also found an appreciable amount of mercury that adsorbed at temperatures as high as 500°C[79].

Gibb et al. found that the mercury retention in dust is related to the carbon content of the dust[127]. As the carbon content in the dust decreased, the vapor phase mercury emissions increased. Approaching 100% retention of Hg was measured when the carbon content of the dust was over 5%. Also, mercury retention in dust was found to increase linearly as the flue gas temperature decreased from 450°C to 150°C. However, over a range of coal chlorine levels (0.11 to 0.44%), no trend was apparent between the coal chlorine content and the mercury retention on the dust. They also found that over 80% of the vapor phase Hg was present in the oxidized form for the highest chlorine content coal.

One approach is to encourage the attachment of mercury to more easily collectible solid particles. Fixed or fluidized beds containing granular sorbent materials are used as a control device before releasing the gases to the atmosphere[128-131]. Currently, the most commonly used sorbent material is activated carbon (AC), and AC saturated with chlorine or iodine, but more typically, sulfur. However, the efficiency of AC is still in doubt because of its low capacity to adsorb mercury, low applicable temperature range, regeneration and slow adsorption rates[132-137].

Another technique used is to electrically induce the oxidation of elemental Hg by the formation of radicals such as OH, O and ozone[138]. In his thesis, Lee also expounds on various

Reproduced with permission of the copyright owner. Further reproduction prohibited without permission.

other methods of mercury removal, including the use of other radicals, which can be used as oxidants and are generated on a titania particle surface when irradiated with ultra-violet light.

These are among the various areas of research being done on either the oxidation of elemental mercury, or the effective removal of mercury from flue gas conditions. However, very few of them seem to be viable commercially, and in fact, there are only less than a dozen or so companies that offer a commercial means of removing mercury from power plant flue gases. Some of these companies and their claims are listed in the following section.

1.6.4 Current Commercial Technology for Hg Removal

As mentioned earlier, activated carbon (AC) is the most commonly used sorbent material, and despite the doubt in AC efficiency, several companies offer a commercial means of removing mercury from flue gases. Injecting AC upstream of electrostatic precipitators (ESP) or fabric filters (FF) is seen as the retrofit technology with the widest potential application for Hg control. Various companies offer Hg control technologies that claim over 90% reduction of vapor mercury in flue gases, and 60% of these companies include the use of AC injection[140]. Table 1.6.4 is a list of companies that offer various technologies to control mercury emissions, and the commercial status.

Reproduced with permission of the copyright owner. Further reproduction prohibited without permission.

Company	Technology	Status
ADA[141-146]	Activated Carbon	Guarantee: 80% removal w/ FF[a], 60% w/ ESP[b]
Babcock Borsig[147-149]	Various Reagents and Activated Carbon	>90% removal demonstrated on MSW[c] units. No test data on PC[d] units.
Lurgi[141]	Activated Carbon	70-95% removal depending on Hg species and PCD[e].
Sorbent Technologies Corporation	Activated Carbon and powdered sorbents	Up to 85% removal demonstrated.
Babcock & Wilcox[150-154]	Reagent injection in wet FGD	Up to 80% removal demonstrated.
Phalman	MnOx[f] Injection	No full-scale test data reported.
Powerspan[155-156]	Electro-catalytic oxidation (ECO)	No full-scale test data reported.
Apogee Sci. Inc.[157-164]	Adsorption processes (MerCAP^{TM})	90% removal demonstrated at one site.

Table 1.6.4: Summary of various companies offering technology to capture mercury, and the status of development[140].

a. FF – fabric filter
b. ESP – electro-static precipitator
c. MSW – municipal solid waste
d. PC – pulverized coal
e. PCD – particulate control device
f. MnOx – manganese oxide

Reproduced with permission of the copyright owner. Further reproduction prohibited without permission.

1.7 Objective of This Project

The objective of this project is to simulate a flue gas system, similar to one from a power plant. This involves matching the composition of the various components in the flue gas, and having a structure able to conform to a temperature versus residence time profile similar to a power plant. The focus is on using flue gas derived from the combustion of power river basin (PRB) coal.

1.7.1 Flue Gas from PRB Coal Combustion

Flue gas derived from the combustion of power river basin (PRB) coal is more difficult to work with because of the composition, which is displayed in Table 1.7.1.

Component	Composition
Nitrogen (N_2)	70%
Oxygen (O_2)	3.5%
Carbon Dioxide (CO_2)	13.5%
Water (H_2O)	13%
Sulfur Dioxide (SO_2)	370 ppmv
Nitrous Oxide (NO)	170 ppmv
Carbon Monoxide (CO)	300 ppmv
Chlorine (Cl)	100 ppmv
Mercury (Hg)	10 $\mu g/m^3$

Table 1.7.1: Summary of component and respective composition, typical to a PRB coal combustion flue gas.

This system is a difficult composition to work with because of the SO_2 and water content – and both components inhibit Hg oxidation. Various researchers, as discussed in previous sections, have shown the effects of water and SO_2 on Hg oxidation, and the general consensus is that both inhibit Hg oxidation. According to the Deacon Reaction (Equation 12), water forms HCl, and HCl is incapable of oxidizing Hg effectively. Similarly, according to equation 11, SO_2 reacts to form SO_3 and consumes the chlorine species in the process, forming HCl.

Reproduced with permission of the copyright owner. Further reproduction prohibited without permission.

It is known that Hg is released in its elemental state upon the combustion of coal, and this is a result of Hg having a boiling point of Hg is 357°C while the boiler is at temperatures in excess of 1700°C. The temperature profile poses an issue with regard to Hg oxidation.

The Deacon reaction is thermodynamically favored in the forward direction at temperatures between 430°C and 475°C. However, at a boiler temperature of 1700°C or higher, the backward reaction is favored, where HCl is the likely species to exist. This results in a lower chance of the oxidation of Hg. The presence of unburned carbon, or fly-ash, would encourage the adsorption of mercury onto it, but in actuality, research has shown that as temperatures increase, the amount of mercury adsorbing on a surface decreases. There are also several dozen competing reactions that probably take place within the system, from the exit of the boiler to the exit of the stack gas. Many of the other problems have been listed in previous sections.

As a result, this composition of flue gas provides a challenging opportunity for mercury oxidation. Other researchers make use of unusual compositions, such as too high of an Hg, SO_2 and NO concentration, or too low of a N_2, O_2 and H_2O concentration. The composition described in Table 1.7.1 is a good balance and is more realistic in terms of actual flue gas compositions as derived from a PRB coal combustion system.

1.7.2 "What this Project Aims to Accomplish"

The purpose is especially to design and construct a laboratory scale system that will allow for the testing of novel oxidants and sorbents, with an end goal of performing experiments involving a combination of the most effective oxidant and sorbent for total mercury.

The design of the system will model a temperature versus residence time profile of a power plant. This will be attained by blending the various gases according to the composition in Table 1.7.1, and heating them to the desired operating temperature. This project, in particular, aims to find a cheap and efficient means of oxidizing mercury in this system.

Reproduced with permission of the copyright owner. Further reproduction prohibited without permission.

The project will make use of cutting edge technology in mercury detection, in particular, the use of an atomic fluorescence mercury analyzer, to detect the concentration of the mercury species present in the flue gas.

Additionally, this project will consolidate experimental data collected from literature and propose a global kinetic mechanism to predict Hg oxidation based on the concentrations of the various constituents in the flue gas stream, the temperature profile of the system, and residence time.

Reproduced with permission of the copyright owner. Further reproduction prohibited without permission.

CHAPTER 2

Laboratory Apparatus

This chapter focuses on the construction of the laboratory apparatus that was used in all the experimental work presented in this thesis. The chapter has been divided into several sections. Each section includes pictures, design specifications and modifications made on the apparatus. Also included are lists of prices of major items purchased, part numbers and the vendor. All prices and part numbers are subject to change and are valid as of the project duration between the years 2002 and 2005.

2.1 Design of the Rig

It was desired that the rig would have the ability to perform homogeneous and heterogeneous mercury oxidation experimental work. Homogeneous mercury oxidation is the process which occurs in the gas phase by the interaction and reaction between gas molecules. Heterogeneous mercury oxidation typically takes place within sorbent or fly ash particles. This thesis focuses on homogeneous mercury oxidation.

The apparatus was initially designed by the combined effort of engineers from Foster Wheeler, North America Corp., Mr. William Betchel and Mr. Matthew Chalmers. Much of the design specifications were drawn up in a CAD. A detailed description is given in later sections. Minor modifications done on the apparatus are also listed in detail.

2.2 Objective of Rig

The objective of the apparatus was to carry out homogeneous and heterogeneous mercury oxidation experimental work. Additionally, the temperature versus residence time profile of the apparatus had to match that of a power plant.

Reproduced with permission of the copyright owner. Further reproduction prohibited without permission.

As mentioned in Chapter 1, most researchers have performed experimental work at temperatures above 1000°C or below 200°C. There is limited work done at temperatures between the exit of the economizer and the stack of a power plant. The apparatus designed for this work had the ability to match the profile from the economizer to the bag-house. Two ideas for achieving the profile were discussed and discarded before the third idea was implemented.

2.2.1 First Idea: Pulverizer and Boiler Construction

The first idea was to build an apparatus consisting of a coal pulverizer and a boiler. This scheme would have been extremely difficult to design and maintain. Additionally, the cost of building would have been higher than the proposed budget.

The burning of pulverized coal would have also resulted in fly ash particles entrained in the flue gas stream. Experimental work involving the homogeneous oxidation of elemental mercury would have not been possible because of particulate matter. This idea was thus discarded.

2.2.2 Second idea: Propane Combustion

The second design of the apparatus was to use a propane combustion system, where propane would have been burnt according to the reaction shown below:

$$C_3H_8\,(g) + 5\,O_2 \rightarrow 3\,CO_2 + 4\,H_2O \qquad (1)$$

Several issues were a concern:

1. The combustion of propane required a flame, which is inherently dangerous.
2. The combustion of propane results in a high mole fraction of CO_2 and H_2O. This would have easily provided the necessary compositions CO_2 and H_2O, but the control of these compositions would have been difficult.
3. The purchase, installation and daily maintenance of a propane combustor would have been expensive and time consuming.

Reproduced with permission of the copyright owner. Further reproduction prohibited without permission.

Due to these issues, the propane combustion design was abandoned.

2.2.3 Third Idea: Blending Gases

Blending of the gas components was chosen as the safer and cheaper idea. The major components of the flue gas were blended together according to the composition as shown in Table 1.7.1. This composition was used in most experiments described in this thesis. The composition listed is typical to a flue gas composition obtained upon the combustion of Powder River Basin (PRB) coal. The gas blend is then heated and experimental work is then carried out. This idea was preferred and implemented.

2.3 Construction of the Apparatus

This section gives a detailed list of the various parts of the apparatus, along with design specifications, vendors, part numbers and costs. Some modifications which were made to the initial design are also included. Figure 2.3-1 is a schematic of the entire apparatus used in this experimental work. It includes the main apparatus, the condenser unit, the carbon trap and the totalizer. Figures 2.3-2 to 2.3-5 are CAD drawings of the same equipment. Figures 2.3-2 and 2.3-3 are of the main apparatus, without the condenser unit, carbon trap and totalizer. These sections of the apparatus were modifications that were added later (Figures 2.3-4 and 2.3-5), and more details are given in following sections.

Reproduced with permission of the copyright owner. Further reproduction prohibited without permission.

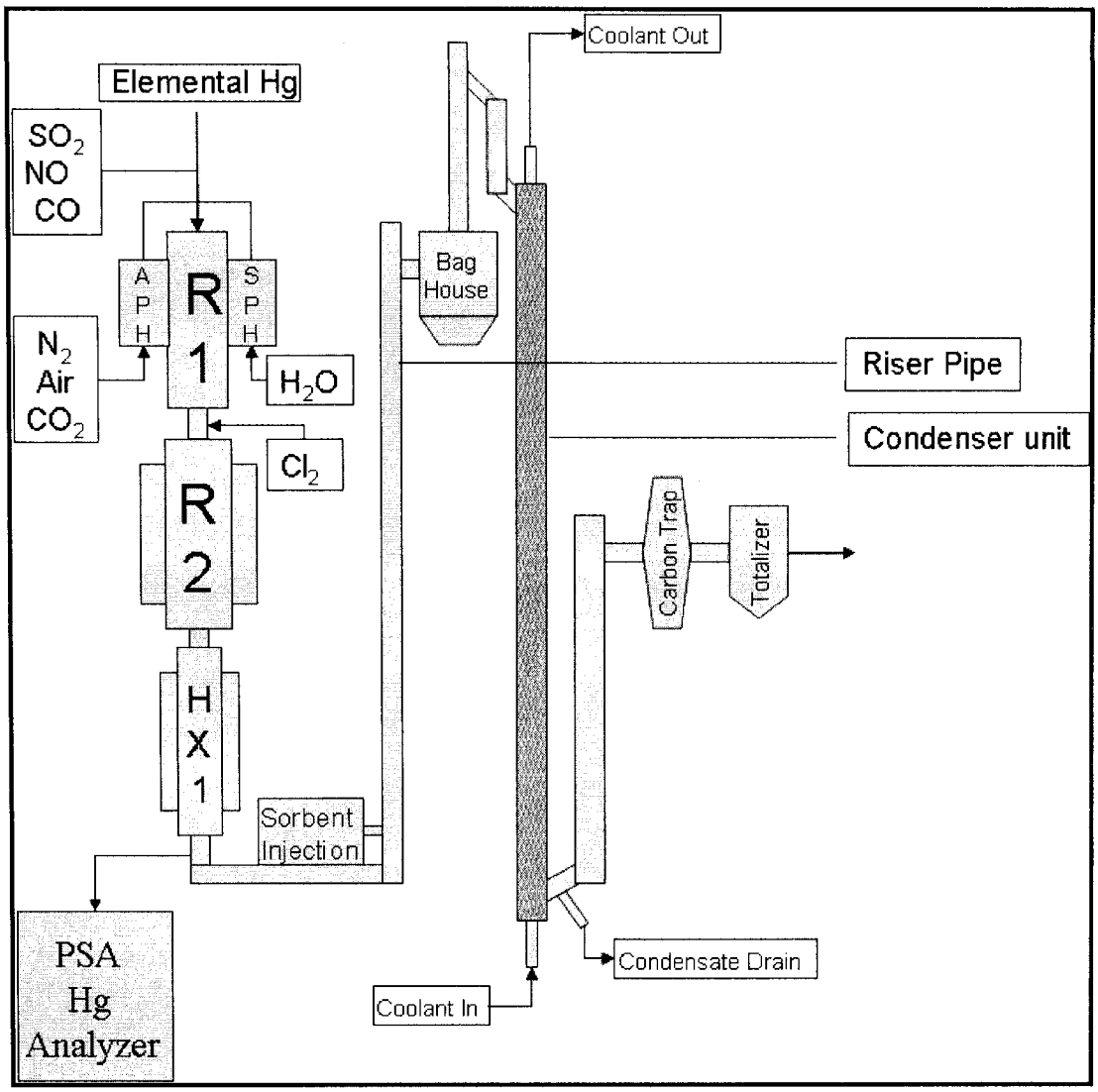

Figure 3.3: Schematic of Testing Facility to perform Hg oxidation tests. Base gas compositions and temperature profile are shown in Tables 3.3 and 3.3.4 respectively.

Reproduced with permission of the copyright owner. Further reproduction prohibited without permission.

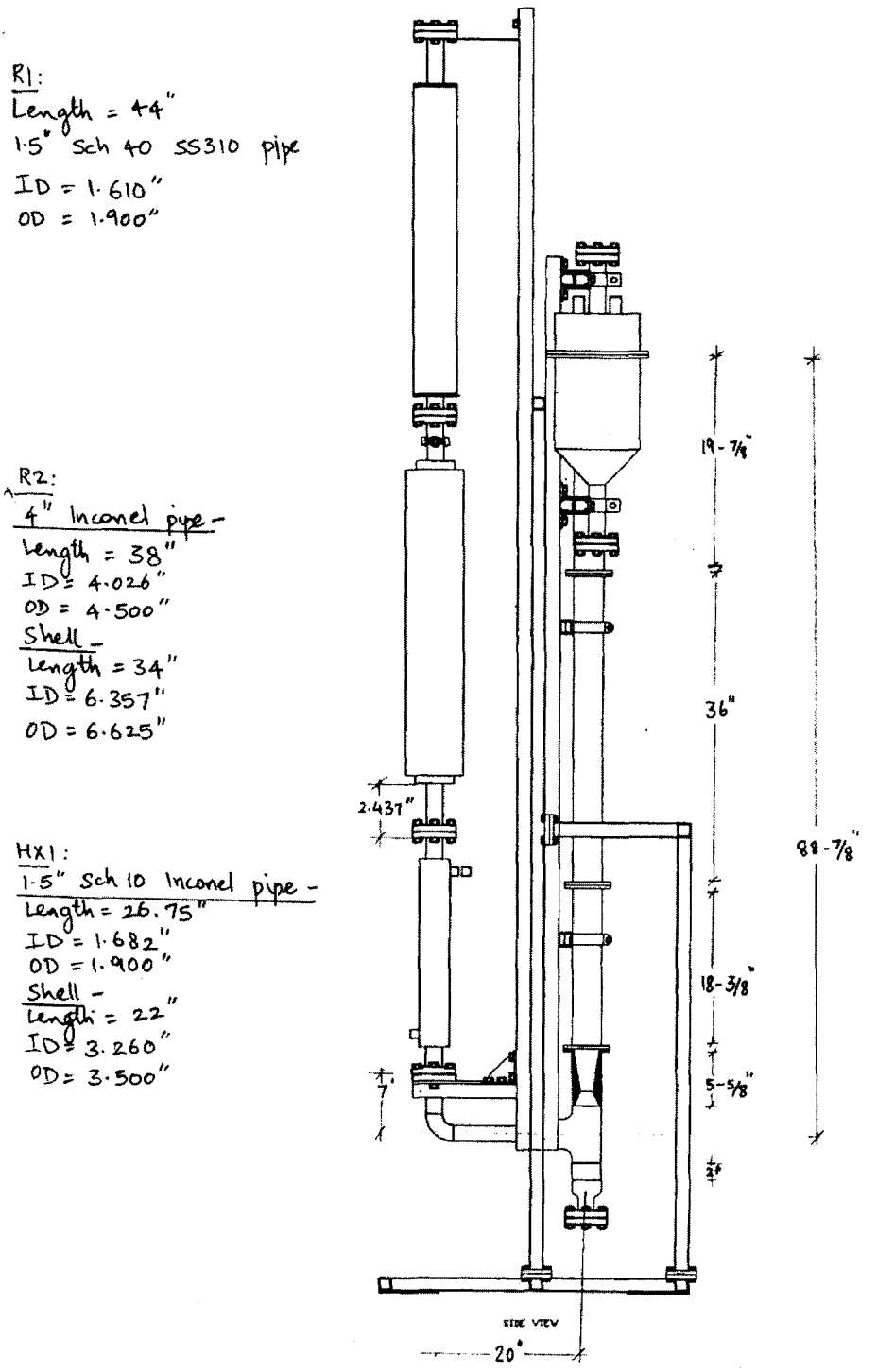

Figure 2.3-2: CAD drawing of the rear view of experimental apparatus without condenser unit.

Reproduced with permission of the copyright owner. Further reproduction prohibited without permission.

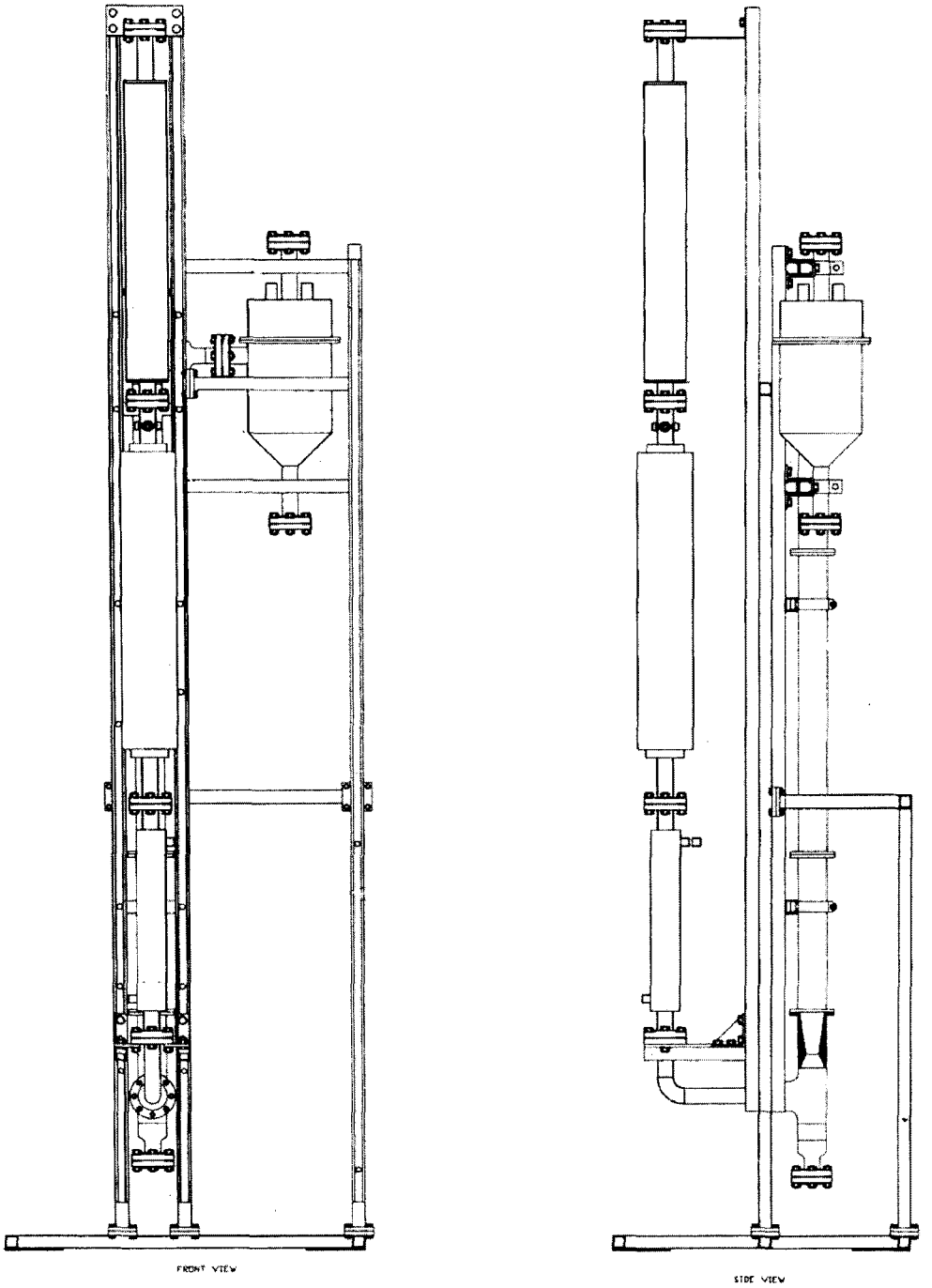

Figure 2.3-3: CAD drawing of the front and side view of experimental apparatus without condenser unit.

Reproduced with permission of the copyright owner. Further reproduction prohibited without permission.

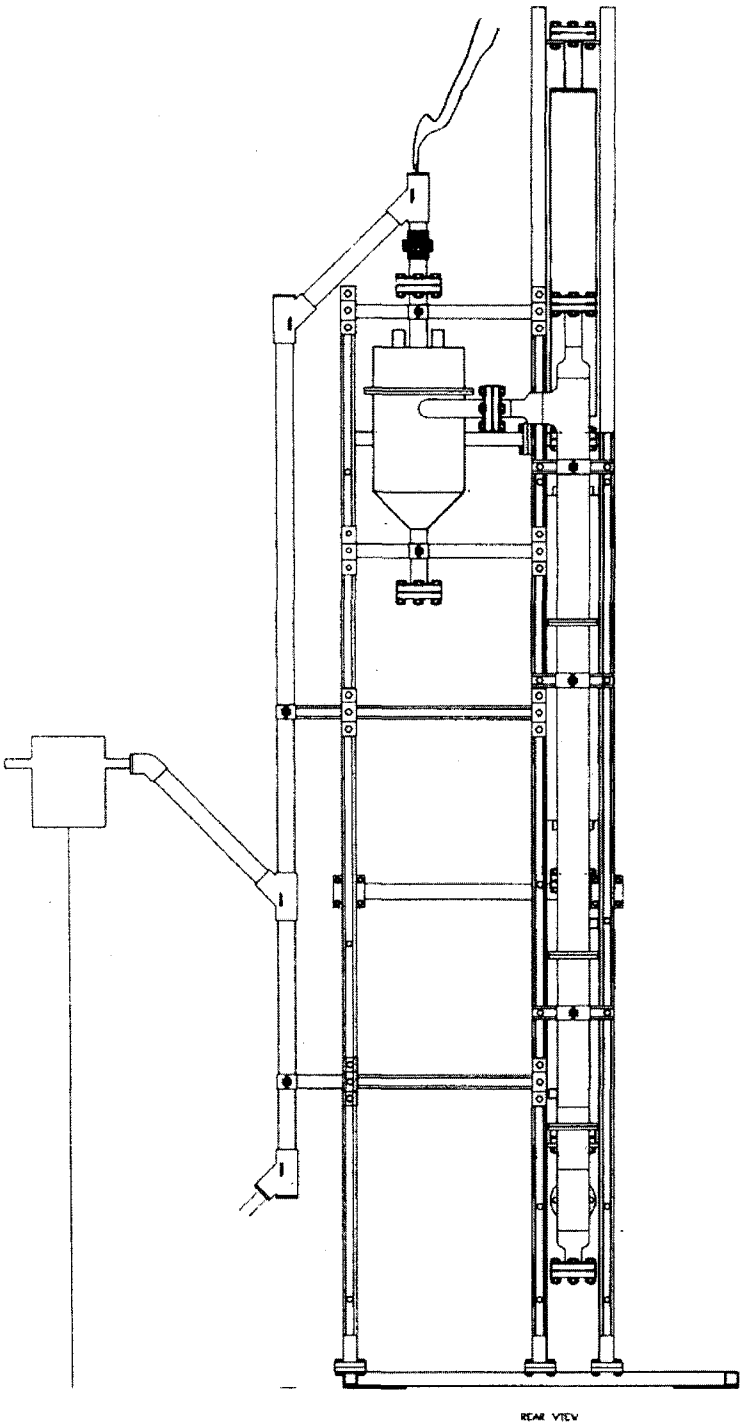

Figure 2.3-4: CAD drawing of the rear view of experimental apparatus with condenser unit.

Reproduced with permission of the copyright owner. Further reproduction prohibited without permission.

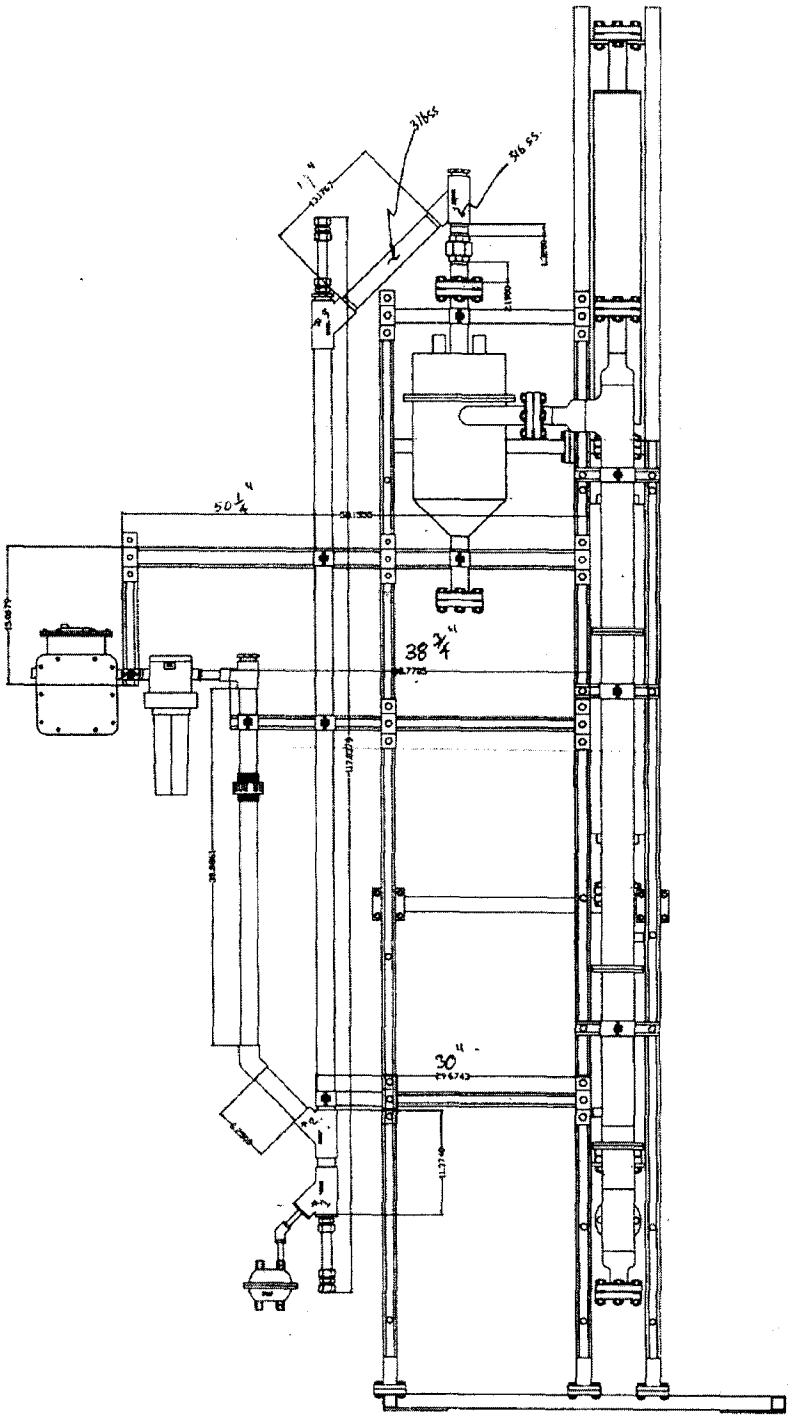

Figure 2.3-5: CAD drawing of the rear view of entire experimental apparatus with condenser unit.

Reproduced with permission of the copyright owner. Further reproduction prohibited without permission.

2.3.1 R1

R1 is the main heater in this apparatus. It is labeled in Figures 2.3.1-1 to 2.3.1-4.

2.3.1.1 Design of R1

The design of R1 is shown in Figure 2.3.1.1-A. The part marked (2) is the pipe itself which is 44 inches long. It is a schedule 40 pipe made of Stainless Steel (SS) 310. It has an outside diameter (OD) of 1.900 inches and an inner diameter (ID) of 1.610 inches[165]. SS310 was used because of its high temperature resistance and good ductility. It can also resist oxidation at temperatures up to 1150°C in the absence of sulfur gases[166].

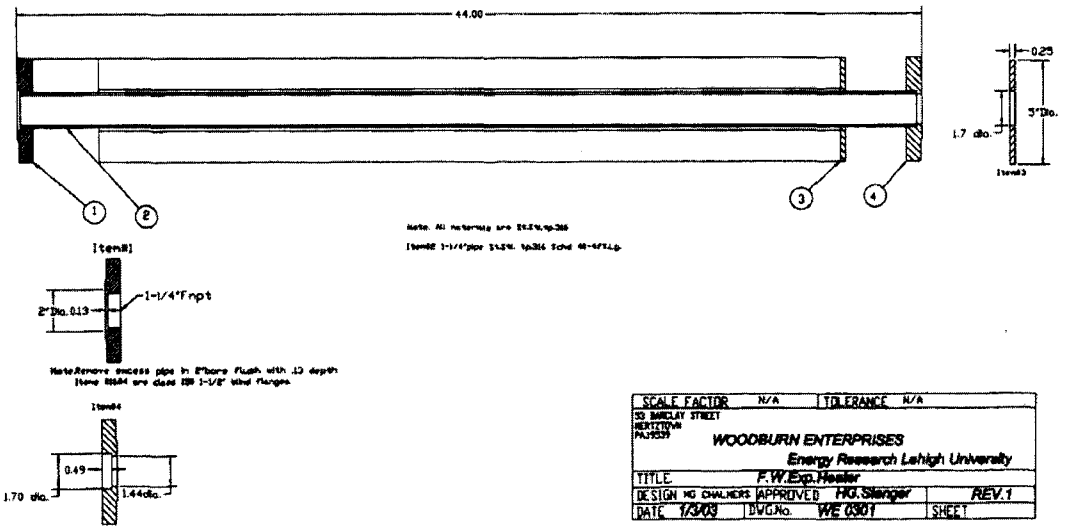

Figure 2.3.1.1-A: CAD drawing of R1.

Reproduced with permission of the copyright owner. Further reproduction prohibited without permission.

The parts marked (1) and (4) are SS316 flanges that were welded to the ends of the pipe. These flanges were bought as blind flanges and the center was bored through. The flanges were then slipped onto the pipe and welded in place. Upon installation, R1 stands upright – part (1) is the top flange and part (4) is the bottom flange. The part marked (3) is a disk that was welded 4 inches above the bottom flange. It is 5 inches in diameter with a ¼ inch thickness. It has a 1.7 inch diameter hole that is cut out of the center, similar to the flanges. The ring slips onto the pipe and is welded in place. It is used to vertically hold the ceramic heaters that encapsulate R1.

R1 is the main heater in this apparatus. The gases flow through it and are heated within the pipe by ceramic heaters. The temperature of the heaters is controlled by a Honeywell control box and is able to reach a maximum value of 1300°C[167]. It was important to ensure that the temperatures at various locations were continuously monitored. 6 K-type thermocouples were used to do this:

i. The first was used to measure the temperature of the gas stream at approximately the center of the pipe.

ii. The second was used to measure the temperature of the gas stream at the exit of R1. This temperature was most important as it determined the temperature and residence time profile of the other sections of the apparatus.

iii. The third was used to measure the skin temperature of the pipe at the quarter length mark from the top of R1.

Reproduced with permission of the copyright owner. Further reproduction prohibited without permission.

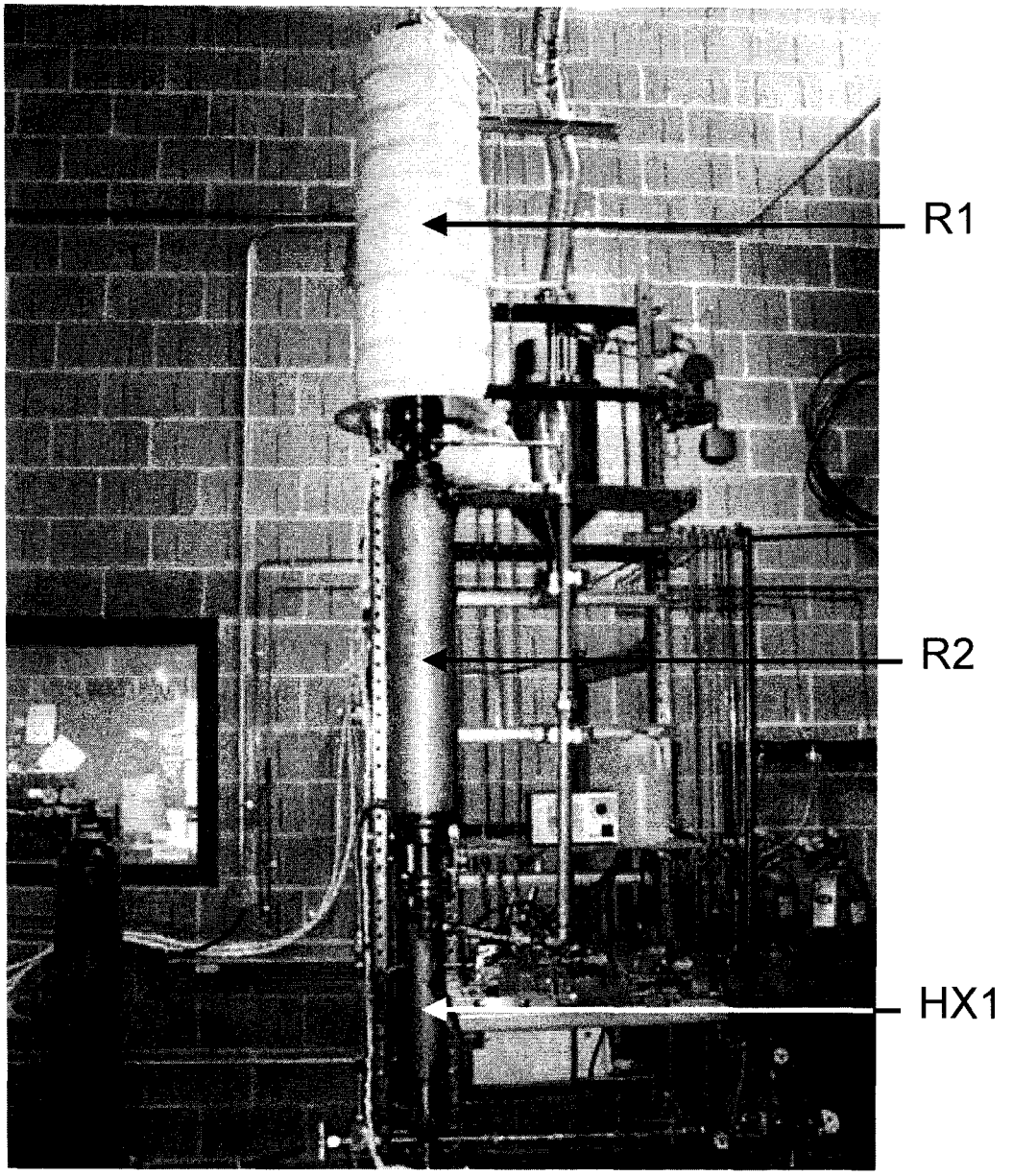

Figure 2.3.1-1: Picture of R1, R2 and HX1 as constructed for experimental work.

Reproduced with permission of the copyright owner. Further reproduction prohibited without permission.

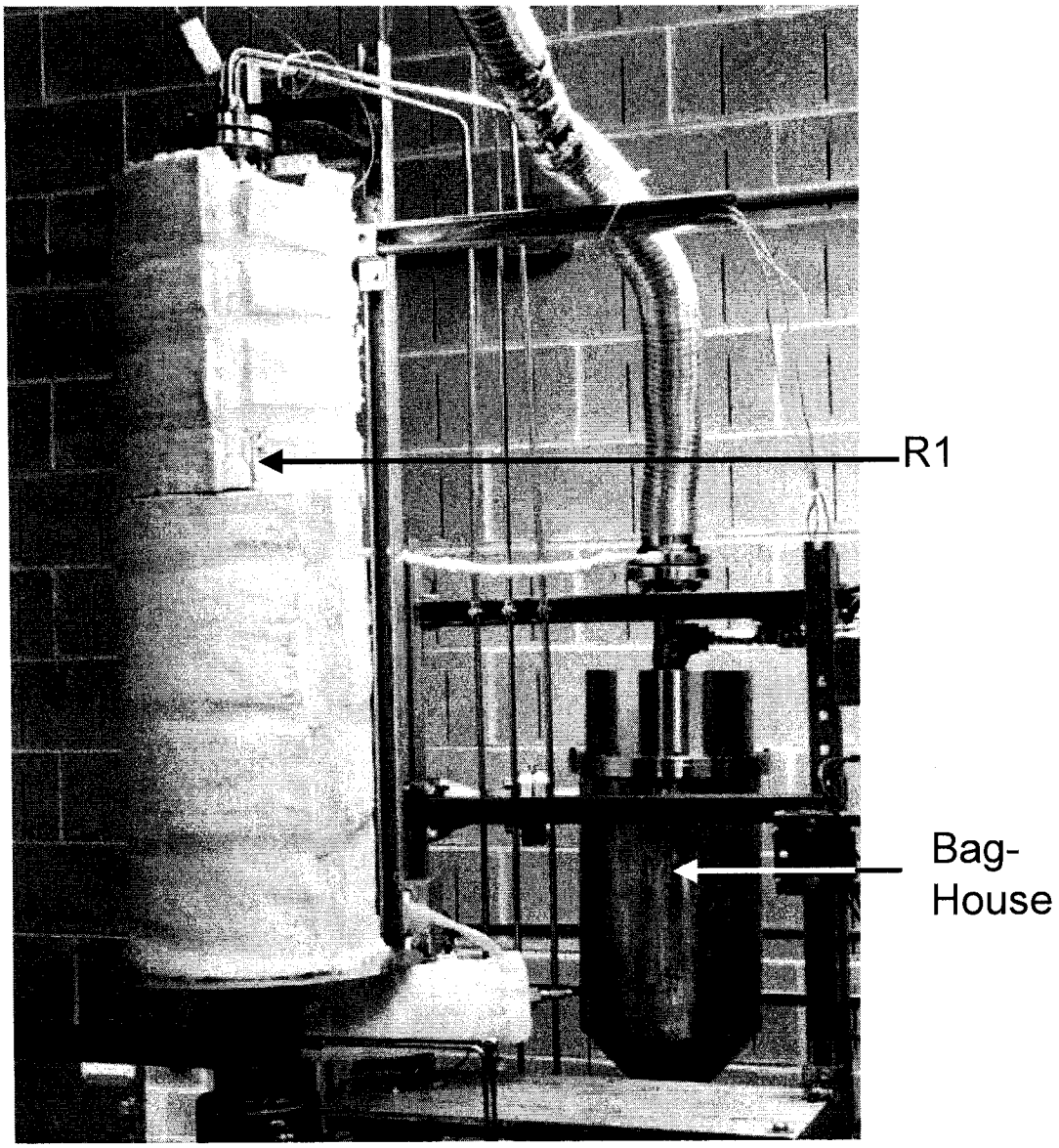

Figure 2.3.1-2: Close-up of insulated R1 and bag-house.

Reproduced with permission of the copyright owner. Further reproduction prohibited without permission.

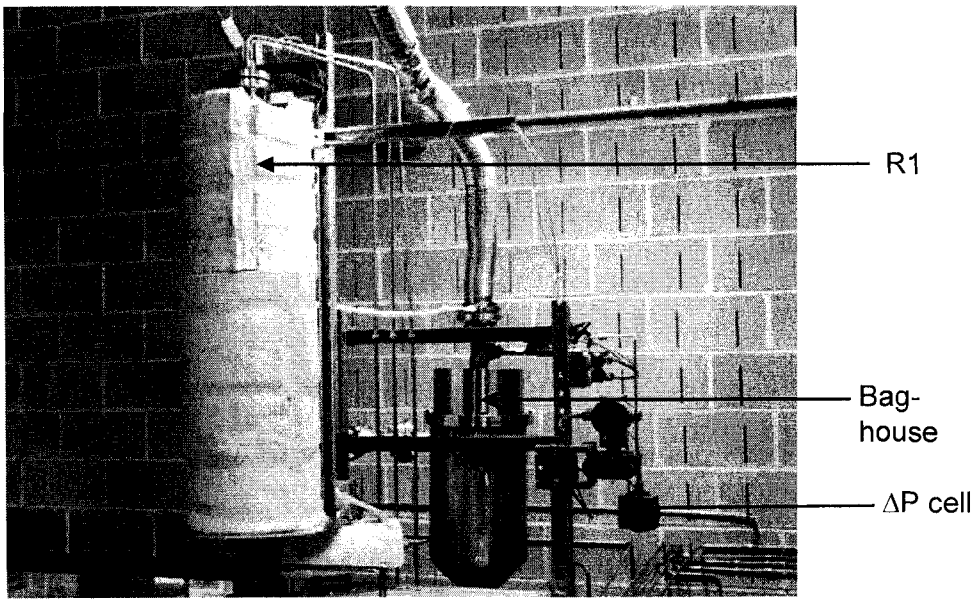

Figure 2.3.1-3: Close up of insulated R1, bag-house and ΔP cell used to send bursts of air into the bag-house.

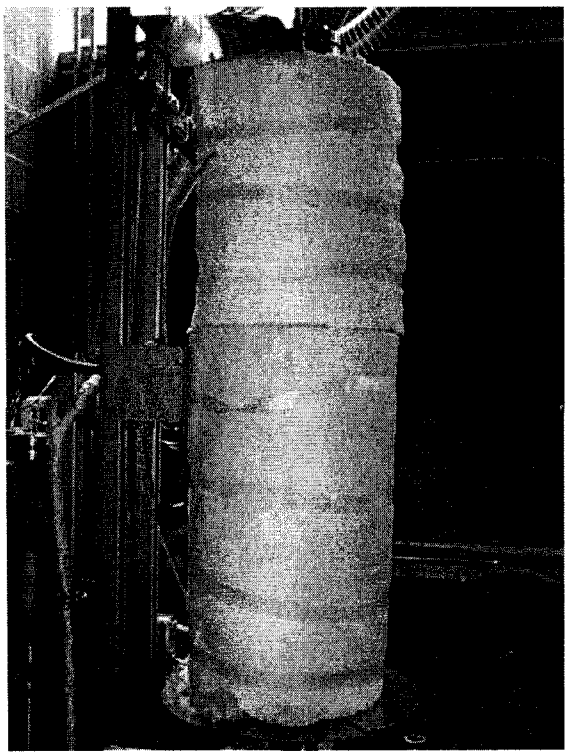

Figure 2.3.1-4:
Close-up of insulated R1.

Reproduced with permission of the copyright owner. Further reproduction prohibited without permission.

iv. The fourth was used to measure the skin temperature of the pipe at the half length mark from the top of R1.

v. The fifth was used to measure the skin temperature of the pipe at the three-quarter length mark from the top of R1.

vi. The sixth was used to measure the skin temperature of the pipe at the bottom of the ceramic heaters, or just above the ring that holds the heaters in place.

The fifth thermocouple that was located at the three-quarter length mark from the top of R1 was connected to the Honeywell control box (Figure 2.3.1.1-1) and was used to control the temperature of the heaters.

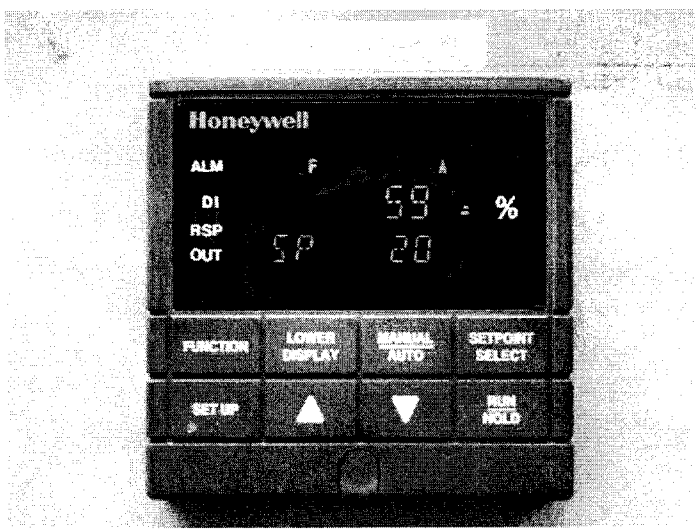

Figure 2.3.1.1-1:
Close-up of Honeywell control box used to control R1 heaters

The ceramic heaters were bought from Thermcraft® [168]. They were half-shells and each was 18 inches long. Each half-shell required 230 volts of operation and gave an output of 1295 watts. Four half-shells were required, and were connected in series to give a total output of 5180 watts.

In order to increase heat transfer and mixing of the gas stream in the pipe, stainless steel wool was packed into R1. The material helped to conduct heat more efficiently, and the packing

Reproduced with permission of the copyright owner. Further reproduction prohibited without permission.

helped to increase the mixing of the gases. The entire setup was also wrapped twice with a 2 inch thick ceramic-fiber insulation blanket. The ceramic fiber has temperature resistance up to 1260°C, and provided adequate heat insulation. The blankets were held in place by fiber-glass tape. The tape is rated for use in between temperatures of -73°C and 260°C.

2.3.1.2 Purchasing Information for R1

Table 2.3.1.2-1 is a list of items purchased, along with the respective part numbers, vendors and prices, as of the duration of the project from 2002 to 2005. The last column is labeled "notes" where miscellaneous information for that item is provided.

Item	Part Number	Vendor	Location	Price ($)	Notes
48" SS 310 pipe	(n/a)	Yeager Supply Inc.	Allentown, PA	125.00	Pipe was cut to 44" length.
Blind Flanges	44695K115	McMaster Carr Supply Company[169]	New Brunswick, NJ	24.56	Flanges were bored out before being welded onto pipe. Figure 2.3.1.2-1.
Socket Weld Flanges	44695K55	McMaster Carr Supply Company	New Brunswick, NJ	30.39	Replaced blind flanges. Figure 2.3.1.2-2
Thermcraft® Heaters	RH246	Thermcraft®	Winston-Salem, NC	105.00	Price is for each half shell. 2-3/8" ID, 18" length. 24" braided leads. 1295 watts each half shell.
Ceramic Fiber Blanket	93315K68	McMaster Carr Supply Company	New Brunswick, NJ	168.30	2" thick x 2' wide x 25' long.
Fiber-glass tape	7574A12	McMaster Carr Supply Company	New Brunswick, NJ	13.83	Used to hold ceramic fiber blanket in place.
Zeetex Insulation Tape	10945-163	VWR[170]	Bridgeport, NJ	10.93	Price per roll. Replaced fiber-glass tape; blanket was tied down.
SS Nuts (7/16")	91845A029	McMaster Carr Supply Company	New Brunswick, NJ	2.98	Price is for a box of 100 nuts. 20 boxes were purchased to fill up pipe. Figure

Reproduced with permission of the copyright owner. Further reproduction prohibited without permission.

					2.3.1.2-3
SS Bolts	92245A726	McMaster Carr Supply Company	New Brunswick, NJ	3.50	Price per bolt. Used to attach R1 to rest of apparatus. SS hex head cap screws; ½" diameter, #13 threading. Figure 2.3.1.2-4
SS Nuts (1/2")	92673A137	McMaster Carr Supply Company	New Brunswick, NJ	8.62	Price per box of 25 nuts. ½" diameter, #13 threading. Figure 2.3.1.2-5.
Thermo-couples	KQIN-18U-12	Omega Engineering[171]	Stamford, CT	27.00	Regular K-type thermocouples to measure temperature. 12" long.
Thermo-couple wire	KXPP-K-20-200	Omega Engineering	Stamford, CT	70.00	K-type thermocouple wire. 200' length.
Thermo-couples	CAIN-18G-18-DUAL	Omega Engineering	Stamford, CT	63.00	Dual K-type Thermocouple: 1 part for temperature control; 1 part for temperature reading
6-Channel panel read-out	DP-462-T	Omega Engineering	Stamford, CT	348.00	6-channel thermocouple output reading. Figure 2.3.1.2-6.
SS310 sheet	(n/a)	Penn Stainless Products	Quakertown, PA	245.00	¼" thick x 6" long x 24" wide. See notes below.
Silver Goop®	MS-TL-SGT	Swagelok[172]	Allentown, PA	40.60	Price per tube. See notes below.
FLEXI-CARB® Gaskets	01501170817	Flexitellic[173]	Local Distributor	72.84	Made of Inconel; placed between flanges

Table 2.3.1.2-1: List of items purchased for R1, with respective vendors and prices.

Reproduced with permission of the copyright owner. Further reproduction prohibited without permission.

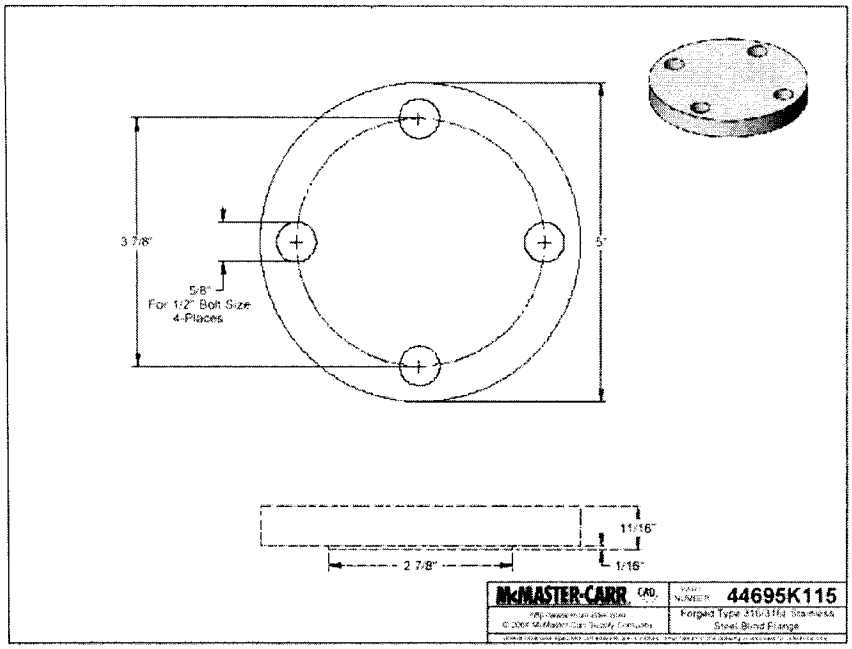

Figure 2.3.1.2-1:
CAD Drawing of blind flange used on R1. Courtesy of McMaster-Carr.

Reproduced with permission of the copyright owner. Further reproduction prohibited without permission.

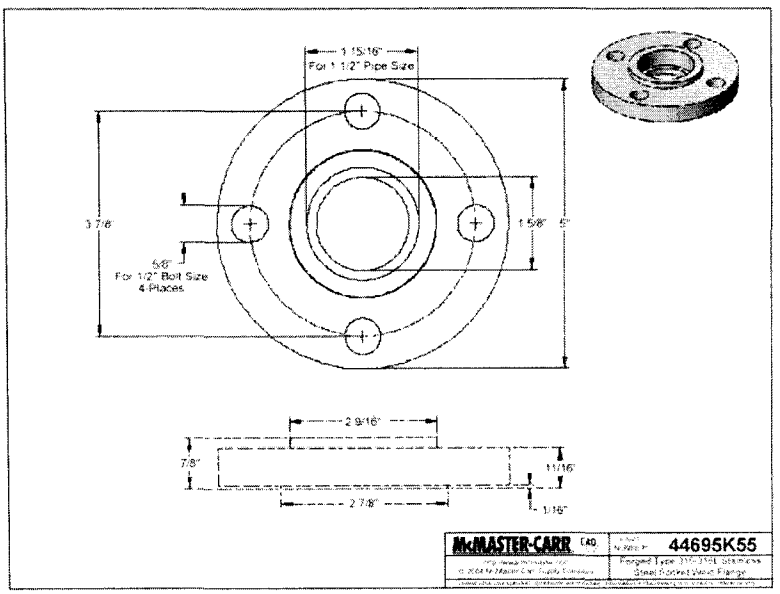

Figure 2.3.1.2-2:
CAD Drawing of socket weld flange used on R1. Courtesy of McMaster-Carr.

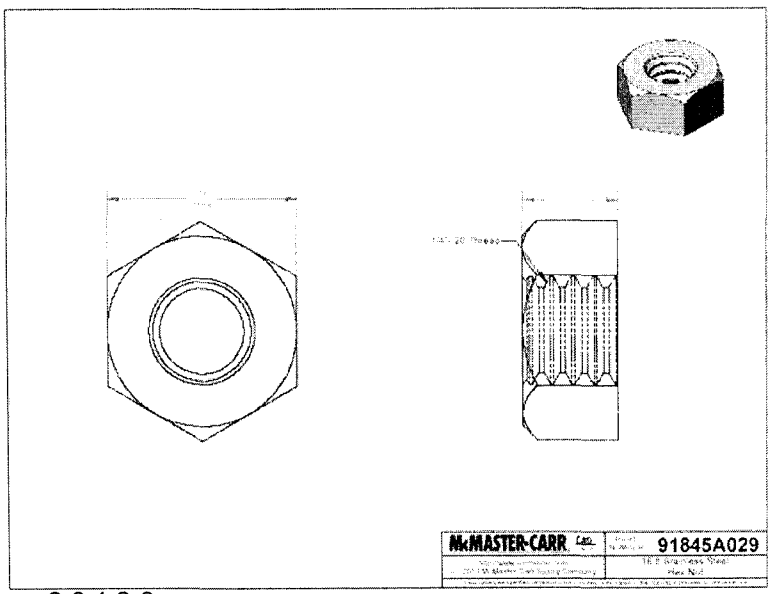

Figure 2.3.1.2-3:
CAD Drawing of SS Nuts used to bolt apparatus together.
Courtesy of McMaster-Carr.

Reproduced with permission of the copyright owner. Further reproduction prohibited without permission.

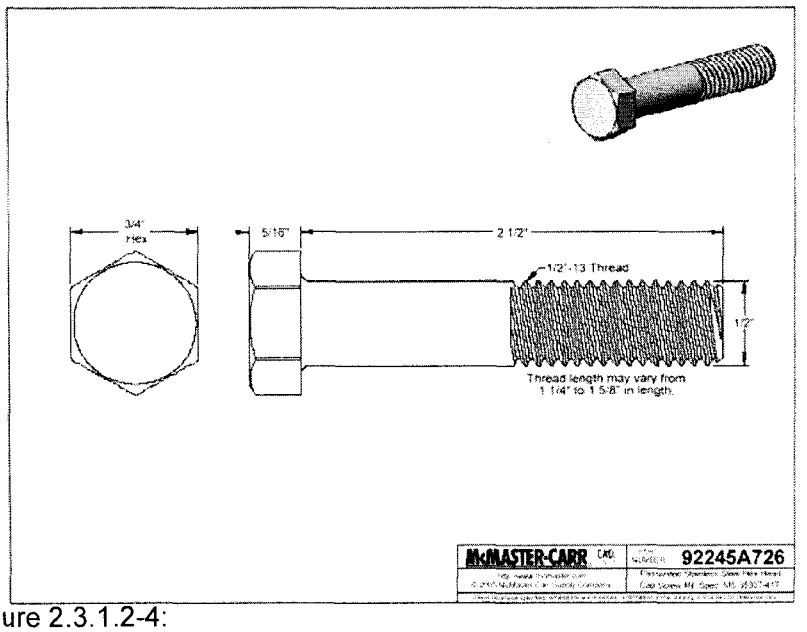

Figure 2.3.1.2-4:
CAD Drawing of SS Bolts used to hold apparatus together.
Courtesy of McMaster-Carr.

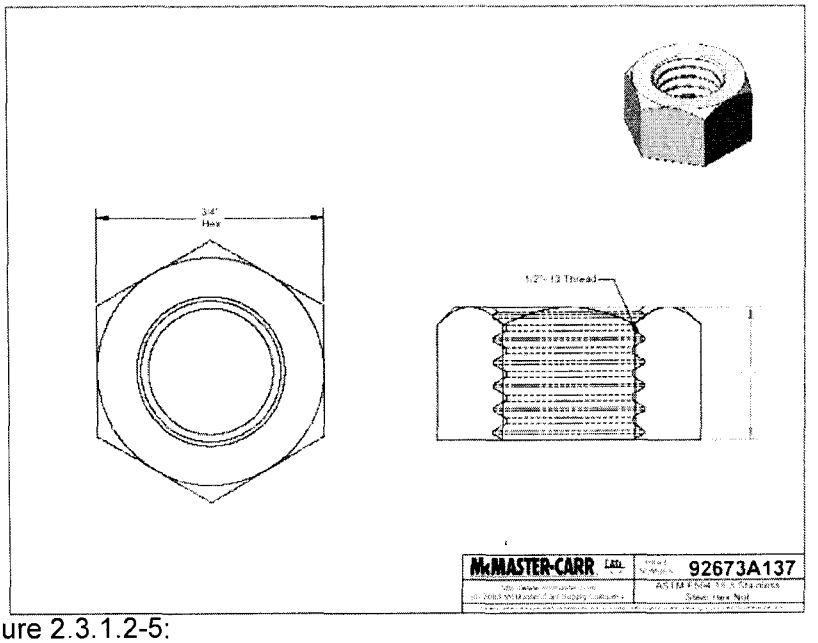

Figure 2.3.1.2-5:
CAD Drawing of SS Nuts used to fill R1 to enhance heat transfer and mixing of gases. Courtesy of McMaster-Carr.

Reproduced with permission of the copyright owner. Further reproduction prohibited without permission.

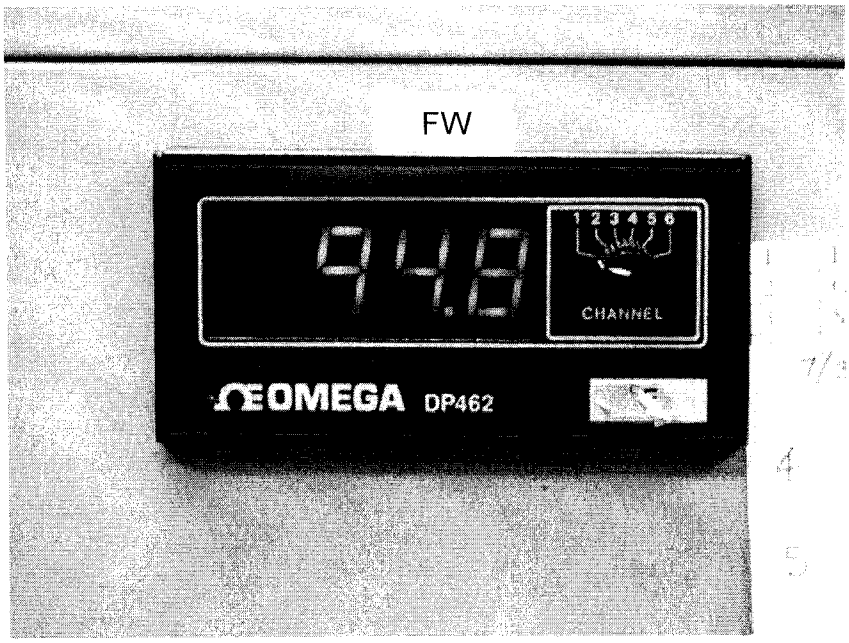

Figure 2.3.1.2-6:
6-channel temperature readout from Omega Engineering. Current settings for reading temperature in °F.

2.3.1.3 Modifications on R1

Some minor modifications had to be made to R1.

i. The process of boring out a blank flange to fit on the SS310 pipe was unnecessary because socket-weld flanges were available from McMaster Carr. These new flanges replaced the blind flanges.

ii. Initially, stainless steel wool was the packing material used in R1 to help mix the gas blend and promote heat transfer. However, at higher temperatures (above 500°C), the steel wool disintegrated and became ineffective. As a result, the wool was replaced by stainless steel nuts. These nuts provided a much better heat transfer capability and did not run the risk of disintegrating into a powder. They also provided adequate mixing of the gas blend.

Reproduced with permission of the copyright owner. Further reproduction prohibited without permission.

iii. A ¼ inch thick SS310 sheet was purchased and a 1.300 inch diameter disk was cut out of it. This disk was inserted into R1 and used to hold the stainless steel nuts in place. 1/8 inch holes were drilled through the disk to allow for the flue gas blend to pass through R1 into R2. The sheet was purchased from Penn Stainless Products in Quakertown, PA, and cost $245.00 per sheet, which had dimensions of 6 inches by 24 inches.

iv. At high temperatures, there is always a danger of the nuts and bolts welding together. If this happens, the process of taking the apparatus apart is almost impossible. To prevent this problem from happening, the threads of the bolts used to fasten R1 to the rest of the apparatus were coated with Silver Goop® purchased from Swagelok in Allentown, PA[172].

2.3.2 R2

R2 is the main reactor in this apparatus. It is labeled in 2.3.1-1 and 2.3.2-1.

Reproduced with permission of the copyright owner. Further reproduction prohibited without permission.

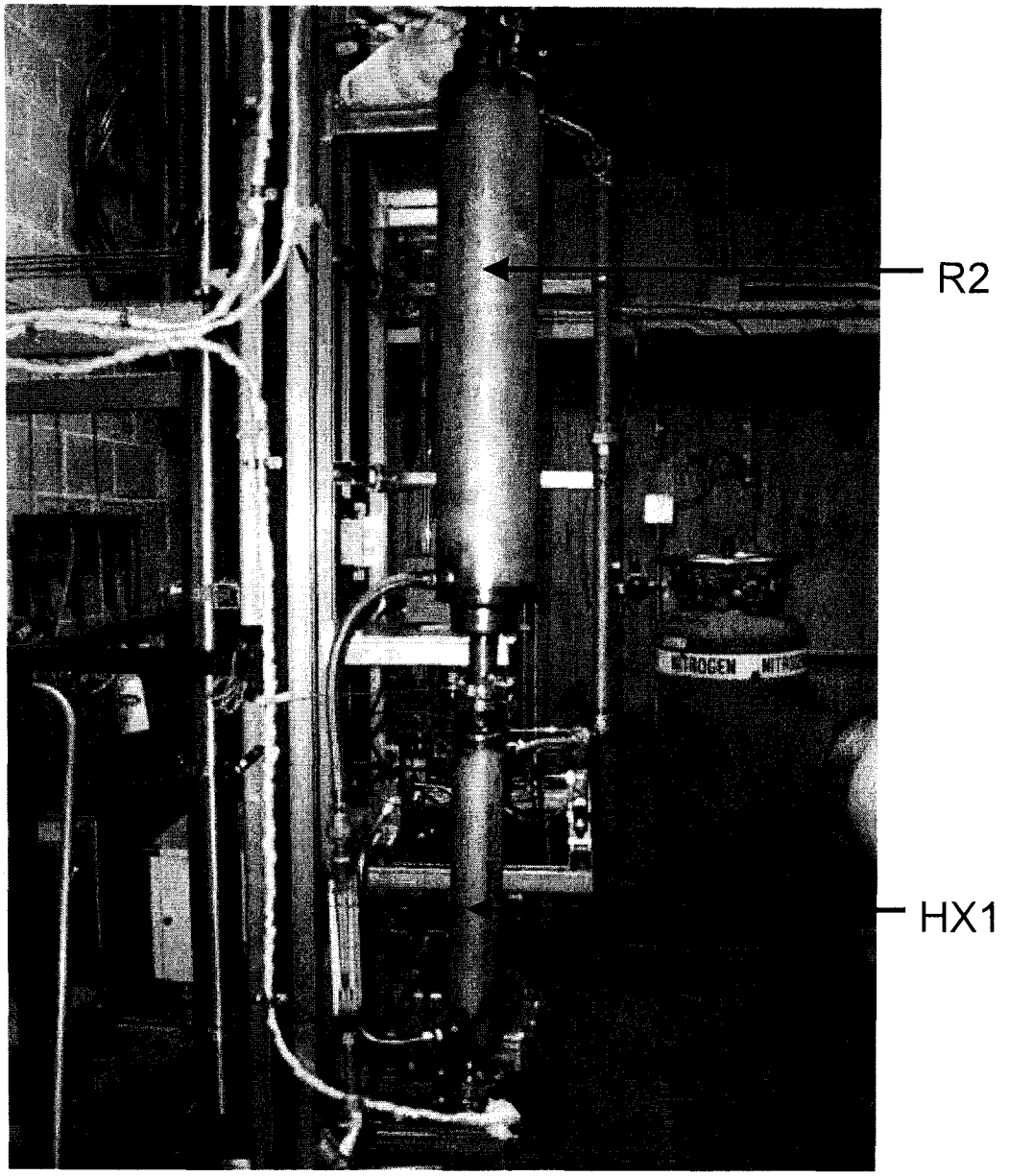

Figure 2.3.2-1: Close up of R2 and HX1 as constructed for experimental work.

Reproduced with permission of the copyright owner. Further reproduction prohibited without permission.

2.3.2.1 Design of R2

The design of R2 is shown in Figure 2.3.2.1-A. R2 was designed to be a shell and tube heat exchanger. The tube section was made of inconel 625®, which is a nonmagnetic, corrosion and oxidation resistant, nickel-base alloy[174]. It has high strength and toughness and can reach temperatures above 1100°C. Table 2.3.2.1-1 lists the main components of inconel 625®.

Component	Percent (%)
C	0.10
Mn	0.50 max
P	0.015 max
S	0.015 max
Si	0.50 max
Cr	20.0 – 23.0
Ni	58.0 min
Co	1.00 max
Ti	0.40 max
Al	0.40 max
Fe	5.0 max
Nb	3.15 – 4.15

Table 2.3.2.1-1: List of main components in Inconel 625®, adapted from Magellan[174].

There are two sections to the tube section of shell and tube heat exchanger, R2:

i. The first section is a pipe length of 4 inches on either side of the shell. These 4 inch pieces have an OD of 1.900 inches and an ID of 1.610 inches. They are labeled (1) in Figure 2.3.2.1-A.

ii. The second section is 38 inches long with an ID of 4.026 inches and an OD of 4.500 inches. This segment is labeled (4) in Figure 2.3.2.1-A.

Reproduced with permission of the copyright owner. Further reproduction prohibited without permission.

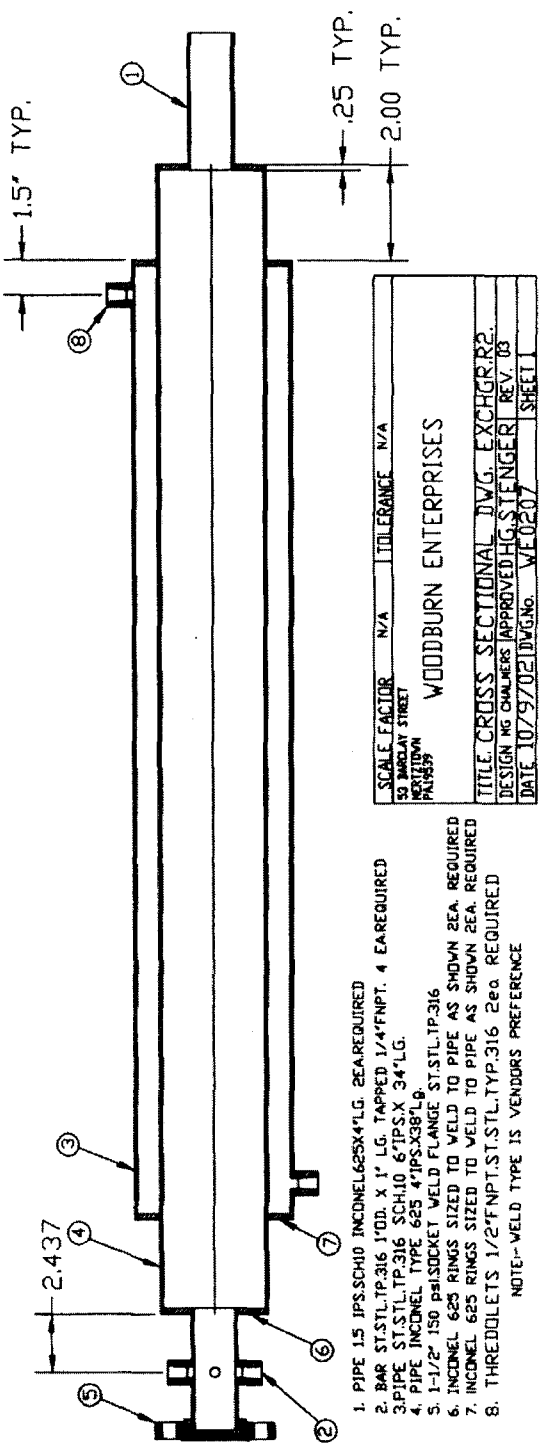

Figure 2.3.2.1-A: CAD drawing of R2.

Reproduced with permission of the copyright owner. Further reproduction prohibited without permission.

Part (4) was designed such that it would increase the residence time of the gases within R2; thereby increasing the reaction time between the gas molecules in the flue gas stream.

Part (3) is the shell section of the shell and tube heat exchanger. It was made of SS 316. It has a length of 34 inches, an ID of 6.357 inches and an OD of 6.625 inches. Part (8) shows threadolets that were welded in place. The threadolets provide fittings for pipes that would be used to feed a coolant through the shell of the heat exchanger.

The parts labeled (2) are similar to the threadolets. A total of four of these connectors were welded into place to allow for oxidant injection or for sample taking. They are made of SS316 with an OD of 1 inch. The threading on these connectors is ¼ inch NPT.

Part (5) is a flange that is similar to that of R1. This flange is bolted to the bottom of R1. An inconel gasket was placed between the two flanges to minimize leaks and prevent corrosion. This gasket is shown in Figure 2.3.2.1-1 and 2.3.2.1-2.

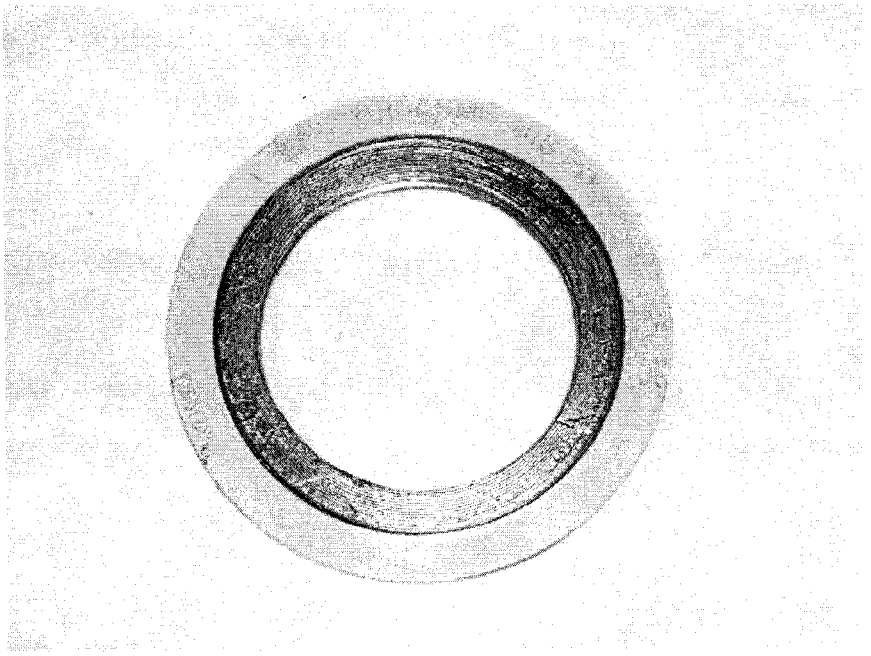

Figure 2.3.2.1-1:
Flexatellic gasket used between flanges of the apparatus.

Reproduced with permission of the copyright owner. Further reproduction prohibited without permission.

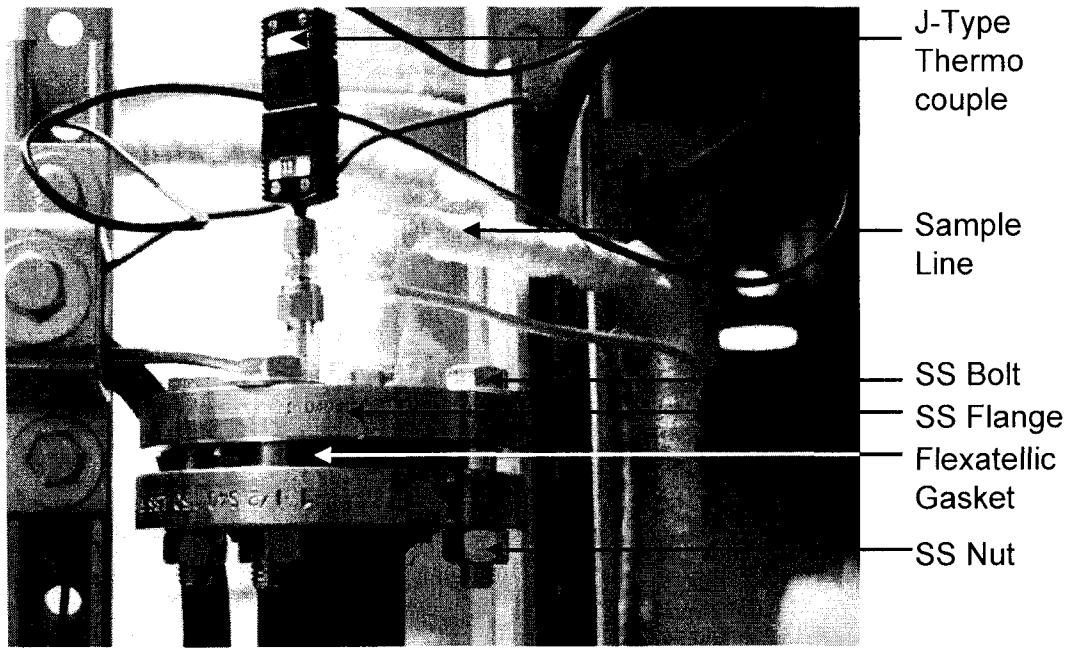

Figure 2.3.2.1-2:
Close up of the section on top of the riser pipe. Picture shows location of the SS bolts, nuts, and the Flexatellic gasket.

A thermocouple was placed at the exit of R2 to measure the gas temperature in the middle of the pipe. In order to maintain the temperature profile, R2 was wrapped with 2 layers of the ceramic fiber blanket used for R1.

2.3.2.2 Purchasing Information for R2

Table 2.3.2.2-1 is a list of items purchased, along with the respective part numbers, vendors and prices, as of the duration of the project from 2002 to 2005. The last column is labeled "notes" where miscellaneous information for that item is provided.

Reproduced with permission of the copyright owner. Further reproduction prohibited without permission.

Item	Part Number	Vendor	Location	Price ($)	Notes
R2	(n/a)	PA Inc.	Houston, TX	3960.60	R2 was fabricated with inconel and SS 316.
Ceramic Fiber Blanket	93315K68	McMaster Carr Supply Company	New Brunswick, NJ	168.30	2" thick x 2' wide x 25' long.
Fiber-glass tape	7574A12	McMaster Carr Supply Company	New Brunswick, NJ	13.83	Used to hold ceramic fiber blanket in place.
Zeetex Insulation Tape	10945-163	VWR	Bridgeport, NJ	10.93	Price per roll. Replaced fiber-glass tape; blanket was tied down.
SS Bolts	92245A726	McMaster Carr Supply Company	New Brunswick, NJ	3.50	Price per bolt. Used to attach R2 to rest of apparatus. SS hex head cap screws; ½" diameter, #13 threading. Figure 2.3.1.2-4
SS Nuts	92673A137	McMaster Carr Supply Company	New Brunswick, NJ	8.62	Price per box of 25 nuts. ½" diameter, #13 threading. Figure 2.3.1.2-5.
Thermo-couples	KQIN-18U-12	Omega Engineering	Stamford, CT	27.00	Regular K-type thermocouples to measure temperature. 12" long.
Thermo-couple wire	KXPP-K-20-200	Omega Engineering	Stamford, CT	70.00	K-type thermocouple wire. 200' length.
6-Channel panel read-out	DP-462-T	Omega Engineering	Stamford, CT	348.00	6-channel thermocouple output reading.
Silver Goop®	MS-TL-SGT	Swagelok	Allentown, PA	40.60	Price per tube.
FLEXI-CARB® Gaskets	01501170817	Flexitellic	Local Distributor	72.84	Made of Inconel; placed between flanges

Table 2.3.2.2-1: List of items purchased for R2, with respective vendors and prices.

Reproduced with permission of the copyright owner. Further reproduction prohibited without permission.

2.3.2.3 *Modifications on R2*

The only modification made to R2 was the installation of a vacuum pump. Initially, the desired temperature profile was not attained. It was suggested that the air pocket in the shell section of R2 was providing insufficient heat insulation. A vacuum pump, which was provided by our sponsor, was installed and a vacuum was pulled on the shell side of both R2 and HX1. The vacuum helped in attaining the temperature profile since heat loss via convection or radiation was minimized.

2.3.3 *HX1*

The purpose of HX1 was to provide additional residence time for the reaction to take place. Additionally, the shell and tube design allowed for cooling down of the gases when needed. It is labeled in Figures 2.3.1-1 and 2.3.3-1.

Reproduced with permission of the copyright owner. Further reproduction prohibited without permission.

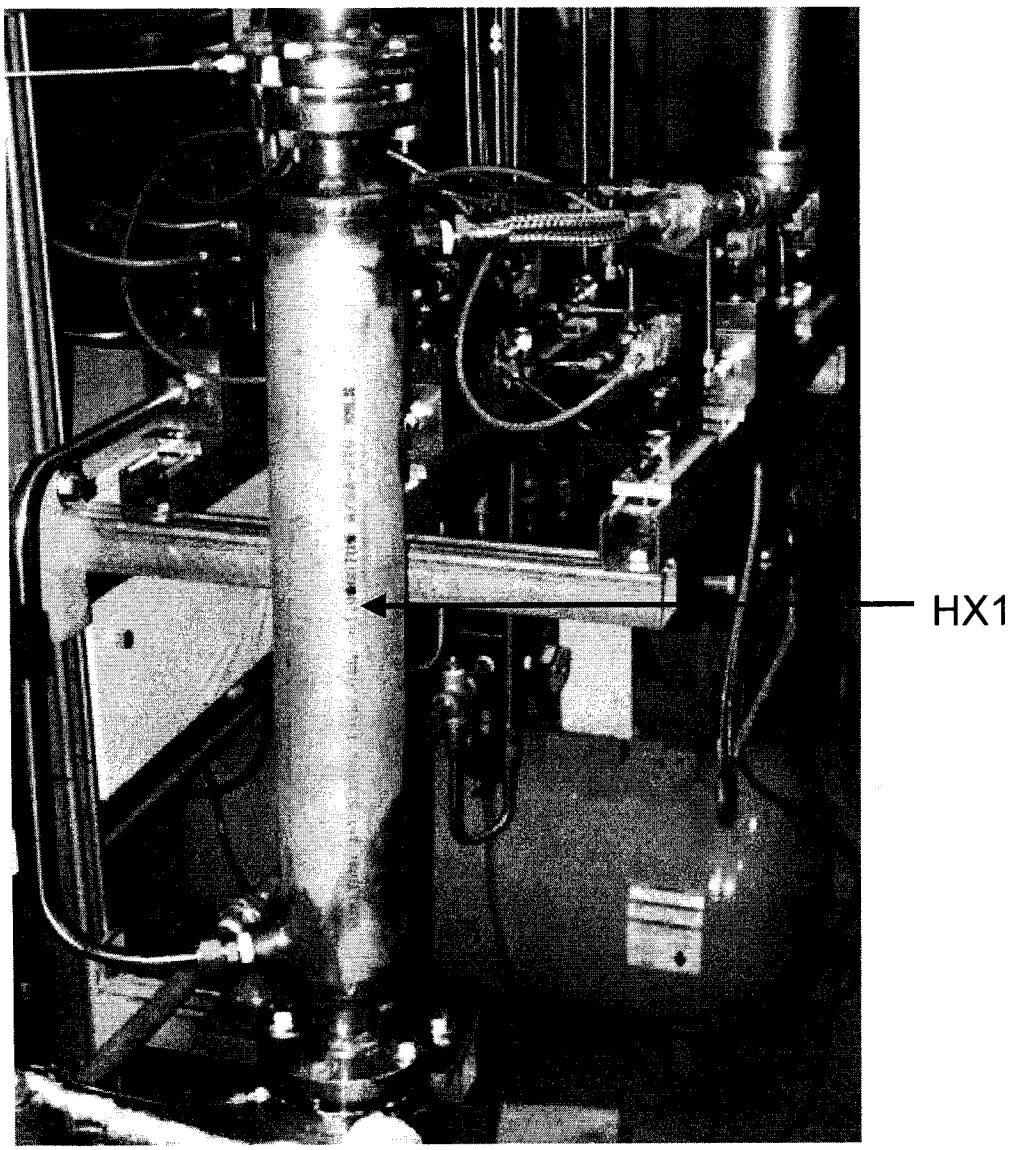

Figure 2.3.3-1: Close up of HX1 as constructed for experimental work.

2.3.3.1 Design of HX1

The design of HX1 is similar to R2 and is shown in Figure 2.3.3.1-A. It is a shell and tube heat exchanger. The tube section, made of Inconel 625®, is labeled (3). It has a length of 26.75 inches, an OD of 1.900 inches and an ID of 1.610 inches. The shell section labeled (2) was made of SS316; it has a length of 22 inches, an OD of 3.000 inches and an ID of 2.650 inches.

Reproduced with permission of the copyright owner. Further reproduction prohibited without permission.

Part (5) was a threadolet welded to the shell section of HX1 to provide fittings for coolant. A thermocouple was placed at the exit of HX1 to measure the gas temperature in the middle of the pipe. In order to maintain the temperature profile, HX1 was also wrapped with 2 layers of the ceramic fiber blanket used for R1 and R2.

No modifications were made to HX1.

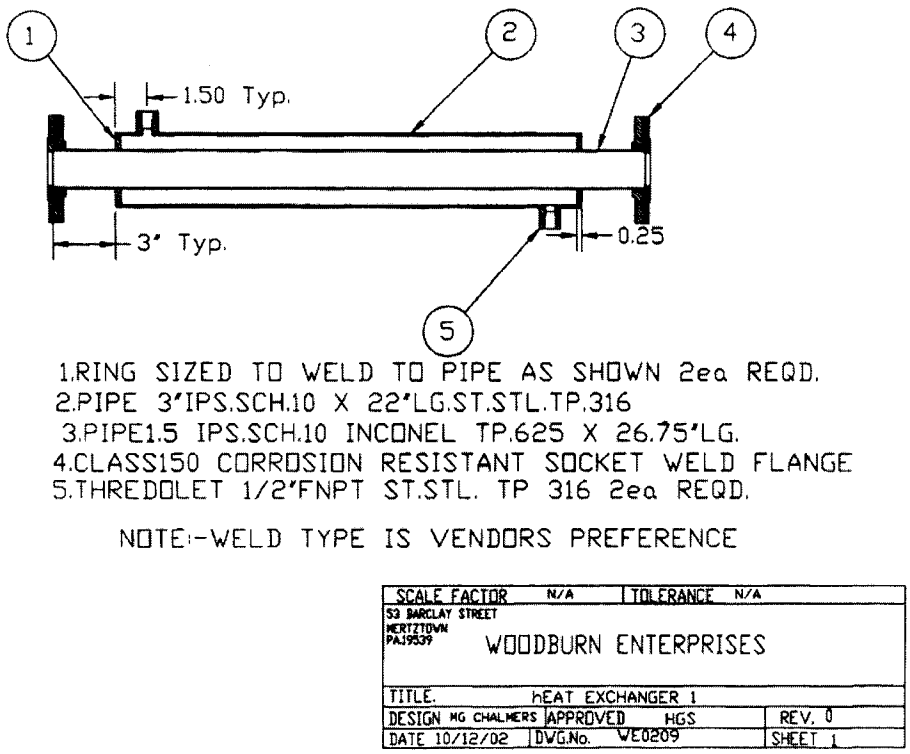

Figure 2.3.3.1-A: CAD drawing of HX1.

Reproduced with permission of the copyright owner. Further reproduction prohibited without permission.

2.3.3.2 Purchasing Information for HX1

Table 2.3.3.2-1 is a list of items purchased, along with the respective part numbers, vendors and prices, as of the duration of the project from 2002 to 2005. The last column is labeled "notes" where miscellaneous information for that item is provided.

Item	Part Number	Vendor	Location	Price ($)	Notes
HX1	(n/a)	PA Inc.	Houston, TX	1342.60	HX1 was fabricated with inconel and SS 316.
Ceramic Fiber Blanket	93315K68	McMaster Carr Supply Company	New Brunswick, NJ	168.30	2" thick x 2' wide x 25' long.
Fiber-glass tape	7574A12	McMaster Carr Supply Company	New Brunswick, NJ	13.83	Used to hold ceramic fiber blanket in place.
Zeetex Insulation Tape	10945-163	VWR	Bridgeport, NJ	10.93	Price per roll. Replaced fiber-glass tape; blanket was tied down.
SS Bolts	92245A726	McMaster Carr Supply Company	New Brunswick, NJ	3.50	Price per bolt. Used to attach R2 to rest of apparatus. SS hex head cap screws; ½" diameter, #13 threading. Figure 2.3.1.2-4
SS Nuts	92673A137	McMaster Carr Supply Company	New Brunswick, NJ	8.62	Price per box of 25 nuts. ½" diameter, #13 threading. Figure 2.3.1.2-5.
Thermo-couples	JQIN-18U-12	Omega Engineering	Stamford, CT	27.00	Regular J-type thermocouples to measure temperature. 12" long.
Thermo-couple wire	EXPP-J-20-200	Omega Engineering	Stamford, CT	54.00	J-type thermocouple wire. 200' length.
FLEXI-CARB® Gaskets	01501170817	Flexitellic	Local Distributor	72.84	Made of Inconel; placed between flanges

Table 2.3.3.2-1: List of items purchased for HX1, with respective vendors and prices.

Reproduced with permission of the copyright owner. Further reproduction prohibited without permission.

2.3.4 Air Pre Heater (APH)

The purpose of the APH was to preheat the bulk gases. The bulk gases consisted of N_2, O_2 and CO_2.

2.3.4.1 Design and Construction of APH

The APH is a 20" long, 1" diameter stainless steel tube heated externally with two 425 watt ceramic heating elements. These are shown in Figure 2.3.4.1-1. The tube is filled with stainless steel packing to enhance mixing and heat transfer. The flow rate of the bulk gases through the APH used in this work was between 70 and 86 standard liters per minute (slpm). The exit gas temperature was controlled between 100°C and 315°C. In order to maintain the temperature profile, the APH was wrapped with a single layer of the ceramic fiber blanket used for R1. The APH is shown in Figure 2.3.4.1-2 and 2.3.4.1-3.

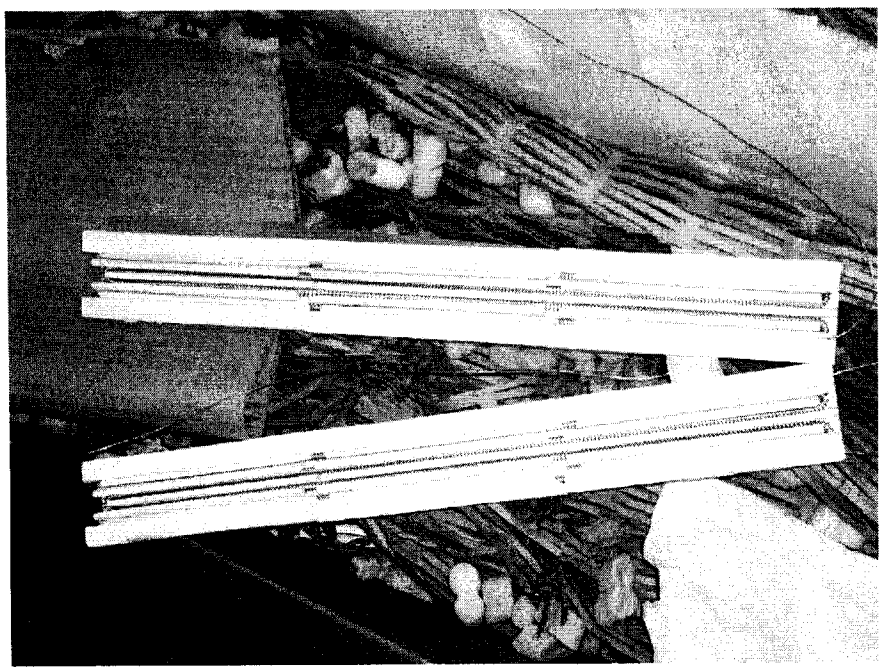

Figure 2.3.4.1-1:
Picture of ceramic heaters used for APH and SPH.
Similar heaters were used for R1, only larger.

Reproduced with permission of the copyright owner. Further reproduction prohibited without permission.

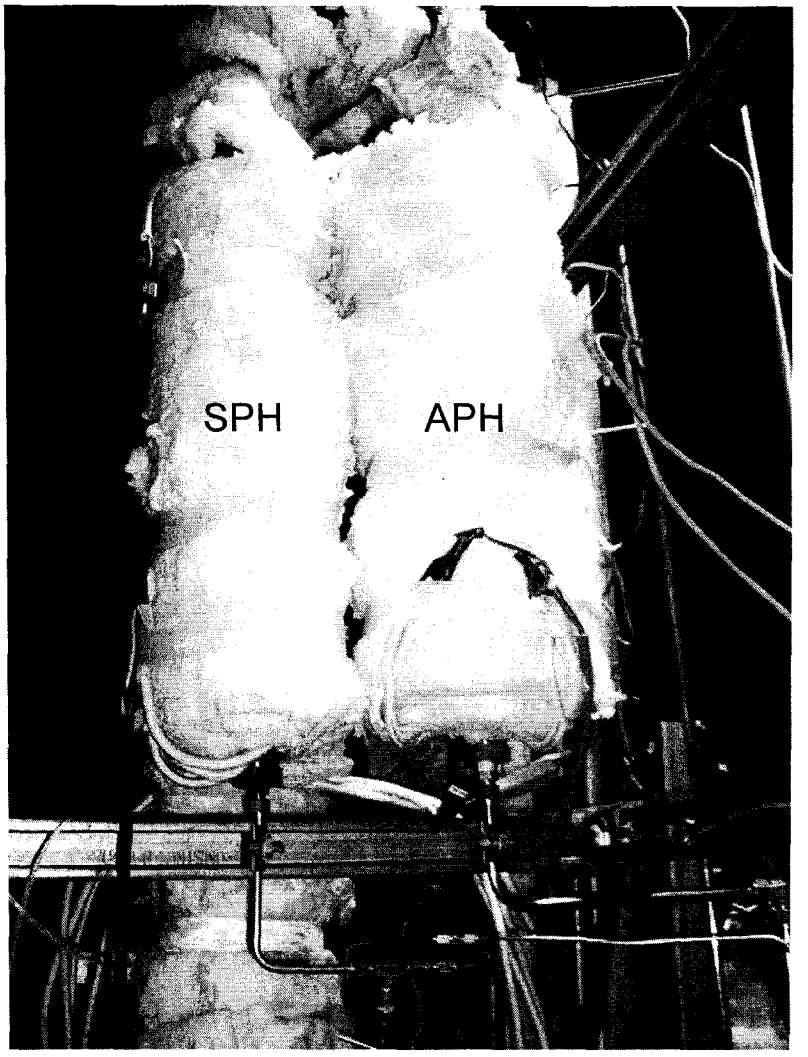

Figure 2.3.4.1-2:
Picture of APH and SPH as used in the experimental work. Both feed heated gases to the top of R1.

Reproduced with permission of the copyright owner. Further reproduction prohibited without permission.

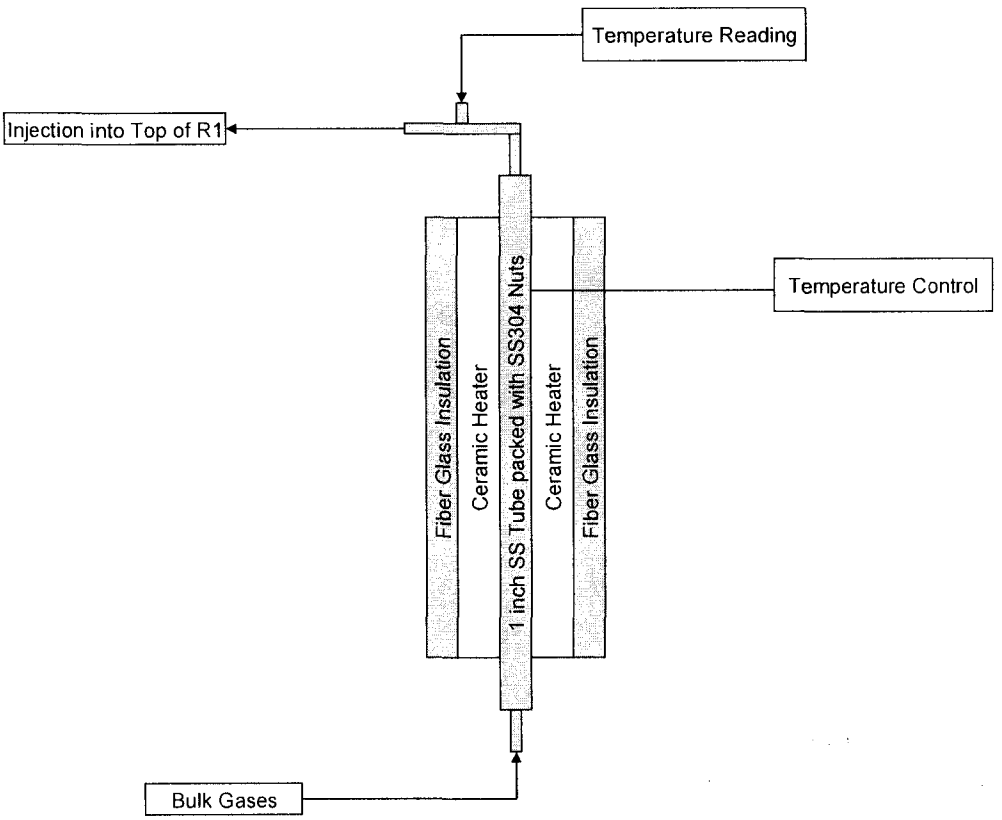

Figure 2.3.4.1-3: Schematic of APH setup.

2.3.4.2 Purchasing information for APH

Table 2.3.4.2-1 is a list of items purchased, along with the respective part numbers, vendors and prices, as of the duration of the project from 2002 to 2005. The last column is labeled "notes" where miscellaneous information for that item is provided.

Reproduced with permission of the copyright owner. Further reproduction prohibited without permission.

Item	Part Number	Vendor	Location	Price ($)	Notes
1 inch Tube	4466K58	McMaster Carr Supply Company	New Brunswick, NJ	47.18	APH fabricated with SS 316 tube.
Thermcraft ® Heaters	RL108	Thermcraft®	Winston-Salem, NC	56.00	Price is for each half shell. 1" ID, 18" length. 24" leads. 425 watts each half shell.
SS Nuts (7/16")	91845A029	McMaster Carr Supply Company	New Brunswick, NJ	2.98	Price is for a box of 100 nuts. 5 boxes used to fill up pipe. Figure 2.3.1.2-3
Ceramic Fiber Blanket	93315K68	McMaster Carr Supply Company	New Brunswick, NJ	168.30	2" thick x 2' wide x 25' long.
Fiber-glass tape	7574A12	McMaster Carr Supply Company	New Brunswick, NJ	13.83	Used to hold ceramic fiber blanket in place.
Zeetex Insulation Tape	10945-163	VWR	Bridgeport, NJ	10.93	Price per roll. Replaced fiber-glass tape; blanket was tied down.
Thermo-couples	KQIN-18U-12	Omega Engineering	Stamford, CT	27.00	Regular K-type thermocouples to measure temperature. 12" long.
Thermo-couple wire	KXPP-K-20-200	Omega Engineering	Stamford, CT	70.00	K-type thermocouple wire. 200' length.
Thermo-couples	JQIN-18U-12	Omega Engineering	Stamford, CT	27.00	Regular J-type thermocouples to measure temperature. 12" long.
Thermo-couple wire	EXPP-J-20-200	Omega Engineering	Stamford, CT	54.00	J-type thermocouple wire. 200' length.
6-Channel panel read-out	DP-462-T	Omega Engineering	Stamford, CT	348.00	6-channel thermocouple output reading. Figure 2.3.4.2-1.
Temp. Controller	CN 2110-T-10	Omega Engineering	Stamford, CT	310.00	Used to control temperature of APH. Also used for SPH. Figure 2.3.4.2-1.

Table 2.3.4.2-1: List of items purchased for APH, with respective vendors and prices

Reproduced with permission of the copyright owner. Further reproduction prohibited without permission.

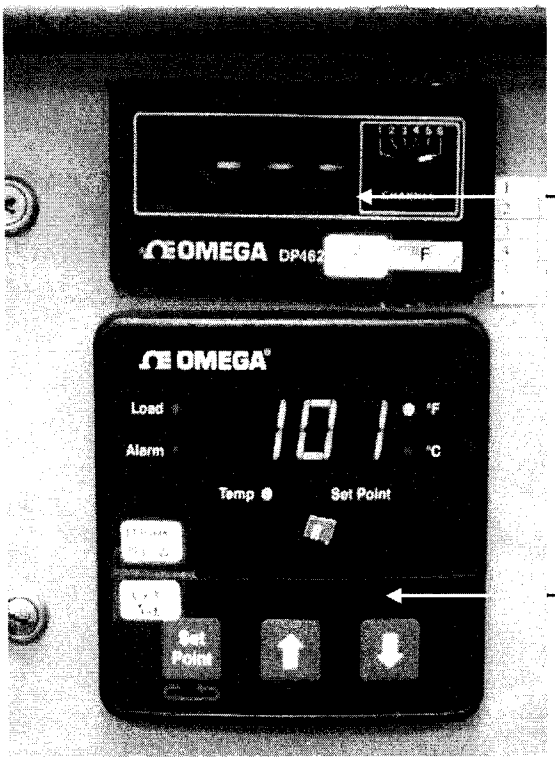

Figure 2.3.4.2-1:
Picture of temperature controller used for SPH and a 6-channel temperature read out used.

2.3.4.3 Modifications on APH

The first modification made was to replace the SS packing material – from SS wool to SS nuts. The nuts proved to be more durable than the wool.

The second modification was to relocate the thermocouple for temperature control. The APH was controlled by a temperature controller purchased from Omega Engineering. Initially, the temperature of the gas at the exit of the APH was used to control the ceramic heaters. This method proved to be ineffective. The thermocouple was then relocated to the skin of the 1 inch tube. Controlling the heaters with this setup was much easier and efficient.

Reproduced with permission of the copyright owner. Further reproduction prohibited without permission.

2.3.5 *Steam Pre Heater (SPH)*

The steam pre-heater has exactly the same design as the APH. All parts used were the same as shown in Table 2.3.4.2-1 and all modifications made to the APH were made to the SPH.

2.3.6 *Riser and Bag-house*

The gas exits the bottom of HX1, makes a 180° turn and enters the sorbent injection system with upward flow. This turn is shown in Figures 2.3.6-1 and 2.3.6-2. In this section, sorbent can be injected into the flue gas stream to study its ability to capture mercury by adsorption. Since this work does not focus on heterogeneous Hg oxidation or Hg capture, the descriptions of each section will be brief.

Reproduced with permission of the copyright owner. Further reproduction prohibited without permission.

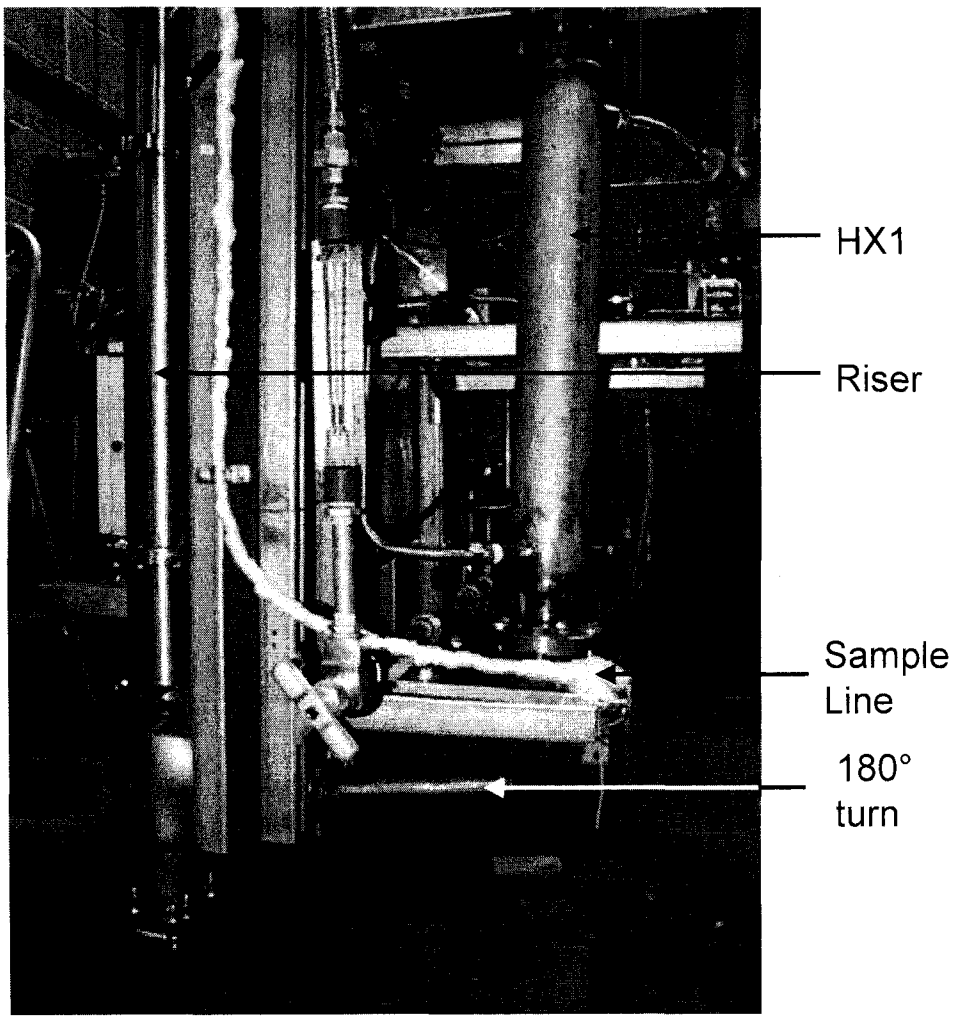

Figure 2.3.6-1:
Picture showing HX1, 180° turn and the riser pipe for sorbent work.

Reproduced with permission of the copyright owner. Further reproduction prohibited without permission.

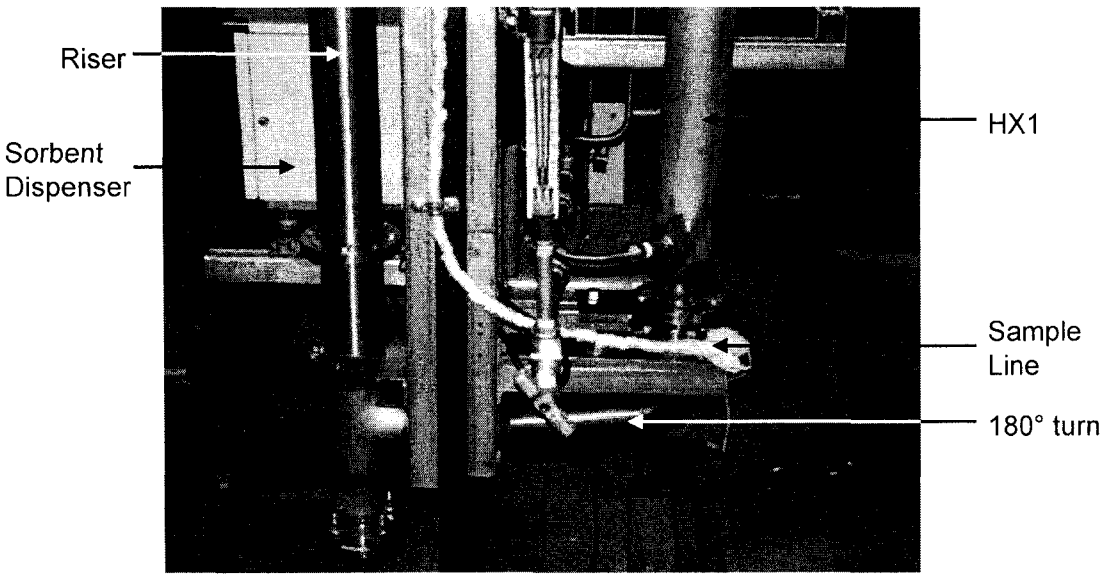

Figure 2.3.6-2:
Close up of 180° turn and bottom of the riser pipe used for sorbent work.

2.3.6.1 Design of Riser and Bag-house

Figure 2.3.6.1-A shows the design of the riser pipe. It has 4 sections to it. The first section is at the bottom, where the 180° turn takes place. This "U" piece is connected to two straight sections, labeled (10) and (6) by flanges, shown in Figures 2.3.6.1-B, 2.3.6.1-1 and 2.3.6.1-2. The fourth piece is labeled (7) in Figure 2.3.6.1-A and has a Tee junction. It is also shown in Figures 2.3.6.1-2 and 2.3.6.1-3. The gas (with sorbent entrained in it) flows upwards, makes a 90° turn and enters the bag-house tangentially. The length of the entire riser pipe is 88 7/8 inches and the diameter is a constant 3 inches. It is made entirely of SS316 and cost $1525 to fabricate. The vendor used was Pocono Machine & Tool Co., Inc, in East Stroudsburg, PA.

Figures 2.3.6.1-C to 2.3.6.1-I are CAD drawings of the bag-house. Figures 2.3.6.1-C, 2.3.6.1-D and 2.3.6.1-10 show the main body of the bag-house. The gas stream exits the riser pipe and enters tangentially into the bag-house via the pipe labeled (5) in Figure 2.3.6.1-C. This is

Reproduced with permission of the copyright owner. Further reproduction prohibited without permission.

also shown in Figure 2.3.6.1-3. The flanges at the bottom of the structure can be undone to collect any deposited material and analyzed for Hg content (shown in Figure 2.3.6.1-4).

The bag-house has a center piece (Figures 2.3.6.1-F, 2.3.6.1-3 and 2.3.6.1-9). It is a plate that holds the fabric filter bags in place. The gas stream passes through the bags and any particles in the stream are stopped by the fabric. The particles then fall to the bottom of the bag-house by gravity.

Figures 2.3.6.1-E and 2.3.6.1-8 show the lid of the bag-house. The top of the lid has 2 holes where a burst of air can enter the bag-house against the flow of the flue. On occasion, the particles build up on the fabric. A burst of air controlled by a delta-pressure (ΔP) cell and solenoid valves help loosen the particles.

Any loosed particles then drop to the bottom of the bag-house and can be collected. The ΔP cell is shown in Figures 2.3.6.1-4 to 2.3.6.1-7.

A cross section CAD drawing of the assembled bag-house is shown in Figure 2.3.6.1-G. Figure 2.3.6.1-H is a CAD drawing of the wire mesh support to hold the fabric filter bags. Figure 2.3.6.1-I is a CAD drawing of the tubes that deliver the burst of air. These tubes, which are welded to the bag-house lid, are seen also in Figure 2.3.6.1-8.

This entire setup was also manufactured by Pocono Machine & Tool Co., Inc, in East Stroudsburg, PA. The cost of fabrication was $2100.

The ash dispenser was purchased separately from Schenck/AccuRate Inc.. The cost of this equipment was $4855. It is shown in Figures 2.3.6.1-11 and 2.3.6.1-12. The purpose of this equipment was to inject ash or powdered sorbent into the gas stream at the side of the riser.

2.3.6.2 Modifications on Riser and Bag-house

Some minor modifications were made to the riser and bag-house:

i. A hole had to be drilled into the side of the riser pipe in order to feed the sorbent or ash into the gas stream. This hole was ½ inch in diameter.

Reproduced with permission of the copyright owner. Further reproduction prohibited without permission.

ii. This section helped cool the gas temperature significantly. A constant temperature of 150°C had to be maintained in order to test for Hg capture by sorbents. A heating coil was thus wrapped around the riser and bag-house to ensure the gas temperature stayed above 150°C.

iii. In order to maintain the temperature within the system, the riser and bag-house were wrapped with fiber glass insulation.

iv. The seal between the bag-house lid, center piece and main body was not good enough. As a result, Pocono Machine had to machine out an o-ring groove on both sides of the center piece. This cost an additional $350. The Viton o-rings (part # 9464K573) used were purchased from McMaster Carr Supply Company and cost $9.45 for a set of 2.

Reproduced with permission of the copyright owner. Further reproduction prohibited without permission.

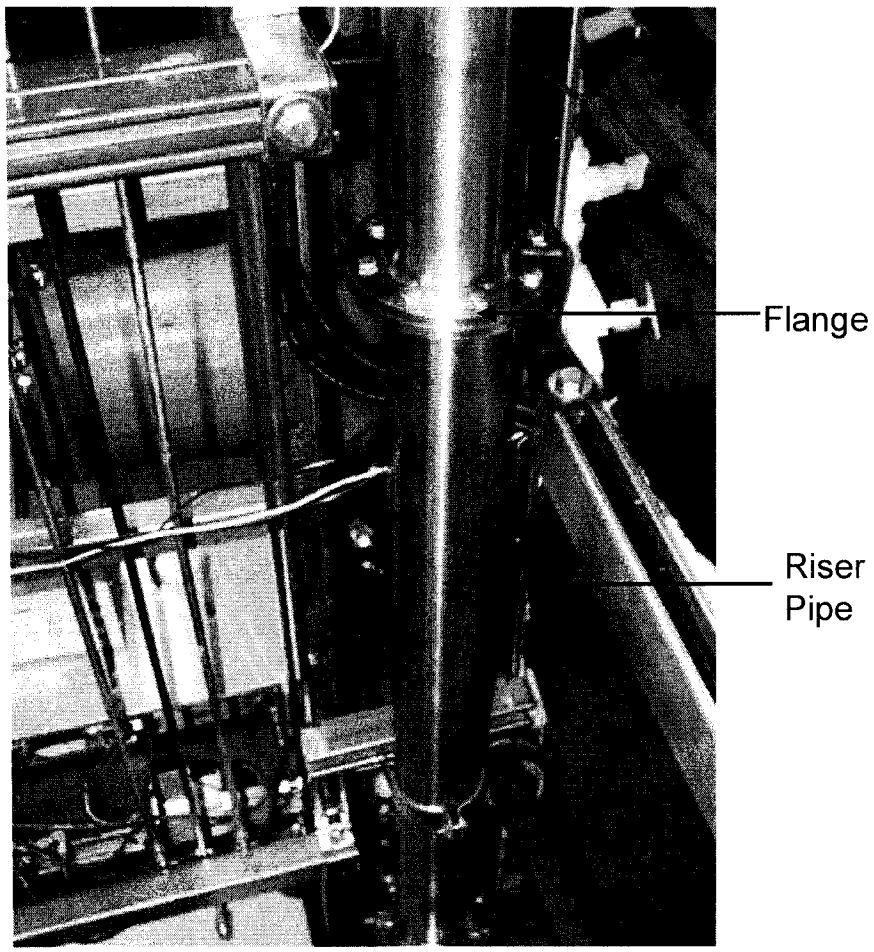

Figure 2.3.6.1-1:
Close up of riser pipe – shows flange used to connect riser pieces together.

Reproduced with permission of the copyright owner. Further reproduction prohibited without permission.

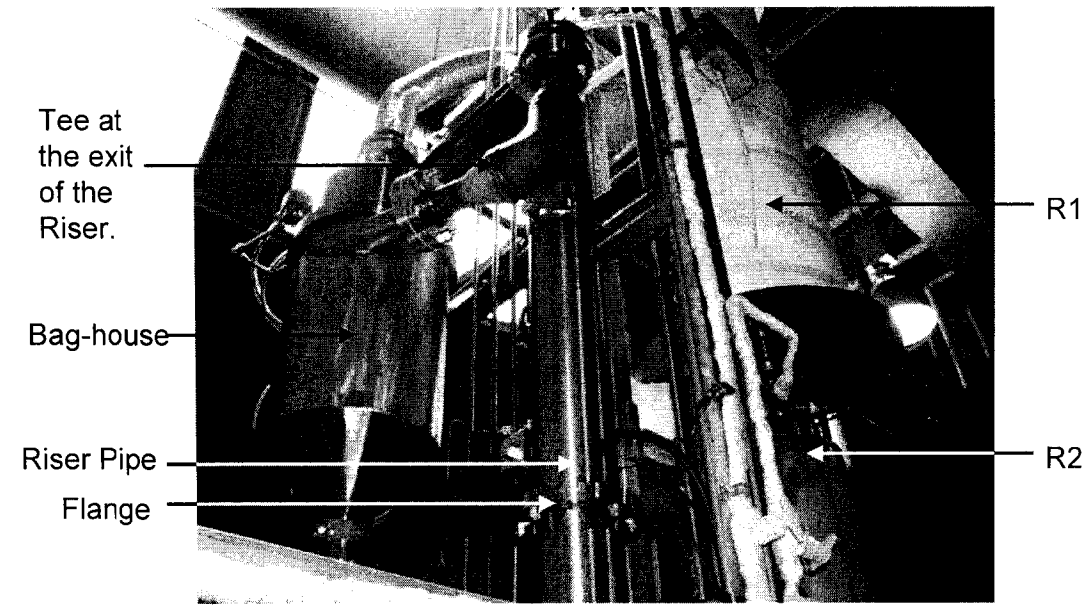

Figure 2.3.6.1-2:
Picture of top of riser and Tee-connection of riser to the bag-house.

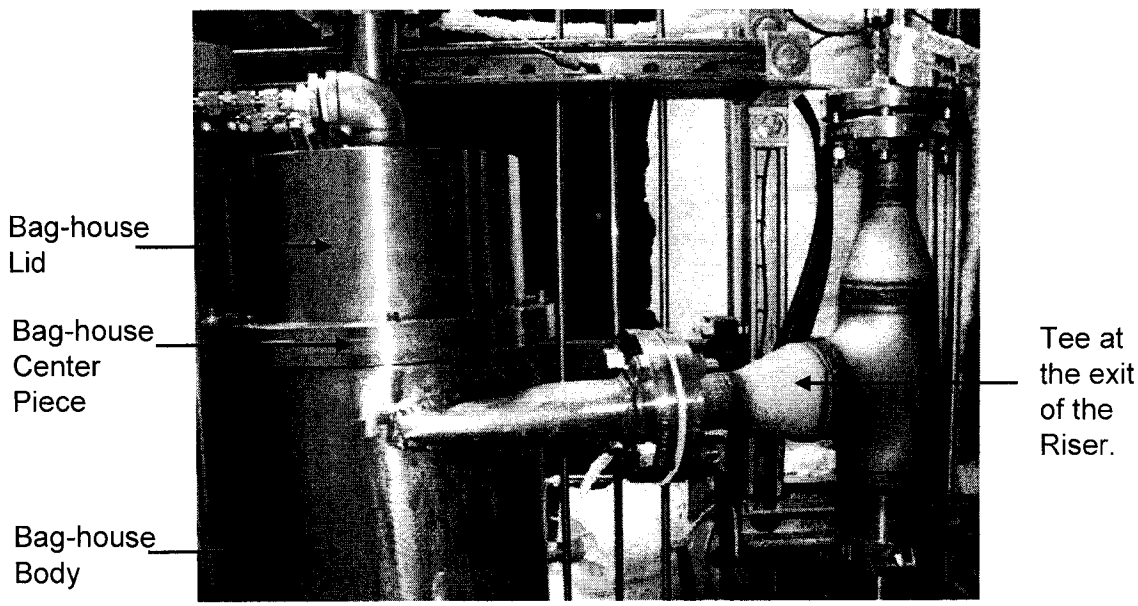

Figure 2.3.6.1-3:
Close up of Tee-junction at the top of the riser. Gas enters bag-house tangentially.

Reproduced with permission of the copyright owner. Further reproduction prohibited without permission.

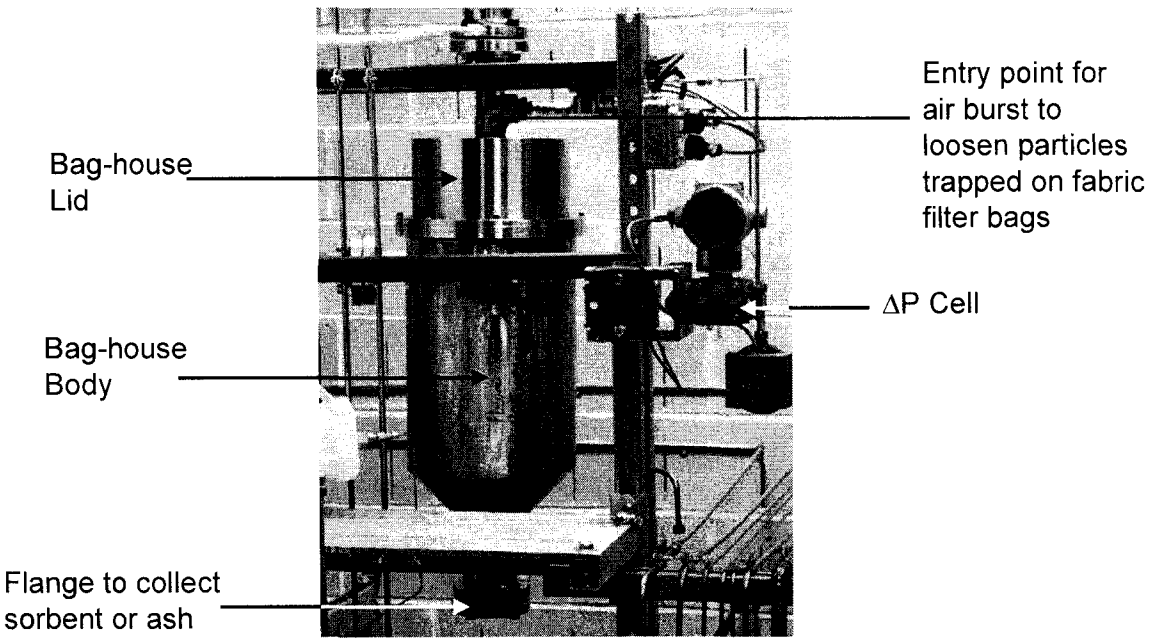

Figure 2.3.6.1-4:
Close up of bag-house.

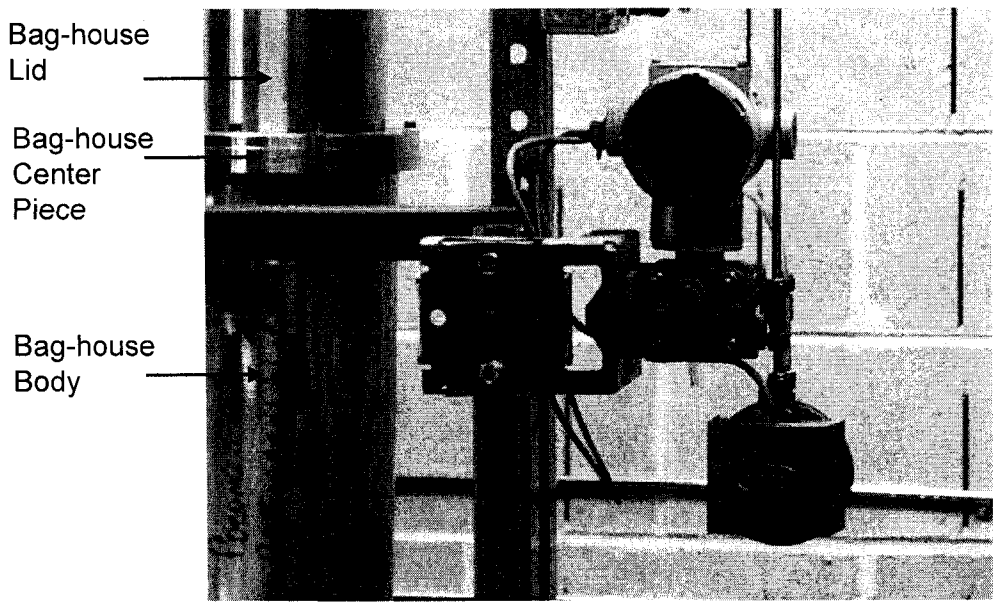

Figure 2.3.6.1-5:
Close up of the ΔP Cell.

Reproduced with permission of the copyright owner. Further reproduction prohibited without permission.

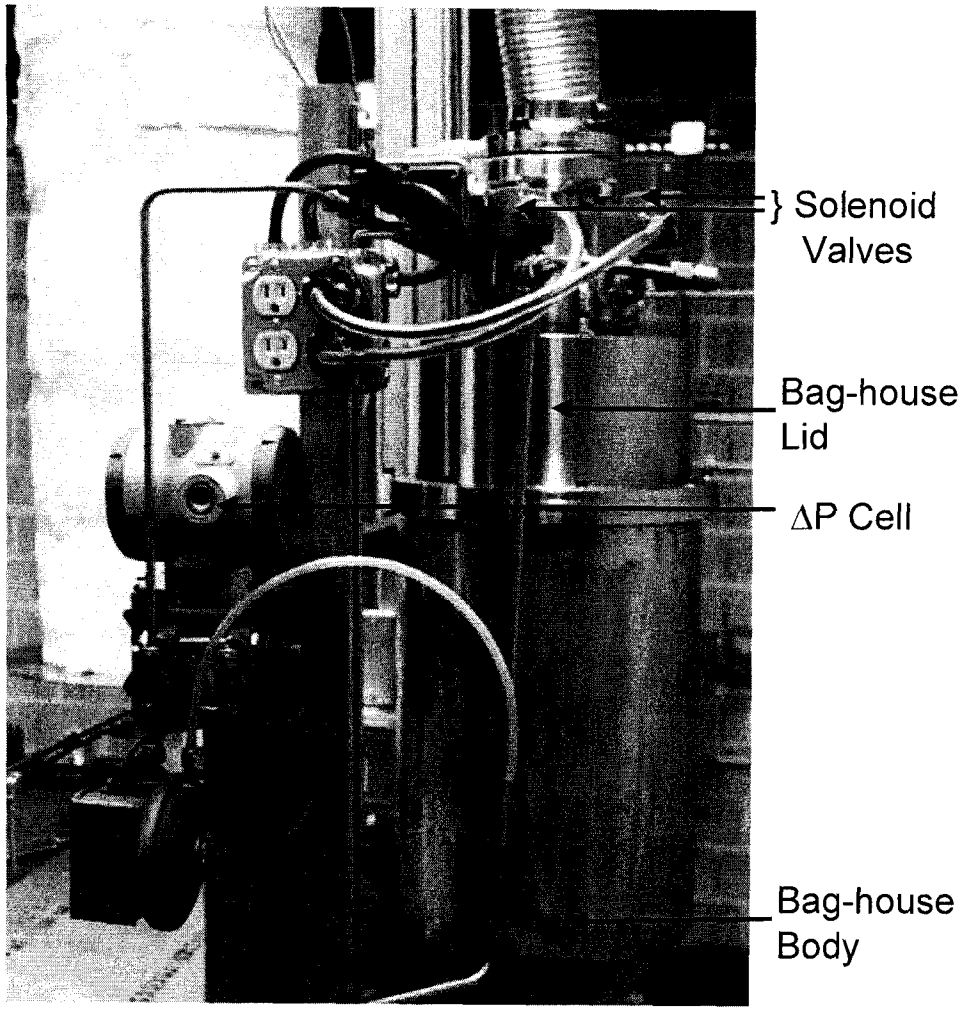

Figure 2.3.6.1-6:
Side view of ΔP Cell and bag-house.

Reproduced with permission of the copyright owner. Further reproduction prohibited without permission.

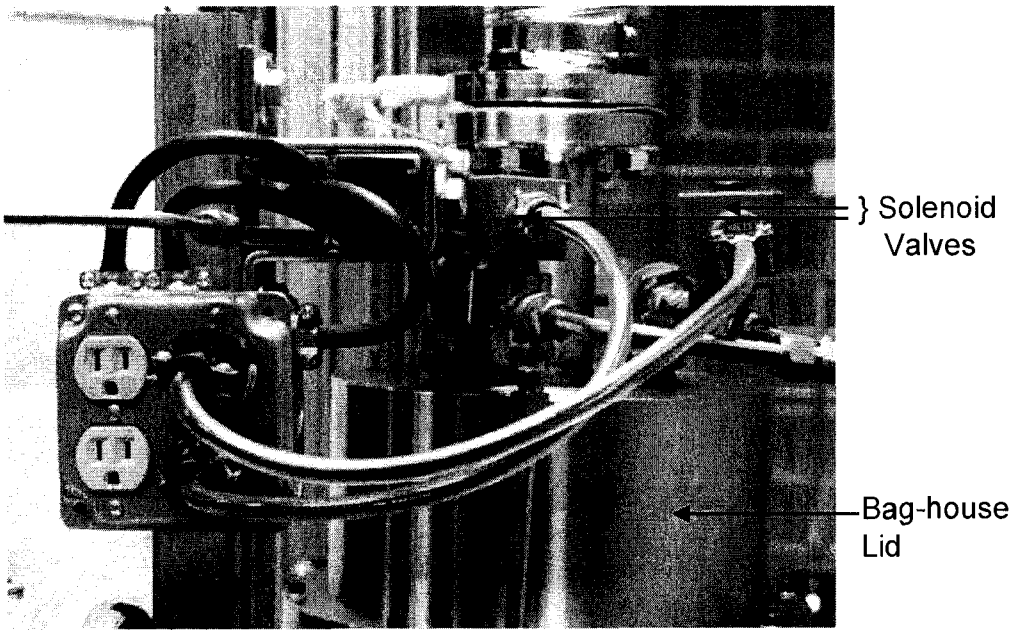

Figure 2.3.6.1-7:
Close up of solenoid valves used to control air burst entering bag-house.

Reproduced with permission of the copyright owner. Further reproduction prohibited without permission.

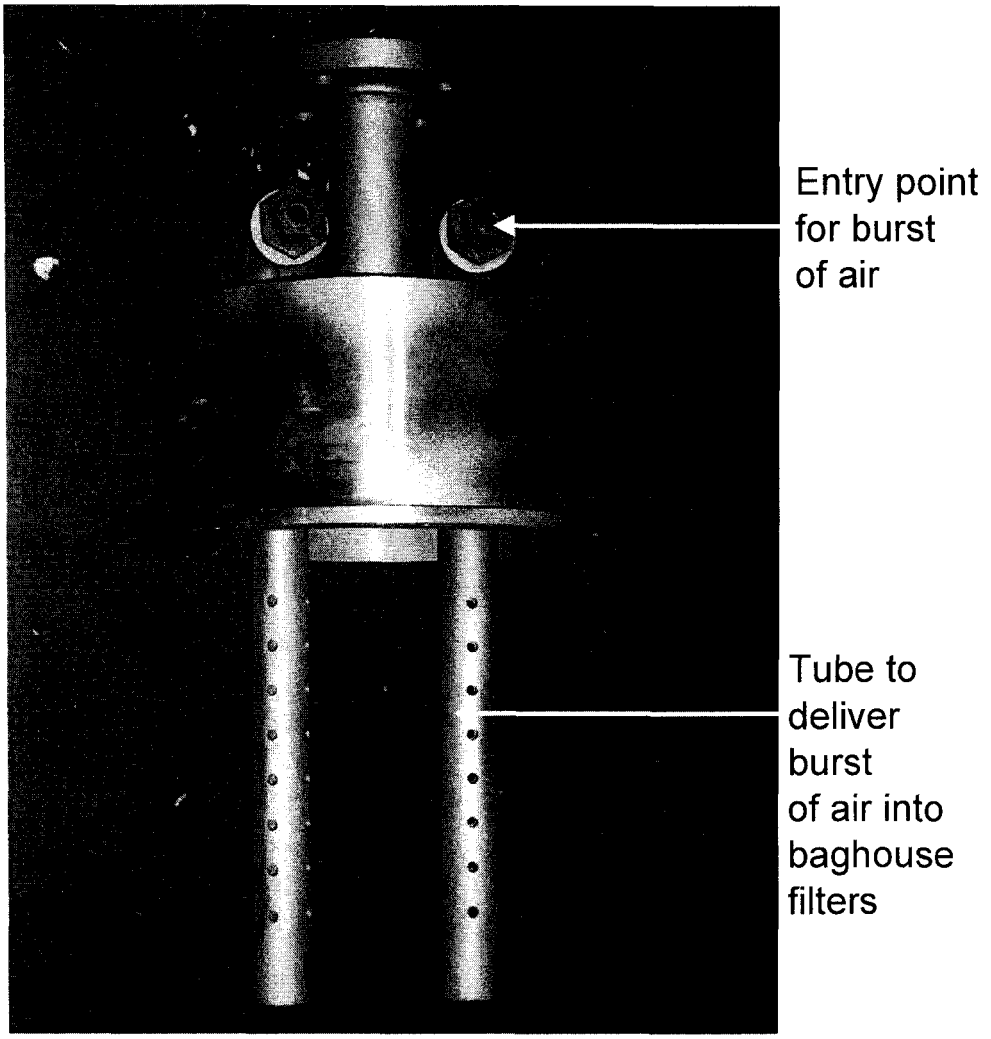

Figure 2.3.6.1-8:
Close up of the bag-house lid

Reproduced with permission of the copyright owner. Further reproduction prohibited without permission.

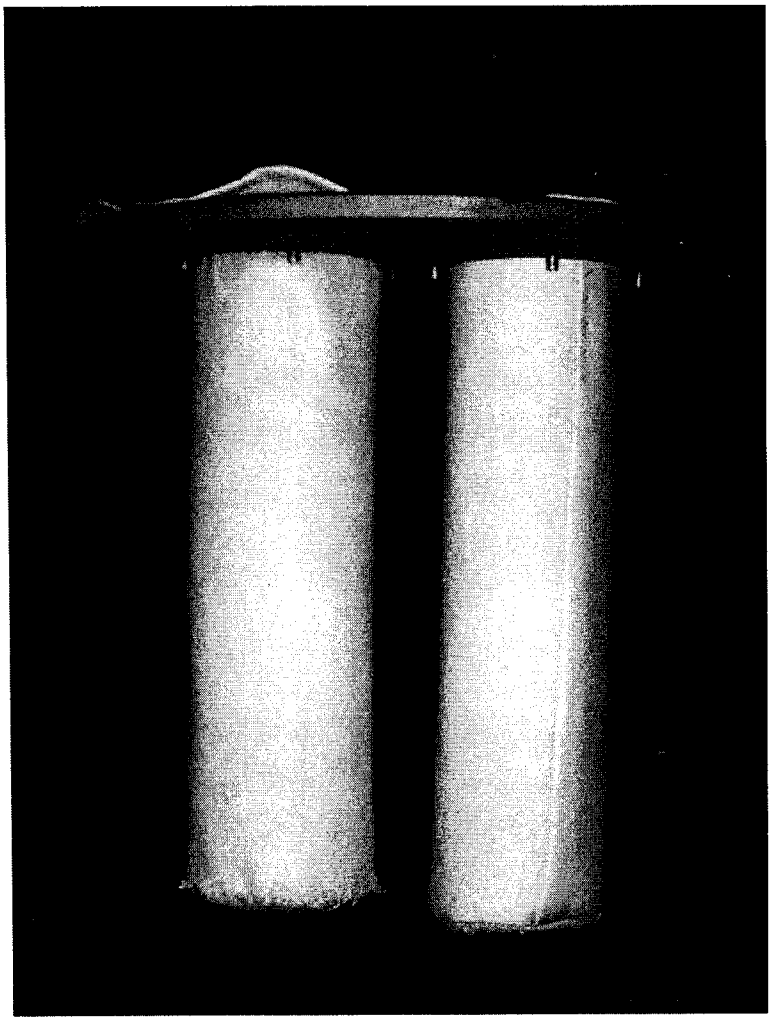

Figure 2.3.6.1-9:
Close up of bag-house center piece with fabric filter bags attached

Reproduced with permission of the copyright owner. Further reproduction prohibited without permission.

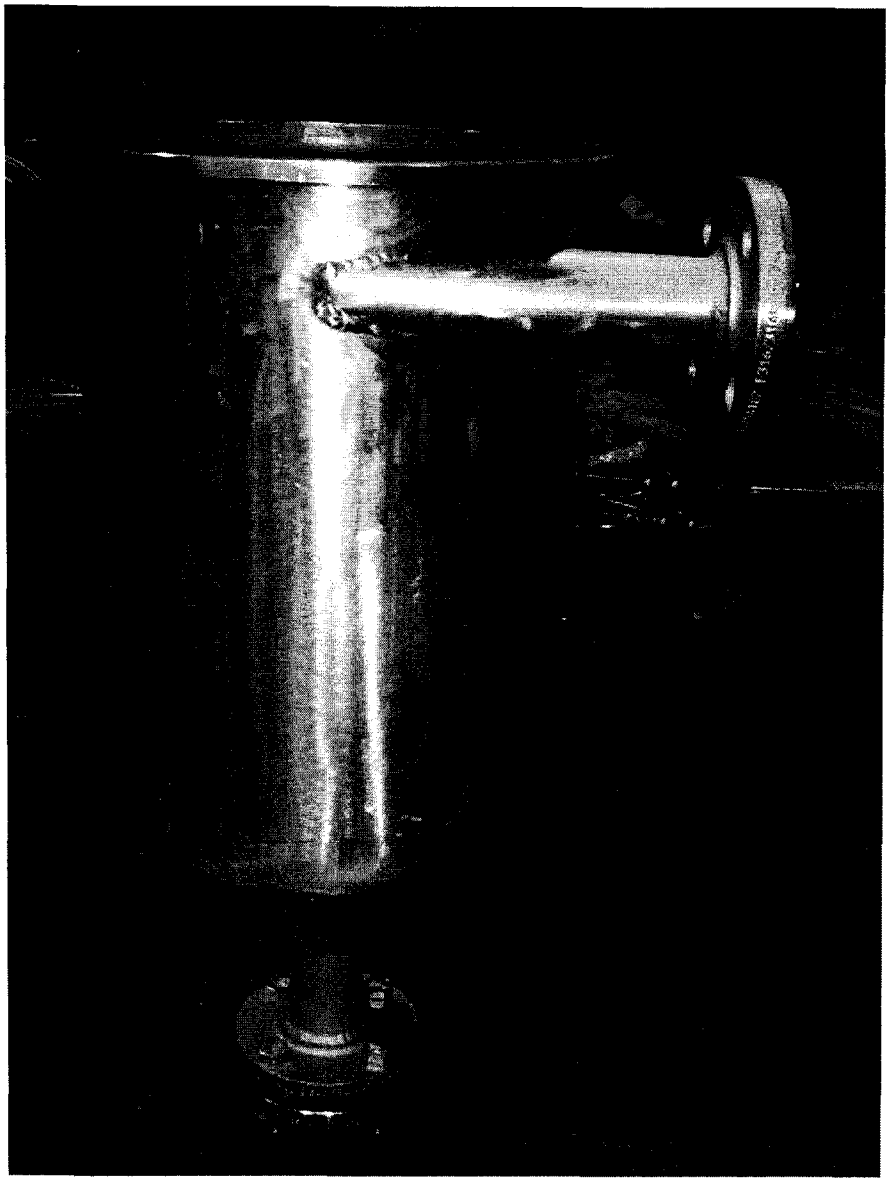

Figure 2.3.6.1-10:
Close up of bag-house body.

Reproduced with permission of the copyright owner. Further reproduction prohibited without permission.

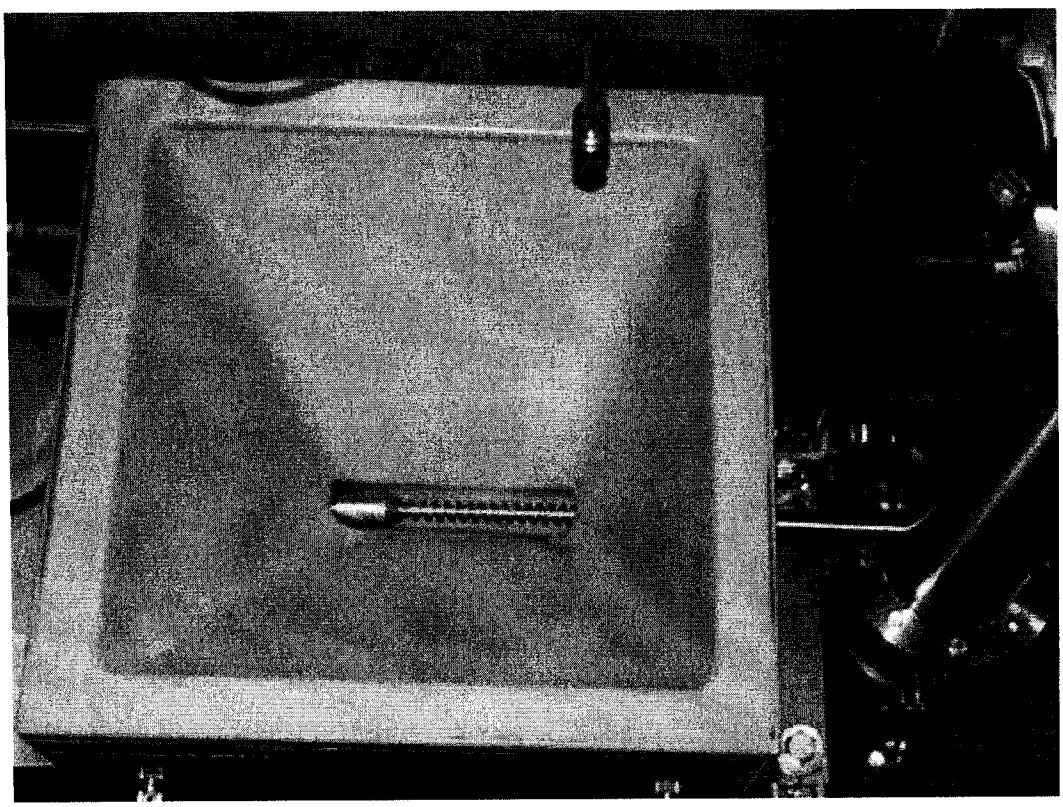

Figure 2.3.6.1-11:
Top view of ash dispenser.

Reproduced with permission of the copyright owner. Further reproduction prohibited without permission.

Figure 2.3.6.1-12:
Controllers for ash dispenser.

Reproduced with permission of the copyright owner. Further reproduction prohibited without permission.

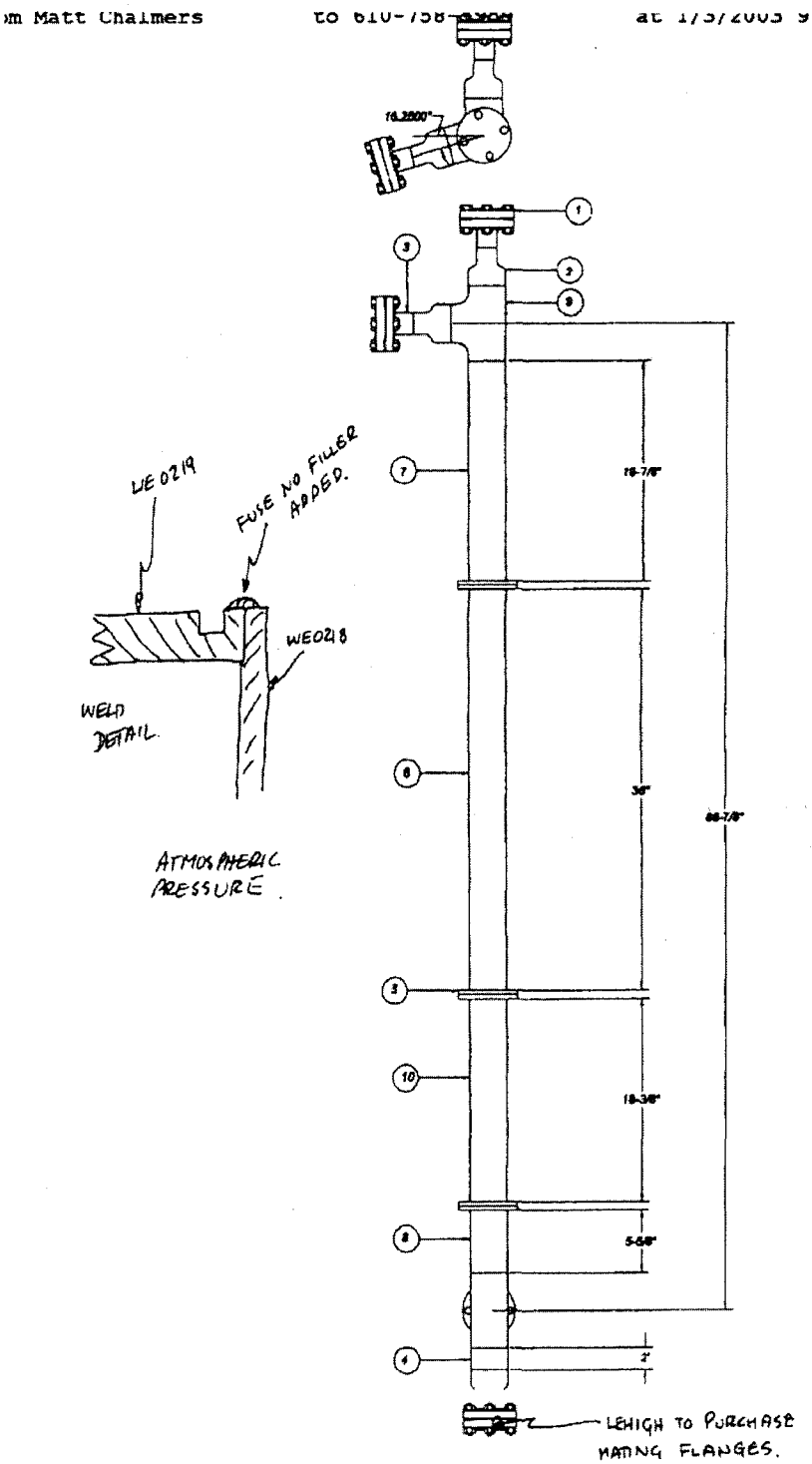

Figure 2.6.3.1-A: CAD drawing of riser section.

Reproduced with permission of the copyright owner. Further reproduction prohibited without permission.

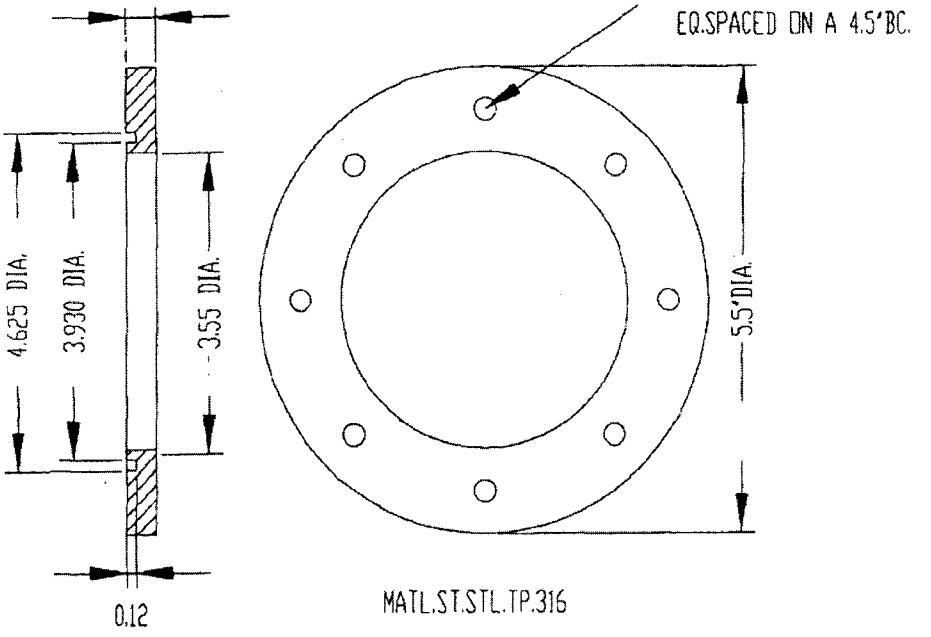

SCALE FACTOR N/A	TOLERANCE N/A	
53 BARCLAY STREET MERTZTOWN PA.19539	WOODBURN ENTERPRISES	
TITLE.	3.5 FLANGE F.W.	
DESIGN MG CHALMERS	APPROVED HG.STENGER	REV. 0
DATE 11/12/02	DWG.No. WE0219	SHEET 1

Figure 2.6.3.1-B: CAD drawing of flanges on riser section.

Reproduced with permission of the copyright owner. Further reproduction prohibited without permission.

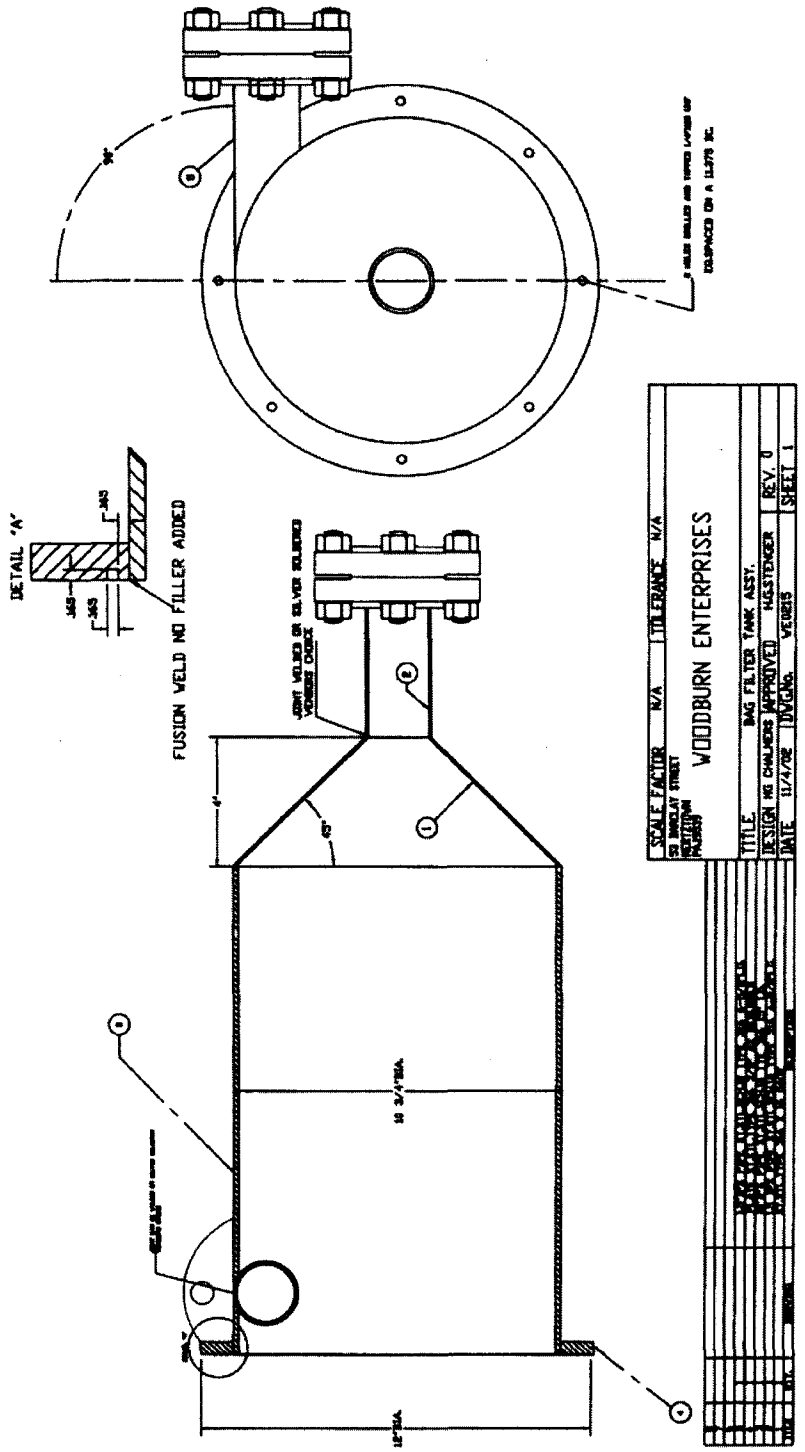

Figure 2.6.3.1-C: CAD drawing of bag-house body.

Reproduced with permission of the copyright owner. Further reproduction prohibited without permission.

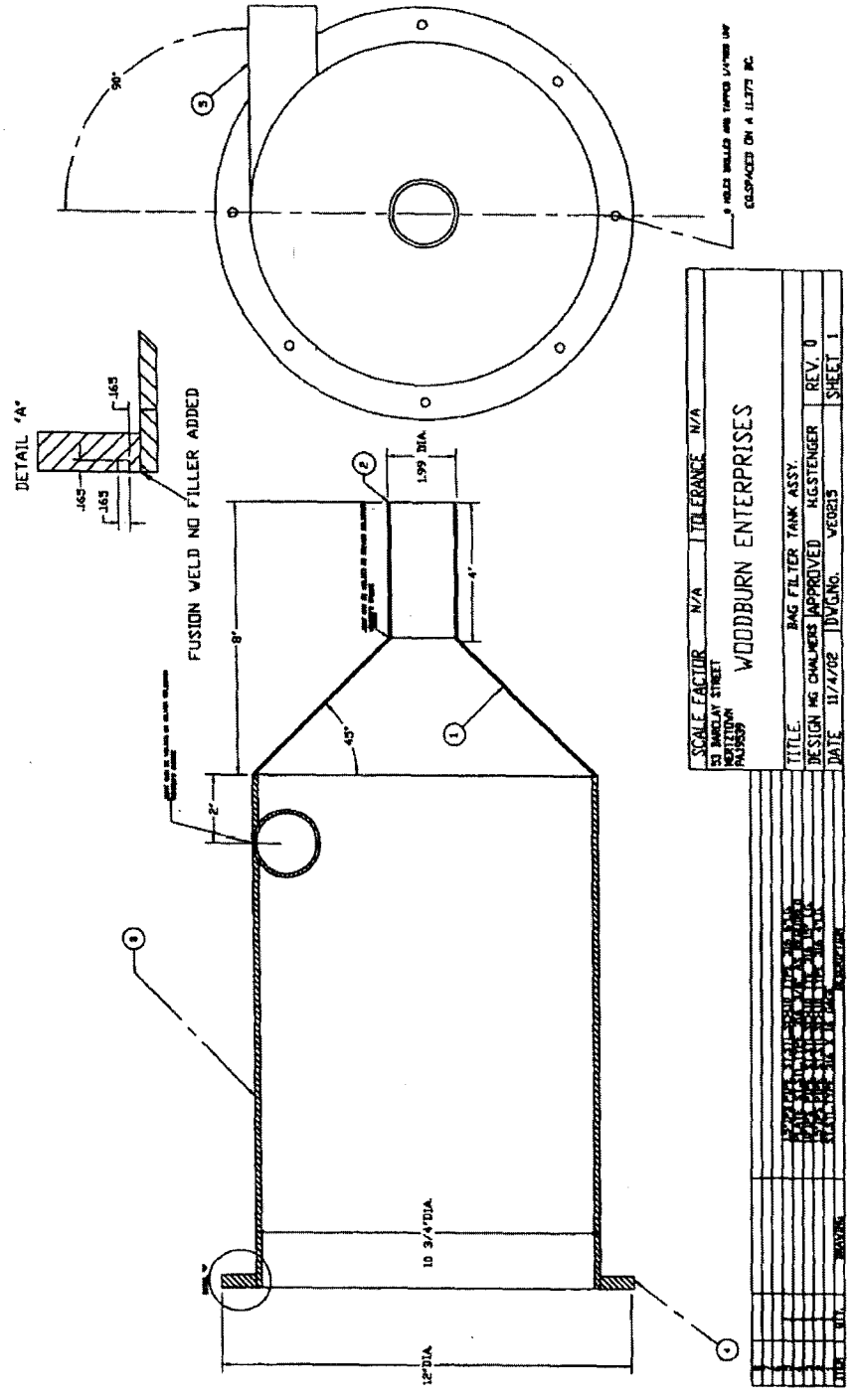

Figure 2.6.3.1-D: CAD drawing of bag-house body. Basic design.

Reproduced with permission of the copyright owner. Further reproduction prohibited without permission.

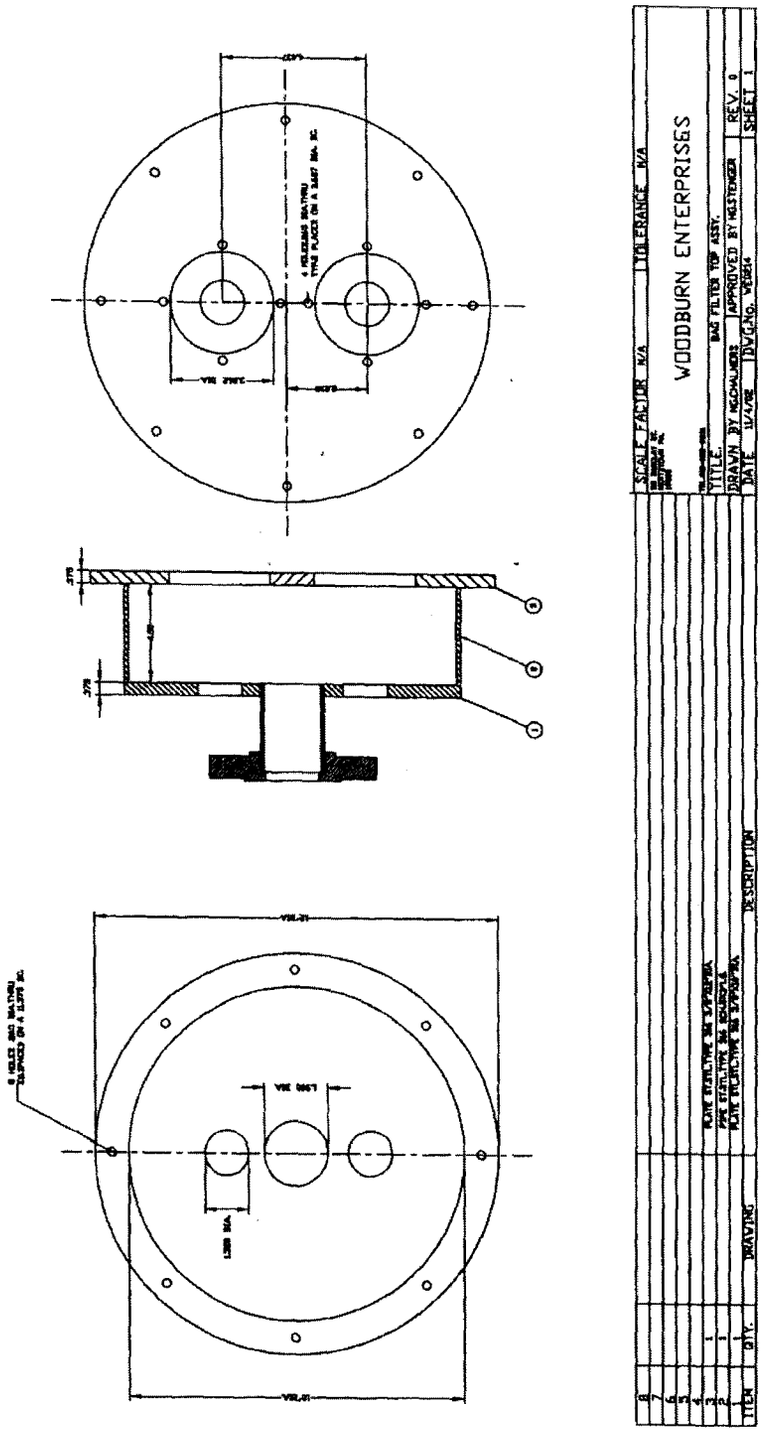

Figure 2.6.3.1-E: CAD drawing of bag-house center piece and bag-house lid.

Reproduced with permission of the copyright owner. Further reproduction prohibited without permission.

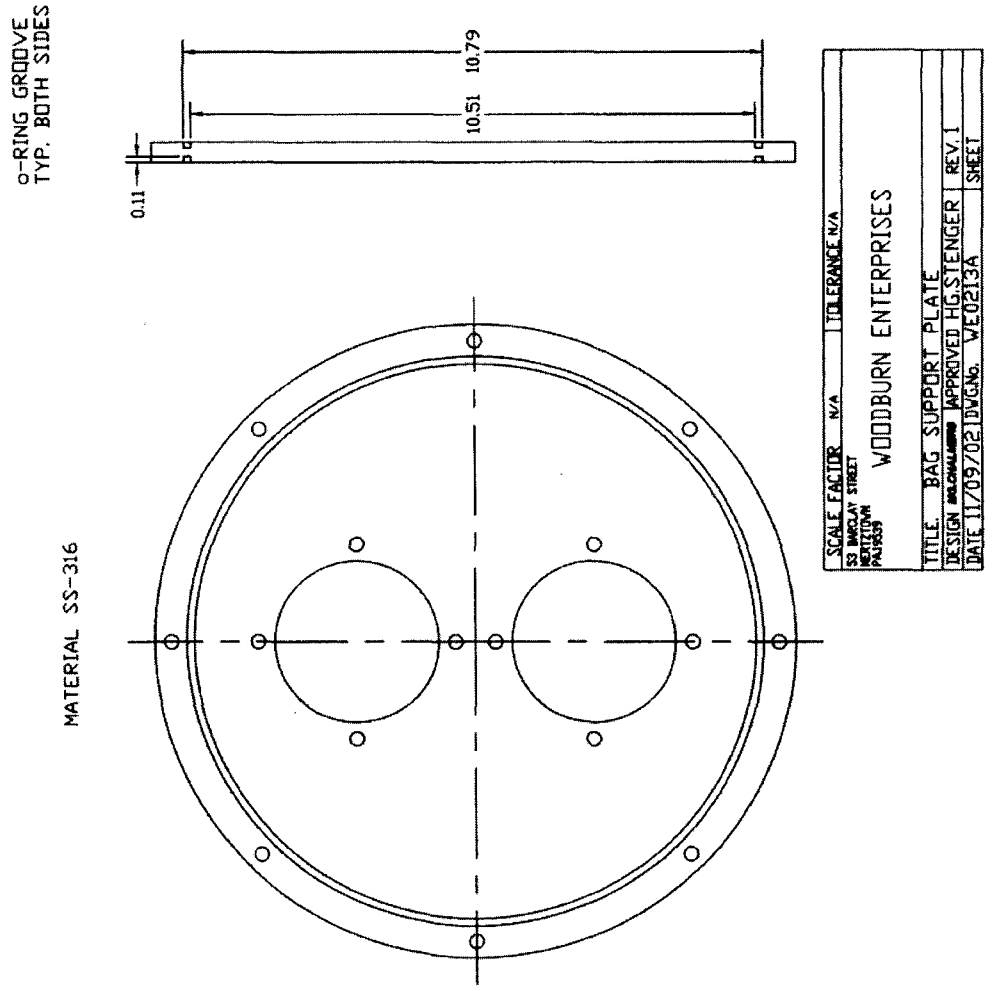

Figure 2.6.3.1-F: CAD drawing of bag-house center piece with "O"-ring grooves.

Reproduced with permission of the copyright owner. Further reproduction prohibited without permission.

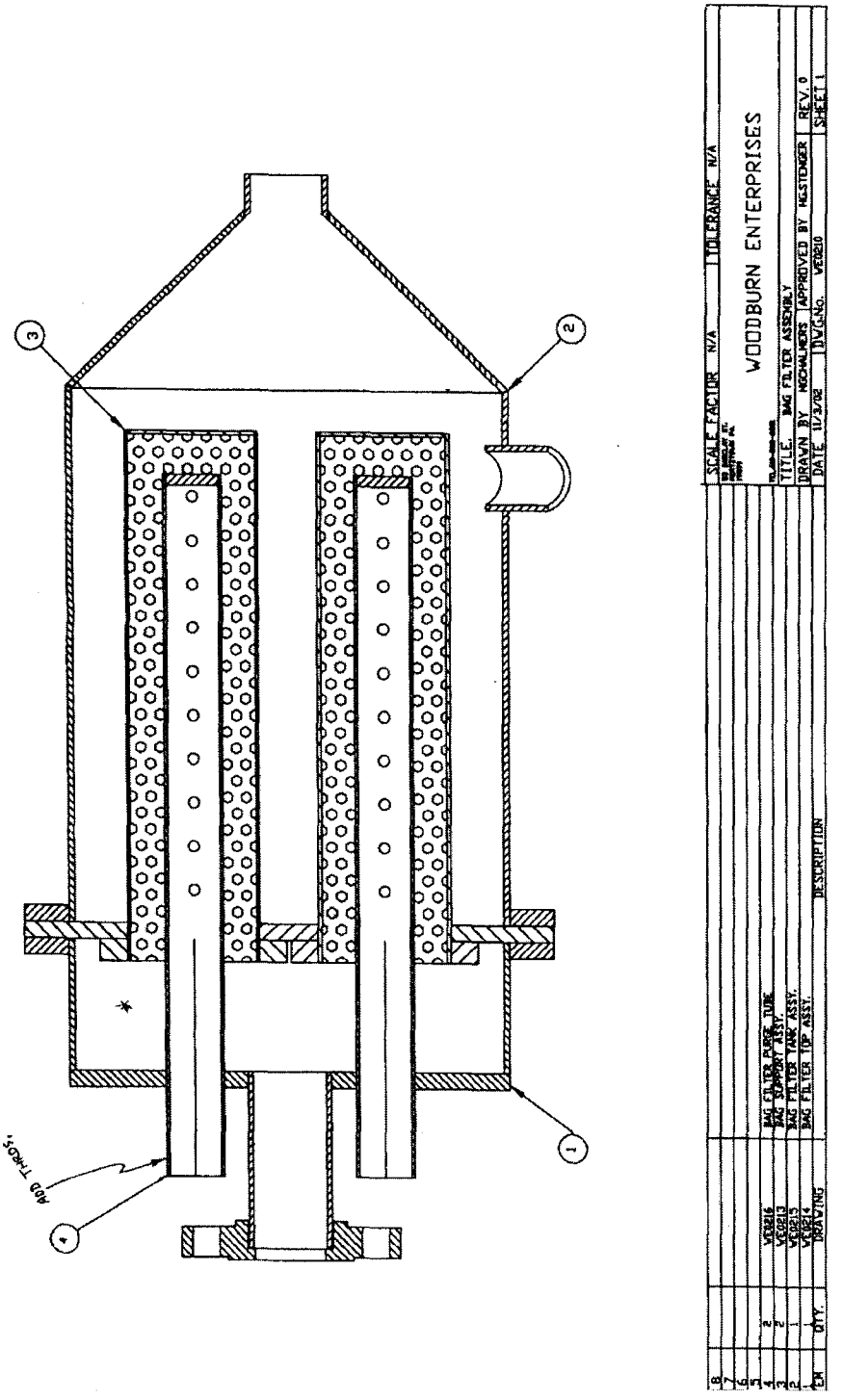

Figure 2.6.3.1-G: CAD drawing of entire bag-house assembly.

Reproduced with permission of the copyright owner. Further reproduction prohibited without permission.

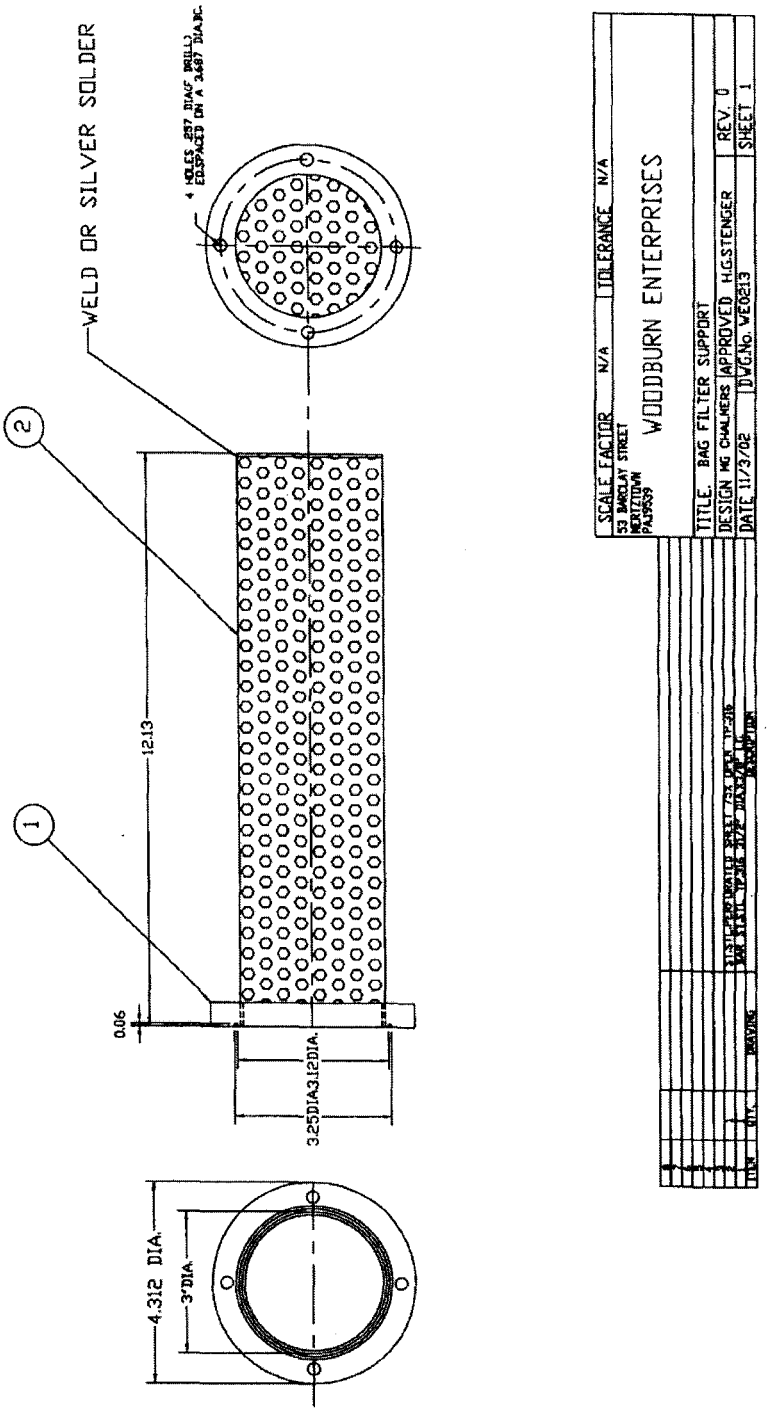

Figure 2.6.3.1-H: CAD drawing of bag-house fabric filter holders.

Reproduced with permission of the copyright owner. Further reproduction prohibited without permission.

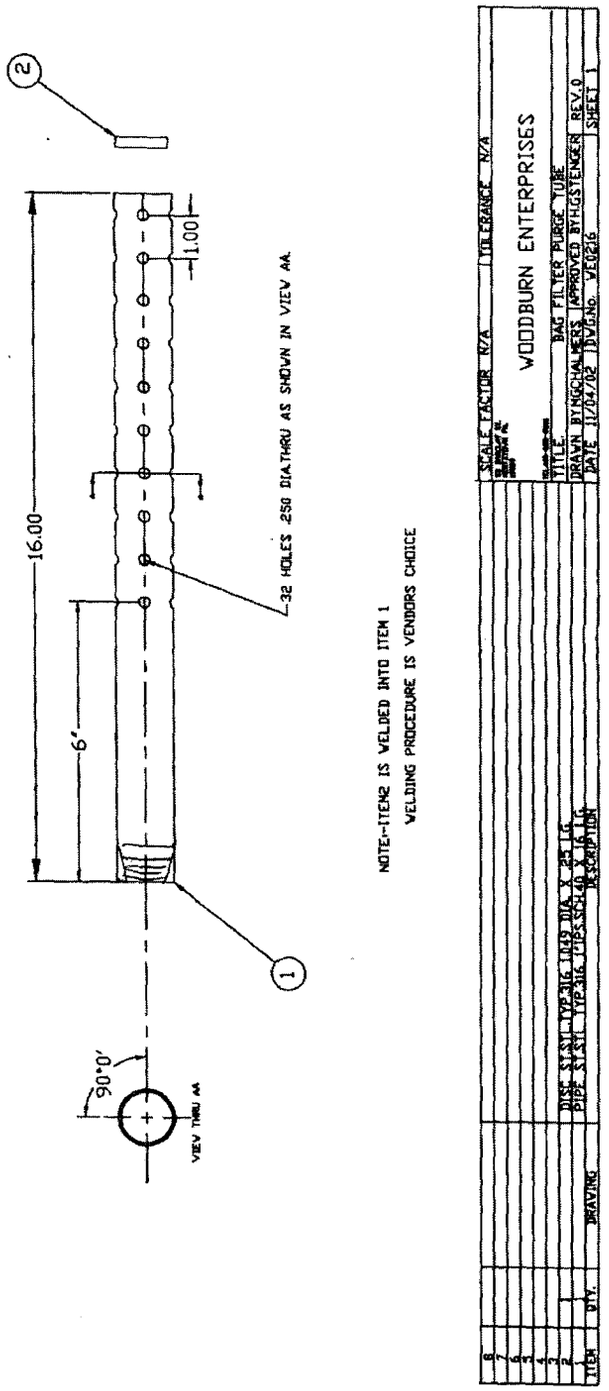

Figure 2.6.3.1-I: CAD drawing of tube within bag-house. The tube delivered bursts of air.

Reproduced with permission of the copyright owner. Further reproduction prohibited without permission.

2.3.7 *Other modifications*

A few other modifications were made on the apparatus, downstream from the bag-house.

2.3.7.1 *Measuring Linear Flow of Gas*

A 30 inch pipe was attached to the top of the bag-house. This pipe had 10 ports tapped on the side which allowed for gas velocity measurement. Each port was ¼ inch in diameter. A unit was purchased to measure linear flow of the gas, but was never installed.

2.3.7.2 *Condenser Unit*

At the exit of the 30 inch pipe, a condenser unit was built. The purpose of the condenser unit was to condense out all the water present in the gas stream. It was designed as a shell and tube heat exchanger. The shell section was made of 1.5 inch OD PVC piping. The tube section was made of a 1 inch OD copper tube. The length of the condenser unit was approximately 85 inches. The condensate used was water.

Water was chilled in a refrigerating unit (Figure 2.3.7.2-1) to near 0°C. The water flowed in an upward direction through the condenser and exited at the top before being re-chilled and recycled. Condensed water was caught in a water trap at the bottom of the condenser (Figure 2.3.7.2-2).

Reproduced with permission of the copyright owner. Further reproduction prohibited without permission.

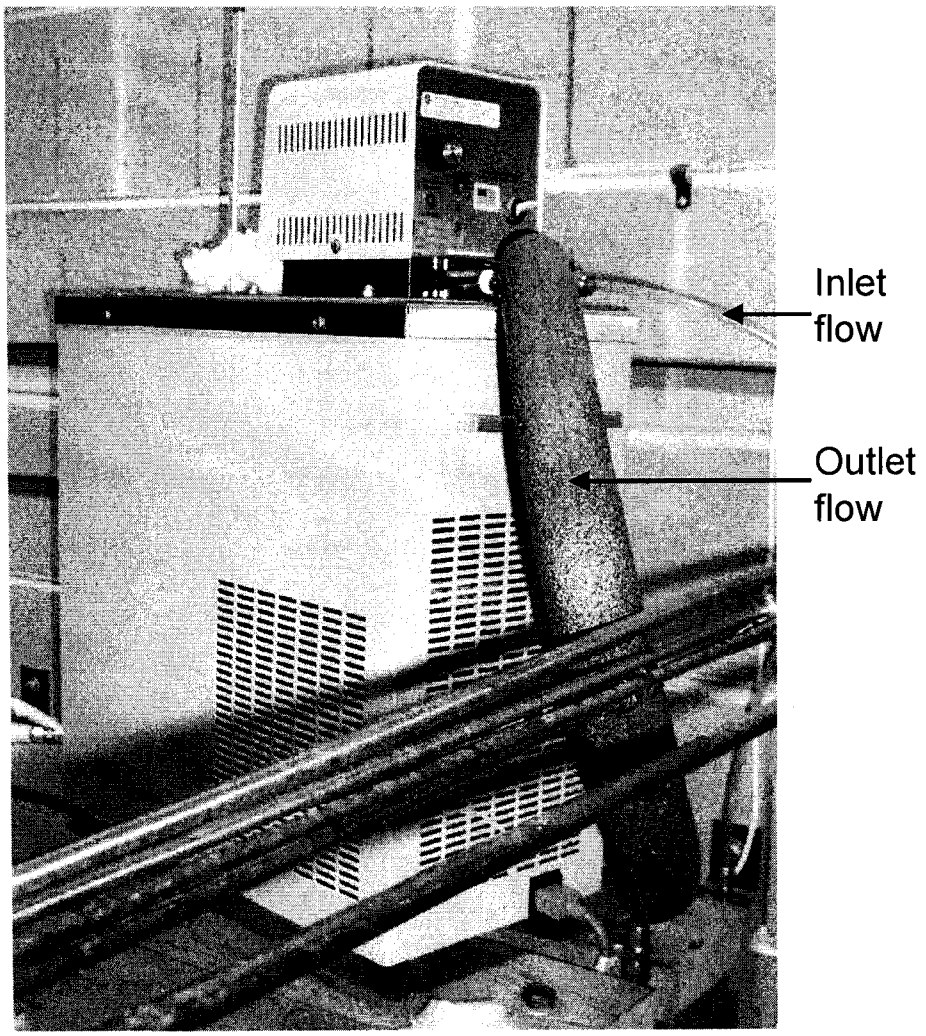

Figure 2.3.7.2-1:
Chiller unit used to cool water flowing through condenser unit. Outlet flow is insulated to prevent heat gain.

Reproduced with permission of the copyright owner. Further reproduction prohibited without permission.

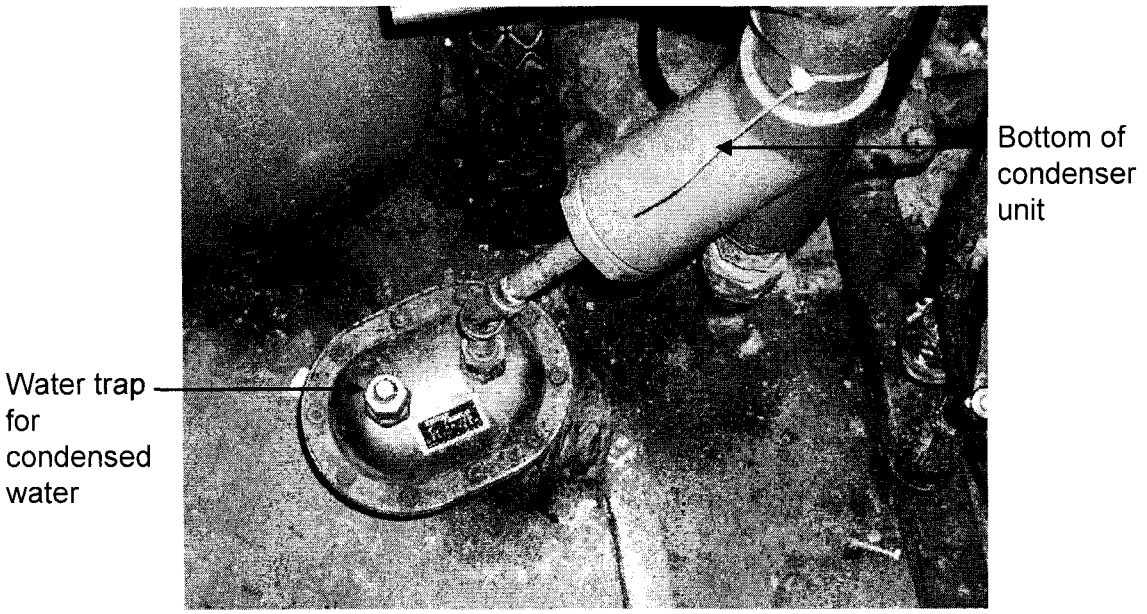

Figure 2.3.7.2-2:
Water trap to drain condensed water.

2.3.7.3 Carbon Filter

Downstream from the condenser unit, a carbon filter was attached to the exhaust line. The purpose of the carbon filter was to prevent any corrosive gases and water from getting to the totalizer (described below). The filter is shown in Figure 2.3.7.3-1. The carbon filter housing (part # 4496K21) and replacement cartridge (part # 4361K22) were purchased from McMaster Carr Supply Company. The filter housing and cartridge cost $53.33 and $6.22 respectively.

Reproduced with permission of the copyright owner. Further reproduction prohibited without permission.

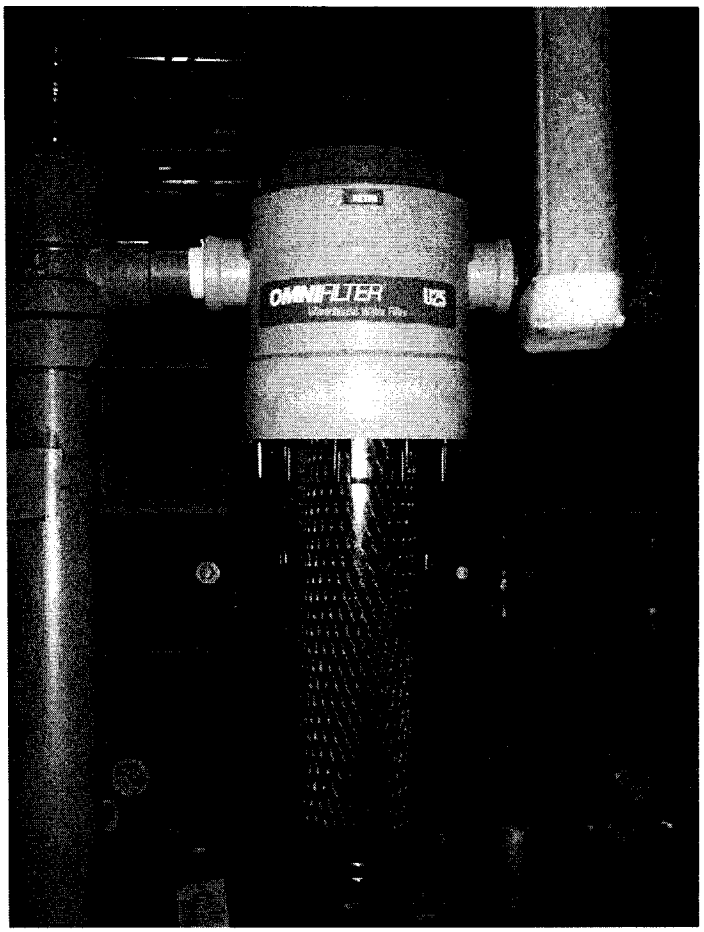

Figure 2.3.7.3-1:
Carbon trap used to remove acid gases and moisture from flue gas stream before entering totalizer.

Reproduced with permission of the copyright owner. Further reproduction prohibited without permission.

2.3.7.4 Totalizer

The purpose of the totalizer was to measure the volumetric flow of the dry gas through the system. The totalizer was attached downstream from the carbon filter and condenser. At this location, the gas stream was assumed to contain no water. The totalizer measured the gas flow in cubic feet per hour. It is shown in Figure 2.3.7.4-1. The totalizer (part # 4360K21) was purchased from McMaster Carr Supply Company and cost $166.90.

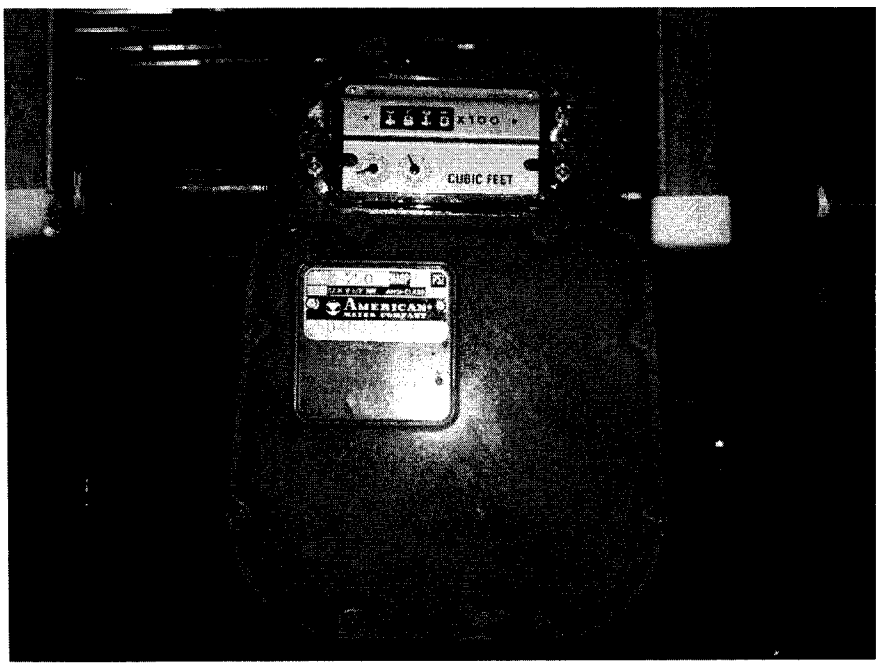

Figure 2.3.7.4-1:
Totalizer used to measure volumetric flow rate of the flue gas in the entire apparatus.

Reproduced with permission of the copyright owner. Further reproduction prohibited without permission.

2.3.7.5 Exhaust Line with Constriction

At the very end of the exhaust line, a constriction was placed before the gas was vented to the atmosphere. It consisted of a 3/8" to ¼" reducing union. The purpose of this constriction was to have a pressure build up in the entire apparatus so that gas samples could be easily taken from any sample port. The maximum pressure within the apparatus was 7 pounds per square inch gauge (psig). It is shown in Figure 2.3.7.5-1.

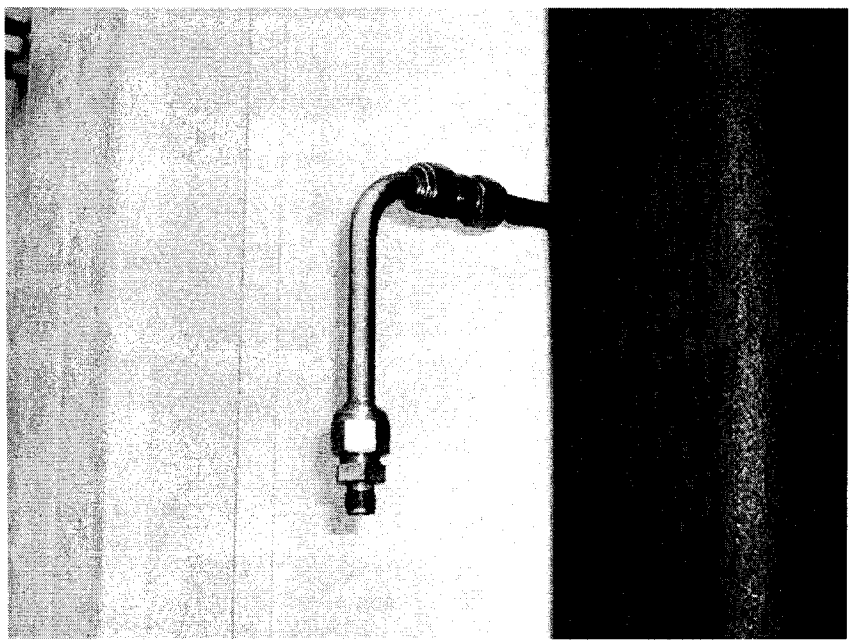

Figure 2.3.7.5-1:
Constriction before flue gas is vented. It is a reducing union from 3/8" to ¼".

Reproduced with permission of the copyright owner. Further reproduction prohibited without permission.

2.3.8 *Sample Lines*

Several sample lines were used to sample for Hg in the gas stream.

i. The first sample line was at the exit of R1. The main purpose of this location was to measure the material balance of Hg in the gas stream. At this location, the Hg has been diluted by all the gases in the stream. Depending on the settings on the Hg source, a concentration of 10 to 15 $\mu g/m^3$ of Hg in the gas stream was desired. It is shown in Figure 2.3.8-1.

ii. The second sample line was located at the exit of R2. This port was used to measure the Hg concentration during the experimental work.

iii. The third sample line was located at the exit of HX1. This port was also used to measure the Hg concentration during the experimental work. This sample line is shown in Figures 2.3.6-1, 2.3.6-2 and 2.3.8-2.

iv. A fourth sample line was located at the same point as the sorbent injection port. This allowed for a slightly additional residence time as the gas flowed around the 180° bend. This port was also larger, with a ½ inch opening. This allowed for easier gas sampling.

v. Additional sample lines were present at the entrance and exit of the bag-house for Hg measurements. However, these were never used in this work.

Reproduced with permission of the copyright owner. Further reproduction prohibited without permission.

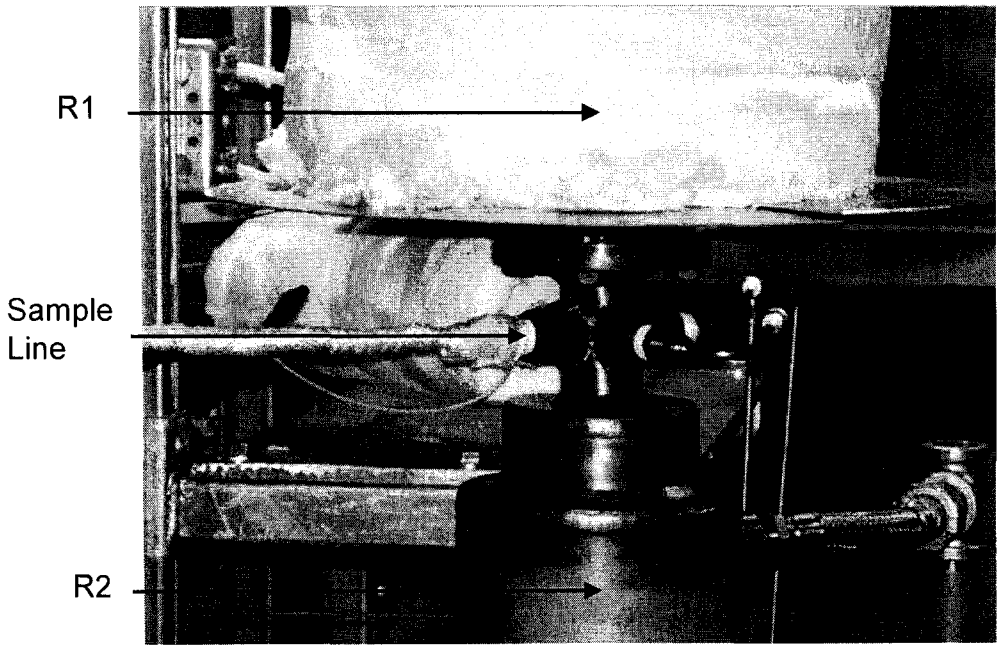

Figure 2.3.8-1:
Close up of section between R1 and R2. Location of sample line and injection point of Cl_2 in all experimental work.

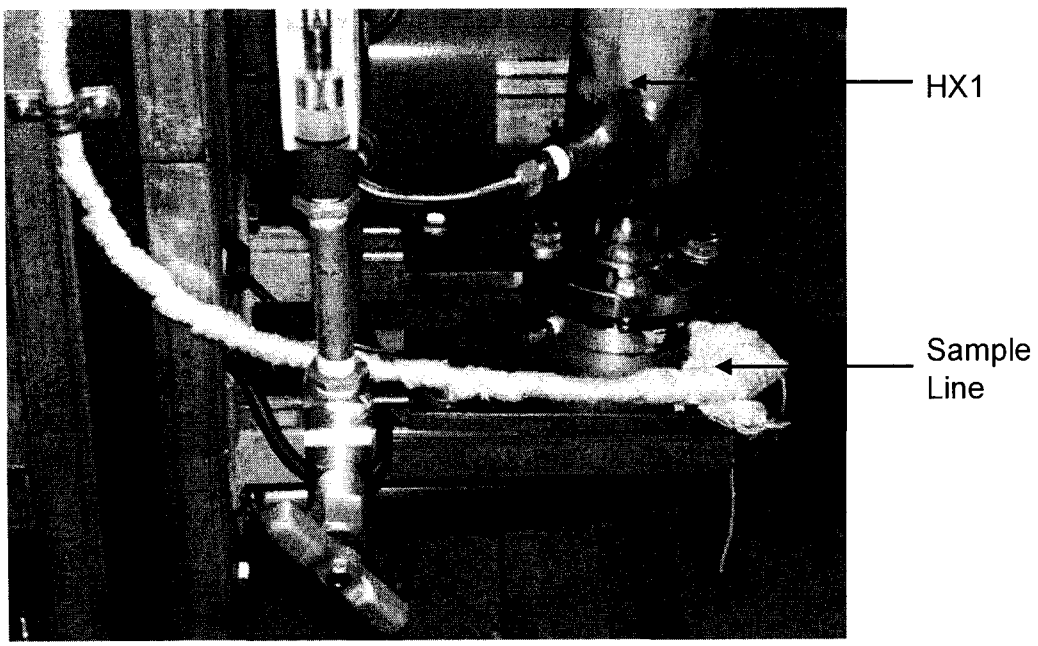

Figure 2.3.8-2:
Sample line at the end of HX1 used to collect gas samples for Hg analysis.

Reproduced with permission of the copyright owner. Further reproduction prohibited without permission.

2.3.8.1 Using Teflon for Sampling

Teflon tubes were used to carry the sample gases to the mercury analyzer. Teflon material was used to prevent mercury losses along the lines. By maintaining the temperature of the lines at approximately 200°C, there would be a reduced amount of water condensation taking place within the lines. It is known that $HgCl_2$ is very soluble in water. Because of this physical property, it is speculated that any $HgCl_2$ present in the gas stream would dissolve in the condensed water within the sample lines. Maintaining the temperature of the lines at 200°C or higher would prevent condensation and mercury losses.

2.3.8.2 Design of Sample Lines

The sample lines were initially designed simply as Teflon tubes wrapped with heating coils and insulated with insulating and fiberglass tape. Teflon tubes (part # 5239K12) were purchased from McMaster Carr Supply Company at $0.97 per foot. The heating coil that was wrapped around the Teflon tubes (part # A-03122-18) were purchased from Cole Parmer and cost $170 for the 18 foot coil. The same insulating and fiberglass tape as mentioned in Table 2.3.1.2-1 was used.

In order to control the power supplied to the heating coil, the coil was attached to a light dimmer switch. These dimmer switches (and the electric boxes) were purchased from a local hardware store. Figure 2.3.8.2-1 shows the arrangement of the dimmer switches in the control room.

2.3.8.3 Modifications on Sample Lines

Over time, the repeated heating and cooling of the Teflon lines by the heating coils resulted in either the tubes melting, or the heating lines burning out. As a result, these sample lines had to be replaced. New sample lines were purchased from APEX Instruments, where the sample lines were constructed for industrial purposes[175]. These self regulated heated sample lines (part # HSRL-4-10) cost $305 for 10 feet length. The sample lines were heated to

Reproduced with permission of the copyright owner. Further reproduction prohibited without permission.

approximately 300°C and remain at this temperature until the power supply was cut off. There was also no longer a need for the light dimmer switches since this new sample line was self regulated.

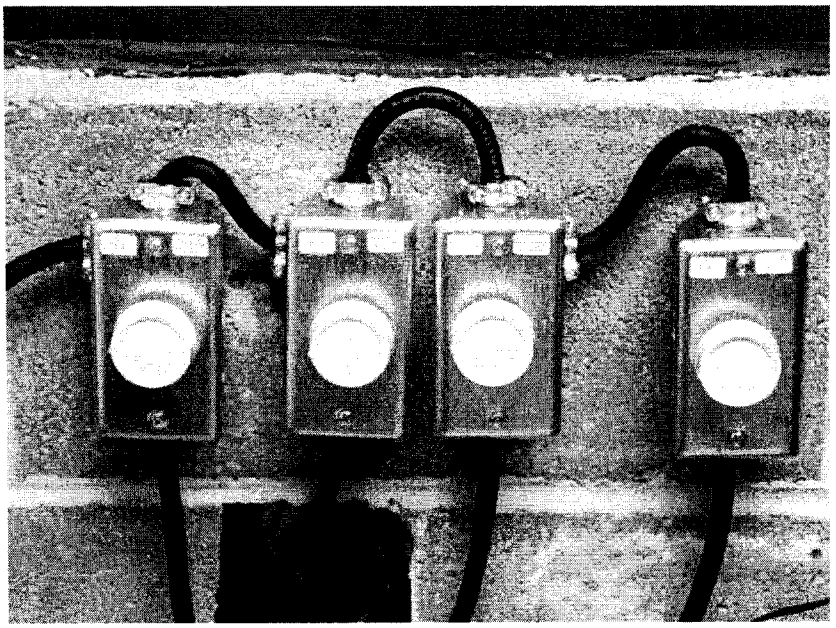

Figure 2.3.8.2-1:
Light dimmer switches used to control heating coils on sample lines.

2.3.9 Gas Blending System

In order to perform experimental work in a cheap, efficient and safe way, the idea of blending gases to form a synthetic flue gas system was proposed. Building a pulverizer and boiler to create a flue gas stream would have been too expensive and complicated to manage. Using propane combustion would have been cheaper, but more dangerous. Several researchers have used this method of blending gases in order to get the desired flue gas composition. This section will present the various steps taken in creating a gas blending system.

2.3.9.1 Using Mass Flow Controllers (MFCs) for All Gases

In order to control the concentration of individual gas components in the flue gas blend, accurate instrumentation had to be used. Mass flow controllers (MFCs) have been regularly used

Reproduced with permission of the copyright owner. Further reproduction prohibited without permission.

as the most accurate means of controlling flow. A separate MFC was purchased for each gas component. The mounted MFCs are shown in Figures 2.3.9.1-1 and 2.3.9.1-2. Each MFC was controlled by an electronic box shown in Figures 2.3.9.1-3, 2.3.9.1-4 and 2.4.2.4-1. Each box has the ability to control 4 MFCs. Table 2.3.9.1-1 lists the items purchased, part number, specifications, price and purpose of use. Under specifications, the flow range of each MFC is listed, along with operating pressure and temperature of calibration. All items were purchased from Omega Engineering.

Item	Part Number	Specifications	Price ($)	Purpose
MFC	FMA-774A	0-100 slpm, 20 psi, 70F	2276.00	MFC used for delivering N_2
MFC	FMA-776A	0-500 slpm, 20 psi, 70F	2900.00	MFC used for delivering N_2
MFC	FMA-776A	0-500 slpm, 20 psi, 70F	2900.00	MFC used for delivering Air
MFC	FMA-773A	0-50 slpm, 20 psi, 70F	2276.00	MFC used for delivering CO_2
MFC	FMA-767A	0-1 slpm, 20 psi, 70F	1164.00	MFC used for delivering NO
MFC	FMA-768A	0-2 slpm, 20 psi, 70F	1164.00	MFC used for delivering SO_2
MFC	FMA-765A	0-200 sccm, 20 psi, 70F	1164.00	MFC used for delivering CO
MFC	FMA-765A	0-200 sccm, 20 psi, 70F	1164.00	MFC used for delivering Cl_2
MFC Controller Box	FMA-78P4	(n/a)	1714.00	4 Sensors per box, 2 purchased

Table 2.3.9.1-1: List of mass flow controllers and the controller boxes purchased for gas flow control.

In the case of NO, SO_2, CO and Cl_2, the gas cylinders purchased were not of the pure components. Each gas was diluted in N_2. For example, Cl_2 was purchased in a cylinder with a 1% Cl_2 and 99% N_2 concentration. A later section lists these items in detail.

Unfortunately, although mass flow controllers are accurate, they are also very sensitive and not corrosive resistant. In the case of NO, SO_2, CO and Cl_2, all the valves in the flow

Reproduced with permission of the copyright owner. Further reproduction prohibited without permission.

controllers corroded and were not functional within a few weeks. Additionally, the flow controller used for air was also damaged by the presence of water in the atmosphere. Ultimately, all flow controllers, except those for N_2 and CO_2 delivery, were replaced with rotometers.

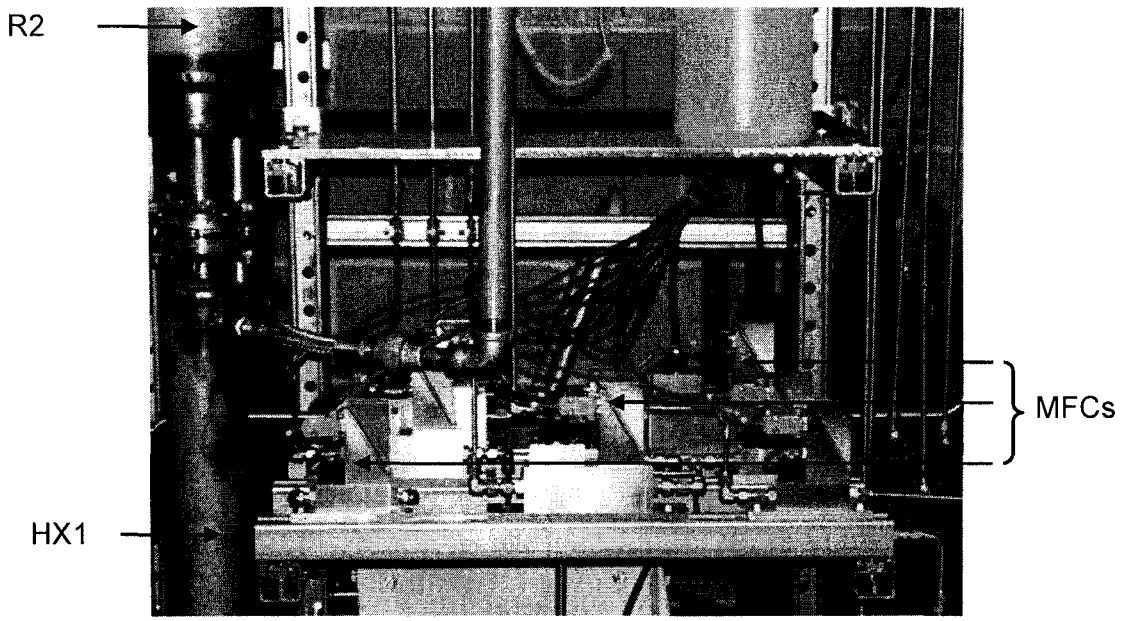

Figure 2.3.9.1-1:
Display of MFCs used in this experimental work before being replaced with rotometers.

Reproduced with permission of the copyright owner. Further reproduction prohibited without permission.

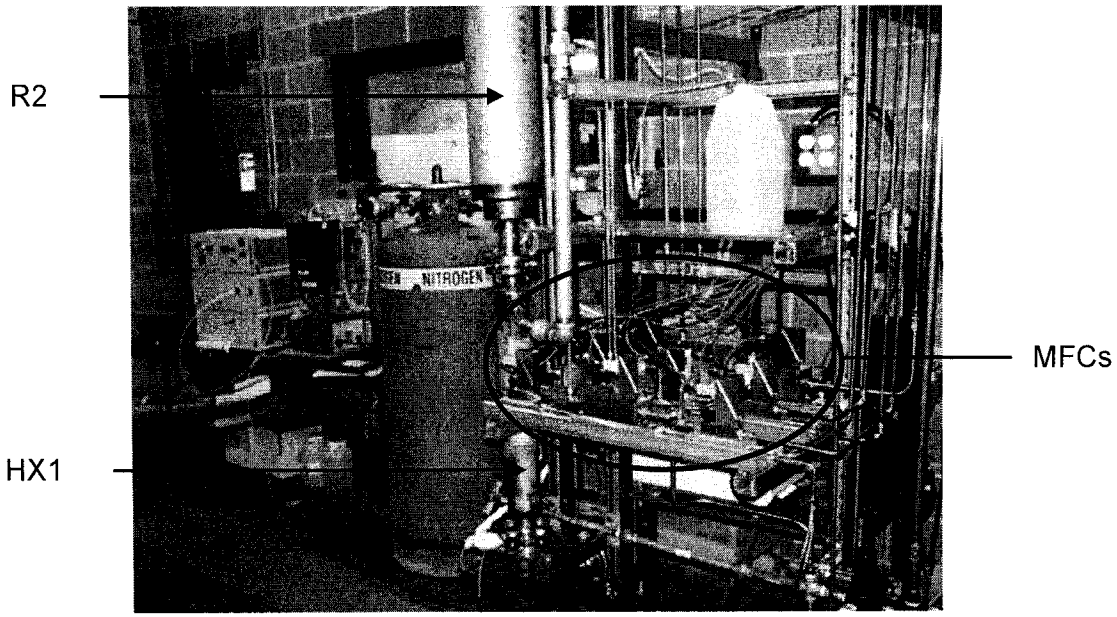

Figure 2.3.9.1-2:
Side view of MFC panel to control all gases flowing into experimental apparatus.

Reproduced with permission of the copyright owner. Further reproduction prohibited without permission.

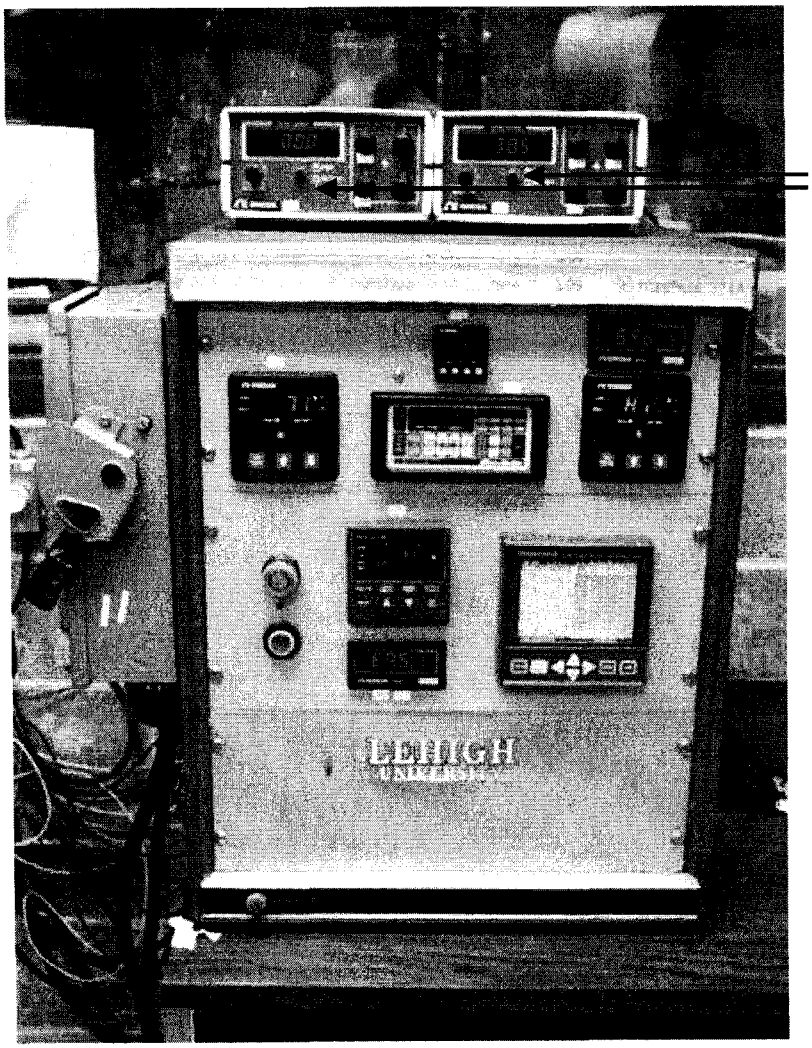

Figure 2.3.9.1-3:
Picture of control panel consisting of temperature read-outs and heater controllers. Also shown are the 4 channel control boxes for MFC control.

Reproduced with permission of the copyright owner. Further reproduction prohibited without permission.

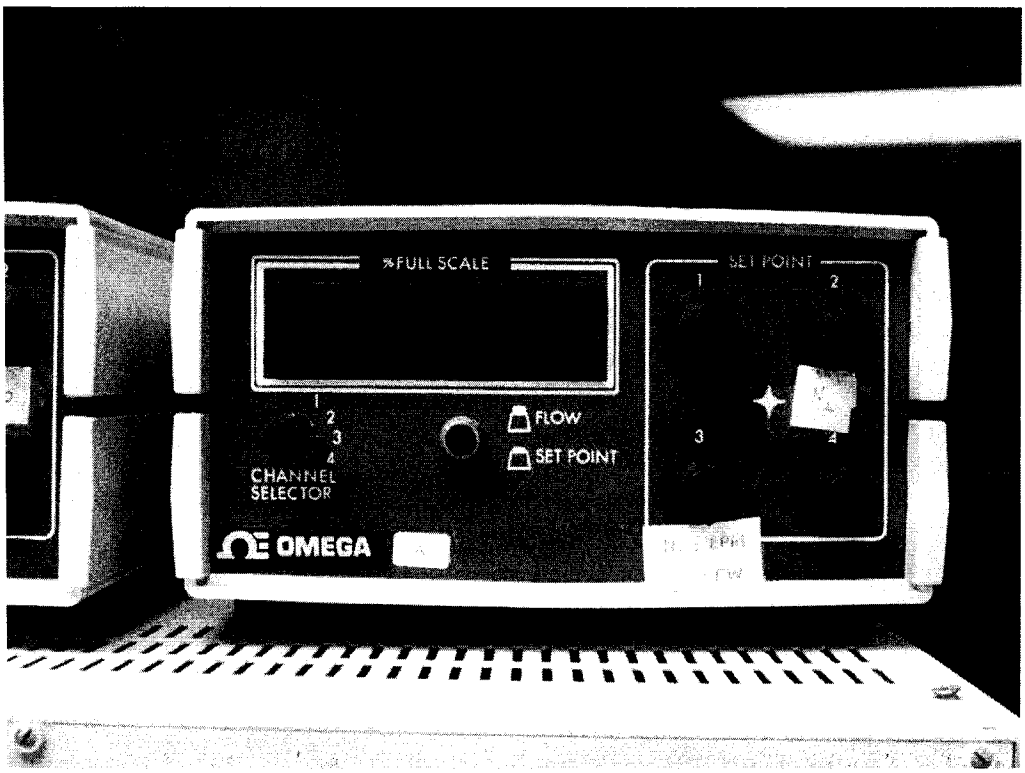

Figure 2.3.9.1-4:
Close up of 4 channel control box for controlling MFCs.

2.3.9.2 Setup for Air Flow

Air was used in the gas blend since it provided the source of O_2. A compact oilless reciprocating air compressor was purchased to pump air from the atmosphere into an air tank. This setup provided a means of delivering air into the apparatus. Additionally, a filter was attached to the compressor to remove any particles that might be present in the air. A modification made to this system was to add a desiccant air dryer unit to remove all moisture from the air before delivering it into the apparatus. Table 2.3.9.2-1 lists the items purchased, part numbers and the prices. All items were purchased from McMaster Carr Supply Company. Figures 2.3.9.2-1 to 2.3.9.2-3 show the air flow setup.

Reproduced with permission of the copyright owner. Further reproduction prohibited without permission.

Item	Part Number	Price ($)
Oilless reciprocating air compressor	8280K22	619.34
Portable compressed air tank	41855K29	53.85
Air Intake Filter	4399K45	34.06
Desiccant Air Dryer	4437K611	378.73
Replacement Desiccants	4437K81	21.91

Table 2.3.9.2-1: List of items purchased for air flow delivery system.

Initially, the air flowing from the compressor to the main heater was controlled by a mass flow controller. However, after a few weeks of use, the mass flow controller was damaged beyond repair. As a result, a rotometer was used in place of the MFC.

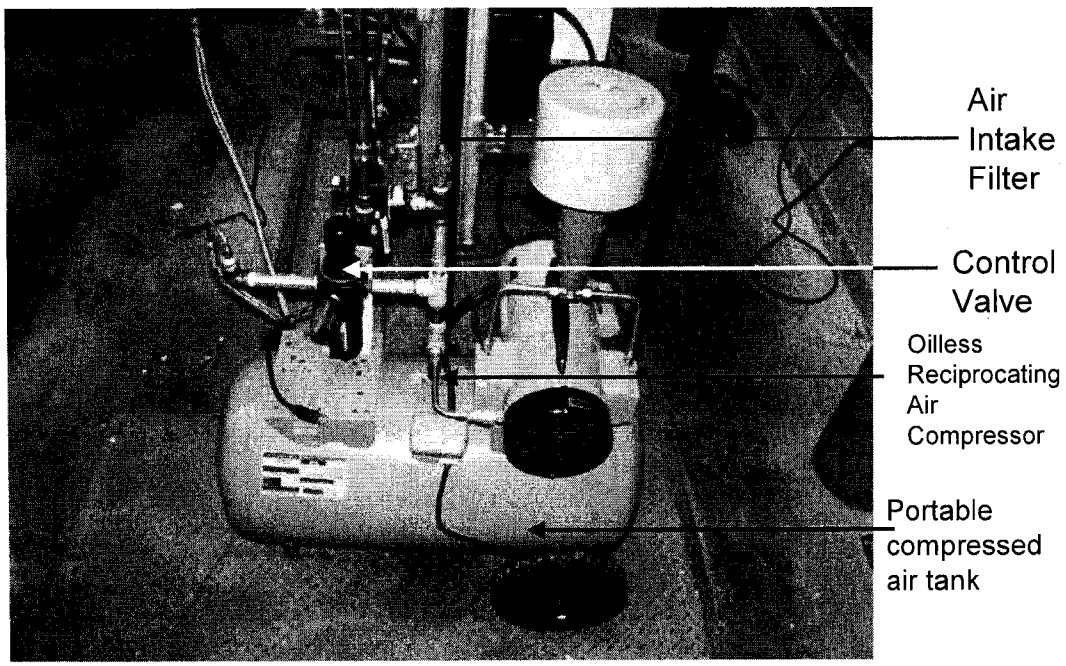

Figure 2.3.9.2-1:
Setup for air flow including air compressor and tank.

Reproduced with permission of the copyright owner. Further reproduction prohibited without permission.

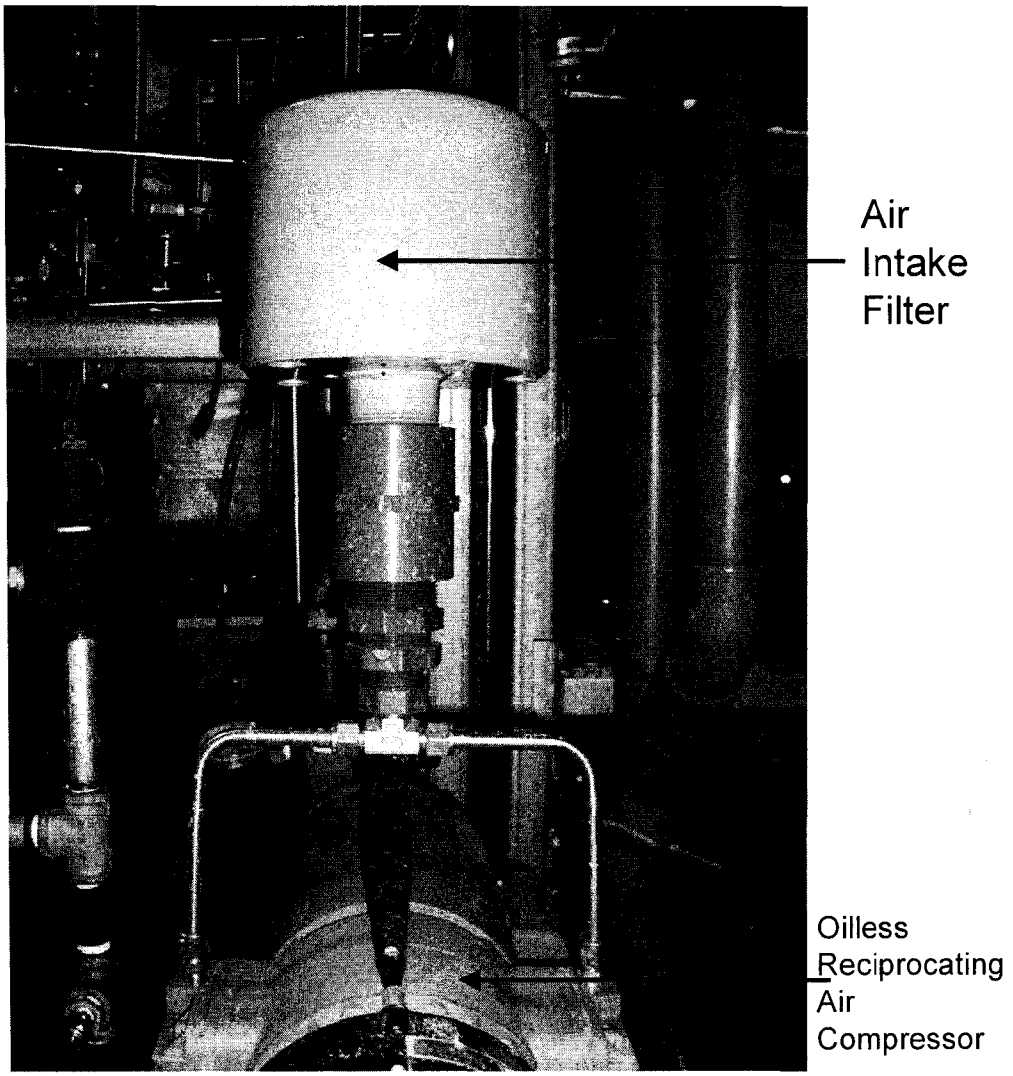

Figure 2.3.9.2-2:
Close up of the top of air flow setup showing air compressor and the air intake filter.

Reproduced with permission of the copyright owner. Further reproduction prohibited without permission.

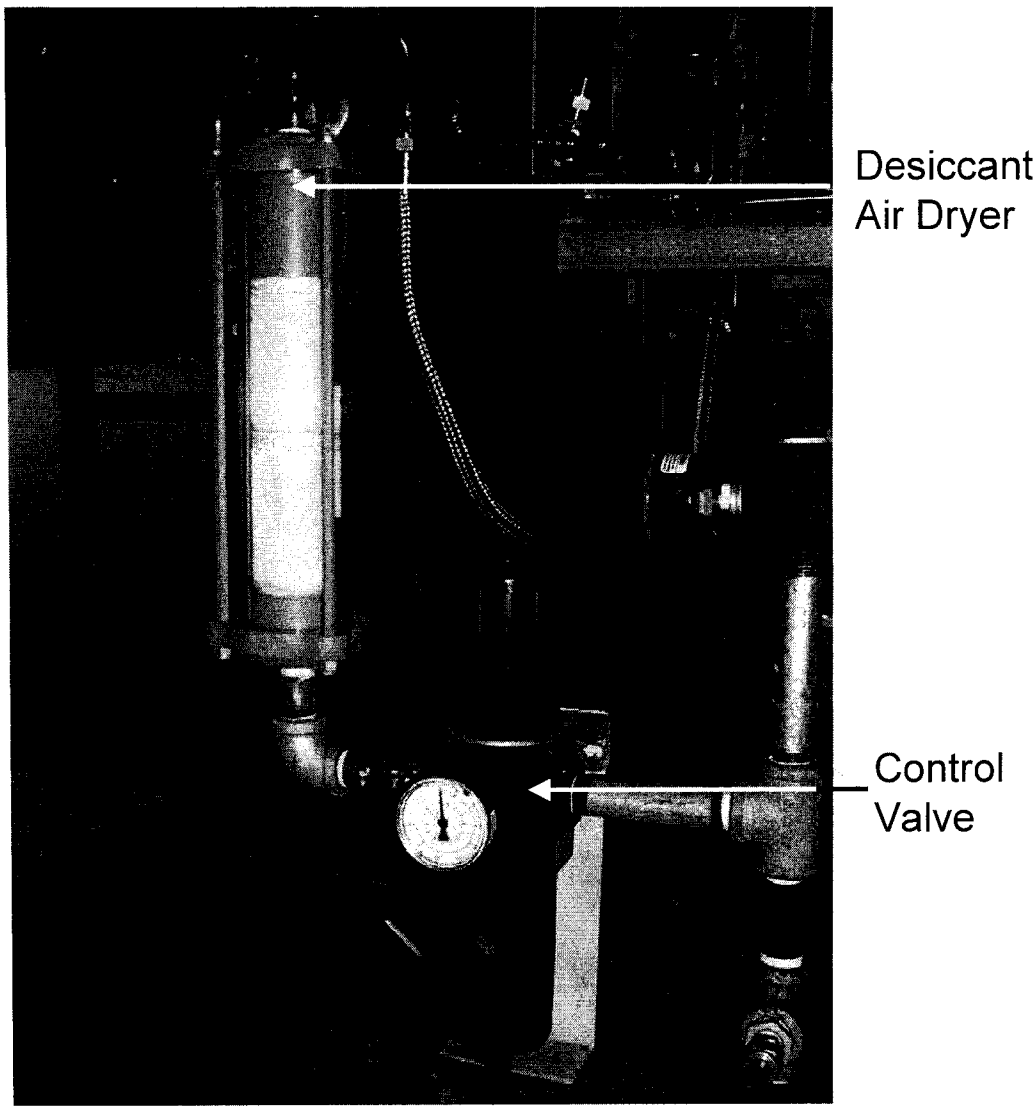

Figure 2.3.9.2-3:
Close up of desiccant – to dry atmospheric air before entering the experimental apparatus.

Reproduced with permission of the copyright owner. Further reproduction prohibited without permission.

2.3.9.3 Using Rotometers for Corrosive Gases

As mentioned in section 2.3.9.1, several of the mass flow controllers were damaged because of the corrosive nature of the gases. In the case of air, the MFC was damaged because moisture in the atmosphere caused the valve in the controller to rust. These MFCs were then replaced by rotometers. All rotometers were purchased from Cole Parmer Instruments Company[176]. Figures 2.3.9.3-1 to 2.3.9.3-3 show some of these rotometers. In the case of air, two rotometers were used to ensure accurate flow readings. Table 2.3.9.3-1 lists the rotometers purchased for each gas stream.

Item	Part Number	Price ($)	Comments
Direct Read Rotometer	C-32035-10	237.00	Replaced Cl_2 MFC; Max. Flow: 1.25 lpm
Direct Read Rotometer Tube	A-32047-60	66.00	Replaced NO MFC; Max. Flow: 1250 mlpm
Direct Read Rotometer Tube	A-03217-13	66.00	Replaced SO_2 MFC; Max. Flow: 374 mlpm
Rotometer	A-32046-09	291.00	Replaced CO MFC; Max. Flow: 104 mlpm
Direct Read Rotometer	C-32461-56	60.00	Replaced Air MFC; Max. Flow: 30 lpm

Table 2.3.9.3-1: Replacement parts (rotometers) for individual gas streams.

Reproduced with permission of the copyright owner. Further reproduction prohibited without permission.

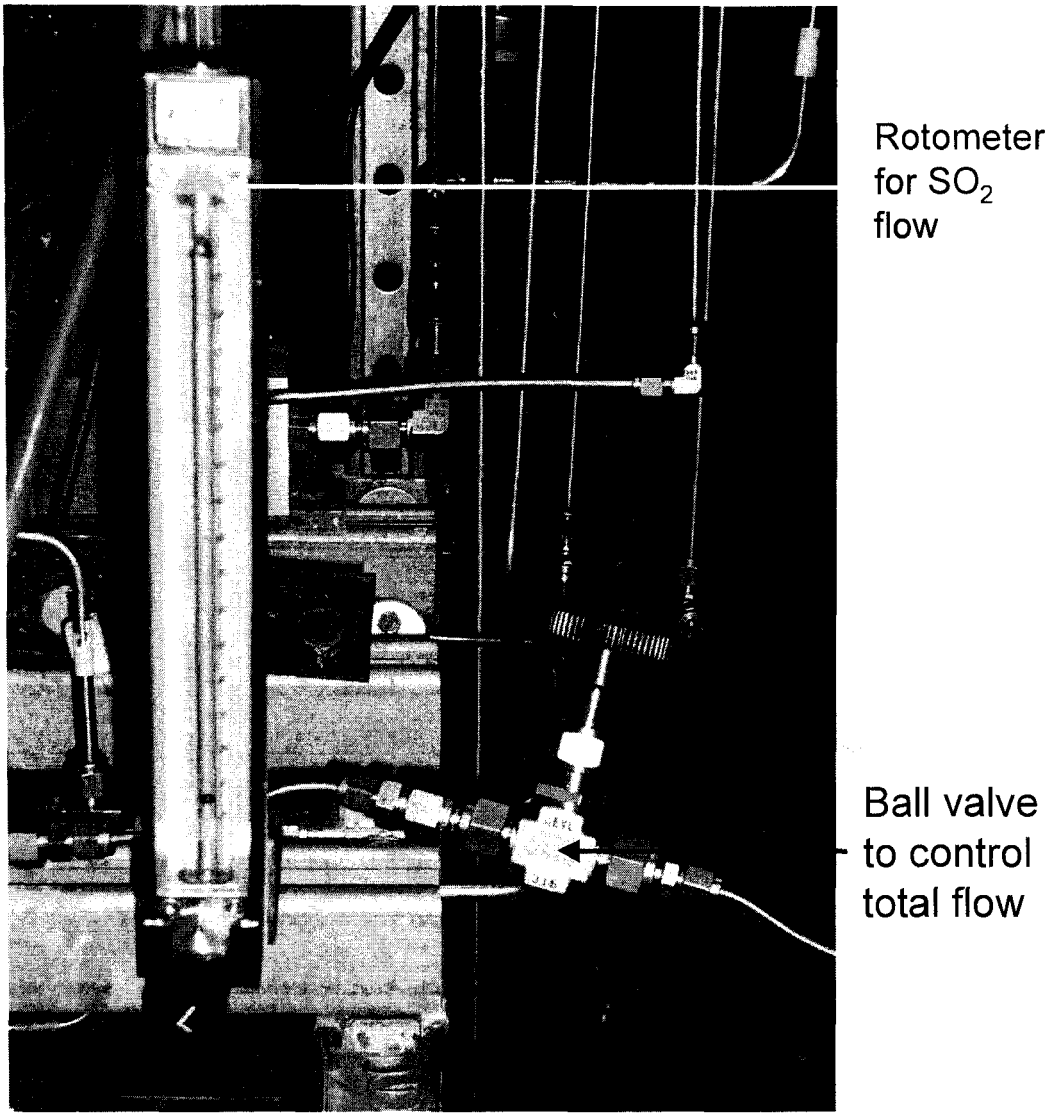

Figure 2.3.9.3-1:
Rotometer and ball valve used for SO_2 flow.

Reproduced with permission of the copyright owner. Further reproduction prohibited without permission.

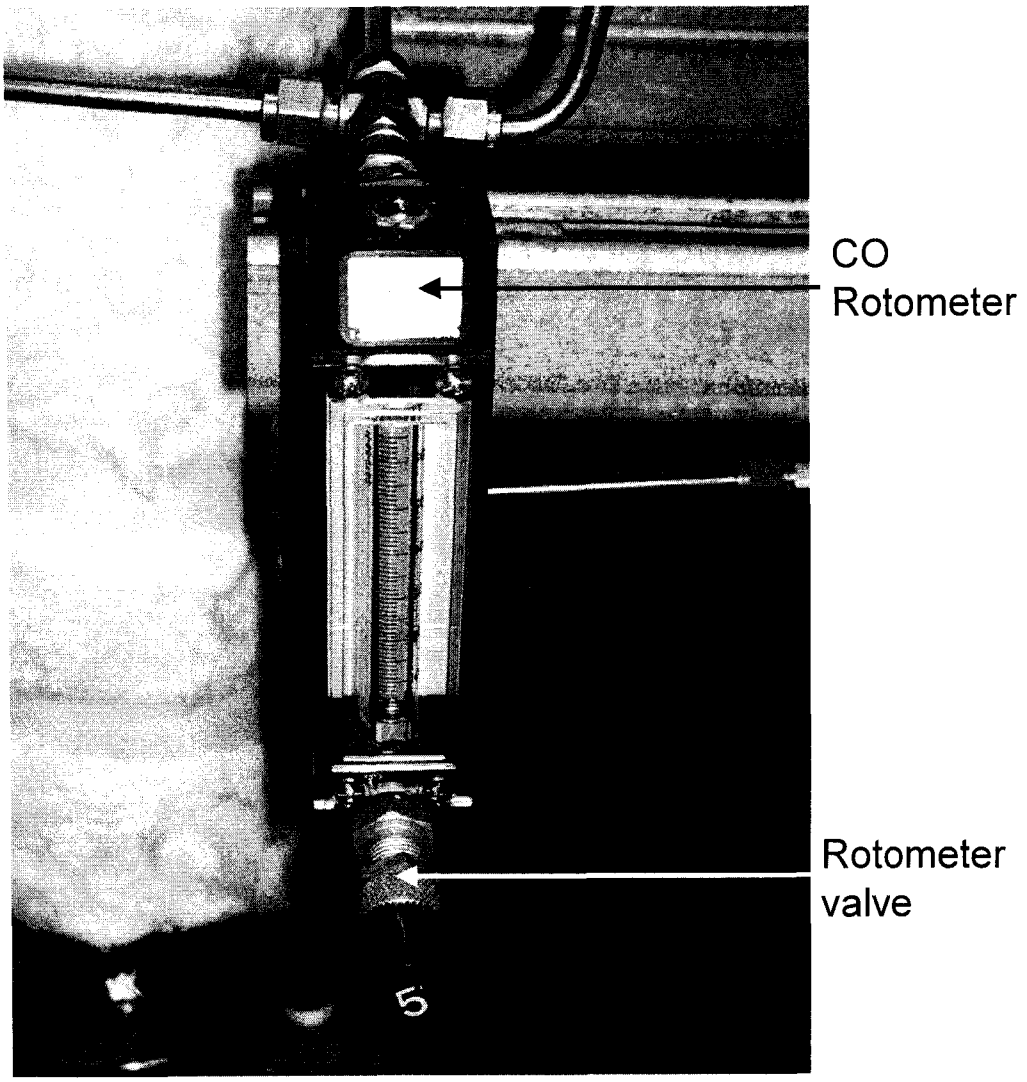

Figure 2.3.9.3-2:
Rotometer used for CO – with built in control valve.

Reproduced with permission of the copyright owner. Further reproduction prohibited without permission.

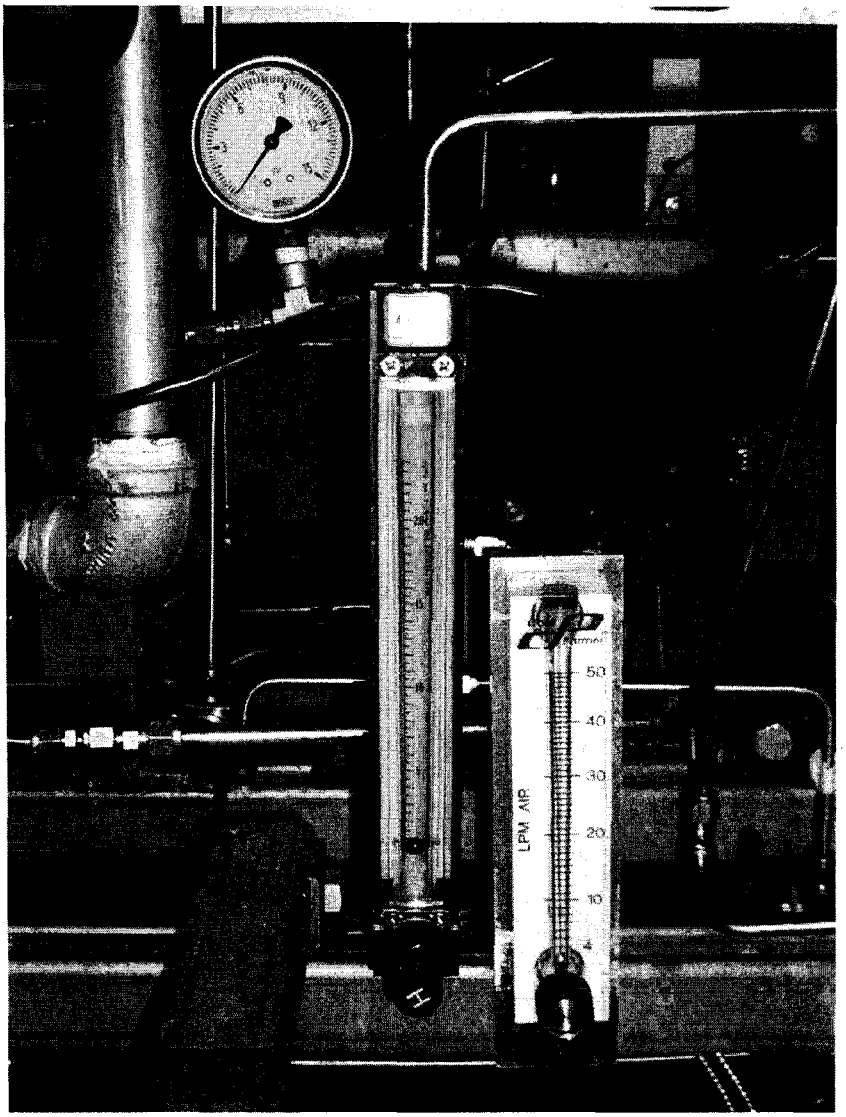

Figure 2.3.9.3-3:
2 Rotometers attached in series to measure air flowrate.

Reproduced with permission of the copyright owner. Further reproduction prohibited without permission.

The rotometers were used to replace the MFCs because they were more corrosion resistant. All the tubes within the rotometers were made of glass, and the concentrations of the gases were not high enough to cause any damage. However, the rotometers were more difficult to control, since they had manual valves. In contrast, MFCs have electronic valves which are more accurate. This resulted in the need to regularly check the rotometers to ensure that the flow of the gas through the tube had not fluctuated significantly. Because of potential fluctuations, the rotometers were more inaccurate than the MFC. For the purposes of this experimental work, the inaccuracies of the rotometers were insignificant and ignored.

2.3.9.4 Combining Gases and Entry Point into R1

Each gas was eventually metered by rotometers. In order to reduce the number of lines connected to R1, the gases were combined into four lines:

i. bulk gas stream consisted of N_2, Air and CO_2
ii. trace gas stream consisted of SO_2, NO and CO
iii. water stream consisted of super heated steam
iv. mercury injection line.

Each line entered at the top of R1, shown in Figures 2.3.9.4-1 and 2.3.9.4-2. The presence of the stainless steel nuts within R1 helped to blend the gases.

Reproduced with permission of the copyright owner. Further reproduction prohibited without permission.

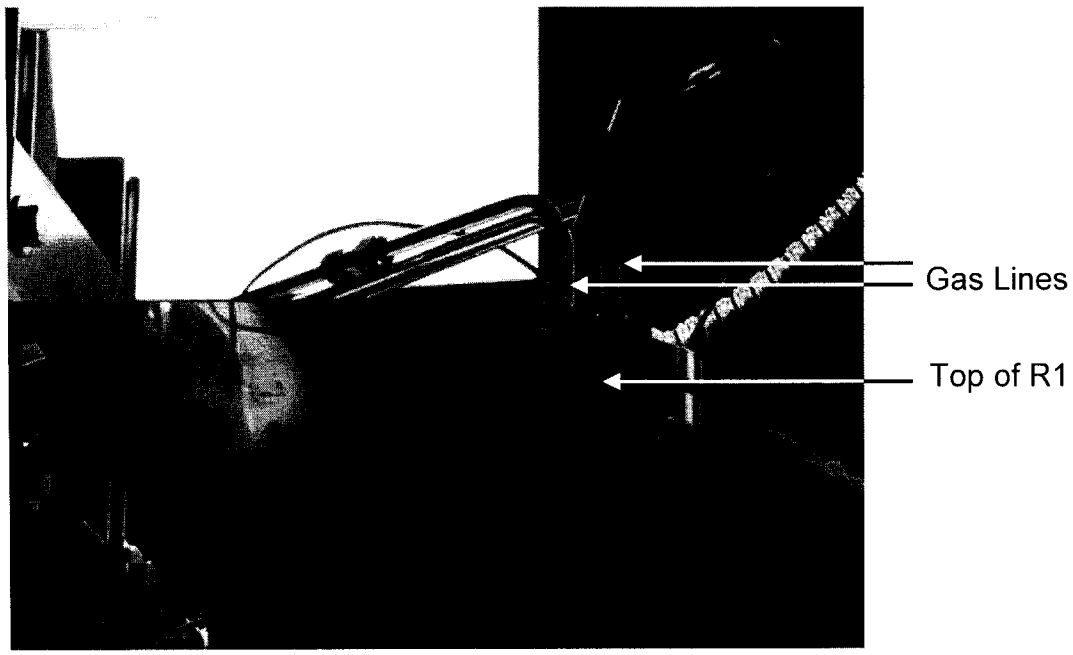

Figure 2.3.9.4-1:
Top view of R1 – entry point of all gases.

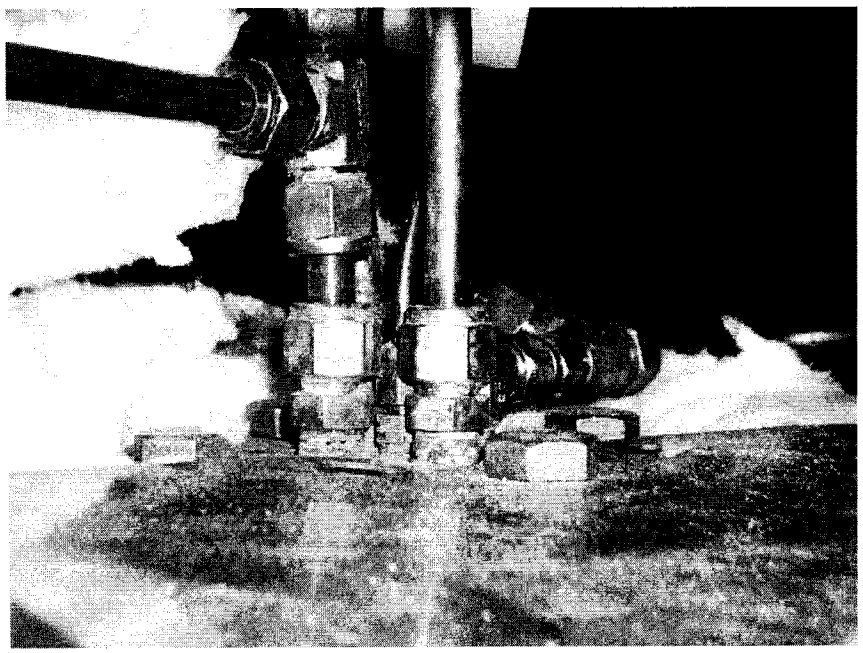

Figure 2.3.9.4-2:
Close up of the top of R1 – entry point of all individual gas streams.

Reproduced with permission of the copyright owner. Further reproduction prohibited without permission.

2.3.9.4.1 Purchasing Information for Gases

Table 2.3.9.4.1-1 lists the gases and the corresponding regulators purchased. All these items were purchased from AirGas in Allentown, PA[177]. The comment column gives more details on the item purchased. Figure 2.3.9.4.1-1 shows some of these gas tanks.

Item	Part Number	Price ($)	Comments
Liquid N_2	NI 180 LT 230	38.22	230 Liters of Liquid N_2. Vaporized to give gaseous N_2.
Liquid N_2 Regulator	ESA-21313	101.71	Used on Liquid N_2 tank
CO_2	CD 50	11.47	Tank of pure CO_2
CO_2 Regulator	APD-3-150-320	229.00	Used on CO_2 tank. Maximum delivery pressure of 150 psig.
10% SO2 / 90% N2	XO2 NI90C15A2018	237.60	Gas tank consists of 10% SO_2 and 90% N_2 mixture.
SO2 regulator	APR-3-150-660	748.25	Used on SO_2 / N_2 tank. Maximum delivery pressure of 150 psig.
Pure SO2	SDAH10	133.64	Tank of pure SO_2
SO2 regulator	Y12 C445D660	491.82	Used on SO_2 tank.
10% NO / 90% N2	XO2 NI90C15AJ211	288.00	Gas tank consists of 10% NO and 90% N_2 mixture
NO regulator	APR-3-150-660	748.25	Used on NO / N_2 tank. Maximum delivery pressure of 150 psig.
1% CO / 99% N2	XO2 NI99C2001415	122.00	Gas tank consists of 1% CO and 99% N_2 mixture
CO regulator	LABE3-125-350	233.40	Used on CO / N_2 tank. Maximum delivery pressure of 125 psig.
1% Cl2 / 99% N2	XO2 NI99C2009231	175.00	Gas tank consists of 1% Cl2 and 99% N_2 mixture
5% Cl2 / 95% N2	XO2 NI95C2002190	286.70	Gas tank consists of 5% Cl2 and 95% N_2 mixture
Cl2 regulator	APR-3-150-330	748.25	Used on Cl_2 / N_2 tanks. Maximum delivery pressure of 150 psig.
Argon	AR Z300	28.00	Argon gas – used for mercury analyzer
Argon regulator	Y12 244F580	220.00	Used on Argon tank. Maximum delivery pressure of 200 psig.
Air (Zero Grade)	AI Z300	15.90	Gas tank consists of 99.0% pure air. Used for mercury analyzer
Air regulator	Y12 244F590	220.00	Used on Air tank. Maximum delivery pressure of 200 psig.

Table 2.3.9.4.1-1: List of Gases and regulators purchased for individual gases.

Reproduced with permission of the copyright owner. Further reproduction prohibited without permission.

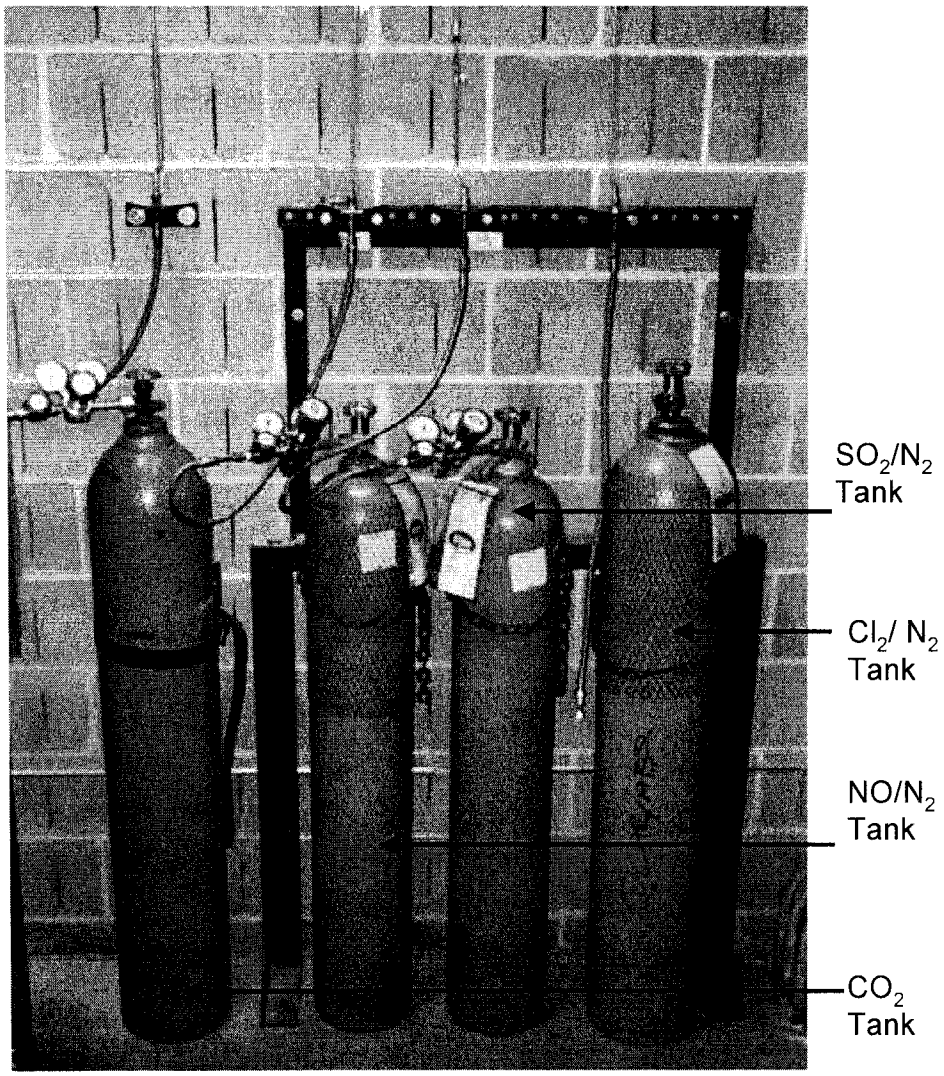

Figure 2.3.9.4.1-1:
Gas cylinders used in the experimental work.

2.3.9.5 Setup for Water Flow

The water injection system was constructed independently of the main apparatus. It was found that adding liquid water into the heated apparatus resulted in large fluctuations of the temperature profile. This procedure was modified and super heated steam (instead of liquid

Reproduced with permission of the copyright owner. Further reproduction prohibited without permission.

water) was injected into R1. In order to get super heated steam, a steam pre heater (SPH) had to be constructed. It had the same design as the APH and is discussed in a previous section.

The SPH was used to vaporize liquid water to super heated steam at temperatures between 100°C and 500°C. Liquid water was pumped via a peristaltic pump at a rate of 10 mlpm. In a flue gas flow of 100 LPM, 10 mlpm of liquid water corresponded to 13.5 LPM of steam. Figure 2.3.9.5-1 shows the pump and the water tank used. The pump was purchased from McMaster Carr Supply Company. The part number was 43205K15 and cost $398.36. Replacement tubes and a pump kit were also purchased from McMaster Carr Supply Company. The part numbers were 43045K22 and 43205K23 respectively. The costs were $13.64 and $34.09 respectively.

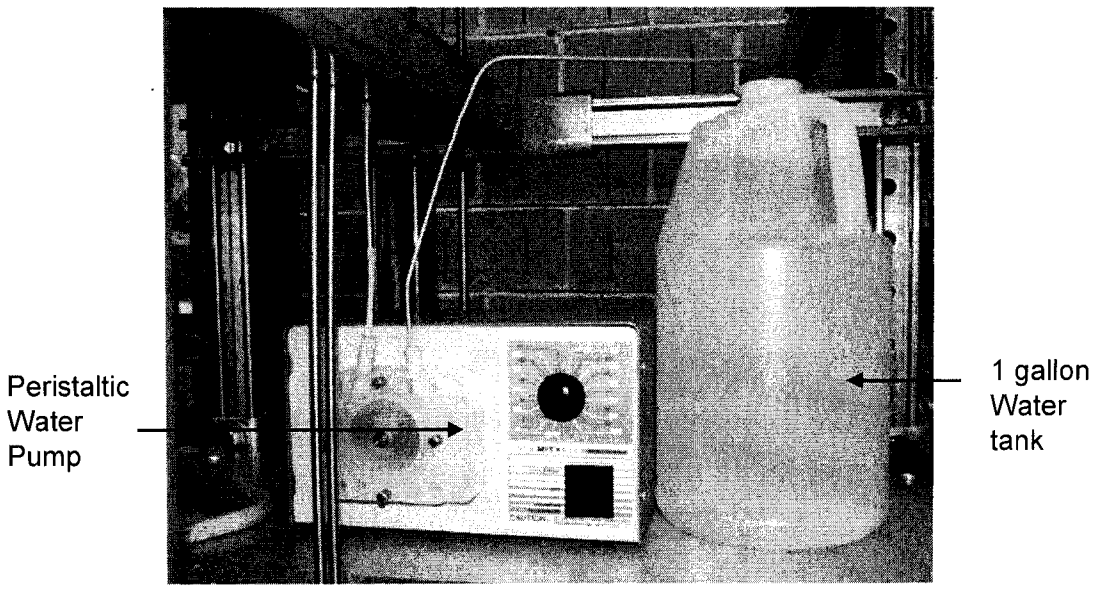

Figure 2.3.9.5-1:
Water delivery system – consisting of water tank and peristaltic pump. Water entered SPH and was vaporized.

2.3.9.6 Frame

The main frame of the apparatus was designed and constructed by Facchiano Iron Works, Inc, in Bethlehem, PA. Figures 2.3.6.1-J and 2.3.6.1-K show the CAD drawings of the frame. The total cost of the frame fabrication was $930.24. It is shown in most of the figures in this chapter. The CAD drawings are shown in Figures 2.3.9.6-A and B.

Reproduced with permission of the copyright owner. Further reproduction prohibited without permission.

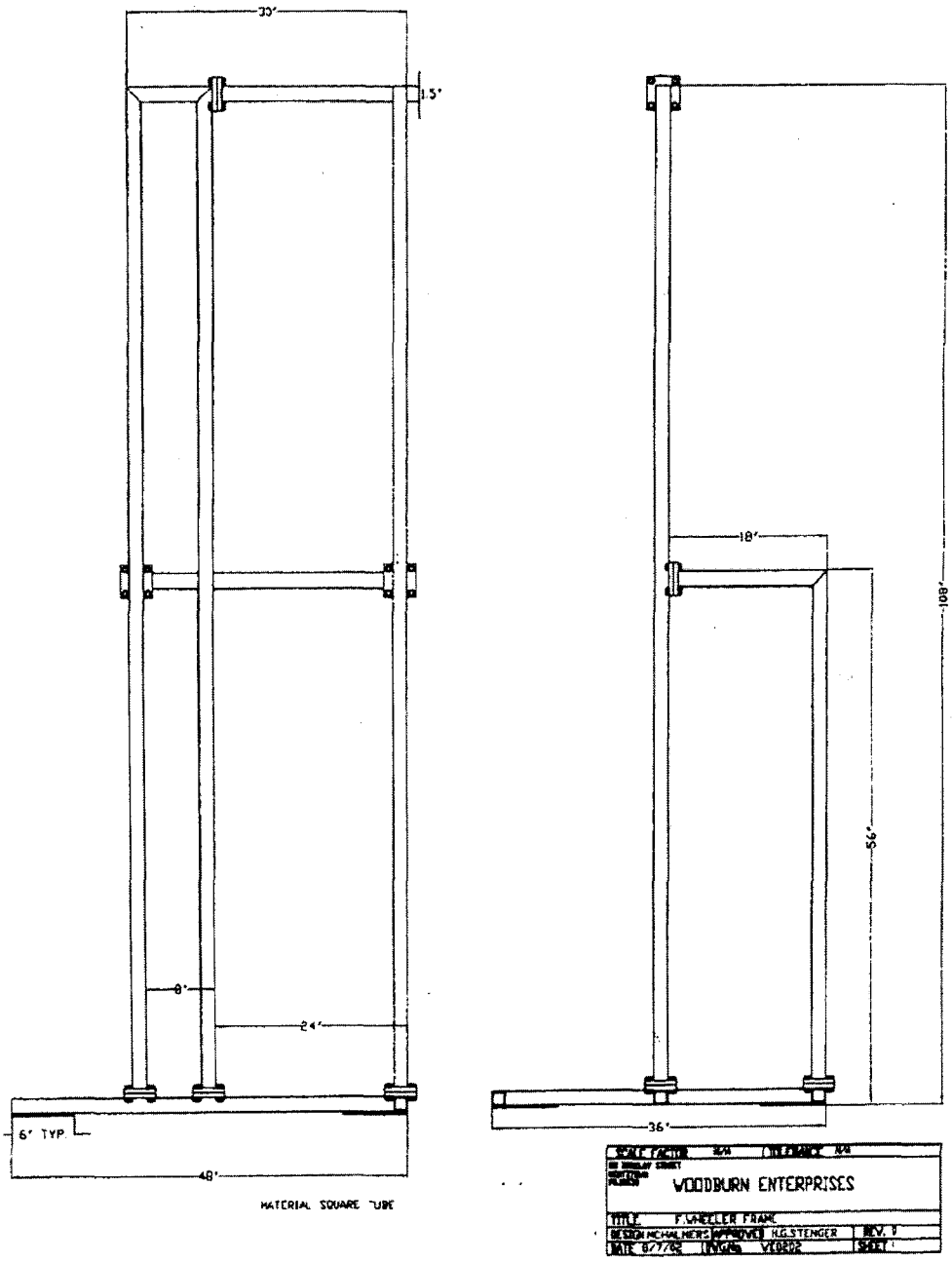

Figure 2.3.9.6-A: CAD drawing of front and side view of frame.

Reproduced with permission of the copyright owner. Further reproduction prohibited without permission.

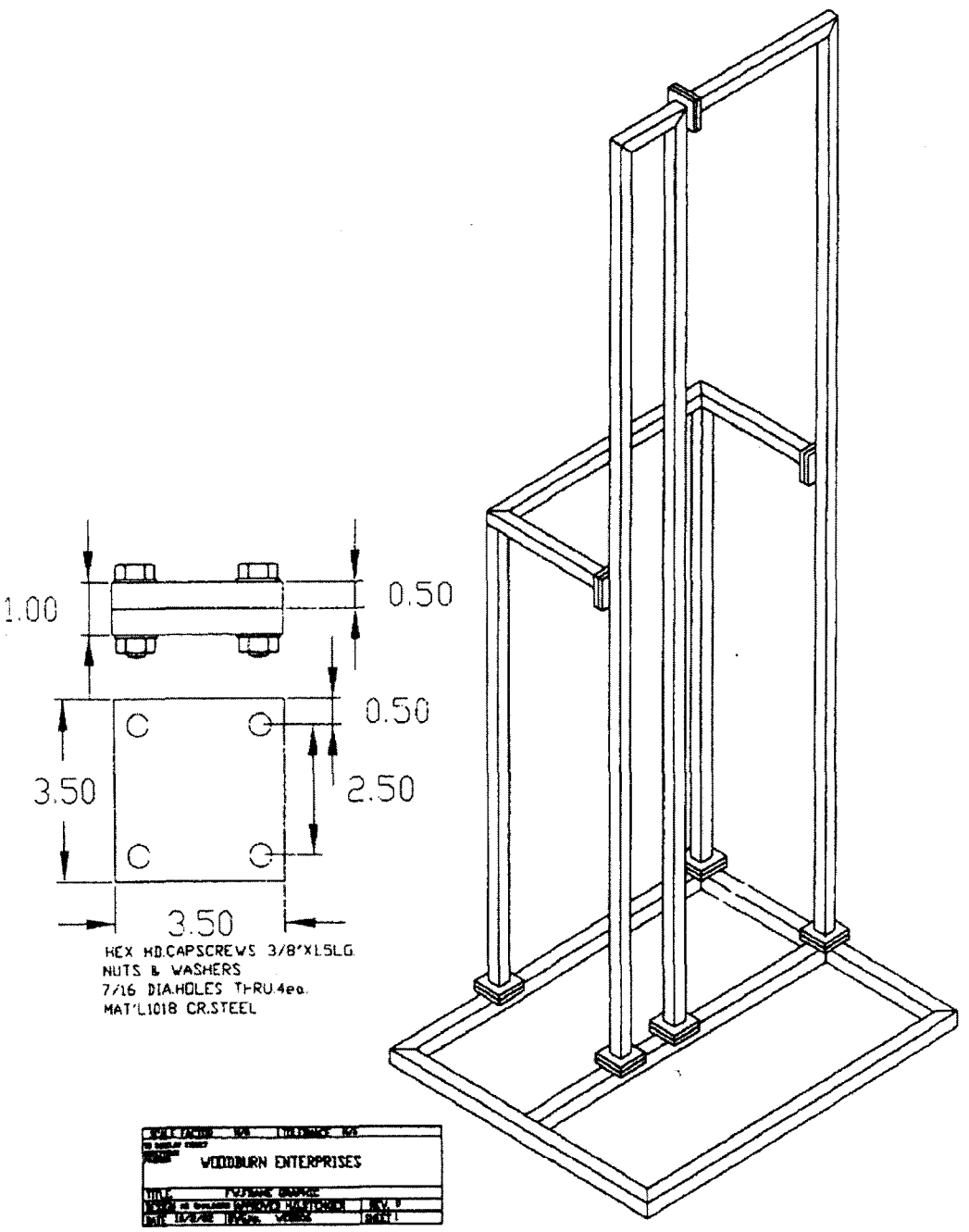

Figure 2.3.9.6-B: CAD drawing of the frame with fittings.

Reproduced with permission of the copyright owner. Further reproduction prohibited without permission.

2.4 Continuous Emissions Monitor (CEM)

This section presents the purpose and use of the mercury analyzer used in this project. It was purchased from the UK and is the PS Analytical 10.525 model[178]. Table 2.4-1 lists the parts of the PSA and other items purchased for it.

Item	Part Number	Vendor	Price ($)	Comments
Sir Galahad II System	PSA 10.525	PSA	39,000	Contained the Gold trap
Online Process Control Software	C210S007	PSA	5,000	Software to control the PSA apparatus
8 Valve Control System (Stream Selector Box)	S665S100/V8	PSA	8,000	Consisted of 8 3-way valves and connectors
Small Scale Conditioner Unit	N001S001	PSA	6,000	The entire conditioning unit
Installation kit for conditioner unit.	N001S002	PSA	500	For installing the conditioner unit
4 Channel Peristaltic Pump	N001S003	PSA	1,500	Peristaltic pump for conditioner unit
Laptop PC for the system	Z586C006	PSA	2,500	Computer to control the entire apparatus
Mercury Vapor Calibrator (CAVKIT)	PSA 10.534	PSA	7,250	CAVKIT unit for elemental mercury delivery
Amasil Gold Sand Trap	G525T004	PSA	635.50	Gold trap for Sir Galahad
Yellow Cones	Z312007	PSA	21.00	Yellow cones similar to ferrules for SS Box tubing
1/8" Tubing for SS Box	Z018T024	PSA	33.50	1/8" replacement tubing
Fan Motor Kit	2FNM-001	Baldwin Inc.	112.50	Motor kit for heater of hot box
Fan Blade Kit	2FNB-001	Baldwin Inc.	3.15	Blade kit for heater of hot box
Pressure-Lock	050031	VICI	68.00	0-250 micro

Reproduced with permission of the copyright owner. Further reproduction prohibited without permission.

Analytical Syringe		Precision Sampling Inc		liter syringe for gas sampling
Sodium Hydroxide	S318-10	Fisher Scientific	82.57	10 kg bucket of NaOH pellets for making impinger solutions
Potassium Chloride	P217-3	Fisher Scientific	49.11	3 kg bottle of KCl pellets for making impinger solutions
Tin (II) Chloride	AA11536A3	Fisher Scientific	135.01	2 kg bottle of SnCl2 powder for making impinger solutions

Table 2.4-1: List of all items purchased for the Continuous Emission Mercury Monitor system.

Reproduced with permission of the copyright owner. Further reproduction prohibited without permission.

2.4.1 *Comparison of PSA to other CEMs*

Several mercury analyzers were compared before the purchase of the PSA model. This section will briefly describe the other analyzers considered. Note that some of the descriptions were valid as of 2001 to 2002. Since the purchase of the PSA analyzer, better and more accurate technology has been developed in the measurements of mercury (total or elemental). As a result, most of this information may be outdated.

The most important factors taken into account in deciding the analyzer purchased are as follows:

i. Flexibility – the analyzer itself had to be portable since there was a possibility of moving the sample lines to different locations on the apparatus.

ii. Durability – the analyzer did not necessarily need to be capable of handling harsh power plant conditions, since it was to be used only in a laboratory setting.

iii. Detection method – at the time of purchase, the amalgamation of mercury on a gold trap seemed to be the most popular and effective means of detecting mercury.

iv. Detection limit – since operating conditions required a mercury concentration of approximately 15μg/m^3, a detection limit of at least 0.05 μg/m^3 was desirable. Several analyzers had detection limits much higher than this.

v. Cost – cost was an issue since some of the analyzers were much too expensive for our conditions and settings.

vi. Speciation – since most of experimental work incorporated the homogeneous oxidation of mercury, it was required that the analyzer be able to distinguish between oxidized mercury and elemental mercury. Several of the analyzers did not have that capability.

vii. Sample time – most analyzers at that time were incapable of instantaneous mercury measurement. They required a certain amount of run-time to process any sample.

viii. Continuous measurement – it was required that the analyzer be an automated continuous monitoring system, as opposed to manually measuring individual samples.

Reproduced with permission of the copyright owner. Further reproduction prohibited without permission.

Tekran Model 1130[179]: The Tekran model had the ability to speciate the mercury. Additionally, it made use of atomic fluorescence to detection mercury concentrations. However, the detection limits were not easily available and the cost of the model was beyond the allotted budget. Few field tests had been done on this model, but none at the laboratory scale.

ADA Technologies[180]: ADA Technologies provided an analyzer that was capable of speciating mercury. The detection limits were less than 1 $\mu g/m^3$, which was higher than the desirable limit. It made use of a thermal converter and an ultraviolet absorption cell. However, the accuracy of this new technology was unclear. Few field tests had been done on this model, but none at the laboratory scale.

GmbH Analytical Technology: This analyzer was based in Germany. It made use of a thermo-catalytic reactor to convert ionic mercury to elemental mercury. As a result of this in-built system, it was impossible to tell how much oxidized mercury was present in the gas stream, since all would have been converted to elemental mercury. This analyzer was installed mainly in Germany, and the detection limits on this model were unclear.

Nippon Instruments Model AM-2[181]: This analyzer was based in Japan. There were two different types of analyzers. The first made use of a reduction catalyst, which had a lifespan of a month or less. The second made use of gold in the amalgamation process and a scrubber to remove harmful trace gases such as SO_2 and NO. However, both types were able to detect only elemental mercury. Additionally, maintenance costs would have been higher than the allowable budget since the catalyst would have to be replaced monthly. No detection limits were available and no reports on the application of these models were found.

Ohio Lumax Company[182]: The Ohio Lumax Company provided an analyzer that made use of the differential atomic absorption spectroscopy technique. Oxidized mercury was reduced and the

Reproduced with permission of the copyright owner. Further reproduction prohibited without permission.

total mercury was measured. Therefore, it would not have been possible to tell how much oxidized mercury was present in the gas stream. No detection limits were available, and no reports on the effectiveness of these analyzers were found.

Senova Corporation: Senova Corporation offered an analyzer with a detection limit of less than 1 $\mu g/m^3$. It made use of a catalytic converter and micro-sensor technology. As a result of this technology, it was not able to speciate between oxidized and elemental mercury. It was also used mainly in power plant settings and not in a laboratory setting.

Most of these analyzers were not able to fulfill the requirements of our experimental work. As a result, the PSA analyzer was chosen. It had the ability to speciate elemental and oxidized mercury. The detection limit was 0.05 $\mu g/m^3$. It also made use of a gold trap to amalgamate the mercury and an atomic fluorescent detector to detect the presence of elemental mercury. Additionally, there were several reports from laboratory settings that suggested the analyzers usefulness, flexibility and cost.

2.4.2 Details of the PSA

This section will give more details on the different parts of PSA analyzer and the uses. The entire analyzer is shown and labeled in Figure 2.4.2-1.

Reproduced with permission of the copyright owner. Further reproduction prohibited without permission.

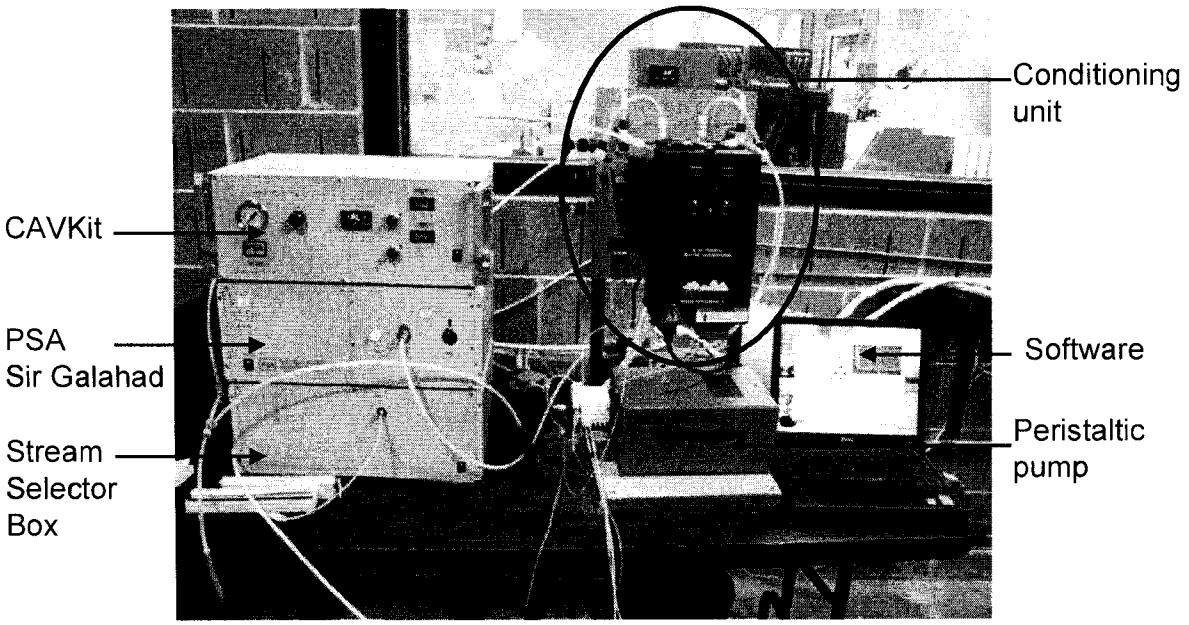

Figure 2.4.2-1: Picture of entire PSA Hg CEM setup.

2.4.2.1 Conditioning Unit

The conditioning unit is shown in Figure 2.4.2.1-1. The unit consists of the hot box, impinger unit, chiller unit and a peristaltic pump (shown in Figure 2.4.2-1).

Reproduced with permission of the copyright owner. Further reproduction prohibited without permission.

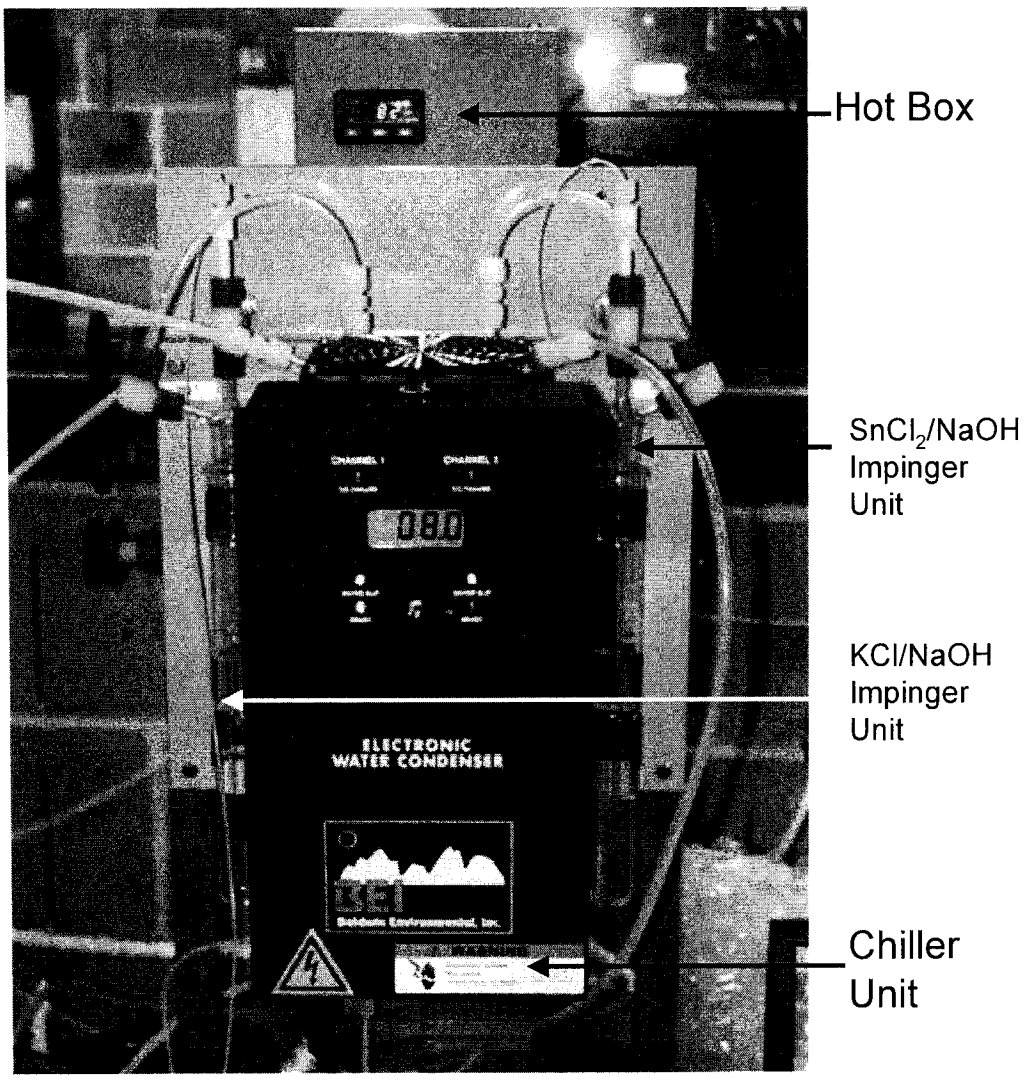

Figure 2.4.2.1-1:
Close up of conditioning unit of PSA Hg CEM analyzer.

2.4.2.1.1 Hot Box

The hot box temperature was maintained at 350°C. The sample gas entered the hot box and was split into two streams, one for each impinger pair. Each stream was further divided into two sub-streams. One of these sub-streams was vented. The other sub-stream entered the

Reproduced with permission of the copyright owner. Further reproduction prohibited without permission.

impinger unit. A schematic of the hot box is shown in Figure 2.4.2.1.1-1. The other purpose of the hot box (aside from splitting the streams) is to maintain a constant temperature of the sample at 350°C to minimize any water condensation from taking place. The heating unit is shown in Figures 2.4.2.1.1-2 and 2.4.2.1.1-3.

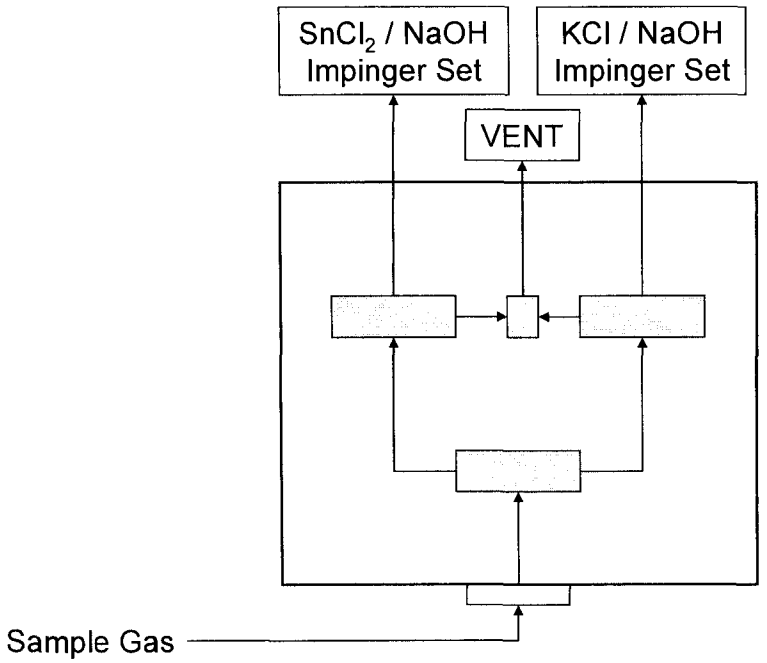

Figure 2.4.2.1.1-1:
Schematic of Hot box. Sample stream is split twice before entering impingers.

Reproduced with permission of the copyright owner. Further reproduction prohibited without permission.

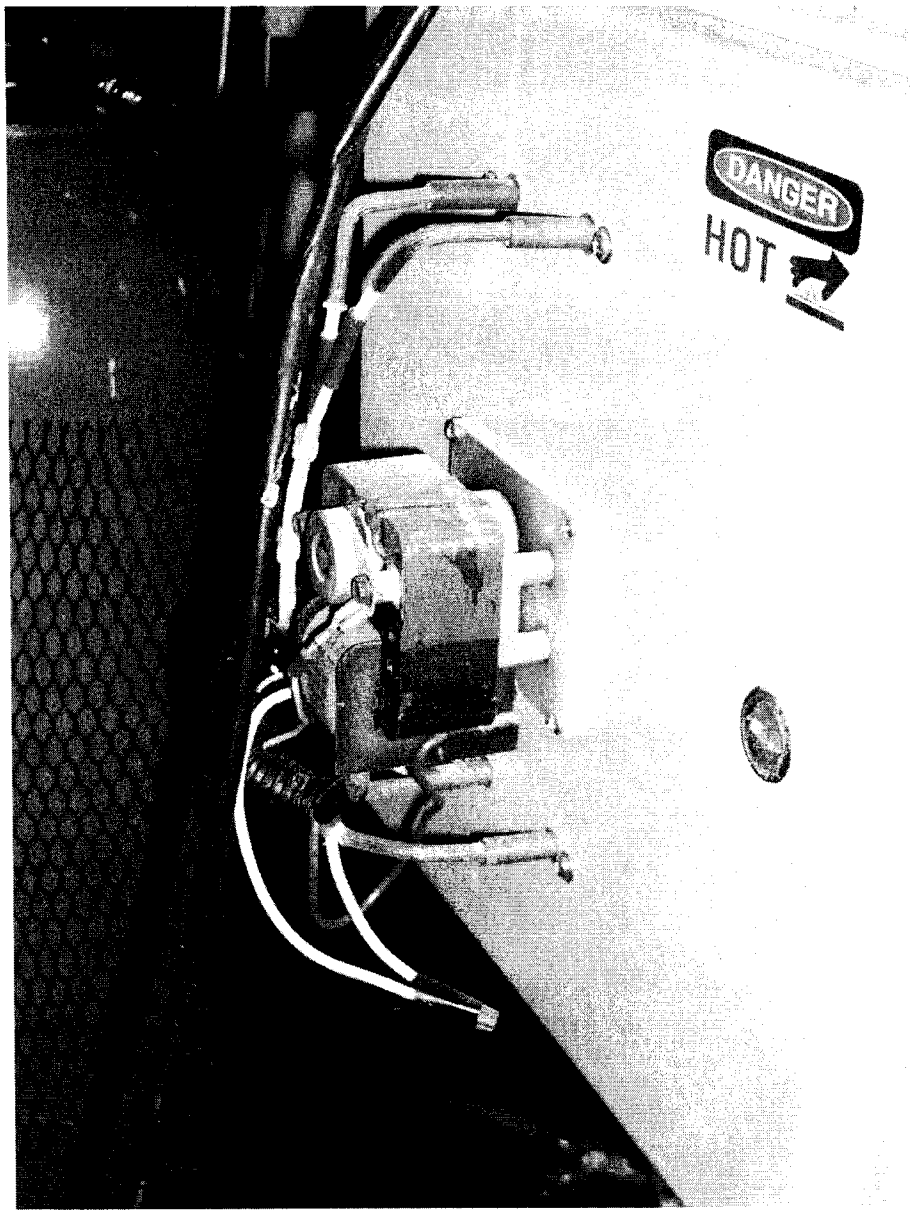

Figure 2.4.2.1.1-2: Heating element of the hot box.

Reproduced with permission of the copyright owner. Further reproduction prohibited without permission.

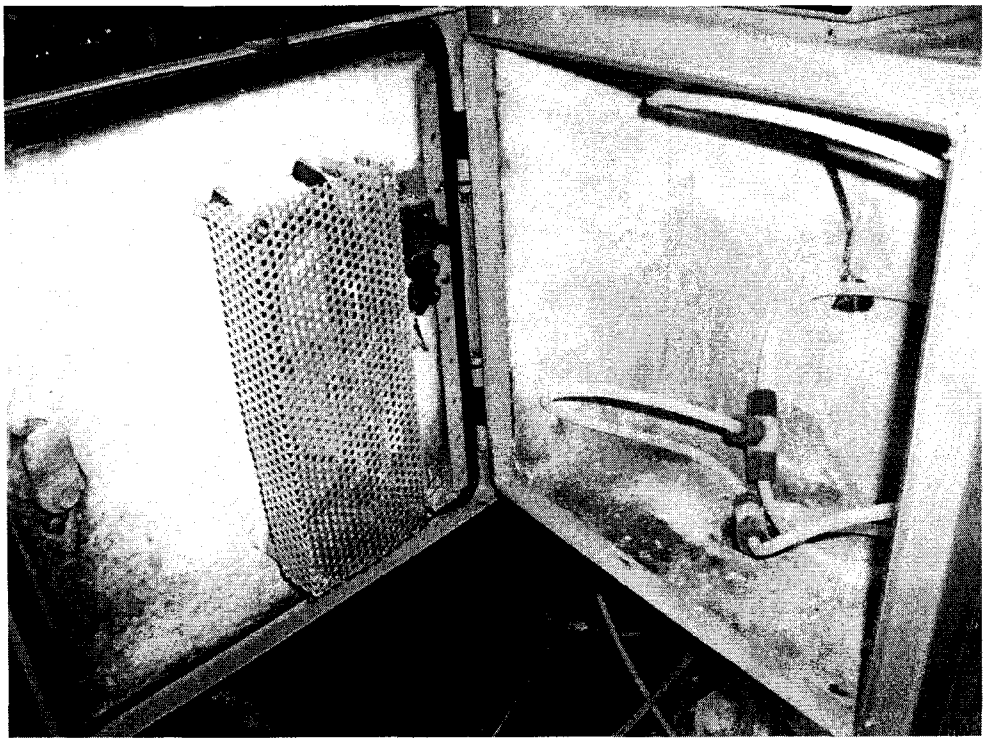

Figure 2.4.2.1.1-3:
Interior of the hot box – shows heating fan and some Teflon tubing.

2.4.2.1.2 Impinger units

There are 2 pairs of impinger units (a total of 4 impingers) present in the conditioning unit. In each pair, one impinger is filled with a solution, and the other is cooled in the chiller unit. This is shown in Figure 2.4.2.1.2-1.

The solution present in the first pair consists of 2% tin (II) chloride (SnCl2) by weight and 20% sodium hydroxide (NaOH) by weight. The purpose of this solution is to reduce any oxidized mercury to its elemental form. It is speculated that the Sn^{2+} is oxidized to Sn^{4+} in the presence of $HgCl_2$. In the process, Hg^{2+} is reduced to Hg^0. NaOH in the solution helps to remove any acidic trace gases (such as SO2 and NO) from getting to the analyzer. The amount of mercury measured from this gas stream represents the total mercury present in the gas stream.

Reproduced with permission of the copyright owner. Further reproduction prohibited without permission.

The solution present in the second pair consists of 10% potassium chloride (KCl) by weight and 10% NaOH by weight. The purpose of this solution is to remove any oxidized mercury species present in the gas stream. NaOH removes the acidic trace gases. The amount of mercury measured from this gas stream is the elemental mercury present in the gas stream. The difference between the total and elemental mercury measurements will be the amount of mercury oxidized in the gas stream.

After passing through the solutions, the gas streams then flow through the second impinger where moisture is removed by condensation. The sample gases then flow into the next unit of the analyzer called the Stream Selector Box.

Reproduced with permission of the copyright owner. Further reproduction prohibited without permission.

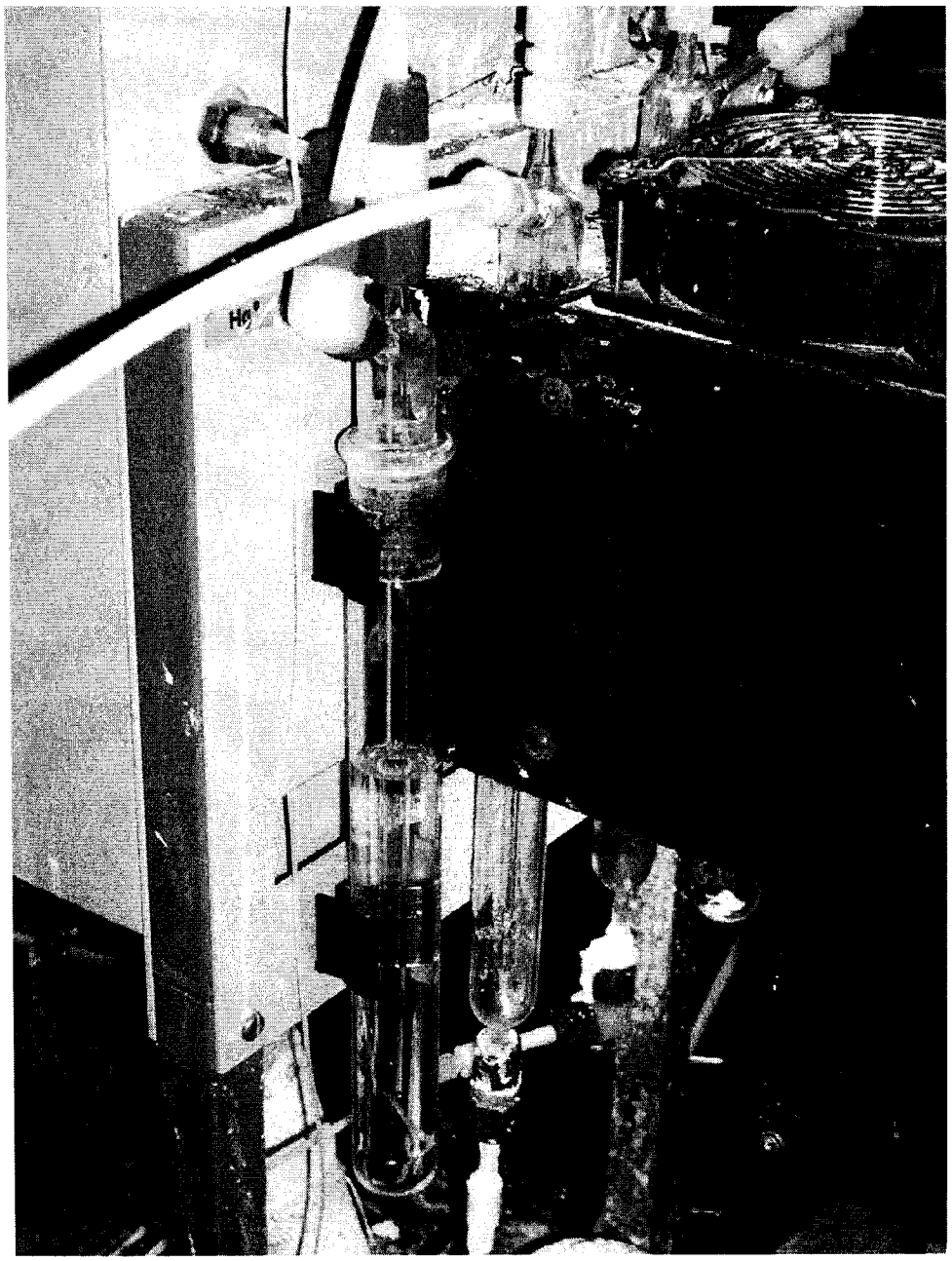

Figure 2.4.2.1.2-1: Close up of impinger unit.

Reproduced with permission of the copyright owner. Further reproduction prohibited without permission.

2.4.2.1.3 Chiller Unit

The purpose of the chiller unit is to ensure that the second impingers in each pair remain at temperatures below 4°C. This would allow all the moisture present in the gas stream to condense out before the gas stream enters the analyzer. It is shown in Figure 2.4.2.1-1.

2.4.2.1.4 Peristaltic Pump

The peristaltic pump serves two purposes. The first is to feed solution to each of the impinger units continuously. This allows the solutions in the impingers to be refreshed continuously during experimentation. Second, the pump also removes any discarded solution and condensed water from the impingers. It is shown in Figures 2.4.2.1.4-1 and 2.4.2-1.

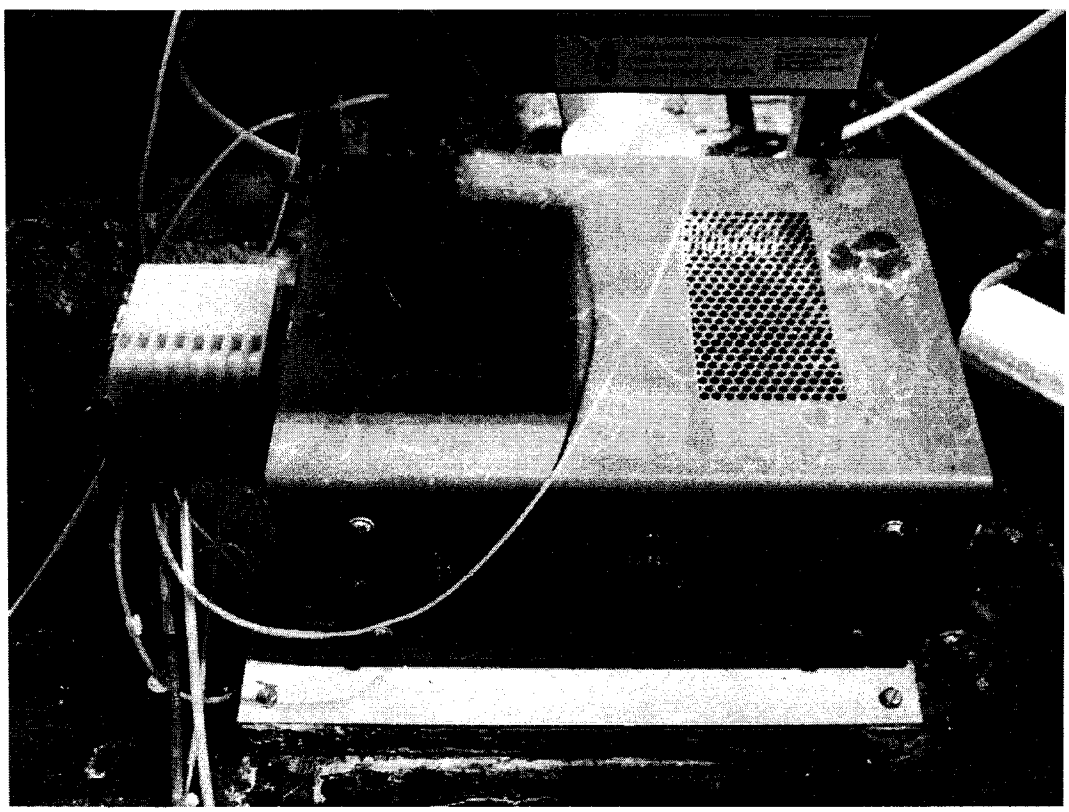

Figure 2.4.2.1.4-1: Close up of peristaltic pump.

Reproduced with permission of the copyright owner. Further reproduction prohibited without permission.

2.4.2.2 Stream Selector Box

The stream selector (SS) box consists of an arrangement of several electrically controlled 3-way valves and tubes (Figure 2.4.2.2-4). The gas stream from the impingers enters the SS Box and is channeled either to the vent or to the Sir Galahad Analyzer. A schematic of the SS Box is shown in Figure 2.4.2.2-1. The functioning of the 3-way valve is shown in Figure 2.4.2.2-2. Figure 2.4.2.2-2A shows that the gas stream is directly vented when the valve is not electrically charged. When the valve is charged with 12 volts, the valve switches to the open position, and the gas stream enters the analyzer. This is shown in Figure 2.4.2.2-2B.

These valves operate simultaneously since at any time there are two sample gas streams entering the SS Box. The analyzer is able to measure the mercury content in only one gas stream at a time. As a result, one of the valves is always in the position shown in Figure 2.4.2.2-2A, where the gas stream is completely vented. The other valve is always in the position shown in Figure 2.4.2.2-2B, where the gas stream is always entering the analyzer. This setup is also shown in Figure 2.4.2.2-3 and 2.4.2.2-4.

Since the analyzer requires only 250 milliliters of gas for sampling purposes, the remainder of the sample gas stream is vented. This takes place in the cross-junction labeled in Figure 2.4.2.2-1.

In order to reduce any mercury losses in the SS Box, the tubes connecting the valves and the cross junction are made of Teflon and are 1/8" in diameter.

Reproduced with permission of the copyright owner. Further reproduction prohibited without permission.

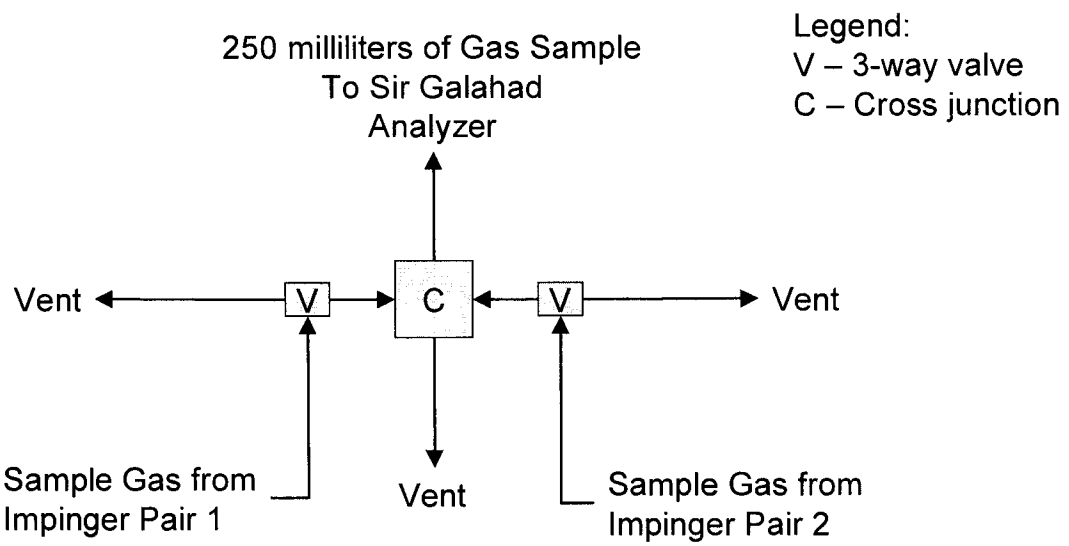

Figure 2.4.2.2-1: Schematic of interior of Stream Selector Box.

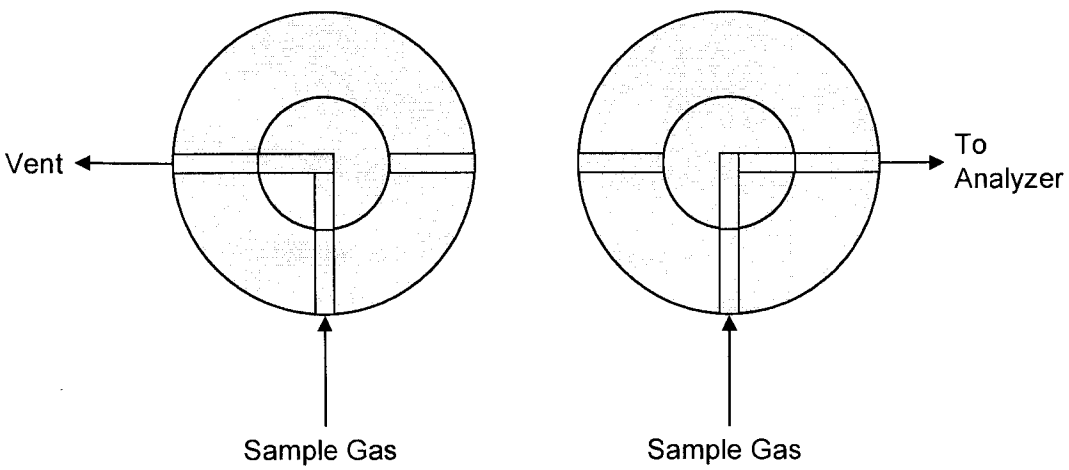

Figure A

Figure B

Figure 2.4.2.2-2:
Schematic of the 3-way valve in Stream Selector Box.

Reproduced with permission of the copyright owner. Further reproduction prohibited without permission.

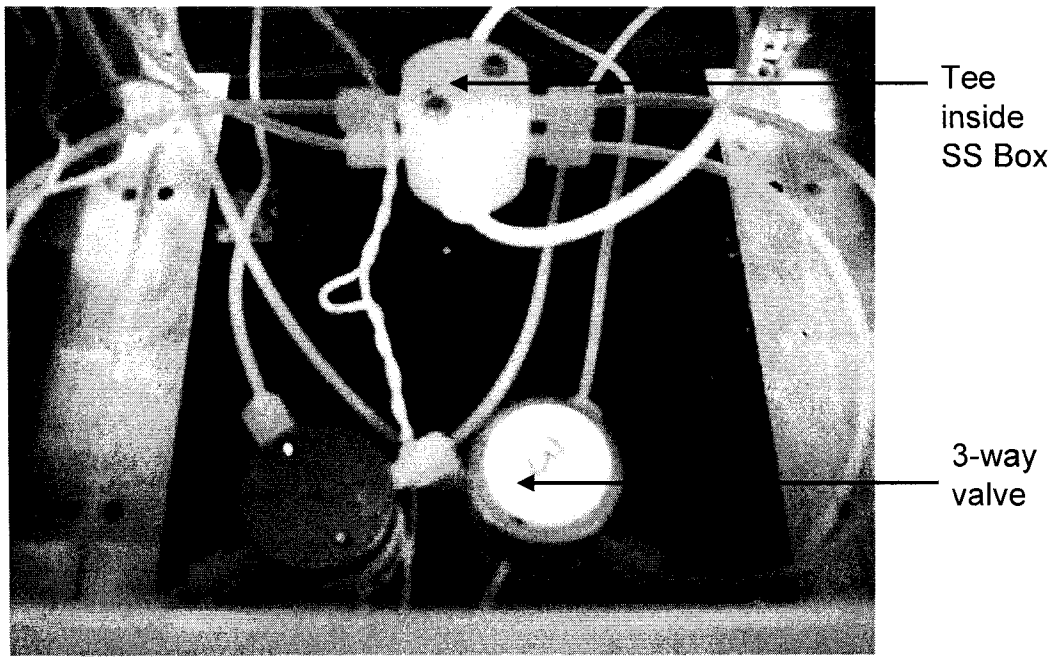

Figure 2.4.2.2-3: Close up of the interior of the Stream Selector Box.

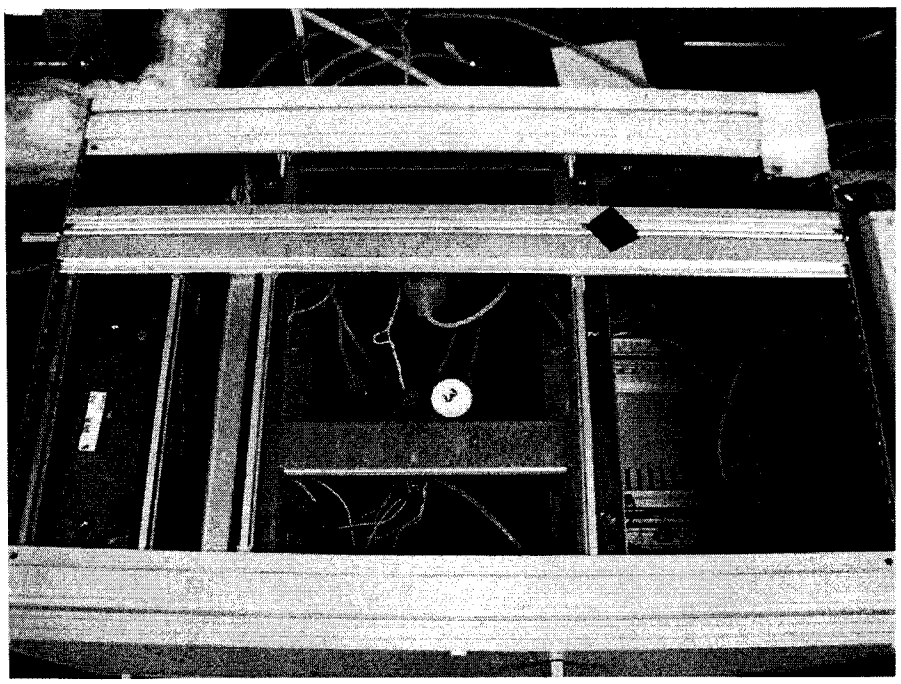

Figure 2.4.2.2-4: Interior of the Stream Selector Box.

Reproduced with permission of the copyright owner. Further reproduction prohibited without permission.

2.4.2.3 Sir Galahad Analyzer

The Sir Galahad Analyzer (10.525) was used in this experimental work to detect elemental mercury concentrations in the gas stream (Figure 2.4.2.3-2). It consists of a gold trap which amalgamates with any elemental mercury present in the gas stream. The interior of the Sir Galahad is shown in Figure 2.4.2.3-3. A closeup of the gold trap is shown in Figures 2.4.2.3-4 and 2.4.2.3-5. Upon heating to 800°C, photons are released from the amalgamated gold trap and are detected by a fluorescent detector. A calibration done prior to experimental work is used to determine mercury concentration based on the amount of fluorescence detected. In between runs, the gold trap is frequently flushed with an inert gas – Argon. This helps to clean the trap of any residual mercury that may remain on the gold trap. Additionally, argon provides an inert environment for amalgamation and fluorescence to be accurately read.

Since 250 milliliters of gas are required for sampling, a rotometer is used to control the volume of gas flowing into the analyzer. This is shown in Figure 2.4.2.3-1.

The calibration process is described in the next section.

Reproduced with permission of the copyright owner. Further reproduction prohibited without permission.

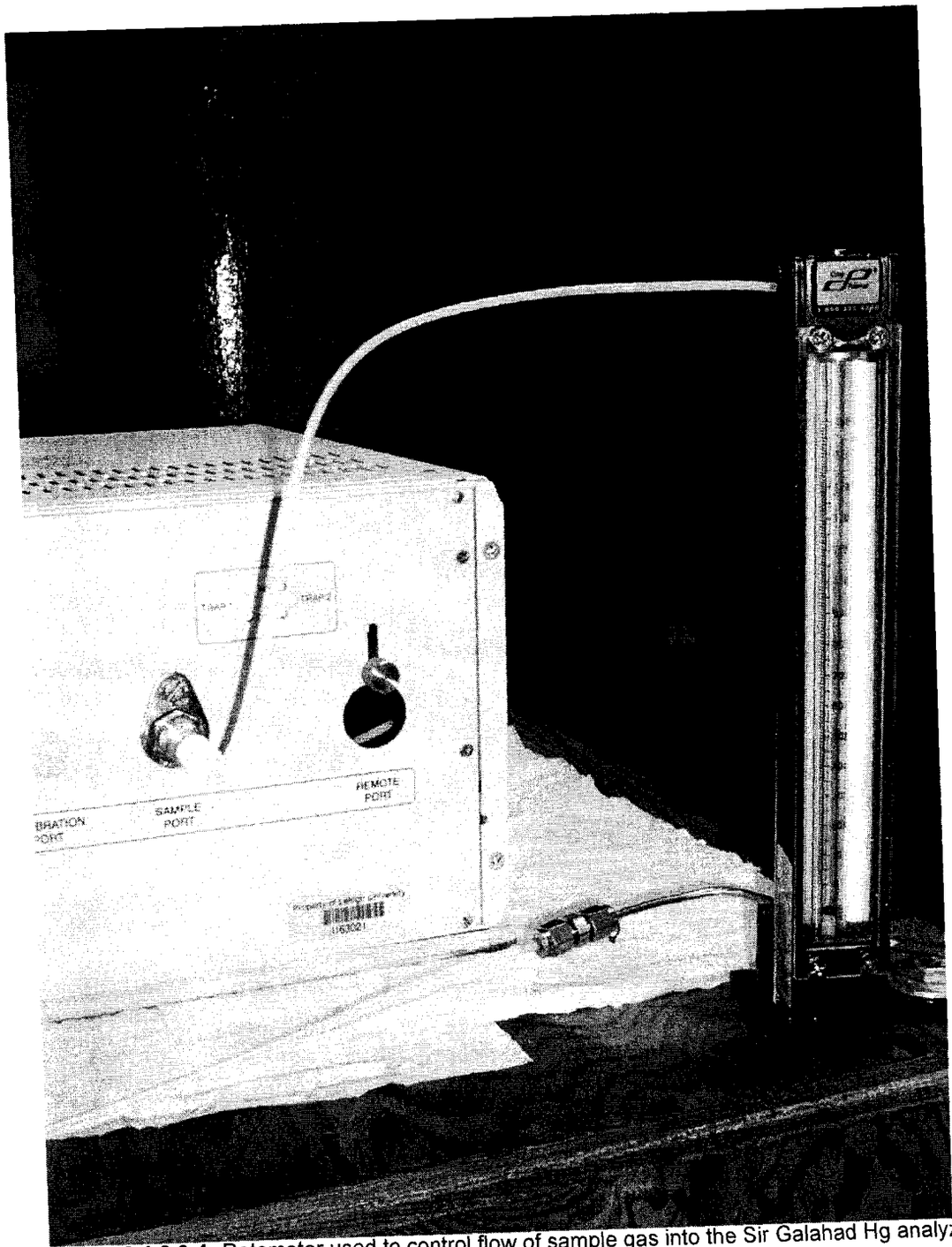

Figure 2.4.2.3-1: Rotometer used to control flow of sample gas into the Sir Galahad Hg analyzer.

Reproduced with permission of the copyright owner. Further reproduction prohibited without permission.

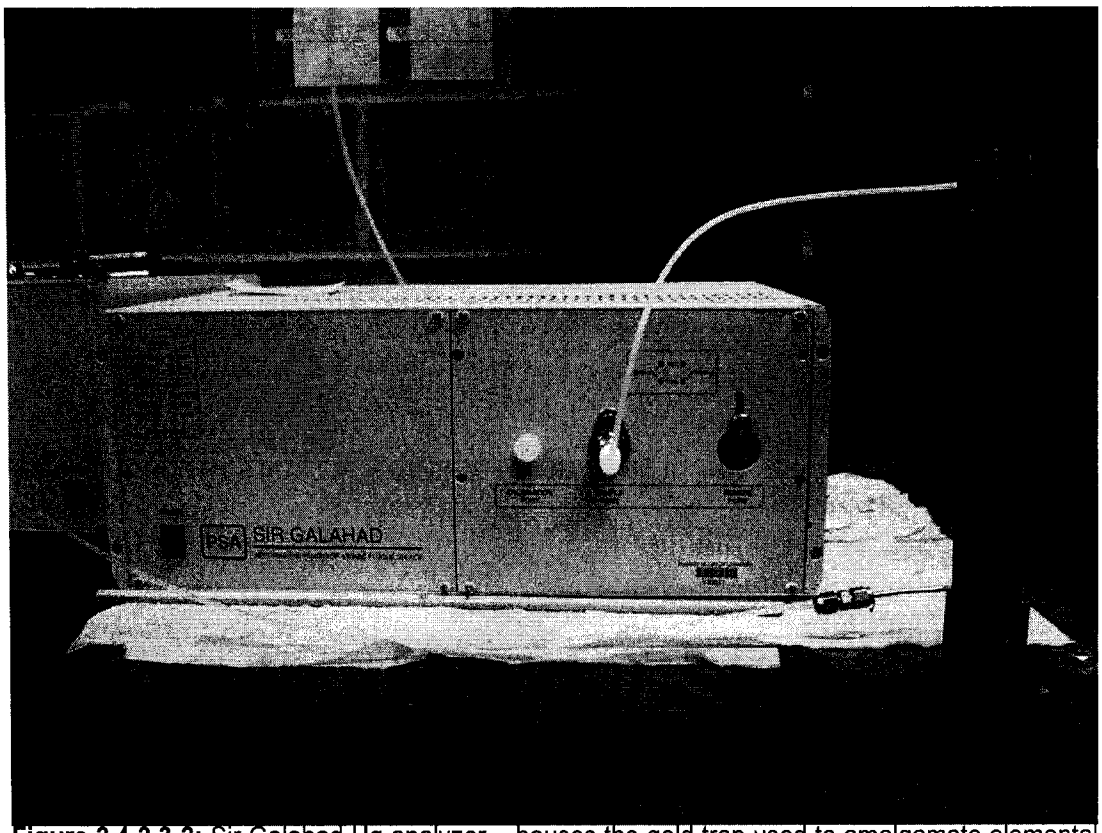

Figure 2.4.2.3-2: Sir Galahad Hg analyzer – houses the gold trap used to amalgamate elemental Hg. Also contains fluorescent detector.

Reproduced with permission of the copyright owner. Further reproduction prohibited without permission.

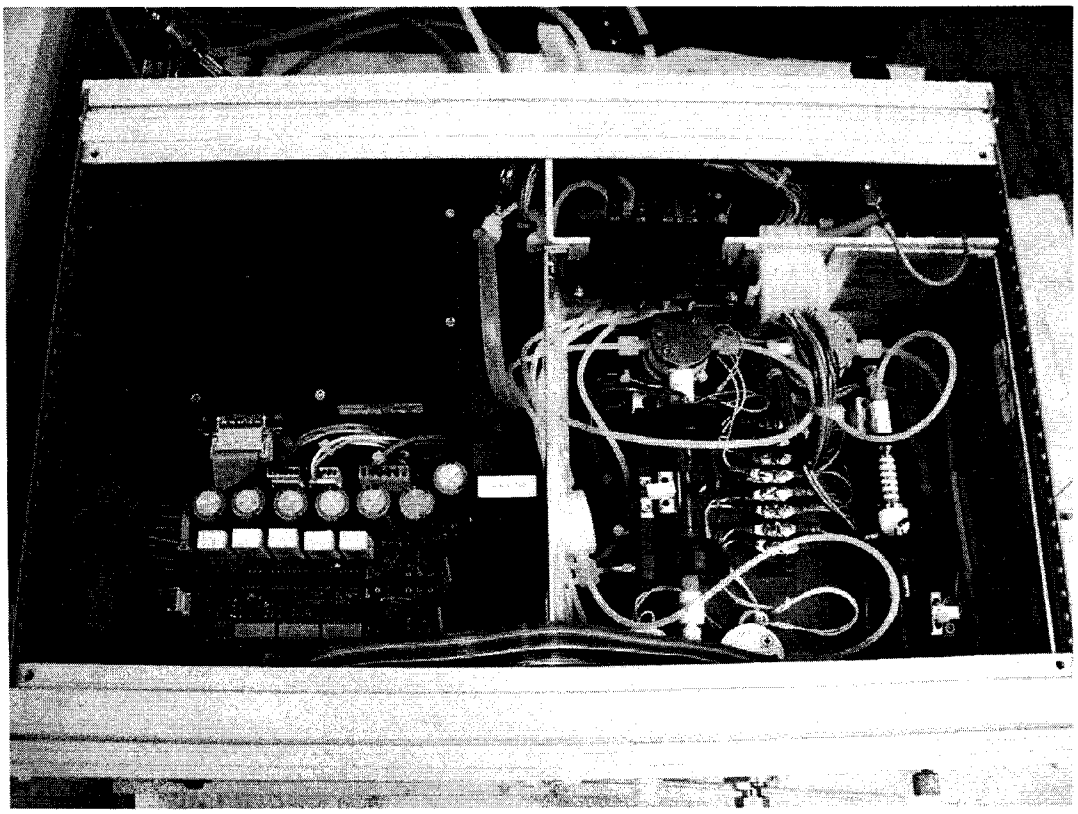

Figure 2.4.2.3-3: Interior view of Sir Galahad.

Reproduced with permission of the copyright owner. Further reproduction prohibited without permission.

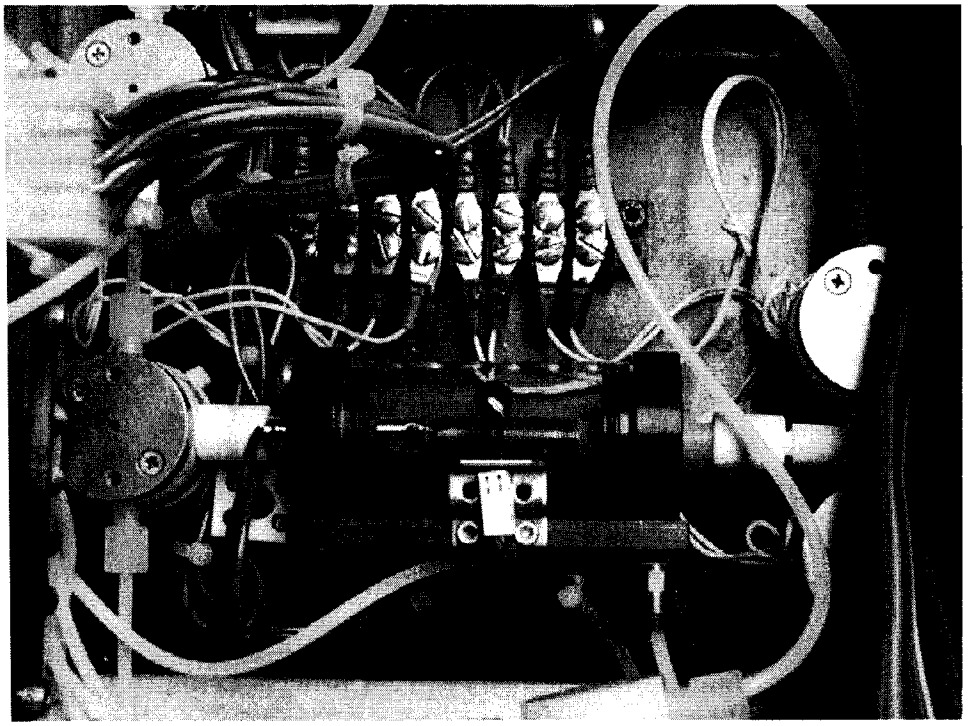

Figure 2.4.2.3-4: Close up of gold trap within Sir Galahad.

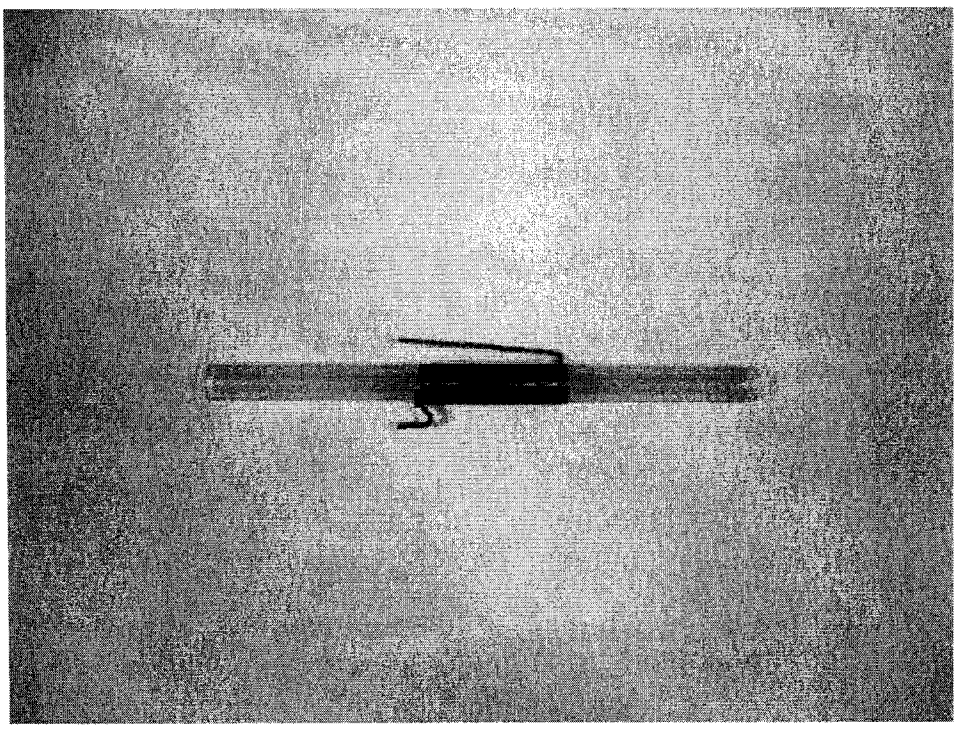

Figure 2.4.2.3-5: Close up of gold trap.

Reproduced with permission of the copyright owner. Further reproduction prohibited without permission.

2.4.2.3.1 Calibration of Sir Galahad Analyzer

The SCEM device is regularly calibrated. A known volume of air with a known concentration of elemental, vapor phase Hg at a measured ambient temperature is injected into the gold trap via a pressure-lock syringe shown in Figure 2.4.2.3.1-2. The syringe samples an air space, via a septum, above liquid mercury in a closed container. This setup is shown in Figure 2.4.2.3.1-1. Because the concentration in the air space is fixed by temperature, the amount of elemental Hg injected into the analyzer can be varied by varying the sample volume. The analyzer records the peak height and area as detected by the fluorescent detector, for each sample. The PSA software plots the peak height or area (as specified by the user) versus the amount of elemental Hg injected. Typically, four mercury amounts were used for the calibration of these experiments: 0, 1, 2, and 5 nanograms (ng). When analyzing unknown gases, typically a sample volume of 250 milliliters is used, which if it contained 5 nanograms, would correspond to a concentration of 20 $\mu g/m^3$.

Reproduced with permission of the copyright owner. Further reproduction prohibited without permission.

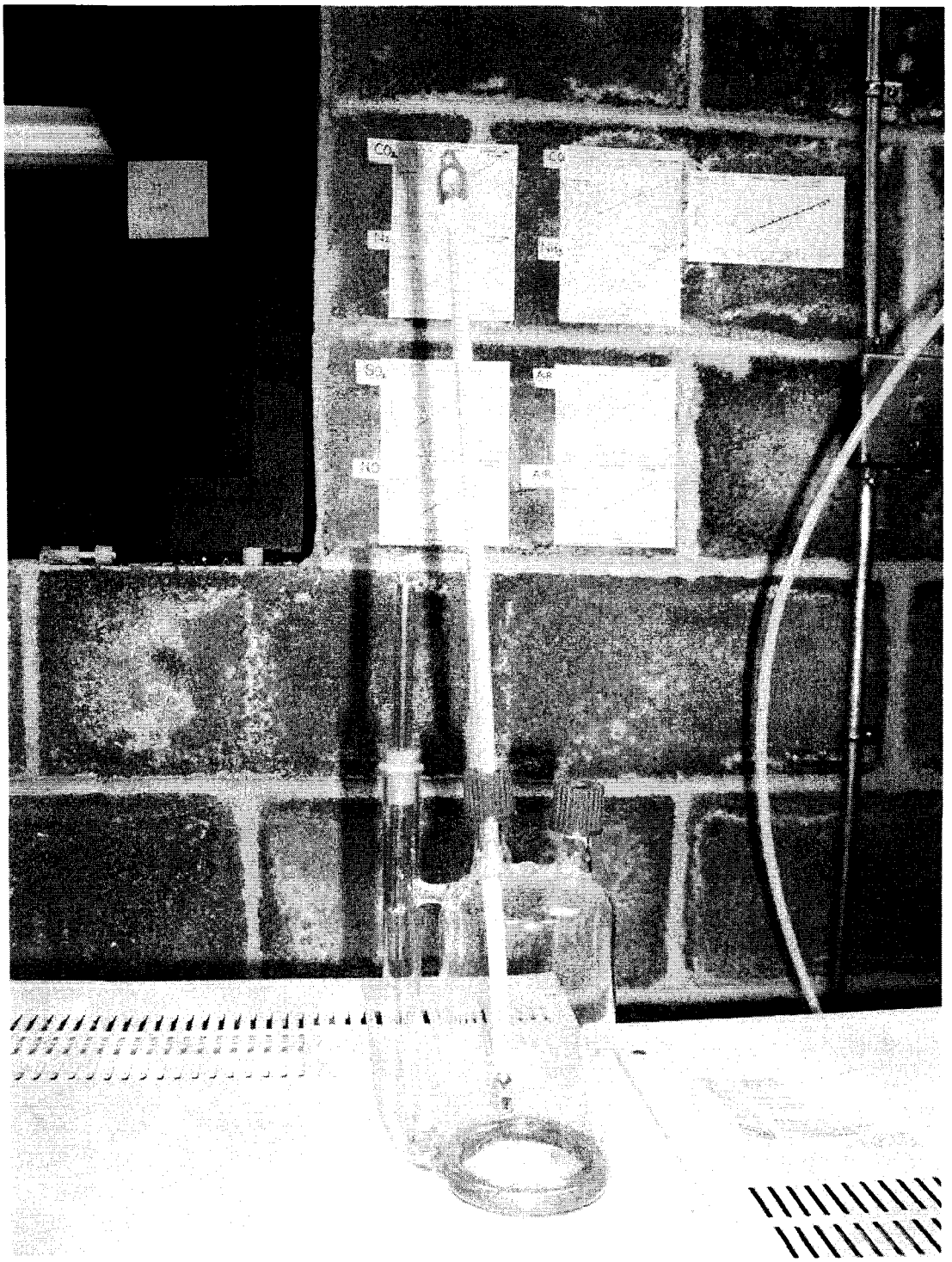

Figure 2.4.2.3.1-1: Mercury contained in a closed container. Used for calibrating Sir Galahad.

Reproduced with permission of the copyright owner. Further reproduction prohibited without permission.

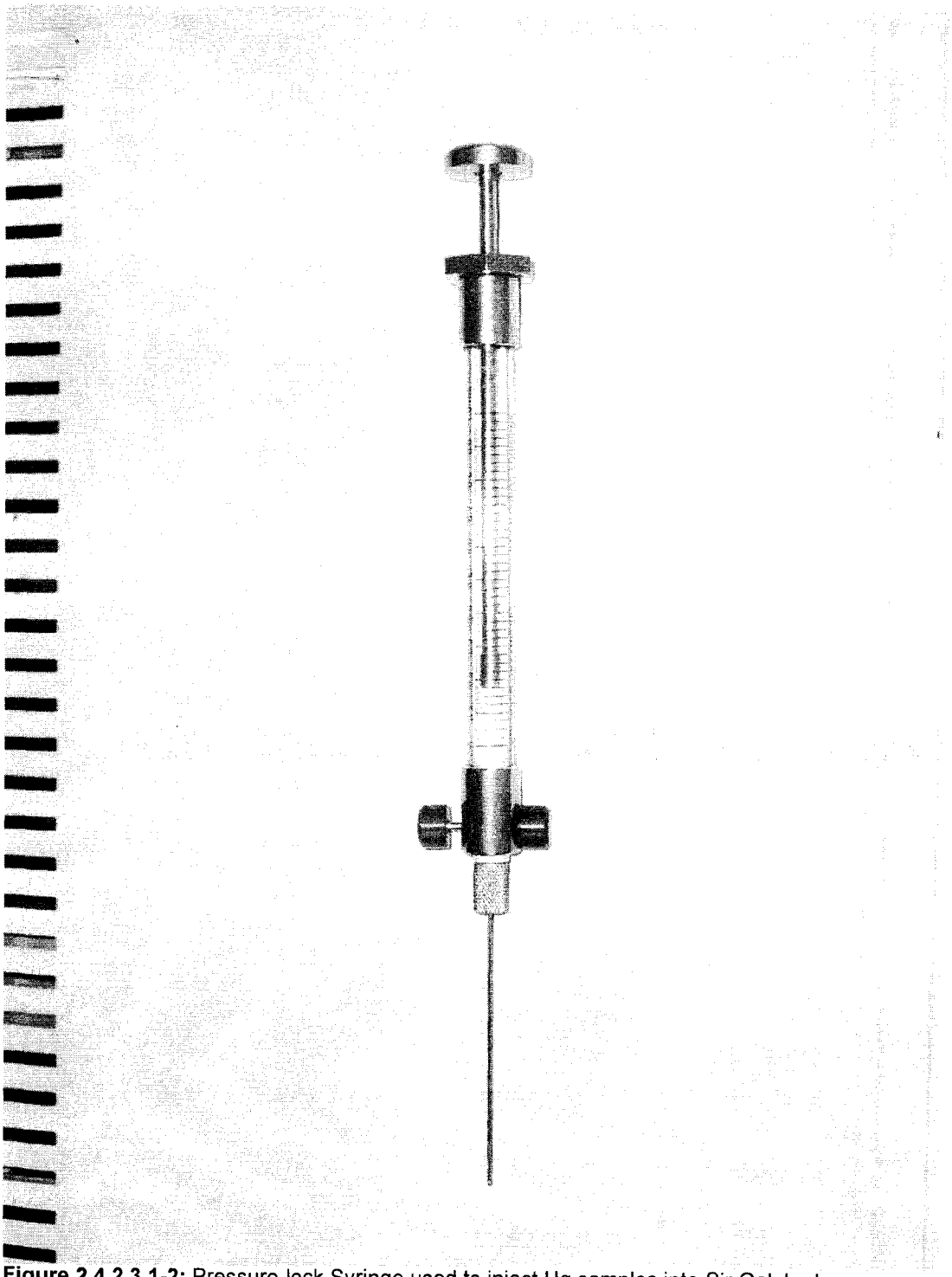

Figure 2.4.2.3.1-2: Pressure-lock Syringe used to inject Hg samples into Sir Galahad.

Reproduced with permission of the copyright owner. Further reproduction prohibited without permission.

2.4.2.4 CAVKIT

The third section of the analyzer is the CAVKIT (Figure 2.4.2.4-1). It consists of a reservoir of elemental mercury. A small flow of N2, called 'reservoir flow', passes over the reservoir and carries the vaporized elemental Hg. The amount of elemental Hg carried by the reservoir flow depends on the temperature of the reservoir – where a higher temperature will result in a higher concentration of elemental Hg in the gas stream. This stream is then diluted by a larger N2 stream called 'dilution flow'. This combined stream flows into the main apparatus. For example, a temperature of 45°C, a reservoir flow of 18 mlpm and a dilution flow of 5 standard liters per minute (slpm), when mixed with the other gases in the apparatus, will result in an approximate elemental Hg concentration of 10μg/m^3.

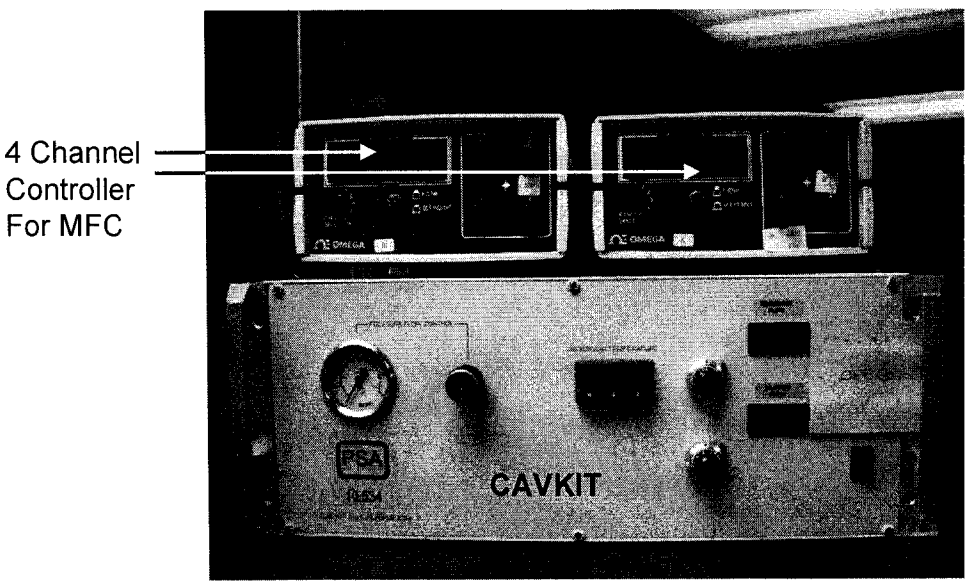

Figure 2.4.2.4-1:
Close up of CAVKIT – used to supply constant amounts of elemental Hg.

Reproduced with permission of the copyright owner. Further reproduction prohibited without permission.

2.4.2.5 Software

The PSA software was used to control the valves in the Stream Selector Box and the Sir Galahad analyzer itself. The software alternated between the valves in the SS box and allowed the appropriate sample to enter the gold trap. The software also recorded the concentration of the mercury in the gas stream based on the calibration curve. Each run was approximately 5 minutes long and consisted of the following process (Table 2.4.2.5-1):

Time (seconds)	Comment
3	Pre Flush – Check Analysis Gas
4	Pre Flush – Check Cooling Gas
5	Pre Flush – Check
60	Allow Gas onto Trap
61	Check
120	Finish Collection Time – Start Flush
121	Check
122	Baseline Measure Start
145	Baseline Measure Stop
150	Heat
151	Peak Measure Start
165	Heat Off
166	Start Cool
167	Check
280	Peak Measure Stop
285	Finish Cool

Table 2.4.2.5-1: Procedure of the 5 minute cycle for each sample point.

Figures 2.4.2.5-1 to 2.4.2.5-11 show the various pages of the software.

Reproduced with permission of the copyright owner. Further reproduction prohibited without permission.

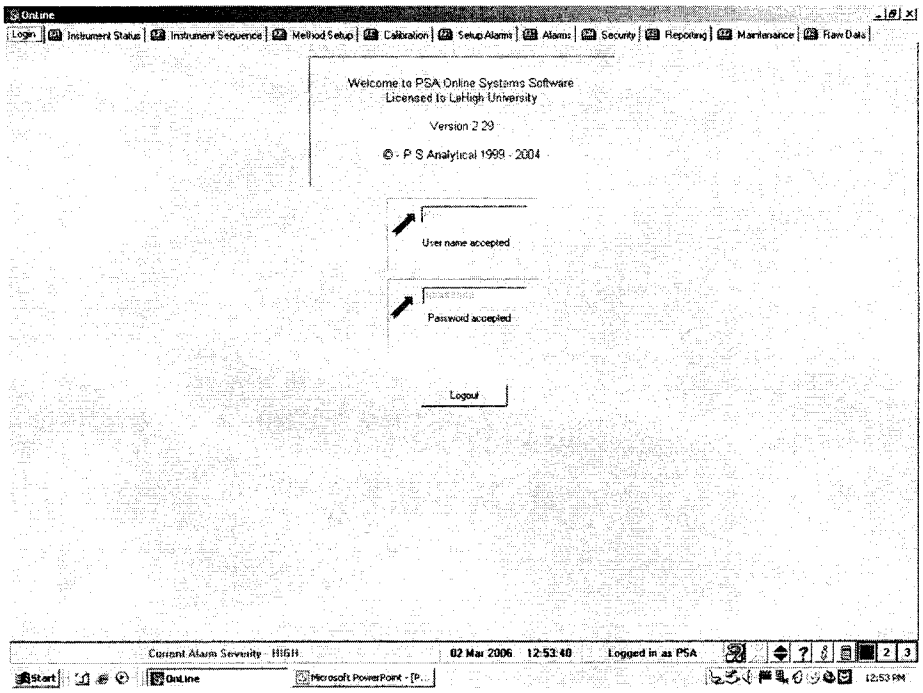

Figure 2.4.2.5-1: PSA Software Page 1 – login page.

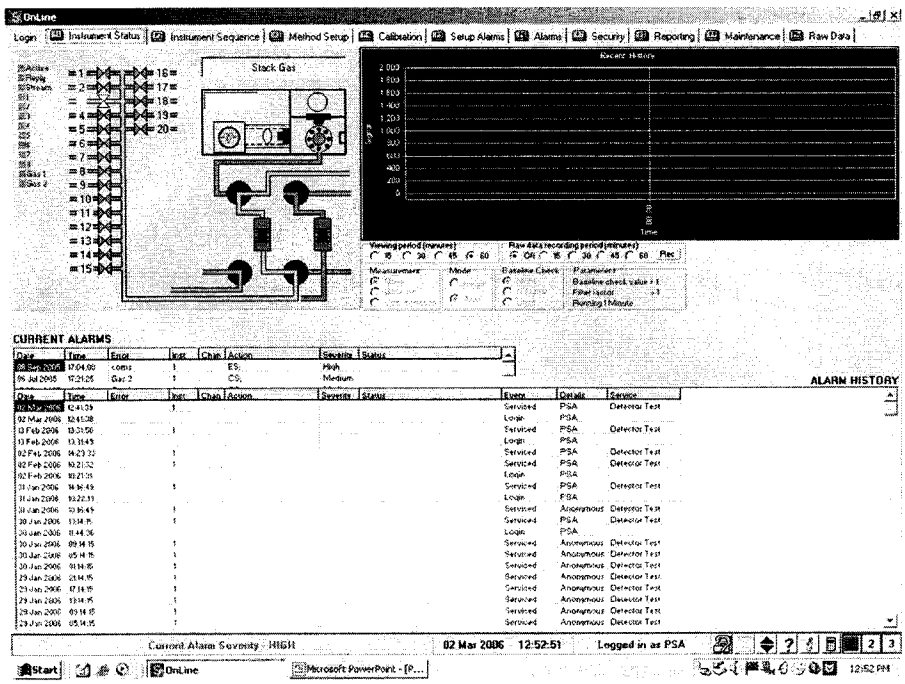

Figure 2.4.2.5-2: PSA Software Page 2 – shows schematic of Sir Galahad and real time reporting of fluorescent signals.

Reproduced with permission of the copyright owner. Further reproduction prohibited without permission.

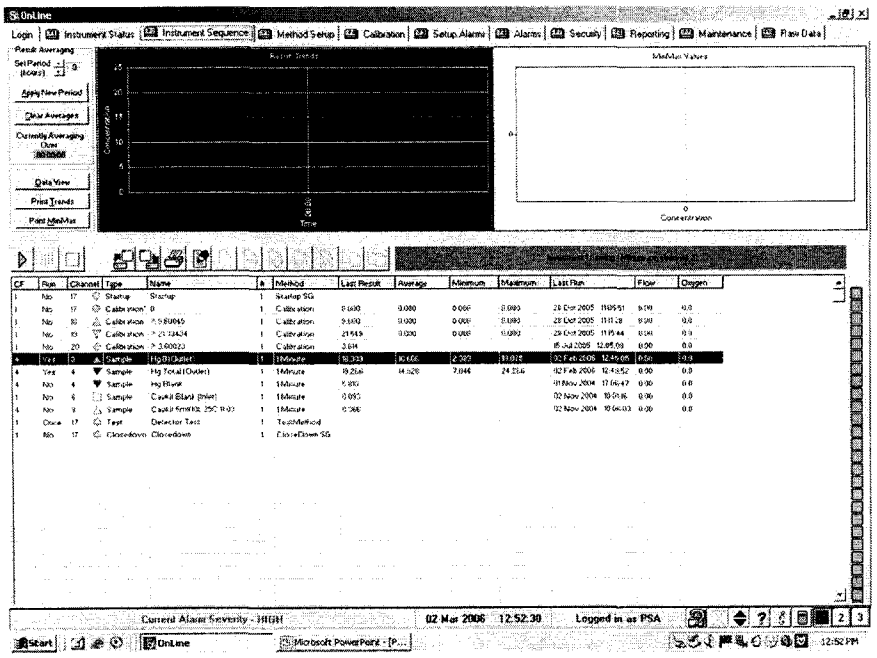

Figure 2.4.2.5-3: PSA Software Page 3 – Instrument Sequence page.

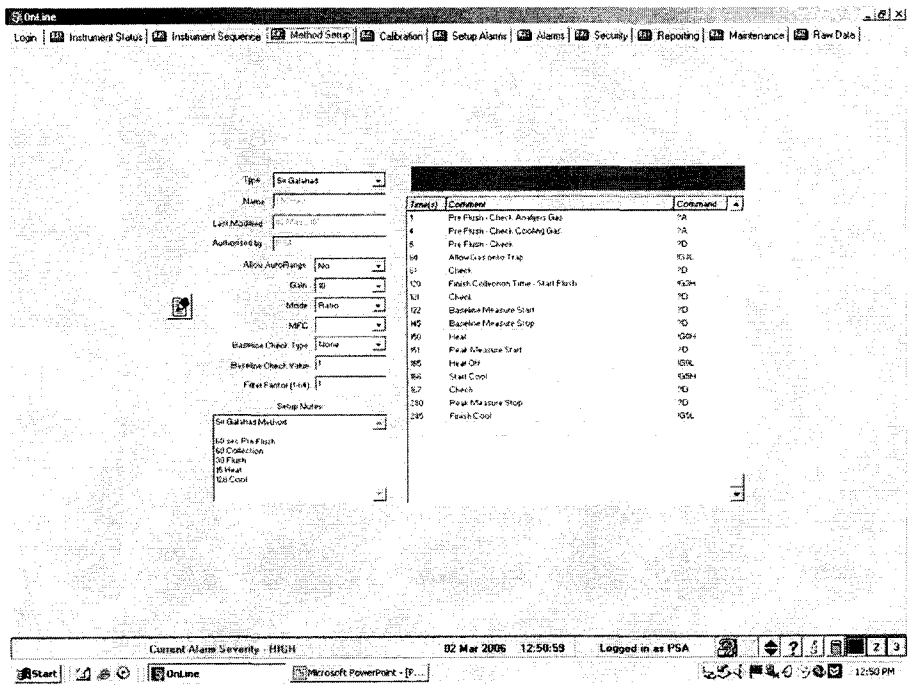

Figure 2.4.2.5-4: PSA Software Page 4 – Method Setup Page.

Reproduced with permission of the copyright owner. Further reproduction prohibited without permission.

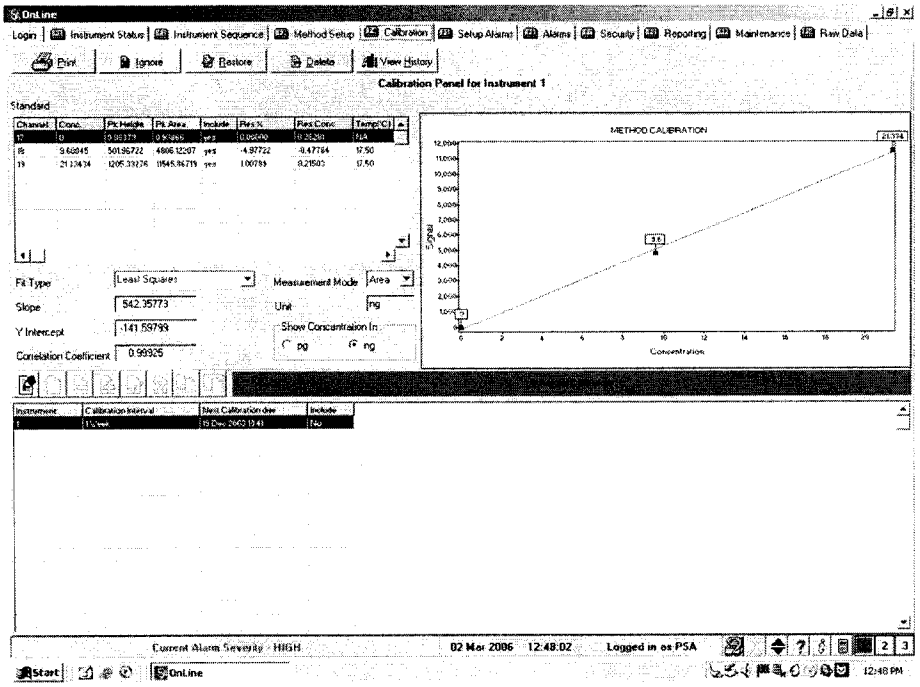

Figure 2.4.2.5-5: PSA Software Page 5 – Calibration curve page.

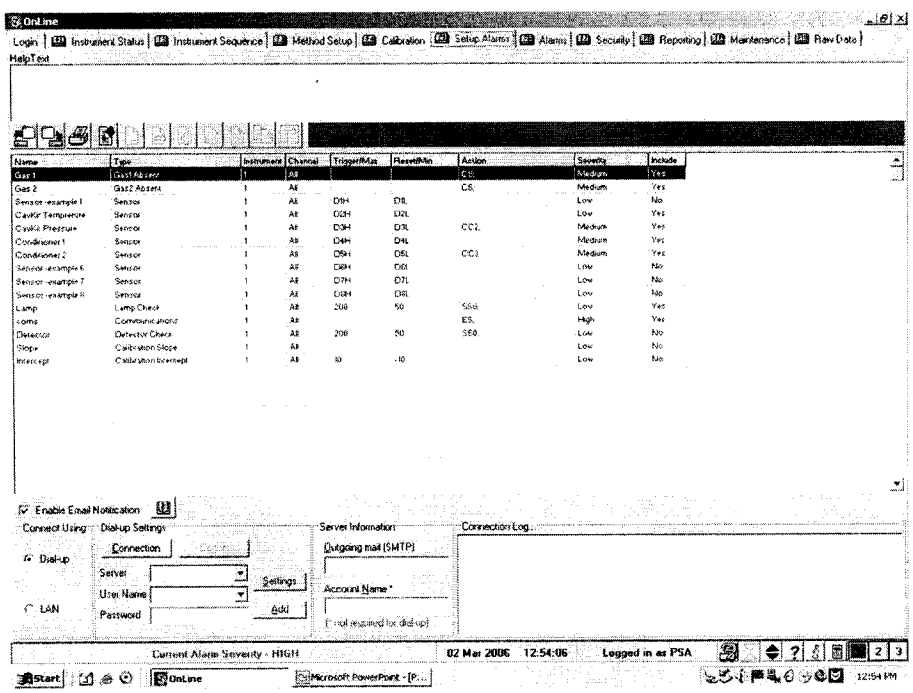

Figure 2.4.2.5-6: PSA Software Page 6 – Setup Alarms Page.

Reproduced with permission of the copyright owner. Further reproduction prohibited without permission.

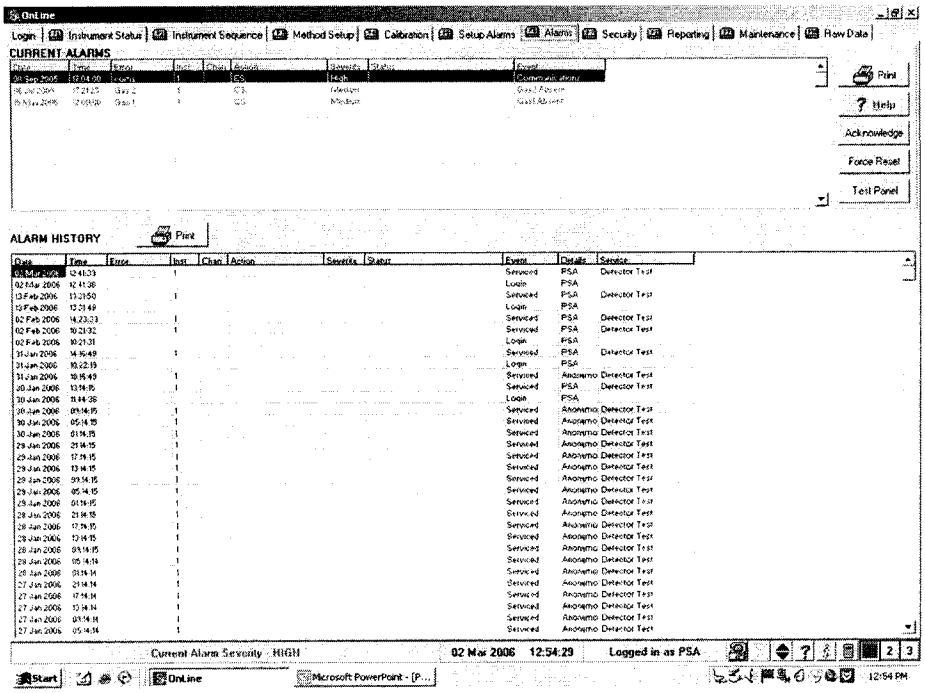

Figure 2.4.2.5-7: PSA Software Page 7 – Alarms Page.

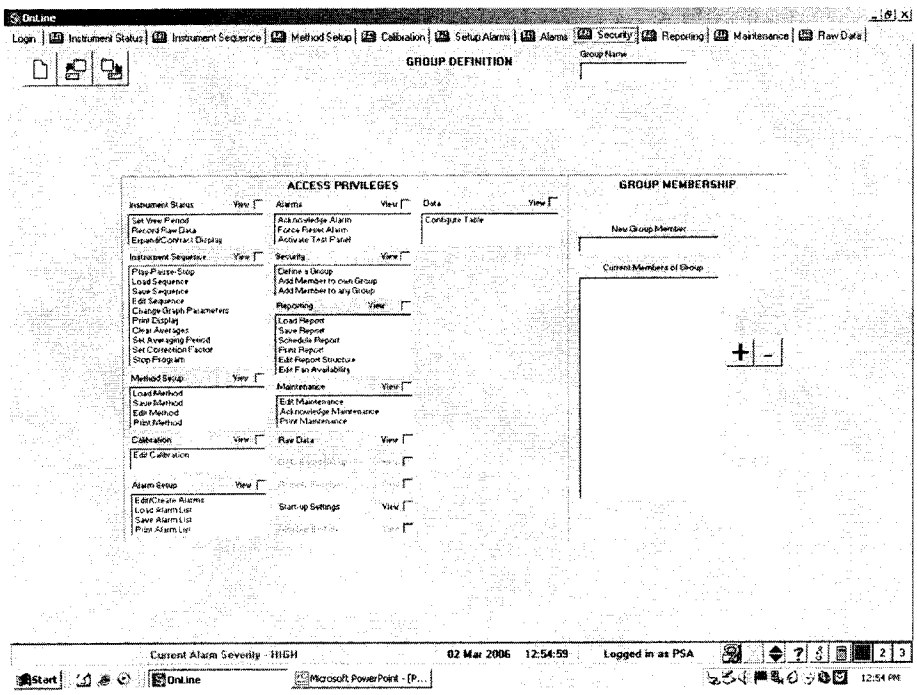

Figure 2.4.2.5-8: PSA Software Page 8 – Security Page.

Reproduced with permission of the copyright owner. Further reproduction prohibited without permission.

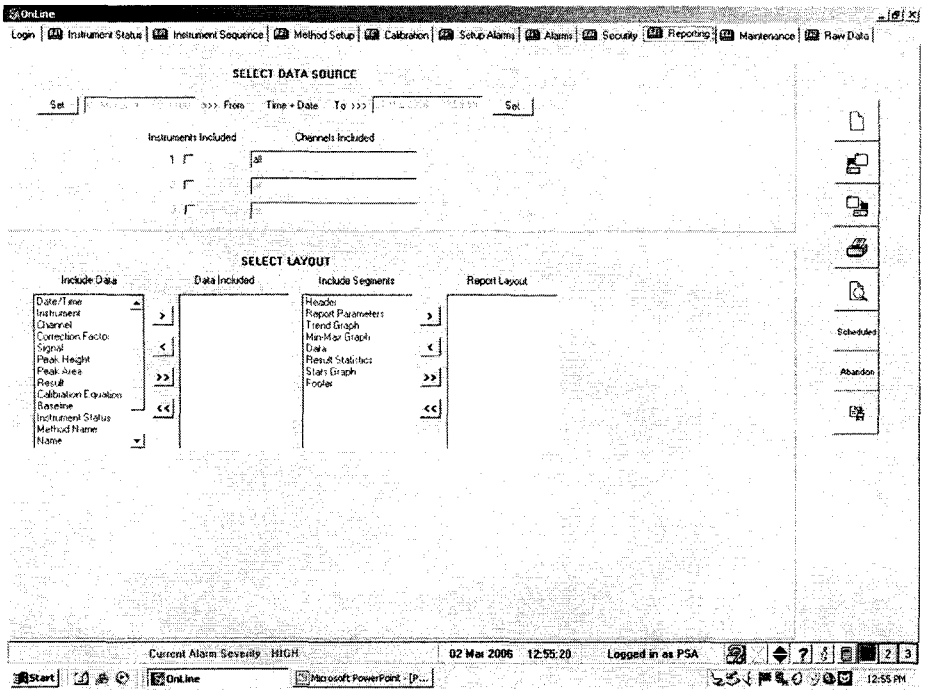

Figure 2.4.2.5-9: PSA Software Page 9 – Reporting Page.

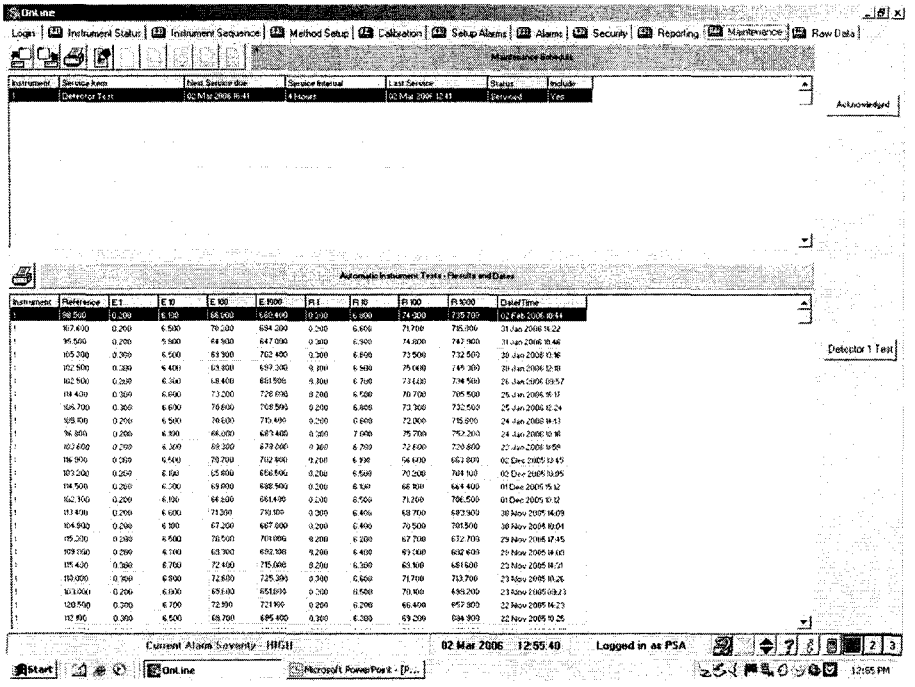

Figure 2.4.2.5-10: PSA Software Page 10 – Maintenance Page.

Reproduced with permission of the copyright owner. Further reproduction prohibited without permission.

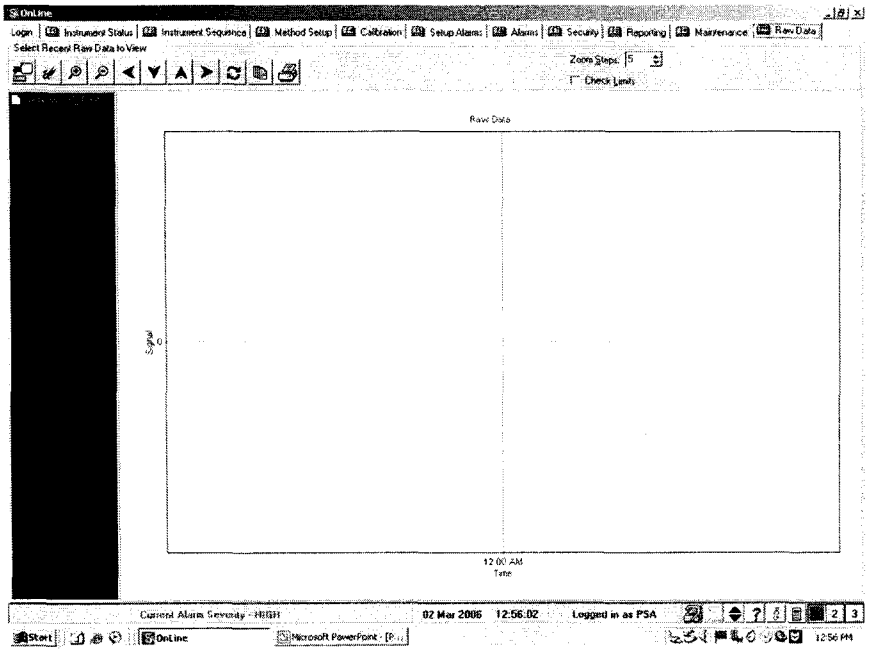

Figure 2.4.2.5-11:
PSA Software Page 11 – Raw Data Page, shows raw data for run.

2.4.3 Trouble-shooting the PSA

The PSA analyzer had numerous problems that had to be overcome. This section lists some of the problems and solutions.

i. The gold trap had to be replaced. The presence of water in the gas stream tends to permanently damage the gold trap. Unfortunately, this happened at least two times in the course of this experimental work.

ii. Several leaks were detected in the connections within the hot-box. These fittings had to be replaced or tightened. This was a significant issue since a lot of the sample gas was lost before reaching the analyzer.

iii. Several leaks were also detected within the stream selector box. Similar to the previous solution, several fittings were replaced or simply tightened.

iv. In the course of experimental work, it was found that the Sn^{2+} present in the impinger solution was reduced to Sn^{0}, or metallic elemental tin. As a result, the tin deposited on

Reproduced with permission of the copyright owner. Further reproduction prohibited without permission.

the inside of the impinger and had to be cleaned off before continuing experimental work. This was done by cleaning the impinger with several milliliters of acid. The acid reacted with the tin and removed it.

v. A similar issue was also seen in the hot-box. A lot of deposition was found within the tubes. These tubes were easily cleaned with copious amounts of water and blow drying them with air.

vi. The chiller unit had to be replaced on one occasion.

vii. The hot-box was heated by a heating element and a fan. The fan eventually had to be replaced since repeated heating and cooling resulted in its deterioration.

viii. The flow rate of sample into the analyzer was controlled by a Mass Flow Controller located in the Stream Selector Box. Similar to the gold trap, the MFC was damaged beyond repair because of the presence of water in the gas stream. As a result, a rotometer was used to control the flow rate of sample entering the analyzer.

2.5 Control Panel

The various parts of the control panel have been mentioned in previous sections. This section will present some pictures and a summary of the various controllers that were used to control the apparatus. The entire control panel is shown in Figure 2.5-1.

Reproduced with permission of the copyright owner. Further reproduction prohibited without permission.

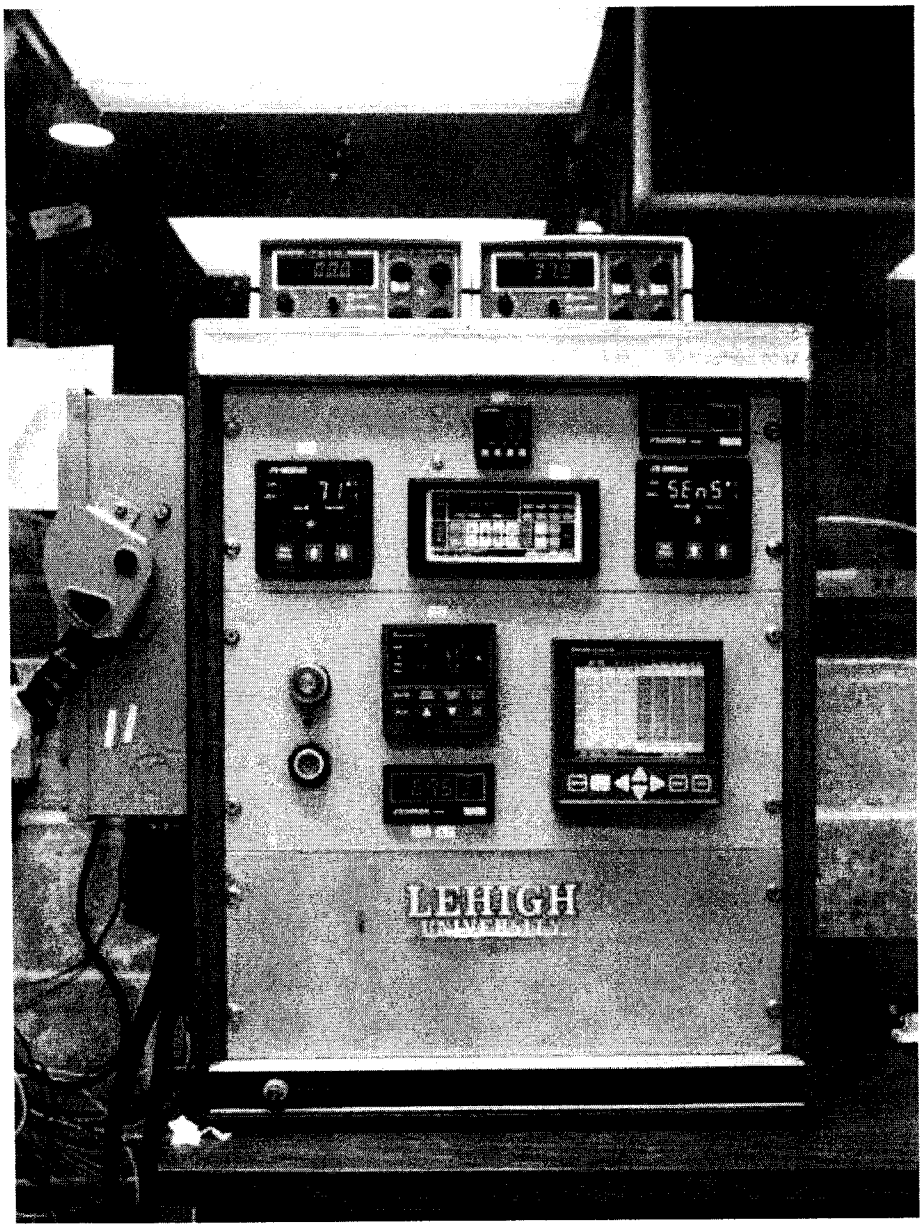

Figure 2.5-1: Control panel.

Reproduced with permission of the copyright owner. Further reproduction prohibited without permission.

2.5.1 *Heater Controllers*

The controllers for R1, APH and SPH are shown. The maximum temperature set-point for the heaters used for the APH and SPH was 800°C. For the APH, at a gas flow rate of 75 SLPM, a set-point of 800°C resulted in a gas temperature of approximately 550°C. For the SPH, at a liquid water flow rate of 10 mlpm, a set-point of 800°C resulted in a super heated steam temperature of approximately 500°C.

The maximum temperature set-point for the heater used for R1 was 1010°C. At a total gas flow rate of 87 LPM of flue gas, the temperature of the gas at the exit of R1 was approximately 865°C.

2.5.2 *Temperature Readouts*

Several thermocouples were used in the apparatus to give temperature readings. These temperatures were read using the 6-channel readout from Omega Engineering. It is shown in Figure 2.3.1.2-6.

2.5.3 *Bag-house Control*

The third major section of the control panel was the pulsating system for the bag-house. The controller had the means of controlling the timing of the air burst to enter the bag-house. In the process of doing this, any ash or sorbent particles caked on the surface of the bags would be released. The controller was not needed in this experimental work.

Reproduced with permission of the copyright owner. Further reproduction prohibited without permission.

CHAPTER 3

The Effects of H_2O, SO_2 and NO on Homogenous Hg Oxidation by Cl_2.

3.1 Abstract

Several researchers have determined that water (H_2O) and sulfur dioxide (SO_2) in a flue gas stream have an impact on the amount of elemental mercury (Hg^0) that is homogeneously oxidized by a chlorine containing species. Generally, it is concluded that H_2O inhibits Hg oxidation by chlorine (Cl_2). However, doubt remains as to whether SO_2 promotes or inhibits Hg oxidation. Further, most published results seem to indicate that nitric oxide (NO) does not have a significant impact on Hg oxidation. This paper will present data taken in a laboratory scale apparatus designed to test these observations. In this work, Cl_2 is intentionally added to a synthetic flue gas stream containing known amounts of elemental mercury. This gas blend is similar to a flue gas obtained by burning Powder River Basin (PRB) coal in a PC-fired power plant and is subject to a time-temperature profile similar to a power plant. The results obtained show that H_2O, SO_2 and NO all have an inhibitory effect on the homogeneous oxidation of Hg by Cl_2. Further, the presence of H_2O increases the inhibitory effect of SO_2 and NO. Two new reactions are proposed to explain these results, in which SO_2 and NO react with Cl_2. The consequences of these reactions are a reduction in the oxidative interactions that take place between Hg and Cl_2, thus decreasing the amount of Hg oxidation that occurs.

Reproduced with permission of the copyright owner. Further reproduction prohibited without permission.

3.2 Introduction

In 1997, the United States Environmental Protection Agency (USEPA) submitted a mercury study report to the U.S. Congress. They projected that of the 158 tons of mercury being released into the environment, 48 tons was derived from coal fired combustion sources[46-52]. On March 15, 2005, the USEPA issued a federal rule to permanently cap and reduce mercury (Hg) emissions from coal-fired power plants. Upon complete implementation, Hg emissions will be reduced by 21% by 2010, and by 70% by 2018. Because of these impending reductions, it is important to find efficient means to remove Hg from power plant flue gases.

Mercury in the flue gas is most commonly classified in three forms: elemental mercury (Hg^0), oxidized mercury (Hg^{2+}) and particulate bound mercury (Hg^P). Details on the reactivity, and physical and chemical properties of each is given in an earlier chapter.

Temperature and flue gas components, such as SO_2, Cl_2 or HCl, and H_2O have strong influences on mercury speciation[44, 81]. Thermodynamic equilibrium calculations performed by Frandsen et al. predict that all gas phase mercury in a coal combustion flue gas should exist as mercuric chloride ($HgCl_2$) at temperatures below 450°C[90]. However, actual mercury speciation data collected by EPA's Information Collection Request (ICR) database shows that at even lower temperatures, elemental mercury still exists in the flue gas[85]. Studies have also shown that the distribution of mercury species is strongly dependent on the type of coal being burnt[89].

Laudal et al. performed several bench scale experiments to determine the effects of various flue gas components on Hg oxidation[76]. Kilgroe et al. showed a negative influence of water and sulfur on mercury oxidation[43]. Norton et al. studied the impact of NO and NO_2 with greater detail[77]. Details on the experimental work by the individual researchers are given in Chapter 1.

In summary, it was found that H_2O inhibits the oxidation of Hg by a chlorine species. The question remains as to whether Cl_2 or HCl is the primary chlorine species responsible for Hg oxidation. Opinions also differ as to whether SO_2 encourages or inhibits Hg oxidation. NO seems to inhibit Hg oxidation, but the published work was done in the presence of particulate matter and not in a homogeneous environment.

Reproduced with permission of the copyright owner. Further reproduction prohibited without permission.

This paper will present data obtained from a laboratory scale apparatus, where the effects of H_2O, SO_2 and NO, on Hg oxidation is studied in systematic detail. Most of the experimental work done by other researchers was performed at temperatures greater than 700°C or below 200°C. Additionally, the individual components of the flue gas were studied in the absence of other major flue gas components such as H_2O and CO_2. This work focuses on temperatures between 550°C and 180°C, and attempts to provide a comprehensive view of the cumulative effects of each of the major flue gas components on Hg oxidation.

3.3 Testing Facility

The testing facility used to perform the Hg oxidation tests has been described in Chapter 2. Table 3.3-1 shows the base case concentrations of the various components of the flue gas used in this work. The specifications closely follow a flue gas stream derived from the combustion of Powder River Basin (PRB) coal.

Component	Composition
Nitrogen (N_2)	70%
Oxygen (O_2)	3.5%
Carbon Dioxide (CO_2)	13.5%
Water (H_2O)	13%
Sulfur Dioxide (SO_2)	370 ppmv
Nitric Oxide (NO)	170 ppmv
Carbon Monoxide (CO)	300 ppmv
Chlorine (HCl or Cl_2)	100 ppmv
Elemental Mercury (Hg)	10 $\mu g/m^3$

Table 3.3-1: Summary of components and composition.

The oxidant used in this chapter is chlorine gas (Cl_2). A cylinder of 1.0% Cl_2 in N_2 was used as the chlorine source. This gas was metered and injected into the heated gas stream between R1 and R2. The same temperature profile, as shown in Table 3.3-2, was used in all three experiments. The concentration of each flue gas component used in this experimental work is shown in Table 3.3-1, except for the concentration of Cl_2 which changes with each experiment.

Reproduced with permission of the copyright owner. Further reproduction prohibited without permission.

Experimental Apparatus		
Location	Temperature (°C)	Cumulative Residence Time (seconds)
Exit R1	538	0.75
Exit R2	389	2.4
Exit HX1	177	2.8
Baghouse Inlet	150	3.7

Table 3.3-2: Values of temperature versus residence time profiles, and the respective locations on the experimental apparatus.

An important feature of the experimental apparatus is its ability to follow a typical power plant time-temperature profile. Figure 3.3-1 shows the close comparison of a power plant temperature profile with the profile obtained in this apparatus when operated at 87 slpm. Table 3.3-2 lists these values of temperature versus residence time as obtained in this apparatus.

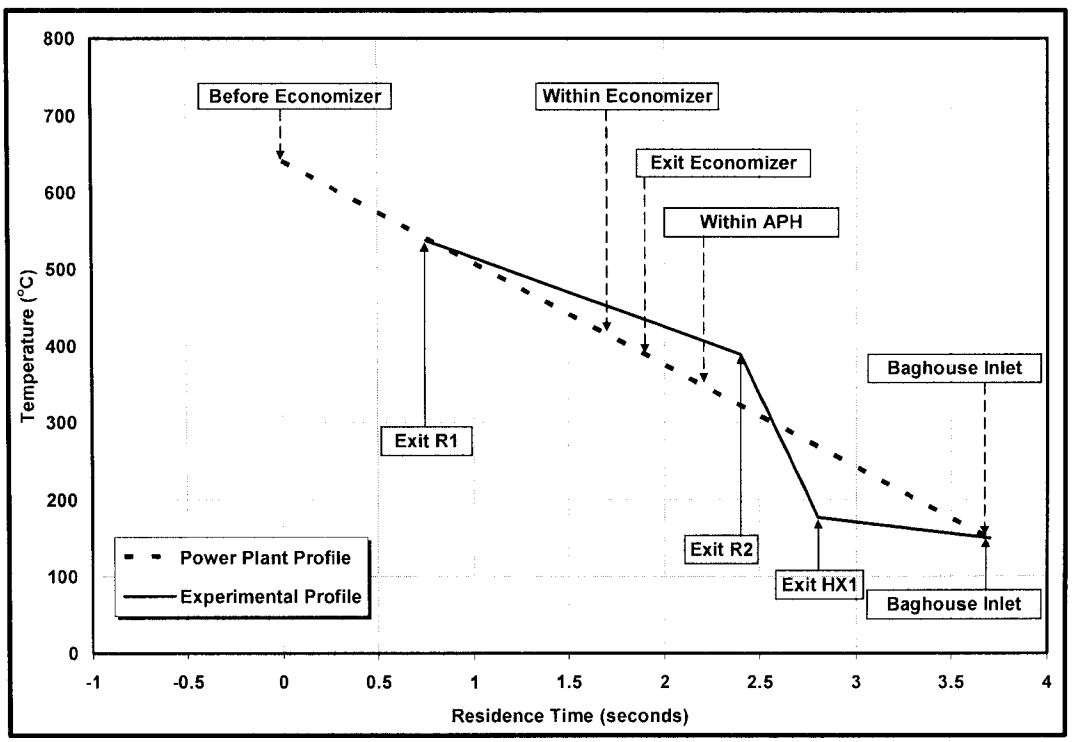

Figure 3.3-1. Comparing temperature versus residence time profiles of a typical power plant and the experimental apparatus. The dashed line represents the profile of a power plant; the solid line represents the profile of the apparatus in this experimental work.

Reproduced with permission of the copyright owner. Further reproduction prohibited without permission.

3.4 Results

There are two major goals for the experiments in this work. First, the experiments are conducted at temperatures different than most other researchers. For example, Kilgroe et al. performed their analysis of the effects of SO_2 and H_2O on Hg oxidation at temperatures greater than 755°C. According to the model by Frandsen, most of the Hg will exist at an elemental state at these temperatures. Conversely, Laudal et al. performed experiments at temperatures below 200°C, and according to Frandsen, most of the Hg will exist in its oxidized form. The temperature profile chosen for this work was between 550°C and 200°C. The second goal of these experiments is to measure the effects of H_2O, SO_2 and NO on the oxidation of Hg by Cl_2. Other researchers agree that H_2O has an inhibitory effect on Hg oxidation, but questions remain concerning the effects of SO_2 and NO.

3.4.1 Experiment 1:

The first experiment performed studied the effects of the gas components on the reaction of Hg with Cl_2. The system was heated with gas flowing until the temperature profile (in Table 3.3-2) was attained. Initially the total gas flow through the system was 87 slpm and consisted of 96.5% N_2, 3.5% O_2 and 10 $\mu g/m^3$ of elemental Hg. Upon reaching the desired temperature, Cl_2 was injected between the R1 and R2 at a rate which would give a 2 ppmv concentration. The SCEM monitored the change in Hg concentration. Once steady Hg values were achieved, the Cl_2 flow was discontinued and the system was allowed to re-equilibrate. Figure 3.4.1 shows the results of this experiment, where elemental Hg concentration (in $\mu g/m^3$) is plotted against the duration of the entire experiment. In the first stage, labeled 1a, 71.7% of the initial amount of Hg was oxidized.

Reproduced with permission of the copyright owner. Further reproduction prohibited without permission.

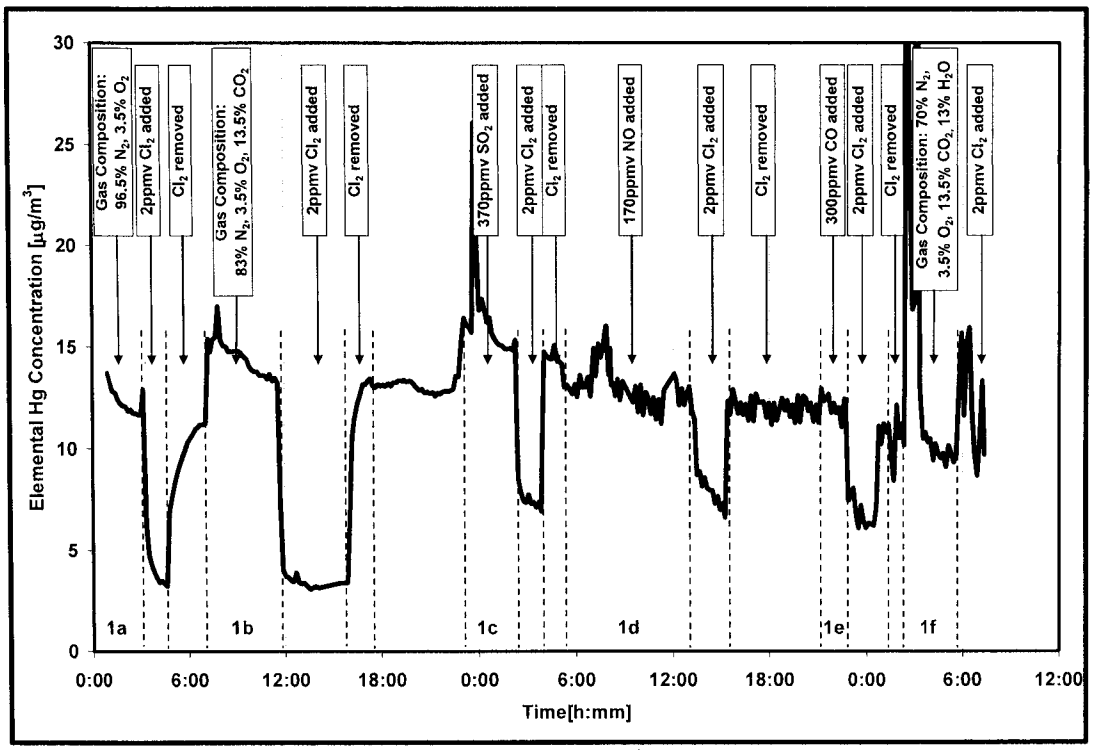

Figure 3.4.1. Plot of elemental Hg concentration ($\mu g/m^3$) with respect to time for Experiment 1. Each stage of the experiment is labeled along with the respective gas composition, and the period of addition and removal of Cl_2.

Next, CO_2 was added and the gas flowing through the system was adjusted accordingly to give 83% N_2, 3.5% O_2, 13.5% CO_2 and 10 $\mu g/m^3$ of Hg^0. At steady temperatures, 2 ppmv Cl_2 was again injected and changes in Hg were measured. This process was repeated for SO_2, NO, CO and H_2O respectively. Table 3.4.1 shows the composition of the gas used in each stage of this experiment, with the percent of Hg oxidized for each stage.

Reproduced with permission of the copyright owner. Further reproduction prohibited without permission.

	Components in Flue Gas Stream									
Stage of	Elemental Hg	N_2	O_2	CO_2	SO_2	NO	CO	H_2O	Cl_2	Elemental Hg Oxidation
Experiment 1	($\mu g/m^3$)	(%)	(%)	(%)	(ppmv)	(ppmv)	(ppmv)	(%)	(ppmv)	(%)
1a	11.6	96.5	3.5	--	--	--	--	--	2.0	72
1b	13.4	83.5	3.5	13.5	--	--	--	--	2.0	77
1c	14.9	83.5	3.5	13.5	370	--	--	--	2.0	52
1d	12.7	83.5	3.5	13.5	370	170	--	--	2.0	46
1e	11.7	83.5	3.5	13.5	370	170	300	--	2.0	47
1f	10.0	70.0	3.5	13.5	370	170	300	13	2.0	0

Table 3.4.1: Composition of gas used in each stage of Experiment 1, and elemental Hg oxidation results.

Figure 3.4.1 also shows that the apparatus has no effect on Hg oxidation by itself. The theoretical concentration of Hg injected into the apparatus was approximately 12 $\mu g/m^3$. As seen in Figure 3.4.1, stages 1a, 1b, 1d, and 1e show that the concentration of Hg before the addition of Cl_2 was approximately 12 $\mu g/m^3$. In the cases of 1c and 1f, the concentration of mercury is slightly different than 12 $\mu g/m^3$ due to drift in flows, but within experimental error.

It is clear from the results in Table 3.4.1 that Cl_2 oxidizes Hg effectively. Stages 1a and 1b show that over 70% of Hg was oxidized. Upon the addition of SO_2 (stage 1c), the percent Hg oxidized dropped from over 70% to 52.3%. This agrees with the results obtained by Kilgroe and Laudal, that SO_2 has an inhibitory effect on Hg oxidation. The addition of NO into the gas stream (stage 1d) further reduced the percent Hg oxidized, from 52.3% to 45.7%. Norton et al. showed similar trends in their work. The addition of CO into the gas stream did not have an impact on the observed Hg oxidation.

In stage 1f, the addition of water completely removes the oxidation effect of Cl_2. Also, the addition of H_2O results in a huge spike of mercury emitted from the apparatus. It is speculated that some elemental and oxidized Hg accumulates on the inner walls of the apparatus over the duration of the experiment, and the presence of H_2O in the gas stream caused an immediate desorption of this elemental Hg. This effect does not last long, since within a few minutes, the concentration of elemental Hg returns to approximately 10 $\mu g/m^3$.

Reproduced with permission of the copyright owner. Further reproduction prohibited without permission.

Following the spike, the addition of 2 ppm Cl_2, showed no measurable oxidation effect. This indicates that 2 ppmv Cl_2 is not able to overcome the oxidation canceling effects of H_2O. Experiments 2 and 3 were then designed and run to determine if increasing the Cl_2 concentration could overcome the effects of water.

3.4.2 Experiment 2:

In this experiment, the gas flow through the system was again 87 slpm and the gas blend consisted of 83% N_2, 3.5% O_2 and 13.5% H_2O. No CO_2, SO_2, NO or CO were added to the gas. The concentration of Cl_2 was increased from 2 to 52 ppmv and the amount of Hg oxidized was measured. The same temperature profile was used as shown in Table 3.3-2. Table 3.4.2 shows the composition of the gas used in each stage of this experiment, along with the percent of Hg oxidized for each stage.

	Components in Flue Gas Stream					
Stage of	Elemental Hg	N_2	O_2	H_2O	Cl_2	Elemental Hg Oxidation
Experiment 2	($\mu g/m^3$)	(%)	(%)	(%)	(ppmv)	(%)
2a	11.6	83.5	3.5	13	2.0	0
2b	12.7	83.5	3.5	13	12.4	83
2c	11.6	83.5	3.5	13	30.9	88
2d	11.4	83.5	3.5	13	52.5	92

Table 3.4.2: Composition of gas used in each stage of Experiment 2, and elemental Hg oxidation results.

In the first stage of Experiment 2 (2a), the same result was obtained as Experiment 1f, where 2 ppmv of Cl_2 had no effect on Hg oxidation. When 12ppmv Cl_2 was added (stage 2b), 82.7% of elemental Hg was oxidized. Further increases of Cl_2 to 31 and 52 ppmv resulted in smaller increases is Hg oxidation of 88.3% and 92.4% respectively. Figure 3.4.2 summarizes the results of this experiment.

Reproduced with permission of the copyright owner. Further reproduction prohibited without permission.

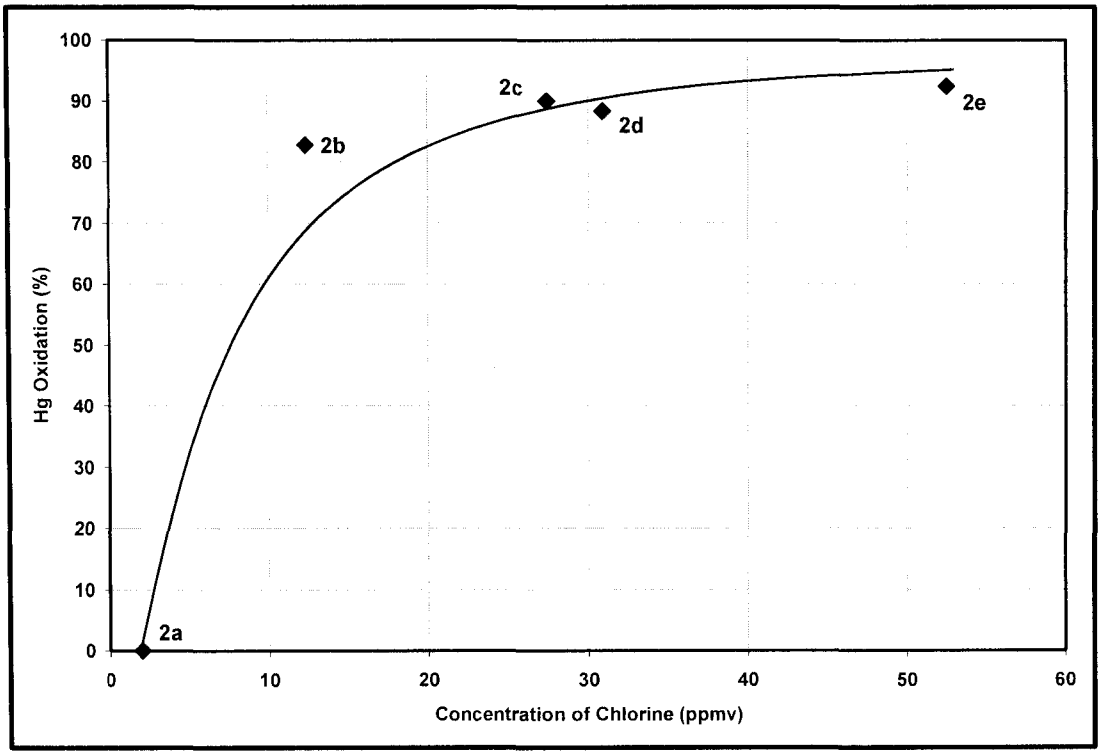

Figure 3.4.2. Plot of percent Hg oxidation versus concentration of chlorine (ppmv). See Table 3.4.2 for the gas composition used in each stage of this experiment.

3.4.3 Experiment 3:

This experiment is the same as Experiment 1, except that 13% water was added and 27.5 ppmv of Cl_2 was injected into the heated gas stream, rather than 2 ppmv in Experiment 1. This amount of Cl_2 was chosen in expectation that the oxidation rates would be strong, allowing the effects of SO_2 and NO to be observed. Table 3.4.3 shows the composition of the gas used in each stage of this experiment along with the percent of Hg oxidized for each stage.

Reproduced with permission of the copyright owner. Further reproduction prohibited without permission.

	Components in Flue Gas Stream									
Stage of	Elemental Hg	N_2	O_2	CO_2	SO_2	NO	CO	H_2O	Cl_2	Elemental Hg Oxidation
Experiment 3	($\mu g/m^3$)	(%)	(%)	(%)	(ppmv)	(ppmv)	(ppmv)	(%)	(ppmv)	(%)
3a	10.5	83.5	3.5	--	--	--	--	13	27.5	90
3b	10.6	70.0	3.5	13.5	--	--	--	13	27.5	90
3c	10.3	70.0	3.5	13.5	370	--	--	13	27.5	57
3d	10.6	70.0	3.5	13.5	370	170	--	13	27.5	46
3e	10.8	70.0	3.5	13.5	370	170	300	13	27.5	45

Table 3.4.3: Composition of gas used in each stage of Experiment 3, and Hg^0 oxidation results.

The results of stage 3a and 3b (effect of CO_2) are similar to that of stages 1a and 1b in Experiment 1 in that the amount of Hg oxidized is high, but the presence of CO_2 had little effect. However, in stage 3c, when adding SO_2, the percent Hg oxidized dropped to 56.7%. When NO was added into the gas (stage 3d), the observed Hg oxidation decreased from 56.7% to 45.6%. Stage 3e showed that the addition of CO did not have an impact on Hg oxidation. Figure 3.4.3 summarizes the results of this experiment and compares them to Experiment 1.

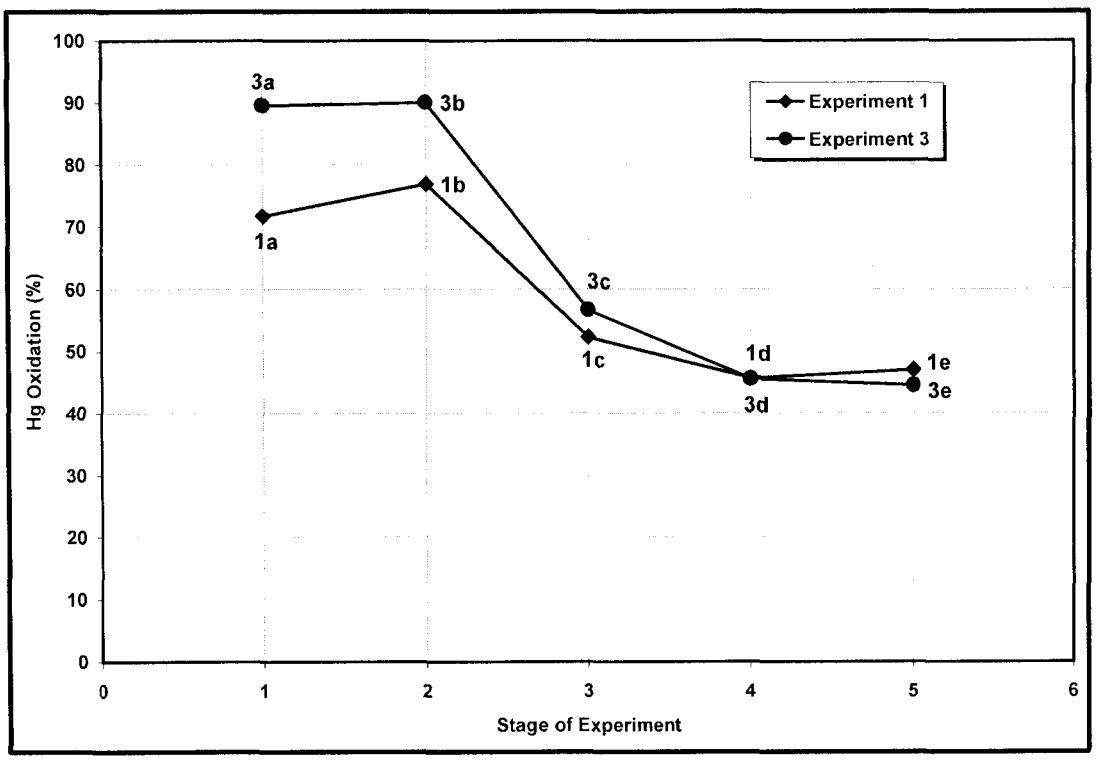

Figure 3.4.3. Plot of percent Hg oxidation versus stage of Experiment 1 and 3. See Tables 3.4.1 and 3.4.3 for the gas composition used in each stage of these two experiments.

Reproduced with permission of the copyright owner. Further reproduction prohibited without permission.

3.5 Discussion

It is known that chlorine compounds can oxidize elemental Hg effectively. However, it has not been shown whether Cl_2 or HCl is the primary species responsible for this oxidation. For instance, Laudal et al. injected Cl_2 into their experimental work and concluded that Cl_2, and not HCl was responsible for Hg oxidation. Conversely, Kilgroe injected HCl in their system, and found that at temperature above 750°C, Hg oxidation occurred very effectively. One way to explain this discrepancy is by assuming the reaction of Cl_2 and water to form HCl and O_2 is reversible.

$$Cl_2\,(g) + H_2O\,(g) \leftrightarrow 2\,HCl\,(g) + \tfrac{1}{2}\,O_2\,(g) \qquad (1)$$

Thermodynamic equilibrium calculations for this reaction at the conditions used in Experiment 3 show that at temperatures below 475°C, and for typical O_2 and H_2O concentrations, Cl_2 dominates HCl and at temperatures above 475°C, HCl dominates over Cl_2. Figure 3.5 shows a plot of equilibrium Cl_2 and HCl concentration with respect to temperature. The constants for the reaction were calculated using the enthalpy and Gibbs free energy of the reaction. The concentrations of water and O_2 were constant at 13.5% and 3.5% respectively. In this work, Cl_2 was injected at 538°C. According to Figure 3.5, some of the Cl_2 injected would have converted to HCl, but at a temperature of 538°C and below, Cl_2 is the dominant species present in the gas stream. Figure 3.5 also helps explain the results obtained by Kilgroe and Laudal. Kilgroe performed experimental work at temperatures above 700°C, and according to Figure 3.5, HCl is the dominant chlorine species present which would most likely oxidize elemental Hg. Conversely, Laudal performed experimental work at temperatures below 200°C, and according to Figure 3.5, Cl_2 would be the dominant chlorine species present and would most likely oxidize elemental Hg.

Reproduced with permission of the copyright owner. Further reproduction prohibited without permission.

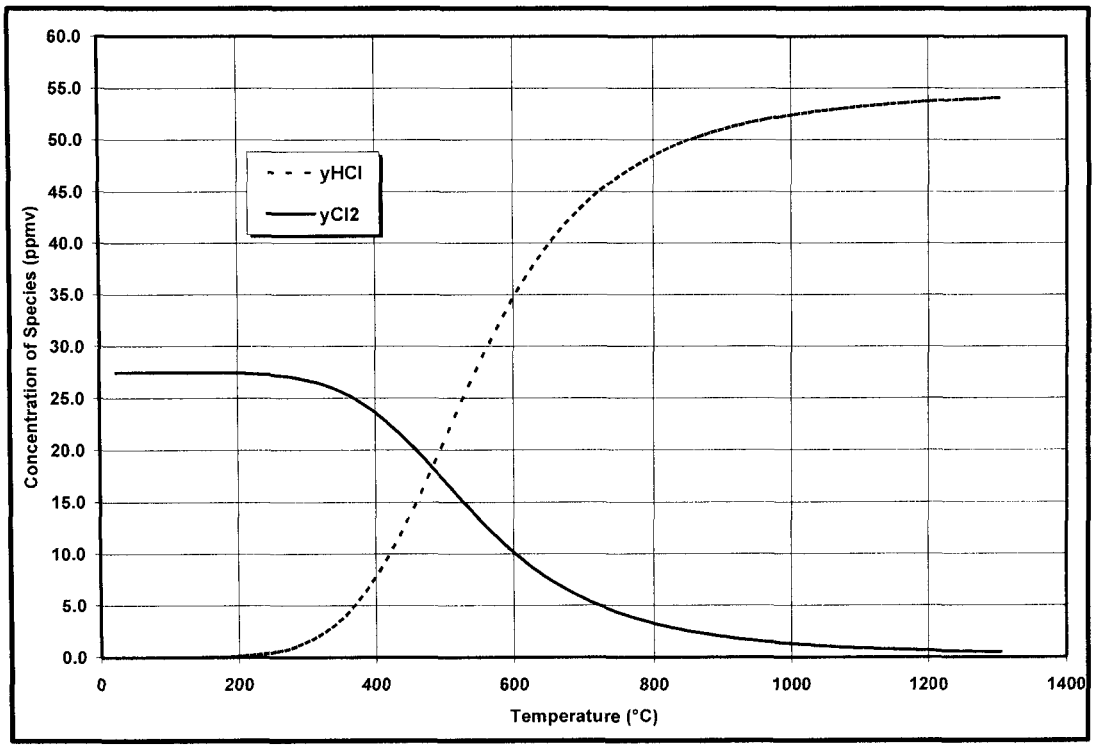

Figure 3.5. Thermodynamic plot of chlorine species concentration versus temperature. The concentration of O_2 and H_2O used in the calculations were 3.5% and 13.5% respectively. Initial concentration of Cl_2 used was 27.5 ppmv.

As a result of electronic structure, Cl_2 is a much stronger oxidizing agent than HCl. The ability of the chlorine atom to accept a valence electron from elemental mercury is significantly lower for HCl since H has already contributed an electron to the outer shell of Cl. This makes the chlorine atom in HCl less reactive than Cl_2, which has a covalent structure that permits its outer shell to be available to those valence electrons available from Hg.

Figure 3.4.2 shows that a critical concentration of Cl_2 exists between 2 and 20 ppmv, where it overcomes water inhibition and rapidly oxidizes mercury. Beyond 50 ppmv, mercury oxidation reaches above 95%, and it is assumed that at excessively high Cl_2 concentrations, the percent of Hg oxidation will eventually reach 100%.

In Experiments 1 and 3 (with and without water), the addition of SO_2 resulted in decreasing Hg oxidation. Comparing stages 1b and 1c in Table 3.4.1, when 370 ppmv SO_2 was added, the observed Hg oxidation dropped from 76.9% to 52.3%. When 370 ppmv SO_2 was

Reproduced with permission of the copyright owner. Further reproduction prohibited without permission.

added in Experiment 3, comparing stages 3b and 3c in Table 3.4.3, Hg oxidation dropped from 90.0% to 56.7%. This indicates that H_2O causes SO_2 to have a stronger inhibition on Hg oxidation.

The inhibitory effect of SO_2 is possibly due to the effect of SO_2 reacting irreversibly with Cl_2. The concentrations of SO_2 in Experiment 1 and Experiment 3 are in greater excess of Cl_2, suggesting that the following reaction may be occurring:

$$SO_2\,(g) + Cl_2\,(g) \rightarrow SO_2Cl_2\,(g) \qquad (2)$$

The reaction of SO_2 and Cl_2 to form SO_2Cl_2 is slightly favorable at temperatures near the end of a typical power plant. For example at 100°C the equilibrium constant for the reaction $SO_2 + Cl_2 \leftrightarrow SO_2Cl_2$ is 102 atm^{-1}. A rough equilibrium extent calculation using the RGIBBS reactor model in Aspen Plus shows that for a partial pressure of SO_2 equal to 0.0002 atm (200 ppm), a chlorine concentration of 2ppm and a temperature of 100°C, up to 5% of the added chlorine could be scavenged by SO_2. This does not cause enough of an effect to account for the data presented in this work. The exact analysis of the equilibrium extent of these reactions is planned as part of future work. This rough estimate is only to indicate that the reaction of Cl_2 with SO_2 is feasible and potentially a reason for decreased mercury oxidation when SO_2 is added.

Similar to SO_2, the addition of NO also resulted in decreasing Hg oxidation. Comparing stages 1c and 1d in Table 3.4.1, when 170 ppmv NO was added, the observed Hg oxidation dropped from 52.3% to 45.7%. In Experiment 3, when 170 ppmv NO was added, comparing stages 3c and 3d in Table 3.4.3, the observed Hg oxidation dropped from 56.7% to 45.6%. Similar to SO_2, NO inhibits Hg oxidation and the presence of H_2O causes NO to exhibit a stronger inhibitory effect on Hg oxidation. The effect is possibly due to a reaction between NO and Cl_2 which would be:

$$2\,NO\,(g) + Cl_2\,(g) \rightarrow 2\,NOCl\,(g) \qquad (3)$$

Reproduced with permission of the copyright owner. Further reproduction prohibited without permission.

The reaction of NO and Cl_2 to form NOCl is thermodynamically favorable at temperatures near the end of a typical power plant. For example at 200°C the equilibrium constant for the reaction NO + 0.5 Cl2 ↔ NOCl is 92 $atm^{-0.5}$. A rough calculation using Aspen Plus (similar to the previous reaction) shows that at a partial pressure of NO equal to 0.0004 atm (400 ppm) and a concentration of Cl_2 of 2 ppm, up to 75% of the added chlorine could be scavenged by NO at 200°C. The exact analysis of the equilibrium of these reactions is planned as part of future work. This rough estimate is only to indicate that the reaction of Cl_2 with NO is feasible and potentially a reason for decreased mercury oxidation when NO is added.

The presence of CO_2 did not have a significant on Hg oxidation. Comparing stages 1a and 1b, the percent of Hg oxidation increased by 5%; comparing stages 3a and 3b, the percent of Hg oxidation increased by 0.5%. But neither value is significant enough to make a conclusion about the effects of CO_2.

Finally, the presence of CO also did not have a significant effect on the percent of Hg oxidation. Comparing stages 1d and 1e, the percent of Hg oxidation increased by 1.3%; comparing stages 3d and 3e, the percent of Hg oxidation reduced by 1.1%. This helps draw the conclusion that CO, in the flue gas stream at these temperatures, does not have an impact on Hg oxidation.

Reproduced with permission of the copyright owner. Further reproduction prohibited without permission.

3.6 Summary and Conclusions

Three experiments were performed to determine the effects of various components of coal combustion flue gas on Hg oxidation. In order to study Hg oxidation by chlorine, various concentrations of Cl_2 were added. It was found that H_2O, SO_2 and NO exhibit inhibitory effects on Hg oxidation. Additionally, two reaction pathways are suggested that may cause these components to demonstrate these characteristics.

The following summarizes the results in this paper:

- A testing facility was built to simulate a temperature versus residence time profile similar to that of a power plant at locations beyond the economizer.
- Chlorine gas (Cl_2) oxidizes Hg effectively. In all these experiments, Cl_2 was intentionally added into a flue gas stream and the percent of Hg oxidation was observed.
- In a gas stream consisting of only N_2, O_2 and CO_2, the observed Hg oxidation increased with increasing Cl_2 concentration and the presence of H_2O. CO_2 did not have appreciable effects on Hg oxidation.
- The addition of SO_2 results in a decrease in Hg oxidation. This may be caused by the reaction of SO_2 with Cl_2 at these temperatures.
- The addition of NO resulted in a further decrease in Hg oxidation. This may be caused by the reaction of NO with Cl_2 at these temperatures.
- The presence of H_2O seems to cause SO_2 and NO to exhibit a stronger inhibitory effect on Hg oxidation and this is clarified by Experiment 3.
- The presence of CO in the flue gas had no effect on Hg oxidation.
- At a fixed gas composition consisting of 83% N_2, 3.5% O_2 and 13.5% H_2O, an increasing amount of Cl_2 resulted in a higher percent of Hg oxidation. It is assumed that at high enough Cl_2 concentrations, the percent of Hg oxidation will eventually reach 100%.

Reproduced with permission of the copyright owner. Further reproduction prohibited without permission.

CHAPTER 4

Development of a Predictive Kinetic Model for Homogeneous Hg Oxidation Data.

4.1 Abstract

Several researchers have developed a kinetic model to predict the effects of various flue gas components on homogeneous mercury (Hg) oxidation. Most of these models make use of over 50 reversible reactions that involve radicals in a combustion or post-combustion system, where temperatures are similar to that of a power plant boiler, in excess of 1700°C. Reaction rate constants are expressed in the form of $k = A*T^{n}*\exp(-E/R/T)$ where the unknown variables are A (pre-exponential factor), n (the exponent of temperature) and E (activation energy). The focus of this paper is the development of a simple kinetic model to predict experimental data in a laboratory scale apparatus. The results obtained show that only 5 reactions are required to predict the data obtained in the experimental work. Two of these reactions are reversible and three are irreversible. None of the reactions involve radicals, and only the pre-exponential factor and activation energy values in the rate constant term for the reactions are determined – the value of 'n' is set at 0. It is found that the predicted values correspond very well with the observed experimental data.

Reproduced with permission of the copyright owner. Further reproduction prohibited without permission.

4.2 Introduction

The key components in the gas stream that are responsible for the conversion of elemental Hg to its oxidized form are molecular chlorine gas (Cl_2) and hydrogen chloride (HCl). Other components, such as water (H_2O), nitrous oxide (NO), and sulfur dioxide (SO_2), also play an important role in this process. It has been found that Hg reacts favorably with Cl_2 at lower temperatures as shown by Mamani-Paco[187], Laudal[76] and Hall[8]. It has been shown that Hg reacts favorably with HCl at higher temperatures as shown by Sliger[82], Kilgroe[43] and Ghorishi[183]. Kilgroe and Sliger also showed that H_2O inhibits the reaction between Hg and HCl. Laudal[76] showed that SO_2 inhibited the reaction between Hg and Cl_2 at low temperatures. Qiu[189] showed that SO_2 inhibited the reaction between Hg and HCl at higher temperatures. In contrast to Laudal and Qiu, Cao[85] and Kellie[89] performed experimental work showing that SO_2 seemed to encourage the oxidation of Hg. This discrepancy was removed by a previously publication showing that SO_2 did have an inhibitory effect[188]. This same work also showed that NO in the gas stream inhibited the reaction between Hg and Cl_2. Data taken in a separate study showed the impact of temperature on the oxidative nature of Cl_2 on Hg[190].

In order to better understand the reaction mechanism that takes place in the gas phase, a model needs to be developed where the percent mercury oxidized can be predicted based on the concentrations of these flue gas components. Several researchers have published predictive mechanisms by using the software Chemkin®. These models use over 50 elementary reactions involving radicals in a gas stream. The presence of radicals in a gas stream may be predicted theoretically. However, to date, no technology is available to experimentally measure these concentrations and offer a comparison to the predictions. Additionally, the use of over 50 of these reactions makes the model bulky and difficult to use. The model makes use of the Arrhenius equation (discussed later) and lists the equations and the corresponding constants. These constants need to be found either by calculations or by finding the best fit to the experimental data. In either case, the two main constants are the pre-exponential factor (A) and the activation energy (E), and both constants have to be a positive number. Several of these values used by other researchers in their modeling work have been negative.

Reproduced with permission of the copyright owner. Further reproduction prohibited without permission.

Sliger et. al. published a model which was used to predict the data obtained in their experimental work[184]. It was found that the model was able to predict about half of their experimental data accurately. However, several activation energy values used in key reactions were negative. Widmer et. al. used a similar approach in their work, where a system of 8 reactions was used to predict the interaction of elemental Hg with a chlorine species[191]. The values used for the constants were similar to that of Sliger, where the activation energy of a key initiation reaction was a negative value. Widmer's model seemed to correspond with experimental data more closely. However, the model did not take into account the effects of other gas components, most notably, SO_2. Edwards et. al. published a model to predict some experimental data[88]. The predictions seemed to correspond well with the experimental data. However, similar to Sliger and Widmer, several of the key constants in the Arrhenius equation were negative. Additionally, the model did not account for the inhibitory effect of SO_2. Niksa et. al. published a kinetic model to predict the importance of NO and H_2O in a gas stream[84]. The predictions seemed to correspond well with the experimental data. However, in order to predict the data accurately, the authors made use of oxygen radicals for initiating the reaction between elemental Hg and Cl radicals. Since oxygen radicals were intentionally added into the model, the results obtained less realistic. Qiu et. al. made use of a similar scheme to predict some experimental data, but also made use of elementary reactions involving the impact of SO_2 on Hg oxidation[189]. The model was able to predict the experimental data very accurately. However, it was unable to predict the data that we obtained. This calls into question the robustness of the model. The experimental work done by Qiu focused on high temperatures, in excess of 1000°C, while the data obtained in our experimental apparatus was done at a maximum temperature of 550°C. This suggests that the model obtained by Qiu was specific for their system and temperature, but was unable to predict lower temperature data.

The experimental data presented in two prior publications were performed in a laboratory scale apparatus that was designed and built for the purposes of performing homogeneous and heterogeneous mercury oxidation[188, 190]. The data presented focuses only on homogeneous mercury oxidation, implying that reactions occurred only in the gas phase. In order to obtain a

Reproduced with permission of the copyright owner. Further reproduction prohibited without permission.

comprehensive explanation of the data collected, it is important to develop a model to predict this data. Several researchers have proposed mechanisms that make use of elementary reactions. Such reactions do not involve molecular interactions, but interactions between radicals. Additionally, these mechanisms have over 50 elementary reactions, which in some cases may contribute to the robustness of the model. However, it was found that the experimental data presented in two prior publications were not predicted well by these models. Additionally, it was found that the constants in the Arrhenius equation for several elemental reactions were negative. As a result, it was important to develop a model that not only predicted the current experimental data, but the data obtained by other researchers as well.

This paper will present a model involving only 5 reactions, where 2 are reversible and 3 are irreversible. The predicted results obtained will be compared to the observed experimental results and it will be shown that the fit is very good.

4.3 Background on Chemical Engineering Kinetics

This section will present a brief overview of chemical engineering kinetics. Consider a generalized reaction written as follows:

$$wA + xB \underset{k_r}{\overset{k_f}{\leftrightarrow}} yC + zD \qquad (1)$$

A and B are the reactants while C and D are the products in this reaction. The terms 'w', 'x', 'y' and 'z' are stoichiometric ratios for the reaction to take place. In the forward reaction case, 'w' moles of A will react with 'x' moles of B to produce 'y' moles of C and 'z' moles of D. The term 'k_f' is the rate constant of the forward reaction. In the reverse reaction case, 'y' moles of C will react with 'z' moles of D to produce 'w' moles of A and 'x' moles of B. The term 'k_r' is the rate constant of the forward reaction.

The rate of the forward reaction (r_f) is dependent on the concentration and stoichiometric ratio of A and B (equation 2) while the rate of the reverse reaction (r_r) is dependent on the concentration and stoichiometric ratio of C and D (equation 3). The square brackets denote concentration of the species.

Reproduced with permission of the copyright owner. Further reproduction prohibited without permission.

$$r_f = k_f \cdot [A]^w \cdot [B]^x \quad (2)$$

$$r_r = k_r \cdot [C]^y \cdot [D]^z \quad (3)$$

The rate of change of concentration with respect to time for each species in the reaction can be written as a differential equation. The term 'R_i' denotes the rate of change of concentration of species 'i' with respect to time. The differential equations for each species in equation 1 are listed below.

$$R_A = \frac{d[A]}{dt} \quad (4)$$

$$R_B = \frac{d[B]}{dt} \quad (5)$$

$$R_C = \frac{d[C]}{dt} \quad (6)$$

$$R_D = \frac{d[D]}{dt} \quad (7)$$

In this reversible reaction, each species is being produced and destroyed. For example, species A is being destroyed in the forward reaction and simultaneously being produced in the reverse reaction. As a result, the rate of change of concentration for species A depends on both the forward and the reverse rates. Equations 4 – 7 can thus be re-written as follows.

$$R_A = \frac{d[A]}{dt} = r_r - r_f = k_r \cdot [C]^y \cdot [D]^z - k_f \cdot [A]^w \cdot [B]^x \quad (8)$$

$$R_B = \frac{d[B]}{dt} = r_r - r_f = k_r \cdot [C]^y \cdot [D]^z - k_f \cdot [A]^w \cdot [B]^x \quad (9)$$

$$R_C = \frac{d[C]}{dt} = r_f - r_r = k_f \cdot [A]^w \cdot [B]^x - k_r \cdot [C]^y \cdot [D]^z \quad (10)$$

$$R_D = \frac{d[D]}{dt} = r_f - r_r = k_f \cdot [A]^w \cdot [B]^x - k_r \cdot [C]^y \cdot [D]^z \quad (11)$$

The reaction rate constants, denoted as k_f or k_r, are found to be well represented by the modified Arrhenius' Law (equation 12)[192]

Reproduced with permission of the copyright owner. Further reproduction prohibited without permission.

$$k = A \cdot T^n \cdot \exp[\frac{-E}{R \cdot T}] \quad (12)$$

where 'A' is the pre-exponential factor, 'T' is the temperature in degrees Kelvin, 'n' is a temperature constant, 'E' is the activation energy of the reaction, and 'R' is the universal gas constant with a value of 1.987 calories per mole per Kelvin (cal/mole/K). Because the exponential term is so much more temperature sensitive than the pre-exponential term, the variation of the 'T^n' term is effectively masked, and equation 12 reduces to:

$$k = A \cdot \exp[\frac{-E}{R \cdot T}] \quad (13)$$

Eventually, the system reaches equilibrium, where the rate of the forward reaction is equal to the rate of the reverse reaction. The equilibrium rate constant (Keq) can thus be determined as shown by equations 14a and 14b.

$$r_f = r_r \Rightarrow k_f \cdot [A]^w \cdot [B]^x = k_r \cdot [C]^y \cdot [D]^z \quad (14a)$$

$$\frac{k_f}{k_r} = \frac{[C]^y \cdot [D]^z}{[A]^w \cdot [B]^x} = Keq \quad (14b)$$

Therefore, after some simple algebraic substitutions, the overall reaction rate for the general reversible reaction can be written as:

$$r = k \cdot \left([A]^w \cdot [B]^x - \frac{[C]^y \cdot [D]^z}{Keq} \right) \quad (15)$$

The value of 'Keq' is typically constant at a specific temperature for a specific reaction. It is known, however, that the value of 'Keq' varies as temperature varies. A simple relation to describe this temperature dependence is shown by equation 16:

$$Keq = \exp\left[M + \frac{N}{T} \right] \quad (16)$$

where M and N are constants. A simple equilibrium calculation using the RGIBBS reactor model in the software Aspen Plus can be done to find the values of M and N, and thus the value of 'Keq'

Reproduced with permission of the copyright owner. Further reproduction prohibited without permission.

as a function of temperature. This process to find 'Keq' for the reversible reactions is used in this work.

It is important to note that the last few steps in this process are not required for an irreversible reaction. For example, if equation 1 was an irreversible reaction, the reaction rate would simply be defined as shown by equation 2. In this work, it was assumed that the irreversible reactions were first order. Therefore, the generalized equation 2 reduces to:

$$r = k \cdot [A] \cdot [B] \tag{17}$$

where the term 'k' is again defined by equation 13.

4.4 Proposing a Reaction Mechanism

The proposed reaction mechanism to predict the experimental data is a simple 5 reaction system, where 2 reactions are reversible and 3 reactions are irreversible. These reactions are listed below.

$$H_2O(g) + Cl_2(g) \xleftrightarrow{k_1} 2HCl(g) + \tfrac{1}{2}O_2(g) \tag{R1}$$

$$Hg(g) + Cl_2(g) \xleftrightarrow{k_2} HgCl_2(g) \tag{R2}$$

$$2NO(g) + Cl_2(g) \xrightarrow{k_3} 2NOCl(g) \tag{R3}$$

$$HgCl_2(g) + SO_2(g) \xrightarrow{k_4} Hg(g) + SCl_2(s,g) + O_2(g) \tag{R4}$$

$$Hg(g) + 2HCl(g) \xrightarrow{k_5} HgCl_2(g) + H_2(g) \tag{R5}$$

where Hg is elemental mercury, Cl_2 is molecular chlorine, $HgCl_2$ is mercury (II) chloride, H_2O is water, HCl is hydrogen chloride, O_2 is molecular oxygen, H_2 is molecular hydrogen, SO_2 is sulfur dioxide, SCl_2 is sulfur dichloride, NO is nitrous oxide and NOCl is nitrosyl chloride. The term '(g)' denotes that the species is in gas phase, and the term '(s,g)' denotes that the species could be in solid (s), gas (g) or both phases.

The reaction rate equations and the corresponding rate constants for the reversible reactions (R1 and R2) can be written following the generalized equations 12, 15 and 16:

Reproduced with permission of the copyright owner. Further reproduction prohibited without permission.

$$r_1 = k_1 \cdot \left([H_2O] \cdot [Cl_2] - \frac{[HCl]^2 \cdot [O_2]^{1/2}}{Keq1} \right) \quad (18)$$

$$Keq1 = \exp\left[M_1 + \frac{N_1}{T} \right] \quad (19)$$

$$k_1 = A_1 \cdot T^{n1} \cdot \exp[\frac{-E_1}{R \cdot T}] \quad (20)$$

$$r_2 = k_2 \cdot \left([Hg] \cdot [Cl_2] - \frac{[HgCl_2]}{Keq2} \right) \quad (21)$$

$$Keq2 = \exp\left[M_2 + \frac{N_2}{T} \right] \quad (22)$$

$$k_2 = A_2 \cdot T^{n2} \cdot \exp[\frac{-E_2}{R \cdot T}] \quad (23)$$

where M_1 and N_1 are the constants for the equilibrium constant (Keq1) for reaction R1, and M_2 and N_2 are the constants for the equilibrium constant (Keq2) for reaction R2.

Additionally, using the generalized equations 8 through 11, the reaction rate equations and the corresponding rate constants for the irreversible reactions (R3, R4 and R5) can now be written as

$$r_3 = k_3 \cdot [NO]^2 \cdot [Cl_2] \quad (24)$$

$$k_3 = A_3 \cdot T^{n3} \cdot \exp[\frac{-E_3}{R \cdot T}] \quad (25)$$

$$r_4 = k_4 \cdot [HgCl_2] \cdot [SO_2] \quad (26)$$

$$k_4 = A_4 \cdot T^{n4} \cdot \exp[\frac{-E_4}{R \cdot T}] \quad (27)$$

$$r_5 = k_5 \cdot [Hg] \cdot [HCl]^2 \quad (28)$$

$$k_5 = A_5 \cdot T^{n5} \cdot \exp[\frac{-E_5}{R \cdot T}] \quad (29)$$

Reproduced with permission of the copyright owner. Further reproduction prohibited without permission.

In this set of equations, there are 5 unknown values of 'A', 5 unknown values of 'E' and 5 unknown values of 'n'. In order to simplify the system of equations and unknowns, some assumptions are made:

i. The 'T^n' term is assumed to be insignificant, and the value of 'n' for all the reactions is set to zero.

ii. Equations (24) and (28) are changed to be first order equations.

As mentioned in the previous section, the values of M_1, N_1, M_2 and N_2 can be found by a simple equilibrium calculation using the RGIBBS reactor in Aspen Tech. The following values were found:

$M_1 = 13.707$
$N_1 = -4769.2$
$M_2 = -17.833$
$N_2 = 17133.1$

Therefore, the final set of reaction rate equations used in this model is as follows.

$$r_1 = A_1 \cdot \exp[\frac{-E_1}{R \cdot T}] \cdot \left([H_2O] \cdot [Cl_2] - \frac{[HCl]^2 \cdot [O_2]^{1/2}}{\exp\left[13.707 - \frac{4769.2}{T}\right]} \right) \quad (30)$$

$$r_2 = A_2 \cdot \exp[\frac{-E_2}{R \cdot T}] \cdot \left([Hg] \cdot [Cl_2] - \frac{[HgCl_2]}{\exp\left[-17.833 + \frac{17133.1}{T}\right]} \right) \quad (31)$$

$$r_3 = A_3 \cdot \exp[\frac{-E_3}{R \cdot T}] \cdot [NO] \cdot [Cl_2] \quad (32)$$

$$r_4 = A_4 \cdot \exp[\frac{-E_4}{R \cdot T}] \cdot [HgCl_2] \cdot [SO_2] \quad (33)$$

Reproduced with permission of the copyright owner. Further reproduction prohibited without permission.

$$r_5 = A_5 \cdot \exp[\frac{-E_5}{R \cdot T}] \cdot [Hg] \cdot [HCl] \quad (34)$$

Following equations 4 through 11, the rate of change of concentration for each species can be written as follows.

$$R_{Hg} = \frac{d[Hg]}{dt} = r_4 - r_2 - r_5 \quad (35)$$

$$R_{HgCl_2} = \frac{d[HgCl_2]}{dt} = r_2 + r_5 - r_4 \quad (36)$$

$$R_{Cl_2} = \frac{d[Cl_2]}{dt} = -r_1 - r_2 - r_3 \quad (37)$$

$$R_{HCl} = \frac{d[HCl]}{dt} = 2r_1 - 2r_5 \quad (38)$$

$$R_{H_2O} = \frac{d[H_2O]}{dt} = -r_1 \quad (39)$$

$$R_{O_2} = \frac{d[O_2]}{dt} = \frac{1}{2} r_1 + r_4 \quad (40)$$

$$R_{SO_2} = \frac{d[SO_2]}{dt} = -r_4 \quad (41)$$

$$R_{SCl_2} = \frac{d[SCl_2]}{dt} = r_4 \quad (42)$$

$$R_{NO} = \frac{d[NO]}{dt} = -2r_3 \quad (43)$$

$$R_{NOCl} = \frac{d[NOCl]}{dt} = 2r_3 \quad (44)$$

$$R_{H_2} = \frac{d[H_2]}{dt} = r_5 \quad (45)$$

These equations can now be solved numerically to find the values of the 10 unknowns.

Reproduced with permission of the copyright owner. Further reproduction prohibited without permission.

4.5 MATLAB Program for Predicting Experimental Data

A MATLAB model was written to solve this system of equations and find the 10 unknown constants for the reaction. The program is a set of 4 files that are given below.

The first file is called 'reactor.m'. This file consists of the modified Arrhenius equation for the rate constants, and lists the reaction rate equations for each of the reactions. As mentioned in the previous section, the stoichiometric coefficients for all the reactions were assumed to be 1 to remove non-linearity in the system. The 'if-else' statement refers to the temperature and residence time profiles of the experimental work. More details on these profiles are given in previous publications[12-13]. The reacting species in the system are listed to be having either variable or constant concentrations. In this work, the species with a constant concentration is H_2O. For example, in a flow rate of 100 liters per minute of gas mixture, 13.5% is comprised of H_2O. In contrast, the concentration of Cl_2 and Hg is $2x10^{-4}$% and $1.2x10^{-7}$%. Since the concentration of H_2O is several orders of magnitudes higher than that of the variable species, it is assumed to be constant. The file 'reactor.m' is shown below.

```
% this function solves the pfr equations
function yprime=reactor(t,y);
global WATER OXYGEN TEMP STOIC ARH EACT kg tres;
% R1 Cl2 + H2O --> 2HCl + 0.5 O2
% R2 Hg + Cl2 --> HgCl2
% R3 2NO + Cl2 --> 2NOCl
% R4 HgCl2+SO2-->Hg+SCl2+O2
% R5 Hg + 2HCl --> HgCl2 + H2
%
% Variable Species 1:Cl2 2:HCl 3:SO2 4:Hg 5:HgCl2 6: NO 7:NOCl 8:O2 9:SCl2 10:H2
% Constant Species WATER:yWater  OXYGEN:yOxygen
%find T

if(t<tres(1)) T=TEMP(1);
elseif(t<tres(2)) T=TEMP(2);
else T=TEMP(3);
end;

k=ARH.*exp(-EACT/1.987/T);

% R1 Cl2 + H2O --> 2HCl + 0.5 O2
Keq1= exp(13.70143007-4769.180023/T);
r(1)=k(1)*(y(1)*WATER - (y(2)^2)*(y(8)^(1/2))/Keq1);

% R2 Hg + Cl2 --> HgCl2
```


Reproduced with permission of the copyright owner. Further reproduction prohibited without permission.

```
Keq2= exp(-17.83302633+17133.09234/T);
r(2)=k(2)*(y(4)*y(1) - y(5)/Keq2);

% R3 2NO + CL2 --> 2NOCL
r(3)=k(3)*y(1)*y(6);

% R4 HgCl2+SO2-->Hg+SCl2+O2
r(4)=k(4)*y(5)*y(3);

% R5 Hg + 2HCl --> HGCL2 + H2
r(5)=k(5)*y(4)*y(2);

yprime=r*STOIC;
yprime=transpose(yprime);
```

The second file is called 'main.m'. The purpose of this file is to initialize all the values of the unknowns being found (A and E) for the respective reactions.

```
clear all;
clc;

% R1 Cl2 + H2O --> 2HCl + 0.5 O2
% R2 Hg + Cl2 --> HgCl2
% R3 2NO + Cl2 --> 2NOCl
% R4 HgCl2+SO2-->Hg+SCl2+O2
% R5 Hg + 2HCl --> HgCl2 + H2

% Constant Values for A and E

A1= 62.271287663137478319;      %Pre-exponential factor for Reaction 1
A2= .37687663751928834888;      %Pre-exponential factor for Reaction 2
A3= 98.681925287893065502;      %Pre-exponential factor for Reaction 3
A4= 138.85335183630201072;      %Pre-exponential factor for Reaction 4
A5= 36.113231663431704987;      %Pre-exponential factor for Reaction 5

E1= 8.8667661287885444210;      %Activation energy for Reaction 1
E2= .89336977740065881548e-1;   %Activation energy for Reaction 2
E3= 23.509278111450633730;      %Activation energy for Reaction 3
E4= 17.638022677706544528;      %Activation energy for Reaction 4
E5= 15.108467962884994051;      %Activation energy for Reaction 5

% this initializes the kinetic parameters you want to find.
AEs=[A1 A2 A3 A4 A5 E1 E2 E3 E4 E5];

% Which constant is up to the code in Hgkineticfinder
A = fminsearch('Hgkineticfinder',AEs)
```


Reproduced with permission of the copyright owner. Further reproduction prohibited without permission.

The function 'fminsearch' is used to find the minimum of a scalar function of several variables, starting at an initial estimate[193]. This is generally referred to as unconstrained nonlinear optimization. In this case, the initial estimate for each of the 10 unknowns is defined by the array called 'AEs'. These values are then called by the next file, 'Hgkineticfinder.m'.

```
function MINERROR=Hgkineticfinder(As)
% R1 Cl2 + H2O --> 2HCl + 0.5 O2
% R2 Hg + Cl2 --> HgCl2
% R3 2NO + Cl2 --> 2NOCl
% R4 HgCl2+SO2-->Hg+SCl2+O2
% R5 Hg + 2HCl --> HgCl2 + H2

% Variable Species 1:Cl2 2:HCl 3:SO2 4:Hg 5:HgCl2 6: NO 7:NOCl 8:O2 9:SCl2 10:H2
% Constant Species WATER:yWater OXYGEN:yOxygen
global WATER OXYGEN TEMP STOIC ARH EACT kg tres;
MINERROR=0;
load reactordata.txt
% data order: Inlet y's:  1:Cl2 2:HCl 3:SO2 in ppm 14:NO in ppm
% except for Hg which is in ug/cum
% followed by WATER, OXYGEN in mole fraction TEMP in C
% followed by Hgzero out in ug/cum
% followed by residence time in seconds
fprintf('\n  Run#   Model Hg conversion   Data Hg conv \n');
ndata=size(reactordata);
for(i=1:1:ndata(1))
   yinit=reactordata(i,1:4); %Hg values from reactor data file
   hgconvdata=(reactordata(i,4)-reactordata(i,10))/reactordata(i,4)*100;
   WATER=reactordata(i,5); %H2O values from reactor data file
   OXYGEN=reactordata(i,6); %O2 values from reactor data file
   MWHg=200.59; % convert Hg to ppm
   yinit(4)=yinit(4)*22.4/1000/MWHg*(1-WATER);
   yinit(5)=0; % zero HgCl2 initially
   yinit(6)=reactordata(i,14); %NO values from reactor data file
   yinit(7)=0; % zero NOCl initially
   yinit(8)=OXYGEN;
   yinit(9)=0; %zero SCl2 initially
   yinit(10)=0; %zero H2 initially
   TEMP(1)=reactordata(i,7)+273.15; % C to Kelvin
   TEMP(2)=reactordata(i,8)+273.15; % C to Kelvin
   TEMP(3)=reactordata(i,9)+273.15; % C to Kelvin
   tres(1)=reactordata(i,11);
   tres(2)=reactordata(i,12);
   tres(3)=reactordata(i,13);
   tmax=tres(3);

   A1= As(1);  %Pre-exponential Factor for Reacton 1
   A2= As(2);  %Pre-exponential Factor for Reacton 2
   A3= As(3);  %Pre-exponential Factor for Reacton 3
   A4= As(4);  %Pre-exponential Factor for Reacton 4
   A5= As(5);  %Pre-exponential Factor for Reacton 5
```


Reproduced with permission of the copyright owner. Further reproduction prohibited without permission.

```
  E1= As(6);  %Activation Energy for Reaction 1
  E2= As(7);  %Activation Energy for Reaction 2
  E3= As(8);  %Activation Energy for Reaction 3
  E4= As(9);  %Activation Energy for Reaction 4
  E5= As(10); %Activation Energy for Reaction 5

  ARH =[A1 A2 A3 A4 A5];
  EACT=[E1 E2 E3 E4 E5]*1e3; %cal/mole

% Stoichiometric Matrix follows, zeros are for species in great excess
% and for species not in reaction
% Variable Species 1:Cl2 2:HCl 3:SO2 4:Hg 5:HgCl2 6:NO 7:NOCl 8:O2 9:SCL2 10:H2
%       1 2 3 4 5 6 7  8  9 10
  str1=[-1  2  0  0  0  0  0  0.5  0  0 ]; %R1 Cl2 + H2O --> 2HCl + 0.5 O2
  str2=[-1  0  0 -1  1  0  0   0   0  0 ]; %R2 Hg + Cl2 --> HgCl2
  str3=[ 0  0  0  0  0  0  0  0   0   0  0 ]; %R3 2NO + CL2 --> 2NOCL
  str4=[ 0  0  0  0  0  0  0  0   0   0  0 ]; %R4 HgCl2+SO2-->Hg+SCl2+O2
  str5=[ 0  0  0  0  0  0  0  0   0   0  0 ]; %R5 Hg+2HCl-->HgCl2+H2
  STOIC=[str1;str2;str3;str4;str5];

  npts=1000; %integration points along reactor
  tspan=0:(tmax/(npts-1)):tmax; % values of time where y's are returned from ODE45
  [t,y]=ode45('reactor',tspan,yinit);
  hgconv=(y(1,4)-y(npts,4))/y(1,4)*100.;
  MINERROR=(MINERROR+(hgconv-hgconvdata)^2);
  fprintf('%3.0f %20.3f %10.3f \n',i,hgconv,hgconvdata);

 end;

MINERROR=MINERROR/ndata(1);
digits(20)
VALUES=sym(As,'d')

% Prints the value of least square error.
fprintf('LS ERROR= %7f \n',MINERROR);

% Prints the values of A – all the Arrhenius pre-exponential factors.
fprintf('\n Constants: \n A1= %7f \n A2= %7f \n A3= %7f \n A4= %7f \n A5= %7f \n',ARH);

% Prints the values of Ea – all the activation energy values.
fprintf('\n E1= %7f \n E2= %7f \n E3= %7f \n E4= %7f \n E5= %7f \n',EACT);
```

This file makes use of the 'fminsearch' function to find the best fit values of A and E for the reactions. The constants for ARH and EACT are imported from the 'main.m' file and used in the matrix shown. The function 'ode45' is based on an explicit Runge-Kutta (4,5) formula, the Dormand-Prince pair[194]. This function is a computing one-step solver for which it needs only the solution at the immediately preceding time point. In general, ode45 is the best function to apply as a "first try" for most time dependent problems[194]. The differential equations used in this work are

Reproduced with permission of the copyright owner. Further reproduction prohibited without permission.

listed as equations 35 through 45 and are solved for with this function. The output of this file presents the updated values of A and E, along with 'MINERROR', or minimum error. The minimum error is calculated by summing the squared difference between the observed and predicted value, and then dividing this value by the number of data points. Initially, the value of MINERROR is zero. Ideally, as the values of A and E become more controlled, the value of MINERROR will tend to zero. This program runs continuously either until the minimum error is zero, or 1000 loops have taken place.

The last file is the data file called 'reactordata.txt' where all the experimental data obtained is presented. The MATLAB file 'Hgkineticfinder.m' calls the values of each of the reacting species, the temperatures and residence times from this file. These values are used in the calculation of A and E.

```
% Reactor Data
% data order: Inlet y's:  1:Cl2 2:HCl 3:SO2 4:Hg in ppm except for Hg which is in ug/cum
% followed by WATER, OXYGEN in mole fraction TEMP in C
% followed by Hgzero out in ug/cum
% followed by residence time in seconds
% Cl2   HCl   SO2   Hg    Water  Oxygen  Temp    Temp    Temp   Hg     tres   tres   tres   NO
% in    in    in    in    in     in      R1exit  R2exit  SL     out    R2     HX1    SL     in
% ppm   ppm   ppm   ug/m3 molfrc molfrc  C       C       C      ug/m3  sec    sec    sec    ppm
%
%
% Runs 1 to 6 from Additive Experiment 1 (2ppm Cl2 Injection)
%
% Run 1: N2 O2
    2     0     0    11.7   0.00   2.9     540     389     177    3.300  1.78   2.00   2.10   0
% Run 2: N2 O2 CO2
    2     0     0    13.4   0.00   2.9     540     389     177    3.100  1.78   2.00   2.10   0
% Run 3: N2 O2 CO2 SO2
    2     0     370  14.9   0.00   2.9     540     389     177    7.100  1.78   2.00   2.10   0
% Run 4: N2 O2 CO2 SO2 NO
    2     0     370  12.7   0.00   2.9     540     389     177    6.900  1.78   2.00   2.10   170
% Run 5: N2 O2 CO2 SO2 NO CO
    2     0     370  11.7   0.00   2.9     540     389     177    6.200  1.78   2.00   2.10   170
% Run 6: N2 O2 CO2 SO2 NO CO H2O
    2     0     370  10.0   12.9   2.9     540     389     177    10.00  1.78   2.00   2.10   170
%
% Runs 7 to 11 from Additive Experiment 2 (27.5ppm Cl2 Injection)
%
% Run 7: N2 H2O O2
   27.5   0     0    10.5   12.9   2.9     540     389     163    1.100  1.78   2.00   2.10   0
% Run 8: N2 H2O O2 CO2
   27.5   0     0    10.6   12.9   2.9     540     389     163    1.055  1.78   2.00   2.10   0
% Run 9: N2 H2O O2 CO2 SO2
```


Reproduced with permission of the copyright owner. Further reproduction prohibited without permission.

```
  27.5   0     370   10.3   12.9   2.9     540    389   163   4.438  1.78  2.00  2.10   0
% Run 10: N2 H2O O2 CO2 SO2 NO
  27.5   0     370   10.6   12.9   2.9     540    389   163   5.751  1.78  2.00  2.10   170
% Run 11: N2 H2O O2 CO2 SO2 NO CO
  27.5   0     370   10.8   12.9   2.9     540    389   163   6.000  1.78  2.00  2.10   170
%
% Runs 12 to 16 from Additive Experiment 2 (49.5ppm Cl2 Injection)
% Continuation from previous section
%
% Run 12: N2 H2O O2
  49.5   0     0     10.5   12.9   2.9     540    389   163   0.570  1.78  2.00  2.10   0
% Run 13: N2 H2O O2 CO2
  49.5   0     0     10.6   12.9   2.9     540    389   163   0.717  1.78  2.00  2.10   0
% Run 14: N2 H2O O2 CO2 SO2
  49.5   0     370   10.3   12.9   2.9     540    389   163   3.443  1.78  2.00  2.10   0
% Run 15: N2 H2O O2 CO2 SO2 NO
  49.5   0     370   10.6   12.9   2.9     540    389   163   5.150  1.78  2.00  2.10   170
% Run 16: N2 H2O O2 CO2 SO2 NO CO
  49.5   0     370   10.8   12.9   2.9     540    389   163   5.000  1.78  2.00  2.10   170
%
% Runs 17 to 25 from Water Experiment
% 3 temperatures, 3 Cl2 concentrations
%
% Run 17: N2 H2O (Exit R1 = 607F)
  12.4   0     0     12.7   12.9   0.0     319    270   163   3.670  2.83  2.83  2.93   0
% Run 18: N2 H2O (Exit R1 = 607F)
  30.9   0     0     12.7   12.9   0.0     319    270   163   1.600  2.83  2.83  2.93   0
% Run 19: N2 H2O (Exit R1 = 607F)
  51.8   0     0     12.7   12.9   0.0     319    270   163   0.800  2.83  2.83  2.93   0
% Run 20: N2 H2O (Exit R1 = 805F)
  11.6   0     0     11.7   12.9   0.0     429    343   163   2.230  2.44  2.44  2.54   0
% Run 21: N2 H2O (Exit R1 = 805F)
  30.5   0     0     11.7   12.9   0.0     429    343   163   1.140  2.44  2.44  2.54   0
% Run 22: N2 H2O (Exit R1 = 805F)
  51.8   0     0     11.7   12.9   0.0     429    343   163   0.630  2.44  2.44  2.54   0
% Run 23: N2 H2O (Exit R1 = 1000F)
  11.6   0     0     11.8   12.9   0.0     538    404   163   2.040  1.78  1.78  1.88   0
% Run 24: N2 H2O (Exit R1 = 1000F)
  30.5   0     0     11.8   12.9   0.0     538    404   163   1.380  1.78  1.78  1.88   0
% Run 25: N2 H2O (Exit R1 = 1000F)
  51.8   0     0     11.8   12.9   0.0     538    404   163   0.900  1.78  1.78  1.88   0
%
% Runs 26 to 35
% Cl2 collection of data - various temperatures, various Cl2 concentrations
% NOTES: Gas composition = 100% N2
%
% Run 26:
  1.00   0     0     1.08   0.00   0.0     166    114   121   0.290  3.17  3.56  3.67   0
% Run 27:
  1.00   0     0     1.15   0.00   0.0     347    194   121   0.544  2.41  2.75  2.86   0
% Run 28:
  1.00   0     0     10.86  0.00   0.0     169    113   121   3.350  3.16  3.54  3.65   0
% Run 29:
  1.00   0     0     11.65  0.00   0.0     353    228   121   5.420  2.32  2.65  2.76   0
% Run 30:
```


Reproduced with permission of the copyright owner. Further reproduction prohibited without permission.

```
  1.00    0      0     11.6    0.00    0.0     582     325     121     5.870  1.78  1.78  1.90  0
% Run 31:
  1.00    0      0     10.9    0.00    0.0     232     121     121     3.260  2.91  3.28  3.39  0
% Run 32:
  5.00    0      0     11.6    0.00    0.0     232     121     121     0.970  2.91  3.28  3.39  0
% Run 33:
  5.00    0      0     14.65   0.00    0.0     385     238     121     1.580  2.24  2.55  2.66  0
% Run 34:
  5.00    0      0     11.2    0.00    0.0     593     327     121     0.250  1.78  1.78  1.88  0
% Run 35:
  1.00    0      0     4.28    0.00    0.0     365     218     121     0.740  2.32  2.65  2.76  0
%
%
% Cl2   HCl    SO2    Hg      Water   Oxygen  Temp    Temp    Temp    Hg     tres  tres  tres  NO
% in    in     in     in      in      in      R1exit  R2exit  SL      out    R2    HX1   SL    in
% ppm   ppm    ppm    ug/m3   molfrc  molfrc  C       C       C       ug/m3  sec   sec   sec   ppm
%
% Run 36:
  0     200    370    10.2    12.9    2.9     860     538     177     5.700  1.35  1.49  1.59  170
% Run 37-38:
  0     300    0.0    9.00    12.9    2.9     860     538     177     2.500  1.35  1.49  1.59  170
  0     200    0.0    7.84    12.9    2.9     860     538     177     2.400  1.35  1.49  1.59  170
% Run 39:
  0     200    0.0    7.50    12.9    2.9     860     538     177     4.000  1.35  1.49  1.59  170
```

Issuing the MATLAB command

```
>> main
```

in the command window would result in a typical result as shown.

Run#	Model Hg conversion	Data Hg conv
1	76.394	71.795
2	76.392	76.866
3	52.318	52.349
4	51.914	45.669
5	51.915	47.009
6	5.787	0.000
7	94.993	89.524
8	94.993	90.047
9	43.642	56.913
10	43.561	45.745
11	43.599	44.444
12	98.998	94.571
13	98.998	93.236
14	61.633	66.573
15	61.414	51.415
16	61.415	53.704
17	99.925	71.102
18	100.000	87.402
19	100.000	93.701
20	94.288	80.940
21	99.920	90.256

Reproduced with permission of the copyright owner. Further reproduction prohibited without permission.

22	99.980	94.615
23	72.439	82.712
24	96.084	88.305
25	98.959	92.373
26	70.561	73.148
27	62.474	52.696
28	70.369	69.153
29	61.204	53.476
30	47.214	49.397
31	68.080	70.092
32	99.669	91.638
33	98.971	89.215
34	94.409	97.768
35	61.249	82.710
36	31.509	44.118
37	75.353	72.222
38	64.232	69.388
39	64.232	46.667

LS ERROR= 88.1340

Constants:

A1= 62.271287663137478319;
A2= .37687663751928834888;
A3= 98.681925287893065502;
A4= 138.85335183630201072;
A5= 36.113231663431704987;

E1= 8.8667661287885444210;
E2= .89336977740065881548e-1;
E3= 23.509278111450633730;
E4= 17.638022677706544528;
E5= 15.108467962884994051;

Reproduced with permission of the copyright owner. Further reproduction prohibited without permission.

4.6 Results and Discussion

The main purpose of this model is to determine the best values of A and E for the least number of reactions. The fewer the reactions used, the better and more efficient the model. It is possible to use a single reaction to predict a single data point, but that would result in over 30 reactions with different A and E values. This would make the model extremely complicated and inefficient.

The values of A and E are shown in Table 4.6, along with the corresponding rate constants for each reaction.

	Reaction	A	E ($x10^3$) (cal/mole)	$k = A \cdot \exp[\frac{-E}{R \cdot T}]$
R1	$H_2O(g) + Cl_2(g) \xleftrightarrow{k_1} 2HCl(g) + \frac{1}{2}O_2(g)$	62.3	8.87	$k_1 = 62.3 \cdot \exp[\frac{-8.87 \times 10^3}{1.987 \cdot T}]$
R2	$Hg(g) + Cl_2(g) \xleftrightarrow{k_2} HgCl_2(g)$	0.377	0.0893	$k_2 = 0.377 \cdot \exp[\frac{-8.93 \times 10^1}{1.987 \cdot T}]$
R3	$2NO(g) + Cl_2(g) \xrightarrow{k_3} 2NOCl(g)$	98.7	23.5	$k_3 = 98.7 \cdot \exp[\frac{-23.5 \times 10^3}{1.987 \cdot T}]$
R4	$HgCl_2(g) + SO_2(g) \xrightarrow{k_4} Hg(g) + SCl_2(s,g) + O_2(g)$	139	17.6	$k_4 = 139 \cdot \exp[\frac{-17.6 \times 10^3}{1.987 \cdot T}]$
R5	$Hg(g) + 2HCl(g) \xrightarrow{k_5} HgCl_2(g) + H_2(g)$	36.1	15.1	$k_5 = 36.1 \cdot \exp[\frac{-15.1 \times 10^3}{1.987 \cdot T}]$

Table 4.6: Summary of the Reactions used in this work with the corresponding A and E constants for the Arrhenius rate constant.

It was important to determine the effectiveness of the reactions used and the corresponding values of A and E. The best way to compare the observed and predicted values was to make a plot, with the observed values on the y-axis and the predicted values on the x-axis. Ideally, all the data points should lie on the y=x line (shown as the solid line) which would imply that the fit was perfect.

Initially, only Reaction R2 was used in the model. Many researchers have determined that this is the main reaction that results in the oxidation of Hg in a gas stream. The results are shown in Figure 4.6-1.

Reproduced with permission of the copyright owner. Further reproduction prohibited without permission.

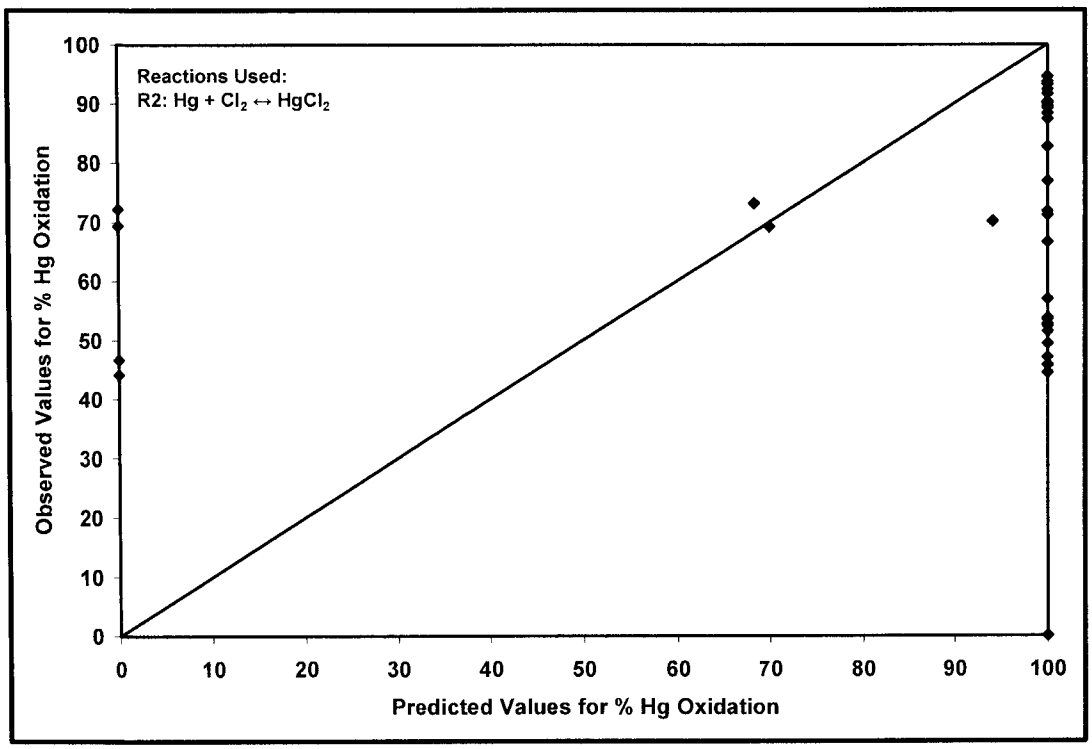

Figure 4.6-1: Plot of Observed % Hg oxidation versus Predicted % Hg oxidation using Reaction 2

As seen in Figure 4.6-1, the use of only R2 in the scheme results in a very poor fit. Most of the predictions are either 0% or 100% Hg oxidation. Only 2 data points seem to be accurately predicted at around the 70% mark. The calculated average error between the predicted Hg oxidation and observed Hg oxidation is 30.4.

Reaction R1 was then included in the modeling scheme. In previous publications, it was discussed that at lower temperatures, Cl_2 is the dominant species that oxidizes Hg, while at higher temperatures, HCl is the dominant species that oxidizes Hg[12-13]. In order to account for the temperature variation within the system, this reaction was used. The result from this step is shown in Figure 4.6-2.

Reproduced with permission of the copyright owner. Further reproduction prohibited without permission.

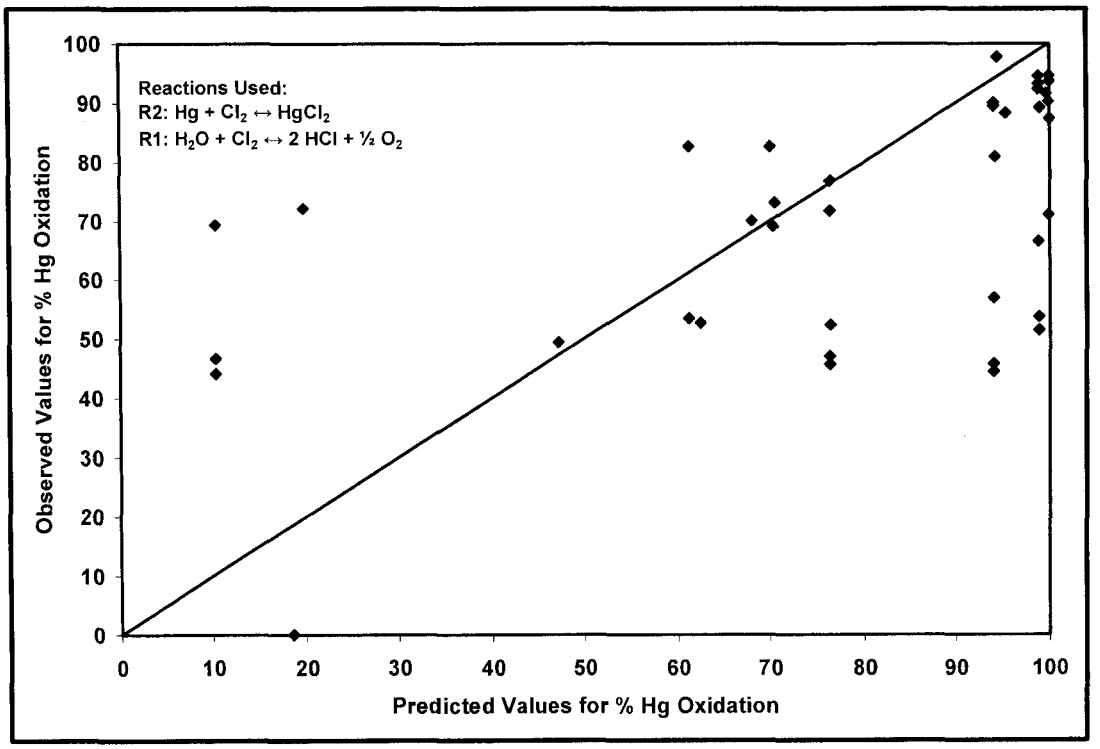

Figure 4.6-2: Plot of Observed % Hg oxidation versus Predicted % Hg oxidation using Reaction 2 and 1.

As seen in Figure 4.6-2, the fit between the observed and predicted values for percent Hg oxidation is slightly better than Figure 4.6-1. The calculated average error between the predicted and observed Hg oxidation values improved to 18.9. Most of the predicted values still do not correspond well with the observed values.

In order to account for the possibility that elemental Hg would react with HCl, Reaction R5 was included in the reaction mechanism as a potential means for Hg oxidation. The result from the addition of this third reaction is shown in Figure 4.6-3.

Reproduced with permission of the copyright owner. Further reproduction prohibited without permission.

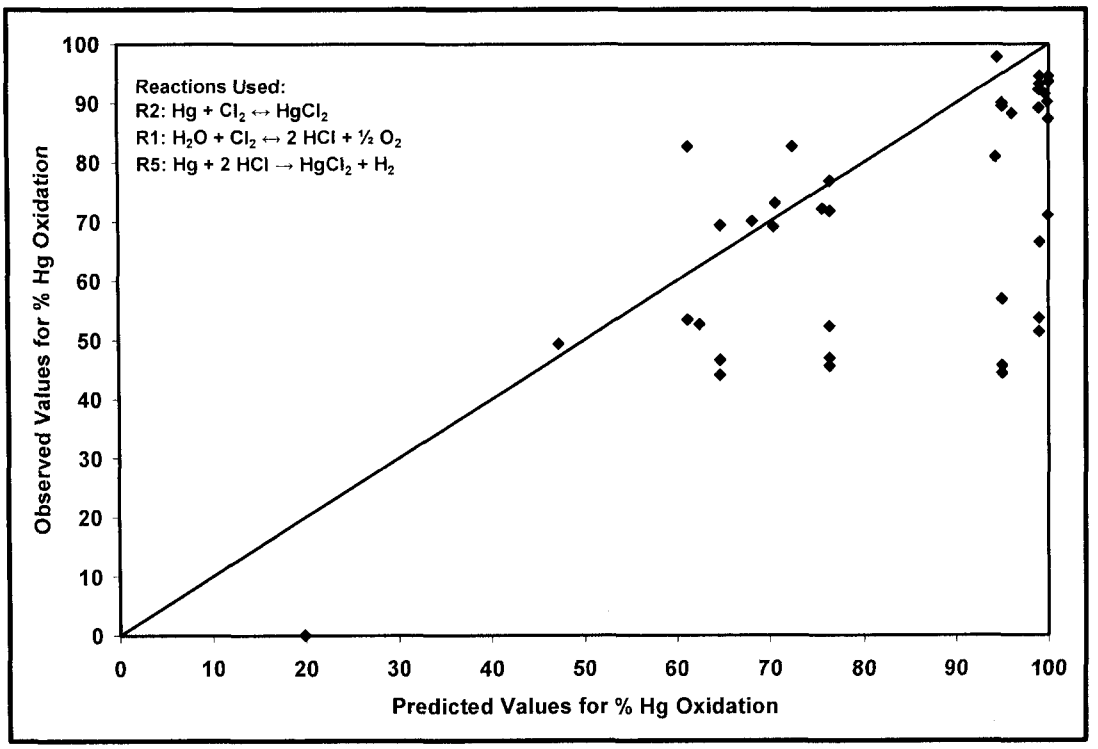

Figure 4.6-3: Plot of Observed % Hg oxidation versus Predicted % Hg oxidation using Reaction 2, 1 and 5.

As seen in Figure 4.6-3, the fit between the predicted and observed percent Hg oxidation values continues to improve. The calculated average error further improved to 15.6. Several of the predicted values are starting to correspond with the observed values.

Based on the experimental work performed in the laboratory apparatus, it was found that SO_2 and NO inhibited the percent of Hg oxidized. As a result, Reactions R3 and R4 were proposed as the possible reactions that result in this inhibitory effect. Reaction R4 was first introduced into the model and the result is shown in Figure 4.6-4. Reaction R3 was then added into the model and the result is shown in Figure 4.6-5.

Reproduced with permission of the copyright owner. Further reproduction prohibited without permission.

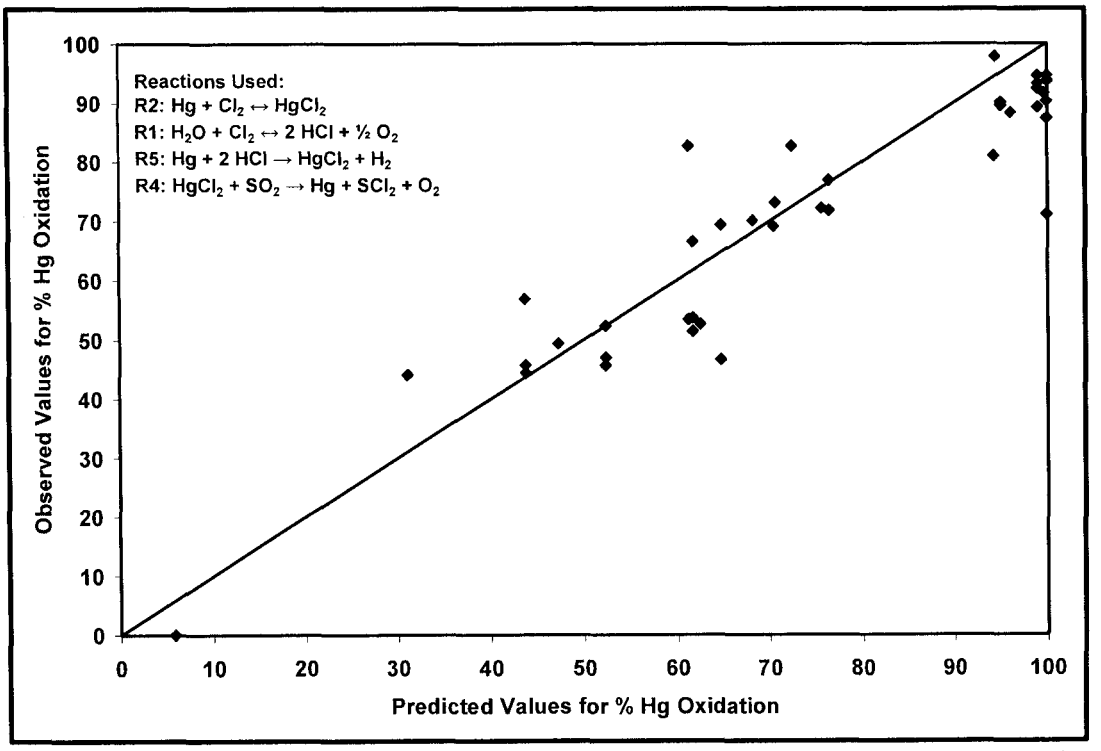

Figure 4.6-4: Plot of Observed % Hg oxidation versus Predicted % Hg oxidation using Reaction 2, 1, 5 and 4.

Reproduced with permission of the copyright owner. Further reproduction prohibited without permission.

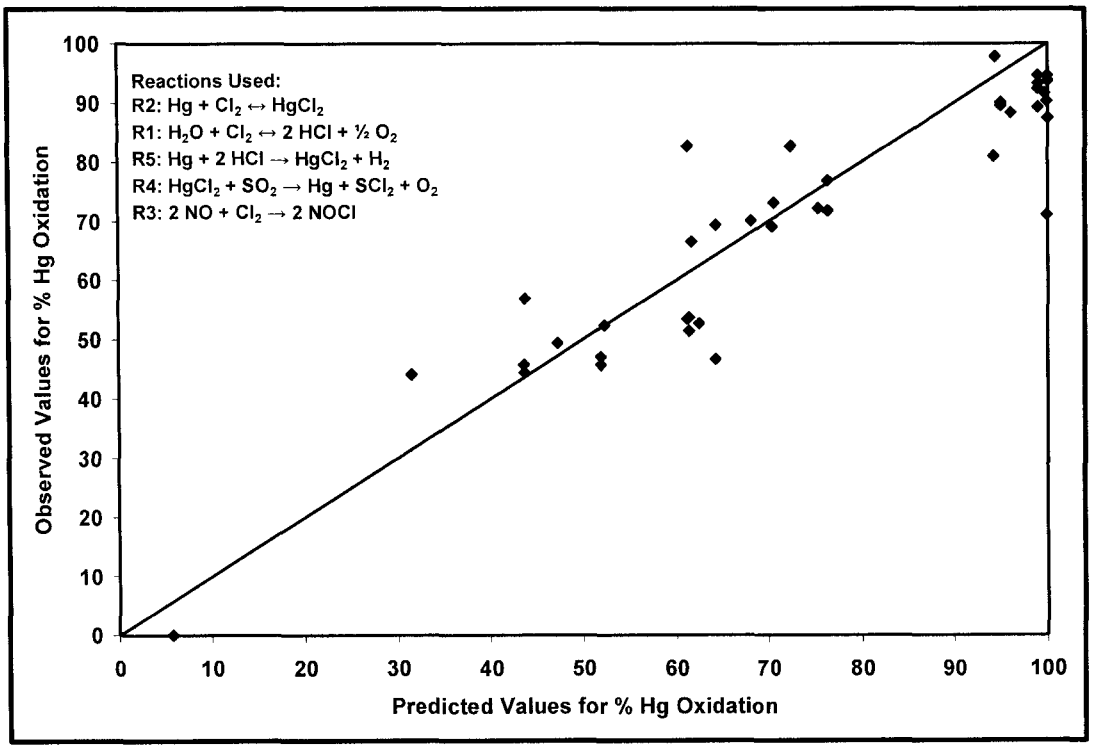

Figure 4.6-5: Plot of Observed % Hg oxidation versus Predicted % Hg oxidation using Reaction 2, 1, 5, 4 and 3.

Figure 4.6-4 shows that the fit continues to improve. The calculated average error was 7.5, a significant improvement from the previous value of 15.6. However, the addition of Reaction R3 seems to improve the fit only slightly. The calculated average error improved slightly to 7.4. This suggests that even though R3 may not be an important reaction in this system, it may still have a minor impact. This reaction is included because of completeness.

Reproduced with permission of the copyright owner. Further reproduction prohibited without permission.

4.7 Conclusions and Future Work

This paper presents a model to predict some experimental data obtained in a chemical engineering laboratory apparatus. It was suggested that 2 reversible and 3 irreversible reactions were needed to accurately predict all the experimental data. Using all 5 reactions, the average error between the predicted and calculated Hg oxidation values is at 7.4.

Future work would involve the use of the entire Arrhenius equation, where the 'T^n' term would not be omitted from the model. The constant 'n' would be a separate set of unknowns in the model and determined in a similar fashion as A and E for each reaction. Additionally, the stoichiometric coefficients for Equations (24) and (28) were assumed to be one. This assumption could be removed to determine if the non-linearity had an effect on determining the values of A and E. Finally, data from other researchers should be used to test the robustness of this model.

Reproduced with permission of the copyright owner. Further reproduction prohibited without permission.

CHAPTER 5

Comparing and Interpreting laboratory results of Hg Oxidation by a Chlorine Species

5.1 Abstract

Several researchers have performed experimental work in attempts to explain the effects of various flue gas components on the oxidation of elemental mercury (Hg^0). Some have concluded that water (H_2O) inhibits Hg oxidation by chlorine (Cl_2). In recently published work, it was found that sulfur dioxide (SO_2) and nitric oxide (NO) also have an inhibitory effect on Hg oxidation. This paper aims to serve three purposes. First, to present some data obtained in a laboratory scale apparatus, designed to test the effects of chlorine species on the oxidation of Hg^0 with respect to temperature. It was found that as temperature increased, Cl_2 was less effective as a Hg oxidizing agent. Second, this paper will present a consolidation of data taken from several sources, where the effects of various flue gas components on the oxidation of Hg^0 is observed and discussed. The summary of these results show the following general trends. At high temperatures, hydrogen chloride (HCl) is the primary chlorine species responsible for Hg^0 oxidation. At lower temperatures, Cl_2 is the dominant species. Additionally, H_2O and SO_2 both have an inhibitory effect on the oxidation of Hg^0 and that NO also exhibits inhibitory effects. Third, a simple two reaction model is presented to predict the experimental data shown in this paper. It is found that the predicted percent Hg oxidation values correspond very well with the observed experimental values.

Reproduced with permission of the copyright owner. Further reproduction prohibited without permission.

5.2 Introduction

This section will describe some of the experimental work performed by individual researchers in greater detail.

Frandsen et al., (1994) performed thermodynamic equilibrium calculations and predicted that all gas phase Hg, derived from the combustion of coal, with typical chlorine contents, would exist as mercuric chloride ($HgCl_2$) at temperatures below 450°C[90]. In contrast, EPA's Information Collection Request (ICR) database shows that elemental Hg still exists in the flue gas at even lower temperatures, indicating that the reaction between elemental Hg and chlorine is kinetically limited[85]. Other studies have shown that the type of coal being burnt, such as lignite, sub-bituminous or bituminous, determines the distribution of the Hg species in the flue gas, since different coal types have different Hg, chlorine, sulfur, moisture and nitrogen content[89]. These components, along with the wide temperature variations within the power plant, have a strong influence on Hg speciation[44, 81].

Laudal et al. performed several bench scale experiments to determine the effects of various flue gas components on Hg oxidation[76]. Kilgroe et al. showed a negative influence of water and sulfur on mercury oxidation[43]. Norton et al. studied the impact of NO and NO_2 with greater detail[77]. Details on the experimental work by the individual researchers are given in Chapter 1.

Ghorishi (1998) studied the effects of temperature on Hg oxidation by HCl[183]. The apparatus used consisted of an oxidation reactor made of quartz. The rest of the connecting lines were made of Teflon. An online Hg analyzer (Buck 400a), with a detection limit of 0.1 $\mu g/m^3$ of Hg^0 was used. The effects of HCl were studied at three temperatures: 515°C, 634°C and 754°C. At 515°C, the residence time was approximately 1.22 seconds, and at 754°C, the residence time was 0.97 seconds. The gas stream consisted of 5% CO_2, 2% O_2, 40 $\mu g/m^3$ elemental Hg, a balance of N_2 and no water. Ghorishi concluded from his results that increasing HCl concentration caused an increase in elemental Hg oxidation at the 754°C temperature experiment. In the 754°C experiment, when 50 ppmv HCl was used, 9.1% Hg oxidation was observed. In the same experiment, when 200 ppmv HCl was used, 27% Hg oxidation was

Reproduced with permission of the copyright owner. Further reproduction prohibited without permission.

observed. Because of the low percent of Hg oxidation, he concluded that gas phase Hg^0 reactions with HCl are relatively slow even at temperatures above 700°C. The results of this work are shown in Table 5.2-1.

HCl (ppmv)	Temp (°C)	Residence Time (sec)	Oxidized Hg (%)
50	515	1.22	5.3
100	515	1.22	9.1
200	515	1.22	16.3
50	634	1.1	5.8
100	634	1.1	10.7
200	634	1.1	18.3
50	754	0.97	9.1
100	754	0.97	15.5
200	754	0.97	27.2

Table 5.2-1: Data adapted from Ghorishi. Gas blend consisted of 40 $\mu g/m^3$ Hg^0, 5% CO_2, 2% O_2 and the balance N_2[183]. Test was done to determine the effects of temperature on Hg oxidation by various HCl concentrations.

Hall et al., (1991) showed the effects of temperature on Hg oxidation by HCl[8]. Their apparatus consisted of a 17kW flue gas generator, which included a propane burner to heat up the flue gas and a 12 meter long flue gas duct made of stainless steel. Gas samples were taken at a flow of 1 liter per minute (LPM) via a PTFE tube, and Hg concentrations were measured by a continuous cold-vapor atomic adsorption (CVAA) spectroscopic method. The gas stream used in the experimental work consisted of 10% O_2, 150 $\mu g/m^3$ Hg^0, and the balance of N_2. At a temperature between 20°C and 300°C, the addition of 100 ppmv of HCl resulted in 25% oxidation of Hg^0. At a temperature of 500°C, the addition of 200 ppmv of HCl resulted in approximately 75% Hg oxidation. At a higher temperature of 700°C, 100 ppmv of HCl resulted in almost 90% Hg oxidation, and at 900°C, 100 ppmv of HCl resulted in almost 97% Hg oxidation. These results are summarized in Table 5.2-2a.

Reproduced with permission of the copyright owner. Further reproduction prohibited without permission.

Gas Temp. (°C)	HCl (ppmv)	Total Residence Time (sec)	Oxidized Hg (%)
20-300	100	2.8 - 2.0	24.0
20-300	200	2.8 - 2.0	26.0
20-300	300	2.8 - 2.0	26.0
500	12.5	1.50	8.0
500	25	1.50	48.9
500	100	1.50	60.8
500	200	1.50	72.2
500	300	1.50	74.4
700	100	1.07	84.9
700	200	1.07	84.9
700	300	1.07	88.5
900	100	0.70	95.3
900	200	0.70	95.8
900	300	0.70	95.8

Table 5.2-2a: Data adapted from Hall et al., Gas blend consisted of approximately 150 $\mu g/m^3$ Hg^0, 10% O_2 and the balance was inert gases[8]. Total residence time varied as shown based on temperature of the system. Test was done to show the effects of increasing HCl concentration on Hg oxidation with respect to temperature.

Hall[8] also studied the effects of Cl_2 on Hg oxidation in a dry gas stream consisting of 10% O_2, 150 $\mu g/m^3$ Hg^0, and the balance of N_2. At 500°C, when 12.5 to 150 ppmv of Cl_2 was added, Hg oxidation increased from 27.8% to 78.5%. The Cl_2 data obtained at 500°C are summarized in Table 5.2-2b.

Gas Temp. (°C)	Cl_2 (ppmv)	Total Residence Time (sec)	Oxidized Hg (%)
500	12.5	1.50	27.8
500	25	1.50	53.5
500	50	1.50	67.8
500	100	1.50	75.3
500	150	1.50	78.5

Table 5.2-2b: Data adapted from Hall et al., Gas blend consisted of approximately 150 $\mu g/m^3$ Hg^0, 10% O_2 and the balance was inert gases[12]. Temperature of the system in this case was constant at 500°C; residence time remained constant at 1.5 seconds. Test was done to show the effects of increasing Cl_2 concentration on Hg oxidation.

Sliger et al., (2000, 2001) performed similar experimental work as Hall et al.[82, 184]. Their apparatus consisted of a 16.1 kW natural gas burner. The furnace chamber was made of refractory material. The EPA Method 29, which uses a quartz probe to sample gases, was used to extract samples and speciate Hg. In their first experiment, HCl, diluted in air, was injected near

Reproduced with permission of the copyright owner. Further reproduction prohibited without permission.

the exit of the furnace. The gas stream consisted of 7.43% O_2, 6.15% CO_2, 12.3% H_2O, 25 ppmv NO_x, between 53 and 137 $\mu g/m^3$ of Hg^0 and the balance being N_2. The temperature of the sample was between 922°C to 1071°C. The data showed that HCl caused Hg oxidation but increasing HCl concentrations did not consistently increase Hg oxidation. Their second experiment varied the concentration of H_2O from 0 mole percent to 14 mole percent, at two HCl levels (39 ppmv and 274 ppmv). This experiment was done in a quartz flow reactor which did not involve the combustion of natural gas, thus giving them the flexibility in selecting compositions of the various flue gas components, most notably, the composition of water in the gas stream. The data showed that higher H_2O concentrations led to lower Hg oxidation. Their data showing the effects of HCl, H_2O and temperature on Hg oxidation are summarized in Tables 5.2-3a to 5.2-3c.

Gas Temp. (°C)	HCl (ppmv)	Oxidized Hg (%)
918	56	0.0
930	172	33.0
929	175	27.0
917	282	41.0
929	453	29.0
868	0	0.0
853	0	2.0
858	131	11.0
1071	0	0.0
1071	638	75.0

Table 5.2-3a: Data adapted from Sliger et al., Gas blend consisted of 7.43% O_2, 6.15% CO_2, 25 ppmv NO_x, between 53 and 137 $\mu g/m^3$ Hg^0 and the balance was N_2[13-14]. Residence time remained constant at 1.4 seconds. Test was done to show the effects of increasing temperature and HCl concentration on Hg oxidation.

Reproduced with permission of the copyright owner. Further reproduction prohibited without permission.

Gas Temp. (°C)	HCl (ppmv)	H_2O Conc. (mole %)	Oxidized Hg (%)
927	39	0.0	100.0
927	39	0.0	96.0
927	39	0.0	92.5
927	39	0.0	85.0
927	39	5.0	93.5
927	39	5.0	80.5
927	39	10.0	68.5
927	39	14.0	69.5
927	39	14.0	63.5
927	39	14.0	38.0
927	39	14.0	31.0
927	39	14.0	24.5

Table 5.2-3b: Data adapted from Sliger et al., Gas blend consisted of 7.43% O_2, 6.15% CO_2, 25 ppmv NO_x, between 53 and 137 $\mu g/m^3$ Hg^0 and the balance was N_2[13]. Residence time remained constant at 1.4 seconds. Test was done to show the effects of increasing H_2O concentration on Hg oxidation by 39 ppmv HCl.

Gas Temp. (°C)	HCl (ppmv)	H_2O Conc. (mole %)	Oxidized Hg (%)
927	274	0.0	100.0
927	274	0.0	95.0
927	274	0.0	86.5
927	274	5.0	95.0
927	274	5.0	79.5
927	274	10.0	79.5
927	274	14.0	96.0
927	274	14.0	75.5
927	274	14.0	74.0
927	274	14.0	71.5

Table 5.2-3c: Adapted from Sliger et al., Gas blend consisted of 7.43% O_2, 6.15% CO_2, 25 ppmv NO_x, between 53 and 137 $\mu g/m^3$ Hg^0 and the balance was N_2[13]. Residence time remained constant at 1.4 seconds. Test was done to show the effects of increasing H_2O concentration on Hg oxidation by 274 ppmv HCl.

Widmer (1998) investigated a simulated municipal waste gas stream, which contained high concentrations of elemental Hg[185]. Their reactor was made of quartz and they used EPA Method 29 to measure Hg concentrations. Their gas stream consisted of 10% O_2, 10% CO_2, 8% H_2O, 3700 $\mu g/m^3$ elemental Hg and the balance was N_2. HCl was injected into the preheated gas stream before entering the reactor. The reactor temperature was varied from 423°C to 876°C and the effects of 300 ppmv and 3000 ppmv of HCl were measured. They observed higher oxidation

Reproduced with permission of the copyright owner. Further reproduction prohibited without permission.

extents at higher temperatures and higher HCl concentrations. For example, upon the addition of 300 ppmv of HCl at 649°C, 22% Hg oxidation was observed. However, the same concentration of HCl at 869°C resulted in 72% Hg oxidation. With the addition of 3000ppmv of HCl at 517°C, approximately 61% Hg oxidation was observed, and over 95% Hg oxidation at 771°C. Widmer concluded that at temperatures above 800°C, complete Hg conversion was observed for 3000 ppmv HCl but at 300 ppmv of HCl, complete oxidation of Hg is possible only at temperatures below 650°C. The results from Widmer are presented in Table 5.2-4.

Gas Temp. (°C)	Residence Time (sec)	HCl (ppmv)	Oxidized Hg (%)
632	0.89	0.0	0.0
423	1.16	3000.0	40.0
517	1.02	3000.0	61.0
771	0.77	3000.0	97.0
876	0.70	3000.0	95.0
538	0.99	300.0	22.0
649	0.87	300.0	22.0
869	0.70	300.0	72.0

Table 5.2-4: Data adapted from Widmer et al., Gas blend consisted of 10% O_2, 10% CO_2, 8% H_2O, 3700 $\mu g/m^3$ Hg^0 and the balance was N_2[185]. Residence time and temperature was varied. Test was done to show the effects of two HCl concentrations (300 and 3000 ppmv) on Hg oxidation.

Mamani-Paco and Helble (2000) investigated the effects of HCl and Cl_2 on the oxidation of elemental Hg[186]. Experimental work was done in a 1.3 meter long insulated quartz tube with three equispaced sampling ports along the length. These ports provided temperature and residence time profiles. The total gas flow was 31 slpm, consisting of 45 $\mu g/m^3$ elemental Hg, 26% by volume of H_2O, 13% CO_2 and 63% N_2. The gas was initially heated to 1080°C. The temperatures and residence time profiles of the apparatus were 520°C and 1.4 seconds at port 1, 350°C and 3.6 seconds at port 2, and 290°C and 6.2 seconds at port 3. The results show that 100 ppmv of HCl alone results in only 2% Hg oxidation. The results also show that Cl_2 is a more effective oxidant than HCl. 50 ppmv Cl_2 resulted in approximately 10% Hg oxidation when sampled from port 1. As the concentration of Cl_2 injected increased, the percent Hg oxidized increased. No effects on sampling position, residence time and sample temperature were

Reproduced with permission of the copyright owner. Further reproduction prohibited without permission.

observed. For example, in the experiment with 50 ppmv Cl_2, Hg oxidation at port 3 was 7% while at port 1 was 10-12%, and in the experiment with 300 ppmv Cl_2, Hg oxidation at port 3 was 69% while at port 1 was 66%. The authors speculate that the reaction between Hg and Cl_2 does not occur at temperatures below 530°C. A selection of the results obtained is summarized in Table 5.2-5.

Temp. Range (°C)	Residence Time (seconds)	Port	HCl (ppmv)	Cl_2 (ppmv)	Oxidized Hg (%)
1080-520	1.4	1	100	0	2
1080-350	3.6	2	100	0	2
1080-290	6.2	3	100	0	2
1080-520	1.4	1	100	50	10
1080-520	1.4	1	0	50	10
1080-520	1.4	1	0	50	12
1080-350	3.6	2	0	50	8
1080-290	6.2	3	0	50	7
1080-520	1.4	1	0	100	45
1080-290	6.2	3	0	100	36
1080-520	1.4	1	0	300	66
1080-290	6.2	3	0	300	49
1080-520	1.4	1	0	500	92
1080-350	3.6	2	0	500	93
1080-290	6.2	3	0	500	92

Table 5.2-5: Data adapted from Mamani-Paco and Helble. Gas blend consisted of 50 $\mu g/m^3$ Hg^0, 26% by volume of H_2O, 13% CO_2 and 63% N_2[186]. Tests were done to show the effects of varying amounts of Cl_2 on Hg oxidation.

Qiu et al., (2003) performed identical experimental work as Mamani-Paco and Helble, except that the gas composition included SO_2[11]. The base composition of the gas used in these experiments was 50 $\mu g/m^3$ elemental Hg, 26% by volume of H_2O, 13% CO_2 and 63% N_2. SO_2 concentration was varied from 0 ppmv to 500 ppmv. Table 5.2-6 lists a selection of these results. The term Φ is defined as the equivalence ratio of the moles of oxygen required and the actual moles of oxygen used in experimental work. In this experimental work, for a Φ value of 1.0, the calculated oxygen concentration in the flue gas was approximately 0.6%. A Φ value of 0.9 yields a calculated oxygen concentration of approximately 2.8% in the flue gas stream. The total residence time of the reaction was approximately 3.5 seconds, and the temperature of the

Reproduced with permission of the copyright owner. Further reproduction prohibited without permission.

apparatus ranged from 1200°C to 350°C. Samples were taken at 350°C. Additional details are given in the paper. In the absence of SO_2 (with Φ=0.9) 250 ppmv Cl_2 results in 64.7% Hg oxidation. Upon the addition of 100 ppmv SO_2, 250 ppmv Cl_2 results in 46.4% (with Φ=0.9) and 27.3% (with Φ=1.1) Hg oxidation respectively. Upon the addition of 500 ppmv SO_2, 250 ppmv Cl_2 results in 21.9% (with Φ=0.9) and 10.4% (with Φ=1.0) Hg oxidation respectively. The results show clearly that as the concentration of SO_2 in the gas stream increases, the percent Hg oxidized decreases. This proves that the presence of SO_2 in the gas stream has an inhibitory effect of Hg oxidation by Cl_2.

Φ	Cl_2 (ppmv)	SO_2 (ppmv)	Oxidized Hg (%)
1.0	250	0	61.0
1.0	500	0	59.1
1.0	250	100	27.3
1.0	500	100	54.8
1.0	250	500	10.4
0.9	250	0	64.7
0.9	500	0	94.5
0.9	250	100	46.4
0.9	500	100	77.4
0.9	250	400	29.7
0.9	500	400	62.4
0.9	250	500	21.9

Table 5.2-6: Data adapted from Qiu et al., Gas blend consisted of, 50 $\mu g/m^3$ Hg^0, 26% by volume of H_2O, 13% CO_2 and 63% N_2[11]. Tests were done to show the effects of varying amounts of Cl_2 and SO_2 on Hg oxidation.

In summary, in the ten investigations cited above, it was found that HCl has a strong Hg oxidation effect at higher temperatures, while Cl_2 has a stronger Hg oxidation effect at lower temperatures. Additionally, higher HCl or Cl_2 concentrations result in higher percent Hg oxidation. Kilgroe and Sliger concluded from their work that H_2O has an inhibitory effect on Hg oxidation by HCl. However, none of the investigations show the effects of H_2O on Hg oxidation by Cl_2. Laudal, Kilgroe, Mamani-Paco and Qiu individually showed that SO_2 has an inhibitory effect on Hg oxidation by HCl or Cl_2. While Kilgroe focused on the use of HCl as the oxidizing agent, Laudal, Mamani-Paco and Qiu showed that SO_2 inhibits Cl_2 as an oxidizing agent as well. However, Kellie suggested that SO_2 encourages the oxidation of Hg but inhibits the amount of oxidized Hg that

Reproduced with permission of the copyright owner. Further reproduction prohibited without permission.

adsorbs onto fly ash particles. Finally, Norton showed that NO also seems to have an inhibitory effect on Hg oxidation by HCl, but since his experimental work was done in the presence of fly ash; the results for Hg oxidation are unclear.

The goal of this study is to obtain critical data not found in other work and to make a quantitative comparison between the data presented by various researchers. This will result in a more comprehensive view of the effects of various flue gas components and temperature on Hg oxidation.

5.3 Testing Facility

The present work reports data obtained in a testing facility that was described in greater detail in Chapter 2. Figure 2.3-1 is a schematic of the testing facility used to perform Hg oxidation tests. The various gas components are metered, blended and heated to the desired temperature. The air pre-heater (APH) was used to preheat the bulk gas stream to temperatures between 100°C and 320°C. The steam pre-heater (SPH) was used to vaporize liquid H_2O to super heated steam at temperatures between 100°C and 300°C. The final pre-heater (R1) allows for heating and mixing of the bulk gases and the steam. The gas temperature at the exit of R1 ranged from 166°C to 570°C. These temperatures were chosen because of the lack of data within this range and that the thermodynamic transition from Hg and $HgCl_2$ occurs in this range. The oxidant used was chlorine gas (Cl_2) and it was injected as a 1% mixture in N_2 at the entrance of R2. The sample gas was transported at a rate of 6 LPM via a Teflon line heated to approximately 150°C. The calculated residence time of the gas stream in the sample line was less than 0.1 seconds.

Reproduced with permission of the copyright owner. Further reproduction prohibited without permission.

5.4 Results:

5.4.1 Hg and Cl_2

The first set of experiments performed was to study the effect of temperature on the oxidation of Hg by Cl_2. The four temperature profiles used in this experiment are shown in Figure 5.4.1-1.

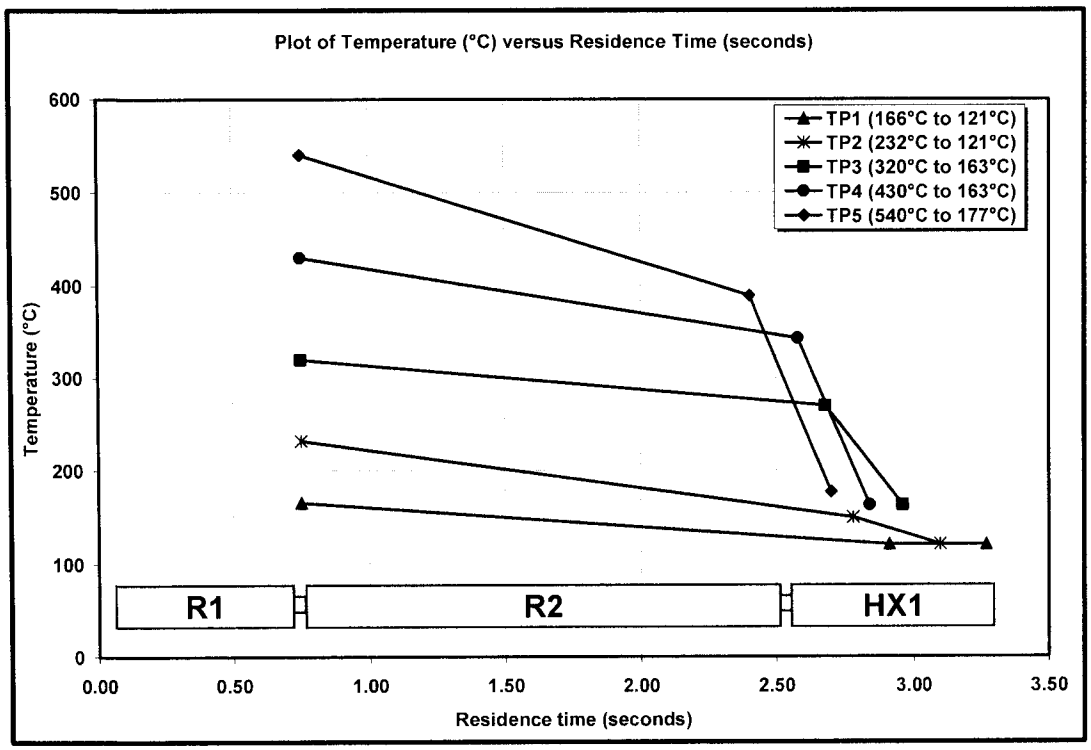

Figure 5.4.1-1: Plot of temperature versus residence time for the apparatus. The first temperature of each profile is that of the gas stream at the exit of R1. The second temperature value is that of the gas stream at the exit of R2. The third temperature value is that of the gas stream at the exit of HX1.

The feed gas contained 10 $\mu g/m^3$ of elemental Hg with the balance being N_2 at a flow of 87 standard liters per minute (slpm). Cl_2 was injected into the gas stream at the exit of R1 at a rate to give a 1 ppmv concentration. The SCEM monitored the exiting elemental Hg concentration and once steady Hg values were achieved the Cl_2 flow was stopped and the system was allowed to return to initial conditions. The temperature of the apparatus was then changed to a new temperature profile. This process was repeated for all temperature profile cases. Figure 5.4.1-2

Reproduced with permission of the copyright owner. Further reproduction prohibited without permission.

shows the results of this experiment, where the plot presents percent Hg oxidation with respect to gas temperature profile as shown in Figure 5.4.1-1.

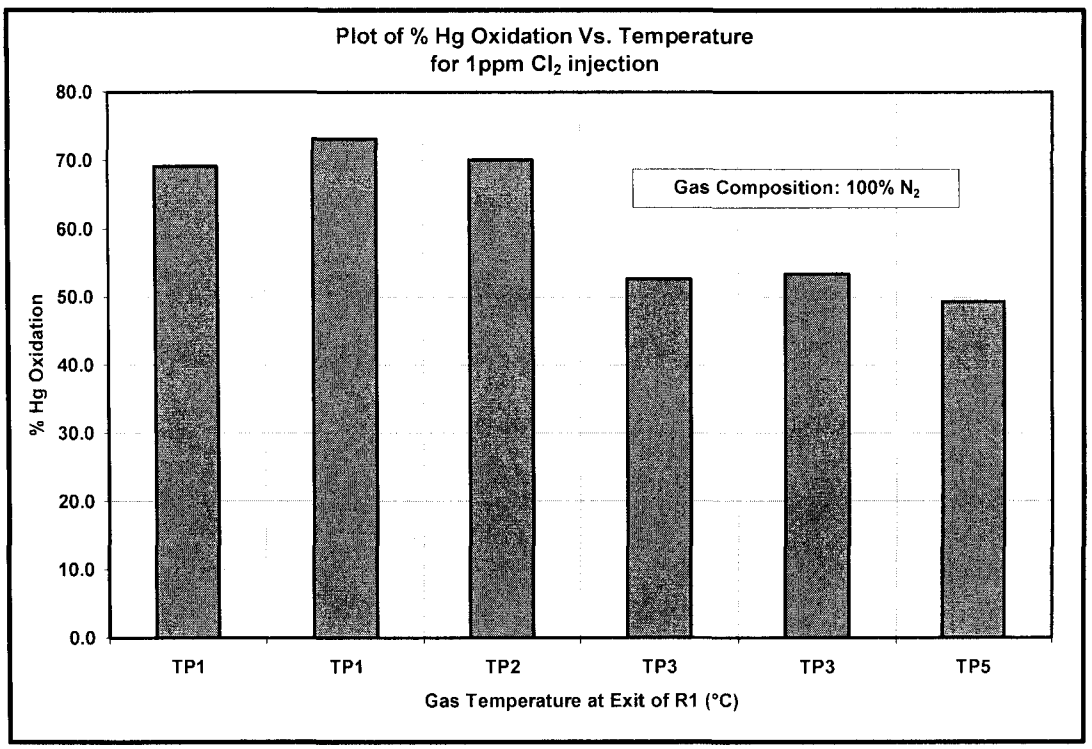

Figure 5.4.1-2: Comparing percent Hg oxidation versus gas temperature profile. Each data point represents a separate experiment. Gas composition consisted of 100% N_2 and 10.0 $\mu g/m^3$ Hg^0.

Two repeat tests were conducted at TP1, where the temperature profile was 166°C to 121°C and the percent Hg oxidation observed was 69% and 73% respectively. For TP2, where the temperature profile was 232°C to 121°C, 70% of the initial amount of Hg was oxidized. For TP3, where the temperature profile was 320°C to 165°C, 53% of the initial amount of Hg was oxidized, and for TP5, where the temperature profile was 538°C to 177°C, 49% of the initial amount of Hg was oxidized. These results show that Cl_2 becomes less effective in oxidizing Hg at higher temperatures.

Reproduced with permission of the copyright owner. Further reproduction prohibited without permission.

5.4.2 Cl_2, H_2O and Hg

In this experiment, the gas flow through the system was again kept at 87 slpm. The gas stream consisted of 10 μg/m^3 elemental Hg, 87.1% N_2 and 12.9% H_2O. Cl_2 was injected into the gas stream at the exit of R1. The percent Hg oxidized was measured at Cl_2 concentrations of 12, 30 and 52 ppmv. This experiment was performed at two temperature profiles TP3 and TP4 shown in Figure 5.4.1-1. This experiment was also done at TP5 and was presented in a previous publication[186]. Figure 5.4.2-1 shows that increasing Cl_2 concentration results in increasing Hg oxidation, however the temperature profile has only a small effect. Also, the difference in percent Hg oxidized between the two temperature experiments narrows as the amount of Cl_2 injected increases.

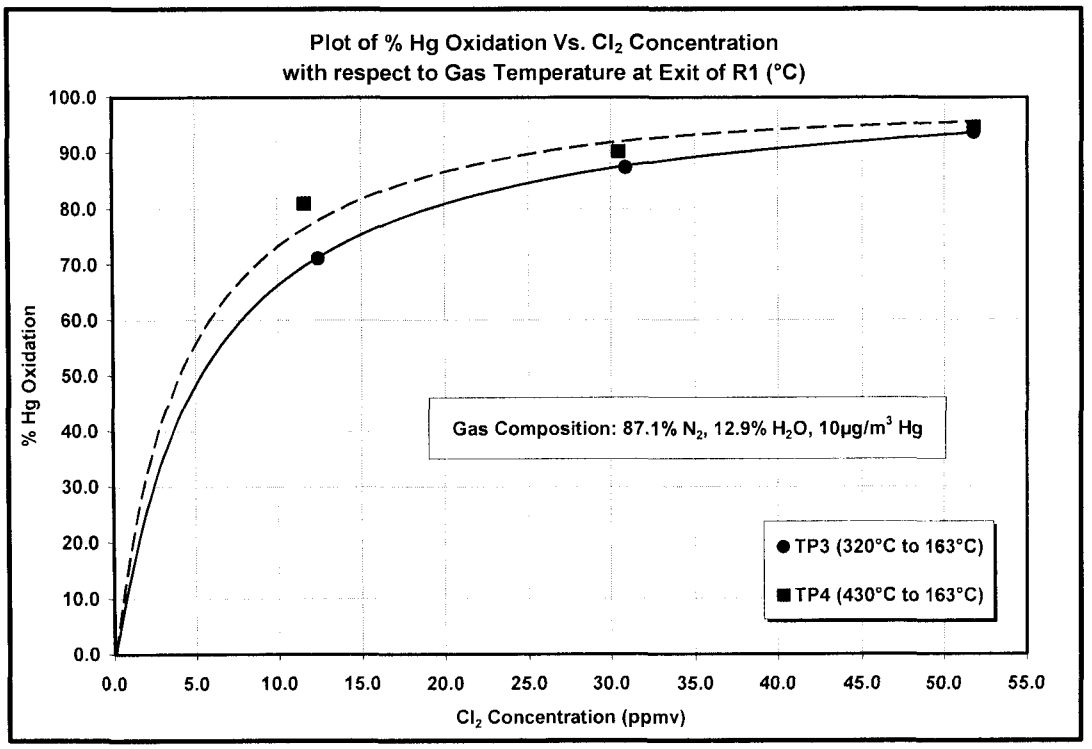

Figure 5.4.2-1: Plot of percent Hg oxidation versus Cl_2 concentration used, with respect to temperature profile of the apparatus. Gas composition consisted of 10.0 μg/m^3 elemental Hg, 87.1% N_2 and 12.9% H_2O. The temperature profile was kept constant as the Cl_2 concentration was increased.

Reproduced with permission of the copyright owner. Further reproduction prohibited without permission.

5.5 Discussion

The results in this work show that Cl_2 can oxidize Hg and that lower temperatures, higher Cl_2 concentrations and the absence of water all increase the extent of oxidation. The experiment at TP1 and TP2 shown in Figure 5.4.1-2 illustrates that in a gas stream consisting of 100% N_2, 1 ppmv Cl_2 resulted in approximately 70% Hg oxidation. This is similar to that reported by Laudal[76] (Table 1.6.2.1-2, row 1) where at a similar temperature of 175°C, he observed Hg oxidation of 84.8% with 10 ppmv Cl_2. The experiment at TP3 and TP5 shown in Figure 5.4.1-2 shows that in a gas stream of 100% N_2, 1 ppmv Cl_2 resulted in approximately 51% Hg oxidation. This is similar to data reported by Hall[12] (Table 5.2-2b, row 2), where the observed Hg oxidation was 53.5% with 25 ppmv Cl_2 in a gas stream consisting of 10% O_2 and the balance of inert gases.

Data in Figure 5.4.2-1 closely resembles the results obtained by Laudal[76], where 11.6 ppmv Cl_2 with 12.9% H_2O and TP4 resulted in 82% oxidation of Hg. This result agrees with that obtained by Laudal (Table 1.6.2.1-2, row 5). This result by Laudal also indicates that HCl is unable to oxidize Hg at low temperatures.

Hall[12] showed that at 500°C, increasing the concentration of Cl_2 in the gas stream resulted in an increase in the percent Hg oxidized. Hall's work was done at a constant temperature of 500°C, which closely resembles the TP5 temperature profile in this work. A similar trend is observed in Figure 5.4.2-1 (TP5) of this work, where an increase in Cl_2 concentration results in an increase in percent Hg oxidized. However, the maximum amount of Cl_2 used in this work was 52 ppmv, while Hall used 150 ppmv Cl_2 and obtained only 78.5% Hg oxidation. It is unclear why Hall required such a large amount of Cl_2 in an inert environment to achieve Hg oxidation similar to those presented in this work. But it does enforce the fact that these experiments are difficult to conduct.

Mamani-Paco and Helble[187] presented Hg-Cl_2 oxidation data at much higher temperatures than those presented in this work. The gas stream used by the authors consisted of 26% H_2O, and the addition of 50 ppmv Cl_2 into the gas stream resulted in only 10% Hg oxidation. In contrast, Figure 5.4.2-1 of this work shows that 50 ppmv Cl_2, added into the gas stream consisting of 87.1% N_2 and 12.9% H_2O, resulted in approximately 93% Hg oxidation. These

Reproduced with permission of the copyright owner. Further reproduction prohibited without permission.

results confirm that H_2O has an inhibitory effect on Hg oxidation – Mamani-Paco and Helble used a higher concentration of H_2O and obtained a lower percent Hg oxidation for the same amount of Cl_2 added. These results also seem to suggest that at higher temperatures, Cl_2 becomes a less effective oxidizing agent. This trend is clearly seen Figure 5.4.2-1, where as the temperature profile of the apparatus increases, Cl_2 becomes less effective in oxidizing Hg.

5.6 Predictive Model

It was thought that a simple two reaction model may be adequate to predict the data obtained in this work. The two proposed reversible reactions are the reaction of Hg with Cl_2 to form $HgCl_2$ (Equation 1) and the reaction of water and Cl_2 to form HCl and O_2 (Equation 2).

$$Hg\ (g) + Cl_2\ (g) \leftrightarrow HgCl_2\ (g) \qquad (1)$$

$$Cl_2\ (g) + H_2O\ (g) \leftrightarrow 2\ HCl\ (g) + \tfrac{1}{2}\ O_2\ (g) \qquad (2)$$

These two reactions are shown to support the observed trends of Cl_2 concentration, temperature, and water addition, as obtained in the experiments. The reactor model used is a non-isothermal plug flow reactor (PFR) system.

At atmospheric pressure, the reaction rates for the two reactions can be written as:

$$r_1 = k_1 \cdot \left(y_{Hg} \cdot y_{Cl_2} - \frac{y_{HgCl_2}}{Keq_1} \right) \qquad (3)$$

$$r_2 = k_2 \cdot \left(y_{H_2O} \cdot y_{Cl_2} - \frac{y_{HCl}^{\,2} \cdot y_{O_2}^{\,1/2}}{Keq_2} \right) \qquad (4)$$

Each 'y' term in Equations 3 and 4 represent the mole fraction of the species in the gas phase. The rates, r_1 and r_2 have the units of ppm per unit time. The temperature dependent terms 'k_1' and 'k_2' are the rate constants for reactions 1 and 2 respectively, and are generally defined by Equation 5:

$$k(T) = A \cdot \exp\left(-\frac{Ea}{R \cdot T}\right) \qquad (5)$$

Reproduced with permission of the copyright owner. Further reproduction prohibited without permission.

where A is the Arrhenius pre-exponential term, Ea is the activation energy (cal/mole), T is the temperature in Kelvin (K) and R is the universal gas constant (cal/mole*K).

The terms 'Keq_1' and 'Keq_2' are the calculated equilibrium rate constants for reactions 1 and 2 respectively and this is shown in the previous chapter.

The concentrations of Hg, $HgCl_2$, Cl_2 and HCl as a function of residence time are shown in Equations 8 to 11, where 't' is the residence time in the reactor system, and the concentrations ([ ]) are in ppm.

$$R_{Hg} = \frac{d[Hg]}{dt} = -r_1 \tag{6}$$

$$R_{HgCl_2} = \frac{d[HgCl_2]}{dt} = r_1 \tag{7}$$

$$R_{Cl_2} = \frac{d[Cl_2]}{dt} = -r_1 - r_2 \tag{8}$$

$$R_{HCl} = \frac{d[HCl]}{dt} = 2r_2 \tag{9}$$

Because the concentrations of H_2O and O_2 are several orders of magnitude higher than the concentrations of the other species in the system, their rate of change are negligible.

Equations 6 to 9 were solved simultaneously using a fourth order Runge Kutta routine (MatLab ODE45), where the temperatures profiles in Figure 5.4.1-1 were used to determine the rate and equilibrium constants. To optimize the appropriateness of the fit between the model prediction and the experimentally measured Hg conversions, a simplex routine was used to minimize the function shown in Equation 12 (MatLab function: fminsearch).

$$ERROR = \sum_{i=1}^{N} (x_{Hg,\text{model}} - x_{Hg,\text{data}})_i^2 \tag{12}$$

where x is the conversion of elemental mercury.

The parameters varied to minimize the function in Equation 12 were A_1, A_2, Ea_1 and Ea_2. A_1 and A_2 are the pre-exponential factors for the reaction rate constants for Reactions 1 and 2 respectively. Ea_1 and Ea_2 are the activation energies for Reactions 1 and 2 respectively. Figure

Reproduced with permission of the copyright owner. Further reproduction prohibited without permission.

5.6-1 is a plot of the predicted percent Hg oxidized versus the observed percent Hg oxidized. The values in Figure 5.6-1 show that the predicted values correlate very well with the observed values. The average difference between the percent Hg oxidation predictions and the observed percent Hg oxidation is 6.4%. Table 5.6-1 lists the reaction rate parameters for Reactions 1 and 2.

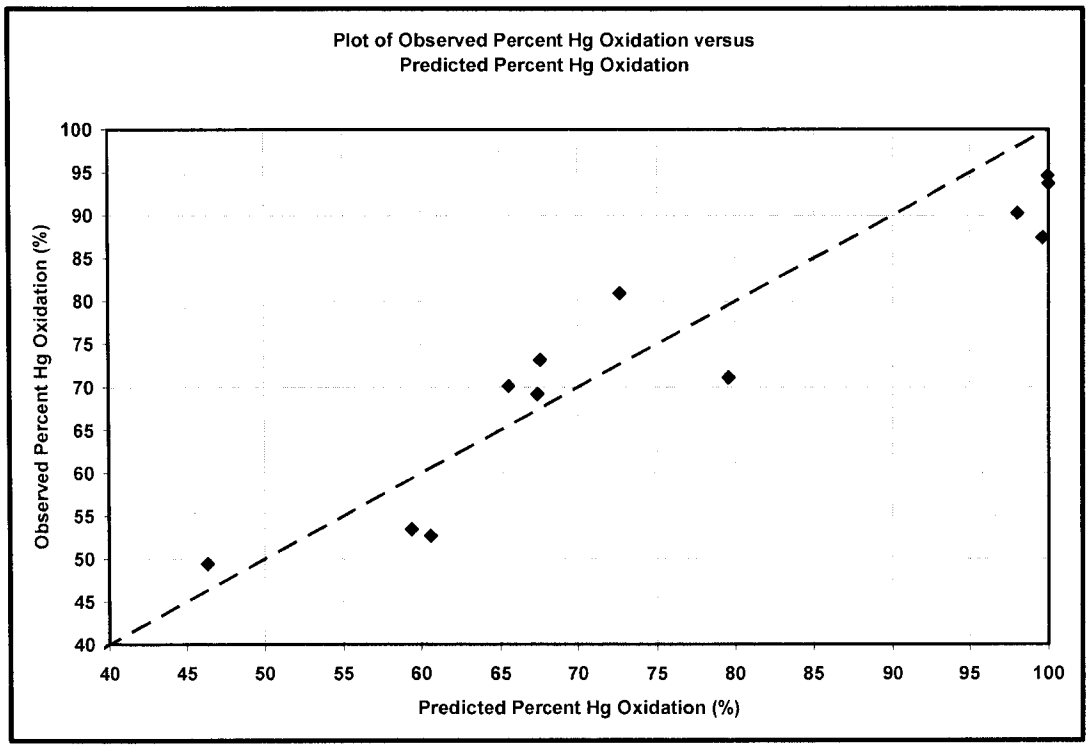

Figure 5.6-1: Plot of observed percent Hg oxidation versus predicted percent Hg oxidation. The constants for A and Ea for Reactions 1 and 2 are given in Table 5.6-1.

	Reaction	A	E ($x10^3$) (cal/mole)	$k = A \cdot \exp[\frac{-E}{R \cdot T}]$
R1	$Hg(g) + Cl_2(g) \xleftrightarrow{k_1} HgCl_2(g)$	0.386	0.145	$k_1 = 0.386 \cdot \exp[\frac{-0.145 \times 10^3}{1.987 \cdot T}]$
R2	$H_2O(g) + Cl_2(g) \xleftrightarrow{k_2} 2HCl(g) + \frac{1}{2}O_2(g)$	0.274	0.198	$k_2 = 0.274 \cdot \exp[\frac{-0.198 \times 10^3}{1.987 \cdot T}]$

Table 5.6-1: Constant values of A and Ea for Reactions 1 and 2, and the corresponding reaction rate constants. These were used to predict the observed data presented in this paper, and Figure 4.6-1 shows the fit.

Reproduced with permission of the copyright owner. Further reproduction prohibited without permission.

5.7 Conclusion

Two sets of experiments were performed in this work to determine the effects of temperature and H_2O on Hg oxidation by Cl_2. In the absence of water, 1ppmv of Cl_2 was able to extensively oxidize elemental mercury, and the extent of oxidation decreased as temperature increased. In the presence of water, much higher concentrations of Cl_2 were needed to gain the same oxidation extent as for the dry gas case. This is due to the reaction of H_2O and Cl_2 to form HCl and O_2, both of which are weaker oxidation species than Cl_2.

A simple two reaction model was used to accurately predict the data presented in this paper. This prediction supported the reaction mechanism proposed. In future work, this model will be expanded to include more experimental data and the data obtained by other researchers.

Reproduced with permission of the copyright owner. Further reproduction prohibited without permission.

CHAPTER 6

A Global Kinetic Mechanism for the Prediction of Hg Oxidation by a Chlorine Species

6.1 Abstract

This chapter presents results from a global kinetic model developed from laboratory test results. The model consists of five reactions - two reversible and three irreversible. These reactions are global reactions and the reaction constants for the Arrhenius expression formulation were determined from a set of 35 experiments. These experiments involve a flue gas composition that include NO, SO_2, Hg, Cl_2; at a range of temperatures and residence times, from 540 to 166°C, and 2.7 to 3.3 seconds respectively. The values obtained for the reaction constants were further used to predict experimental data from eleven experimental mercury data sources in the literature. It was found that the predictions from the model correspond very well with the observed published data.

6.2 Introduction

Several researchers have studied the impact of various flue gas components on the oxidation of elemental Hg. The following is a brief outline of the experimental results obtained by some of these studies. More details are given in a previous chapter.

Fry et al. (2005) investigated the effects of Cl_2 on Hg oxidation at two different quench rates[195]. In Fry et al.'s experiments, natural gas was burnt in a quartz tube and the gas composition obtained consisted of 25 $\mu g/m^3$ Hg^0 together with, 18.1 percent H_2O, 3.3 percent O_2, 58 ppm_v NO, 48 ppm_v CO and a balance of N_2. Mercury concentrations were measured by a Tekran 2537A Hg vapor analyzer. The concentration of Cl_2 used ranged from 0 to 300 ppm_v. Fry et al. assumed that at their initial temperature of 1130°C, molecular chlorine dissociated to

Reproduced with permission of the copyright owner. Further reproduction prohibited without permission.

chlorine radicals or HCl, resulting in an equivalence HCl concentration of 0 to 600 ppm_v. Fry et al. also concluded that as the concentration of chlorine species increased, the percent Hg oxidized increased. Additionally, the high quench rate in their experiments resulted in a higher percent of Hg oxidized at a faster rate. Conversely, the lower quench rate resulted in a lower percent Hg oxidized at a slower rate.

The summary of all the relevant literature data is as follows: it has been reported that temperature plays an important role in Hg oxidation. HCl is important in oxidizing Hg at higher temperatures (above approximately 700°C), while Cl_2 oxidizes Hg at lower temperatures (below 700°C). It has also been reported that SO_2 and H_2O inhibit the oxidation of Hg by either of the chlorine species. Given the importance of these effects, it will be desirable to be able to predict the speciation of Hg using a simple model that can estimate the results of the data presented within this section. All of the experimental data described in this chapter is summarized in Table 6.2-1. Due to the wide range and variety of data collected, a global kinetic mechanism would be best suited to predict all the data obtained by the various researchers, with a good degree of accuracy. This chapter introduces such a model, where five global reactions are used. These reactions are:

$$Hg(g) + Cl_2(g) \xleftrightarrow{k_1} HgCl_2(g) \quad (1)$$

$$H_2O(g) + Cl_2(g) \xleftrightarrow{k_2} 2HCl(g) + \tfrac{1}{2}O_2(g) \quad (2)$$

$$Hg(g) + 2HCl(g) \xrightarrow{k_3} HgCl_2(g) + H_2(g) \quad (3)$$

$$HgCl_2(g) + SO_2(g) \xrightarrow{k_4} Hg(g) + SCl_2(s,g) + O_2(g) \quad (4)$$

$$2NO(g) + Cl_2(g) \xrightarrow{k_5} 2NOCl(g) \quad (5)$$

Reactions 1 and 2 are reversible, while reactions 3, 4 and 5 are irreversible.

Reproduced with permission of the copyright owner. Further reproduction prohibited without permission.

Reproduced with permission of the copyright owner. Further reproduction prohibited without permission.

Author	Gas Composition								Oxidant		Temperature Range	Total Residence Time	Reactor Type	Hg Analyzer Type	Hg Oxidation
	N2	O2	CO2	SO2	NO	CO	H2O	Hg	Cl2	HCl					
	(%)	(%)	(%)	(ppmv)	(ppmv)	(ppmv)	(%)	($\mu g/m^3$)	(ppmv)	(ppmv)	(°C)	(seconds)			(%)
Laudal[76]	71	4	15	1500	0	0	10	20	10	50	175	1.00	Teflon	O-H Method[a]	98.1
				0						0					99.5
				1500					0						15.2
				0						50					99.3
										0					99.7
				1500					10	50					97.9
									0						21.3
															99.9
Norton[77]	82	6	12	1600	300	0	0	12	0	0	180	1.00	Stainless Steel	O-H Method	0.0
				0						50					9.0
				1600	0										2.0
					300										5.0
Ghorishi[183]	93	2	5	0	0	0	0	40	0	200	754 - 25	0.97	Quartz	CEM[b]: Buck 400a	27.3
										100					15.5
										50					9.0
										200	634 - 25	1.00			18.3
										100					10.8
										50					5.8
										200	515 - 25	1.22			16.3
										100					9.0
										50					5.3
Kilgroe[43]	93	2	5	0	0	0	0	40	0	50	754 - 25	0.97	Quartz	CEM: Buck 400a	9.0
				500						100					16.0
										200					26.0
										50					3.5
										100					6.0
										200					17.5
	91.3						1.7			50					1.8
										100					8.0
										200					17.0

Fry[195]	78.6	3.3	0	0	58	48	18.1	25	0	0	1127 - 175	6.00 Fast Quenching	Quartz	CEM: Tekran 2537A	0	0.0
															100	10.0
															200	15.6
															300	28.8
															400	66.2
															500	83.0
															600	86.1
												6.00 Slow Quenching			0	0.0
															100	100.0
															200	24.0
															300	39.2
															400	71.0
															500	83.0
															600	88.0
Qiu[189]	71.2	2.8	0	0	0	0	26	50	250	0	1080 - 25	1.40	Quartz	EPA Method 29 & CVAAS	0	0.0
				100					500						100	16.0
				400					250						200	64.2
				500					500						300	85.0
	73.4	0.6		0					250						400	91.0
				100					500						500	94.0
				500					250						600	96.0
															0	0.0
															100	29.2
															200	68.3
															300	85.0
															400	91.0
															500	96.0
															600	98.0
									250							67.7
									500							94.5
									250							46.4
									500							77.4
									250							29.7
									500							62.4
									250							21.9
									500							61.0
									250							89.1
									500							27.3
									250							54.8
																10.4

Reproduced with permission of the copyright owner. Further reproduction prohibited without permission.

Mamani - Paco[187]	61	0	13	0	0	26	50	50	0	1080 - 25	1.40	Quartz	EPA Method 29 & CVAAS[c]	10.0
											6.20			7.0
											3.60			7.1
											1.40			12.0
											6.20			36.0
											1.40			45.0
											6.20			69.0
											1.40			66.0
											3.60			93.0
											6.20			92.0
											1.40			92.0
											1.40			2.0
											6.20			2.0
											3.60			2.0
											1.40			10.0
Qiu[189]	71.2	2.8	0	0	0	0	26	50	50	0	1080 - 25	1.40	Quartz	EPA Method 29 & CVAAS	67.7
										100					94.5
										300					46.4
										500					77.4
										0					29.7
										100					62.4
										200					21.9
										0					61.0
										12.5					89.1
										300					27.3
										100					54.8
										200					10.4
										0					8.0
	73.4	0.6								100					74.4
										150					88.5
										0					24.0
Hall[8]	90	10	0	0	0	0	0	150	500	0	500 - 25	1.40	Stainless Steel	CVAAS	26.0
										100					75.3
										150					78.5

Reproduced with permission of the copyright owner. Further reproduction prohibited without permission.

Sliger[82]	74.12	7.43	6.15	0	25	0	12.3	100	0	56	997 - 25	1.40	Furnace lined with refractory material and/or Quartz	Simplified EPA Method 29	0.0
										172					33.0
										175					27.0
										282					41.0
										453					29.0
										0	868 - 25				0.0
										0					2.0
										131					11.0
										0	1071 - 25				0.0
										638					75.0
	86.42						0			274	927 - 25				86.5
	81.42						5								79.5
	76.42						10								79.5
	72.42						14								75.5
															74.0
															71.5
Widmer[185]	72	10	10	0	0	0	8	3000	0	0	632 - 25	0.89	Quartz	EPA Method 29	0.0
										3000	631 - 25	0.89			80.0
											771 - 25	0.77			97.0
											876 - 25	0.70			95.0
										300	869 - 25	0.70			72.0
											649 - 25	0.87			22.0
											538 - 25	0.99			22.0

Reproduced with permission of the copyright owner. Further reproduction prohibited without permission.

Reproduced with permission of the copyright owner. Further reproduction prohibited without permission.

Agarwal[188, 190]	96.5	3.5	0	0	0	0	0	11.6	2	0	538 - 177	2.70	Stainless Steel	CEM: PSA	72.0
	83.5		13.5	370	170	300		13.4							77.0
								14.9							52.0
								12.7							46.0
								11.7							47.0
	70							10.0							0.0
	83.5		0	0	0	0	13	12.7	12.4						83.0
								11.6	30.9						88.0
								11.4	52.5						92.0
	70		13.5	370	170	300		10.5	27.5						90.0
								10.6							90.0
								10.3							57.0
								10.6							46.0
								10.8							45.0
	83.5		0	0	0	0		10.5	27.5						94.6
	70		13.5	370	170	300		10.6							93.2
								10.3							66.6
								10.6							51.4
								10.8							53.7
	100	0	0	0	0	0	0	1.1	1.0		166 - 121	3.27			73.1
								1.2			347 - 121	2.96			52.7
								10.9			169 - 121	3.27			69.2
								11.7			353 - 121	2.96			53.5
								11.6			582 - 121	2.70			49.4
								10.9			232 - 121	3.10			70.1
								4.3			365 - 121	2.96			82.7
								11.6	5.0		232 - 121	3.10			91.6
								14.7			385 - 121	2.96			89.2
								11.2			593 - 121	2.70			97.8
	87	0	0	0	0	0	13	12.7	12.4		320 - 163	2.96			71.1
									30.9						87.4
									51.8						93.0
								11.7	11.6		430 - 163	2.84			80.9
									30.5						90.3
									51.8						94.6

Table 6.2-1: Summary of data from 11 unique sources. Data includes gas composition, chlorine species used, gas temperature profile, residence time, mercury measurement device, and observed percent Hg oxidation.

[a] O-H Method – Ontario-Hydro Method; [b] CEM – Continuous Emissions Monitor; [c] CVAAS – Cold Vapor Atomic Adsorption Spectroscopy

6.3 Testing Facility

The proposed global reaction scheme was formulated from data obtained in a testing facility that was described in greater detail in an earlier chapter. Figure 2.3-1 shows a schematic of the testing facility. The air pre-heater (APH) was used to preheat the bulk gas stream to temperatures between 100 and 320°C. The steam pre-heater (SPH) was used to vaporize liquid water to superheated steam at temperatures between 100 and 300°C. The temperature of the gas mixture at the exit of R1 ranges from 166 to 570°C. These temperatures were chosen because of the lack of Hg data within this range and that the thermodynamic transition from Hg and $HgCl_2$ occurs in this range. The oxidant used was chlorine gas and it was injected as a 1 percent mixture in N_2 at the entrance of R2. A PS Analytical Sir Galahad 10.525 semi-continuous Emissions Monitoring system (SCEM) used to measure elemental and total Hg in the gas stream. The data obtained from this experimental rig is included in Table 6.2-1.

6.4 Numerical Model:

An introduction to the reactions used in the global kinetic model used in this work is given in prior chapters. As mentioned in the introduction section, five global reactions were proposed for this model, where two reactions are reversible and three reactions are irreversible. Reaction 1 is the global mercury oxidation reaction, where elemental Hg reacts with Cl_2 to form $HgCl_2$. Reaction 2 is the Deacon reaction which was chosen since at high Cl_2 concentrations, this reaction is kinetically favored in the forward direction and water consumes Cl_2 to form HCl. This would result in less Cl_2 remaining to oxidize elemental Hg at lower temperatures. Since HCl is formed by the Deacon Reaction, Reaction 3 was chosen to account for the reaction between Hg and HCl at high temperatures to form $HgCl_2$ and H_2. Reaction 4 accounts for the inhibitory effect of SO_2 by reducing $HgCl_2$ to elemental Hg. Lastly, Reaction 5 was proposed in a prior publication and accounts for the inhibitory effect of NO on the oxidation of Hg by Cl_2 since NO reacts with Cl_2 to form NOCl[15]. The reactor model used is a non-isothermal plug flow reactor (PFR) system.

At atmospheric pressure, the reaction rates for the two reactions can be written as:

Reproduced with permission of the copyright owner. Further reproduction prohibited without permission.

$$r_1 = k_1 \cdot \left(y_{Hg} \cdot y_{Cl_2} - \frac{y_{HgCl_2}}{Keq_1} \right) \quad (6)$$

$$r_2 = k_2 \cdot \left(y_{H_2O} \cdot y_{Cl_2} - \frac{y_{HCl}^{\ 2} \cdot y_{O_2}^{\ 1/2}}{Keq_2} \right) \quad (7)$$

$$r_3 = k_3 \cdot \left(y_{Hg} \cdot y_{HCl}^{\ 2} \right) \quad (8)$$

$$r_4 = k_4 \cdot \left(y_{HgCl_2} \cdot y_{SO_2} \right) \quad (9)$$

$$r_5 = k_5 \cdot \left(y_{Cl_2} \cdot y_{NO}^{\ 2} \right) \quad (10)$$

Each 'y' term in Equations 6 to 10, except for H_2O and O_2, represents the concentration of each species in ppm. This is different for H_2O and O_2 for which the concentration is in mole fraction. The rate constants, k_1 to k_5 are temperature dependent and are defined by Equation 11:

$$k = A \cdot \exp[\frac{-E}{R \cdot T}] \quad (11)$$

where A is the pre-exponential factor, E is the activation energy (in kcal/mole), R is the universal gas constant (1.987 cal/mole/K), and T is the temperature in Kelvin. Typically, the Arrhenius equation includes a third term (T^n). The value of 'n' was set to zero for all reactions.

Since Reactions 1 and 2 are reversible, the rates of these reactions are dependent on the equilibrium constants, which are function of temperature. A simple equilibrium calculation using the RGIBBS reactor model in the software Aspen Plus was performed to find this temperature dependence[190]. Therefore, the reaction rates for each of the reactions can be written as:

$$r_1 = A_1 \cdot \exp[\frac{-E_1}{R \cdot T}] \cdot \left([Hg] \cdot [Cl_2] - \frac{[HgCl_2]}{\exp\left[-17.833 + \frac{17133.1}{T} \right]} \right) \quad (12)$$

Reproduced with permission of the copyright owner. Further reproduction prohibited without permission.

$$r_2 = A_2 \cdot \exp[\frac{-E_2}{R \cdot T}] \cdot \left([H_2O] \cdot [Cl_2] - \frac{[HCl]^2 \cdot [O_2]^{1/2}}{\exp\left[13.707 - \frac{4769.2}{T}\right]} \right) \quad (13)$$

$$r_3 = A_3 \cdot \exp[\frac{-E_3}{R \cdot T}] \cdot [Hg] \cdot [HCl]^2 \quad (14)$$

$$r_4 = A_4 \cdot \exp[\frac{-E_4}{R \cdot T}] \cdot [HgCl_2] \cdot [SO_2] \quad (15)$$

$$r_5 = A_5 \cdot \exp[\frac{-E_5}{R \cdot T}] \cdot [NO]^2 \cdot [Cl_2] \quad (16)$$

The concentrations of the pertinent species as a function of residence time are shown in Equations 17 to 20. The term, 't', is the residence time in the reactor system, and the concentrations ([ ]) are in ppm. Since the concentrations of O_2 and H_2O are several orders of magnitude higher than the concentrations of the other species, their rates of change are insignificant.

$$R_{Hg} = \frac{d[Hg]}{dt} = r_4 - r_1 - r_3 \quad (17)$$

$$R_{HgCl_2} = \frac{d[HgCl_2]}{dt} = r_1 + r_2 - r_4 \quad (18)$$

$$R_{Cl_2} = \frac{d[Cl_2]}{dt} = -r_1 - r_2 - r_5 \quad (19)$$

$$R_{HCl} = \frac{d[HCl]}{dt} = 2r_2 - 2r_3 \quad (20)$$

Equations 17 to 20 were solved in a similar fashion as mentioned in the previous chapters. The pre-exponential factors (A_1, A_2, A_3, A_4, A_5) and activation energies (E_1, E_2, E_3, E_4, E_5) for the five reactions were varied to minimize the function (Equation 12) in Chapter 5.

Reproduced with permission of the copyright owner. Further reproduction prohibited without permission.

6.5 Results and Discussion

The values of A and E were determined for the five reactions involved in the global kinetic model. Table 6.5-1 includes a summary of the values of these constants.

	Reaction	A	E ($x10^3$) (cal/mole)	$k = A \cdot \exp[\frac{-E}{R \cdot T}]$
1	$Hg(g) + Cl_2(g) \xleftrightarrow{k_1} HgCl_2(g)$	0.24	0.13	$k_1 = 0.24 \cdot \exp[\frac{-0.13 \times 10^3}{1.987 \cdot T}]$
2	$H_2O(g) + Cl_2(g) \xleftrightarrow{k_2} 2HCl(g) + \frac{1}{2}O_2(g)$	80.55	12.10	$k_2 = 80.55 \cdot \exp[\frac{-12.10 \times 10^3}{1.987 \cdot T}]$
3	$Hg(g) + 2HCl(g) \xrightarrow{k_3} HgCl_2(g) + H_2(g)$	32.65	29.99	$k_3 = 32.65 \cdot \exp[\frac{-29.99 \times 10^3}{1.987 \cdot T}]$
4	$HgCl_2(g) + SO_2(g) \xrightarrow{k_4} Hg(g) + SCl_2(s,g) + O_2(g)$	129.86	13.32	$k_4 = 129.86 \cdot \exp[\frac{-13.32 \times 10^3}{1.987 \cdot T}]$
5	$2NO(g) + Cl_2(g) \xrightarrow{k_5} 2NOCl(g)$	9.64	249.76	$k_5 = 9.64 \cdot \exp[\frac{-249.76 \times 10^3}{1.987 \cdot T}]$

Table 6.5-1: Summary of the values for the pre-exponential factor (A) and activation energy (E) for each of the reactions used in this model.

It was important to determine the effectiveness of the scheme proposed and the corresponding values of A and E. A plot was made that includes observed values on the y-axis and the predicted values on the x-axis from all the experimental data from the literature. Figures 6.5-1 to 6.5-5 include a trend-line along with the corresponding equation and best-fit (R^2) value. The trend-line (depicted by a solid line) is the best fit equation for the data as the line passes through the origin. Ideally, all the data points should lie on the y=x line (shown as the dashed line), with an R^2 value of 1.000, which would imply that the fit was perfect.

Reaction 1 is the global mercury oxidation reaction that has been used to determine the concentration of the oxidized species of Hg. As expected, this reaction itself is insufficient to predict the research data that has been published. Figure 6.5-1 shows a plot of observed percent Hg oxidation versus the predicted percent Hg oxidation using only Reaction 1. As seen, most of the predicted data is clustered around the axes. The R^2 value is -0.5013. Reaction 2 is the Deacon Reaction. It is known that the Deacon Reaction requires a catalyst to proceed. The experimental work presented in previous publications was carried out in a stainless steel and

Reproduced with permission of the copyright owner. Further reproduction prohibited without permission.

Inconel pipe[186, 190]. Inconel is known to contain iron and traces of manganese, silicon and aluminum[173]. The oxides of these metals are potential catalysts for the Deacon Reaction to take place as shown by Deacon[98] and Edwards[88]. The result of adding this reaction to the model is shown in Figure 6.5-2. The data is still scattered, the R^2 value improves to 0.4145, which suggests that more than half of the data points do not correlate well with the model. Reaction 3 is a second mercury oxidation reaction. As determined by Kilgroe, Sliger and Widmer et al., HCl is an effective oxidizing agent at high temperatures. Reaction 1 itself does not account for the reaction between elemental Hg and HCl. As a result this third reaction was added to the scheme. The results are shown in Figure 6.5-3. The correlation between the observed and predicted data improved, the R^2 value is now 0.7772.

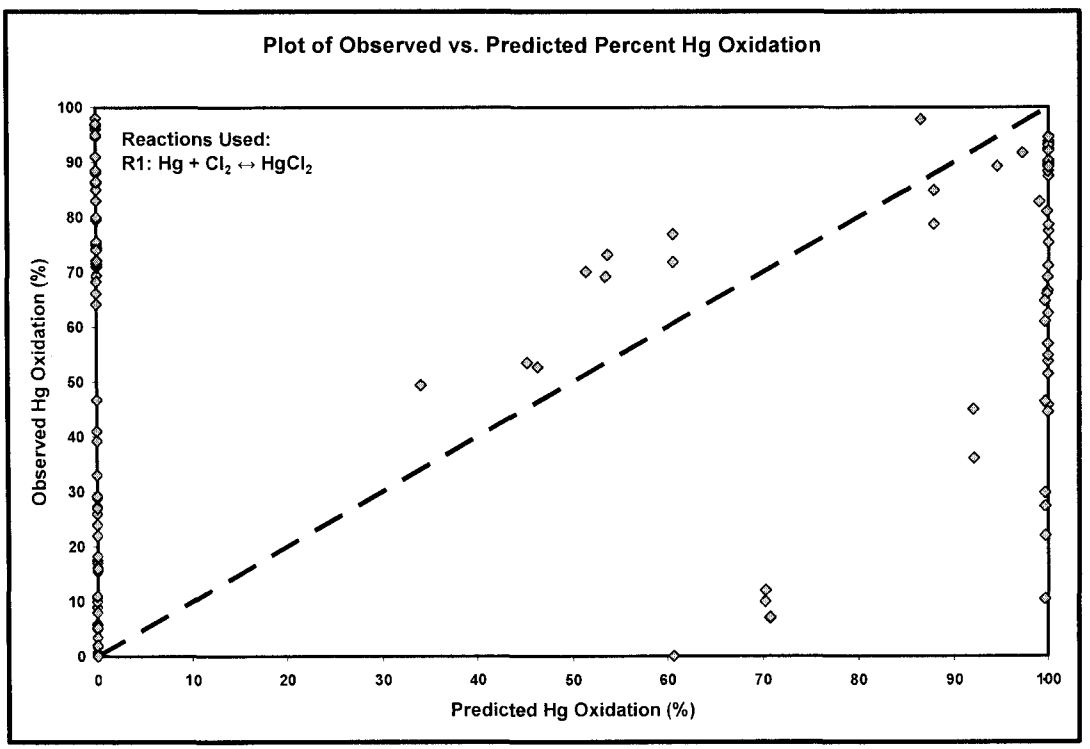

Figure 6.5-1: Plot of Observed Hg oxidation versus Predicted Hg Oxidation, using Reaction 1.

Reproduced with permission of the copyright owner. Further reproduction prohibited without permission.

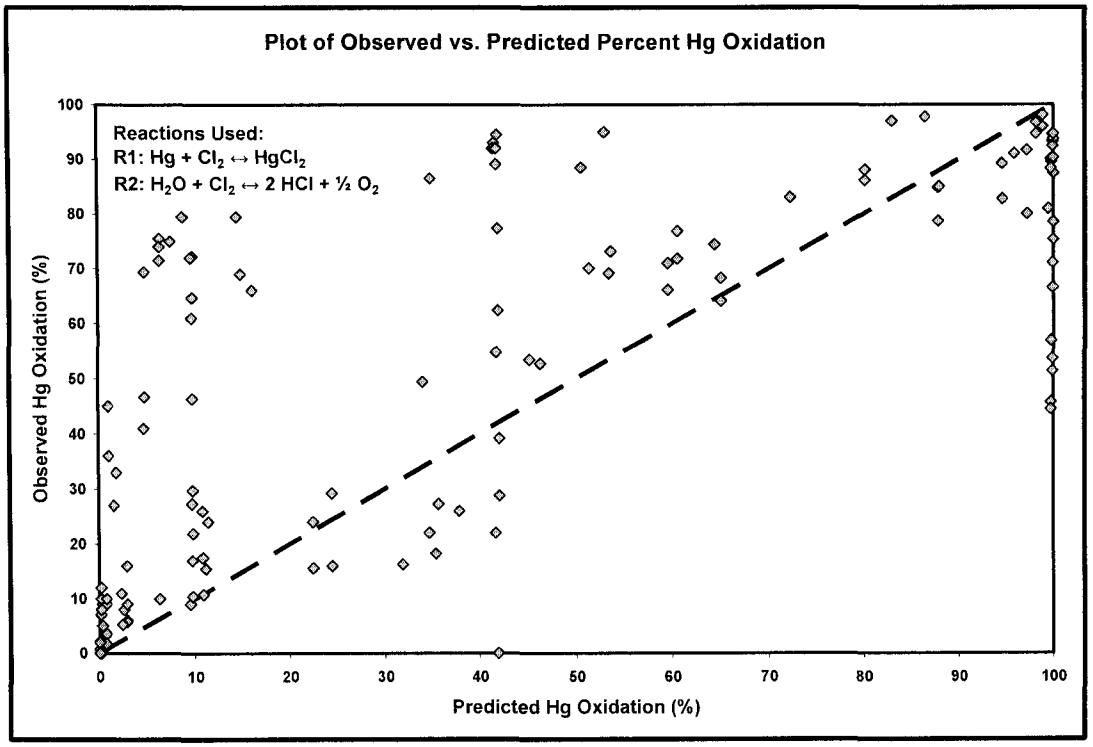

Figure 6.5-2: Plot of Observed Hg oxidation versus Predicted Hg Oxidation, using Reaction 1 and 2.

Reproduced with permission of the copyright owner. Further reproduction prohibited without permission.

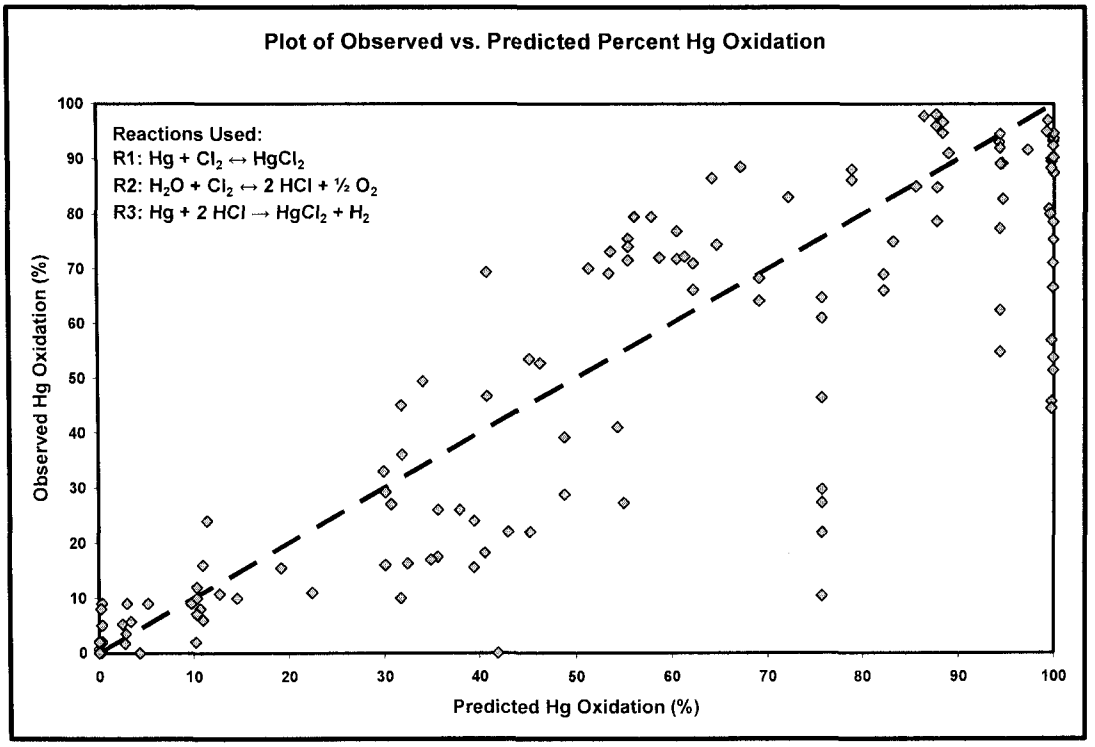

Figure 6.5-3: Plot of Observed Hg oxidation versus Predicted Hg Oxidation, using Reaction 1, 2 and 3.

Reaction 4 is a new reaction that is proposed in this work. There is limited published information that accounts for the inhibitory effect of molecular SO_2 on the oxidation of Hg by a chlorine species. Qiu et al. has suggested this inhibitory effect and proposed two reactions involving SO and SCl[189]. The authors stated that these radicals scavenge chlorine radicals, which may be present at higher temperatures. It is postulated that the chlorine radical is important for the initial oxidation reaction that converts elemental Hg to HgCl[84]. However, a reaction is proposed that does not involve radicals, but instead reacts and reduces $HgCl_2$ in the gas phase to elemental Hg, SCl_2 and O_2. The result of adding this reaction to the model is shown in Figure 6.5-4. The R^2 value for the data pool moved to 0.8916, which suggests that nearly 90 percent of the predictions correspond with the observed value.

Reproduced with permission of the copyright owner. Further reproduction prohibited without permission.

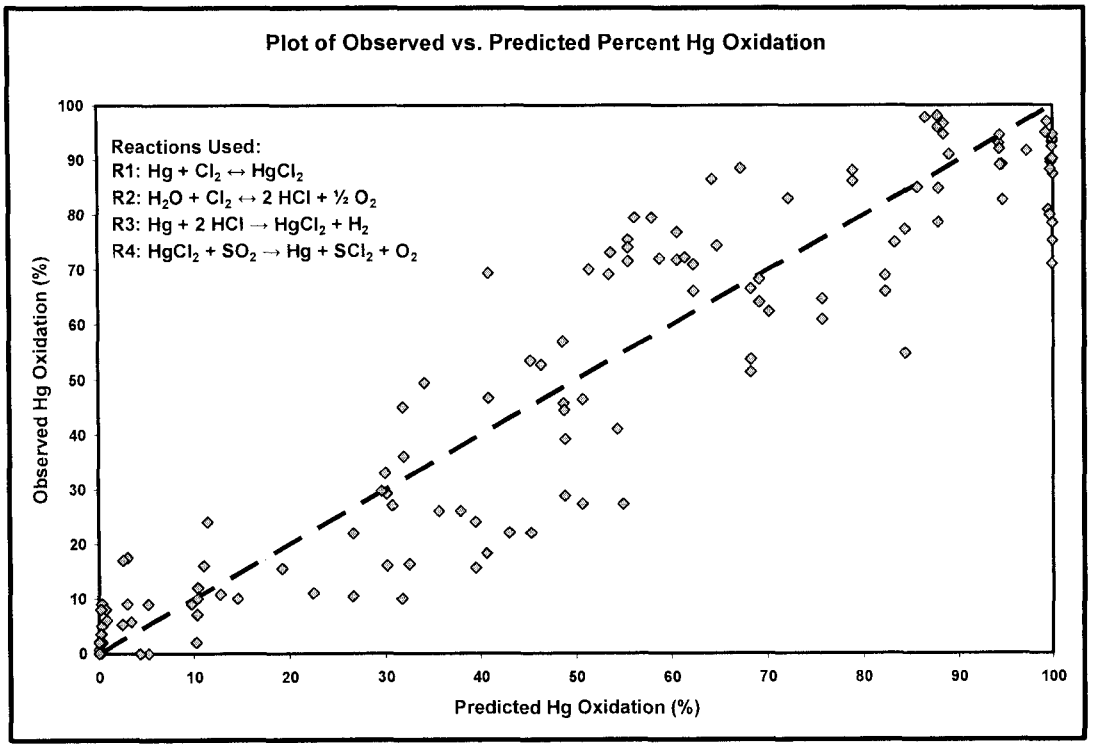

Figure 6.5-4: Plot of Observed Hg oxidation versus Predicted Hg Oxidation, using Reaction 1, 2, 3 and 4.

Reaction 5 was proposed in a previous publication to take into account the inhibitory effect of NO on Hg oxidation by Cl_2[186]. The results of adding this reaction to the model did not seem to affect the fit in any way. Comparing Figures 6.5-4 and 6.5-5, the slope and R^2 value of the best fit line are almost identical. However, this reaction was included in the model for completeness.

Reproduced with permission of the copyright owner. Further reproduction prohibited without permission.

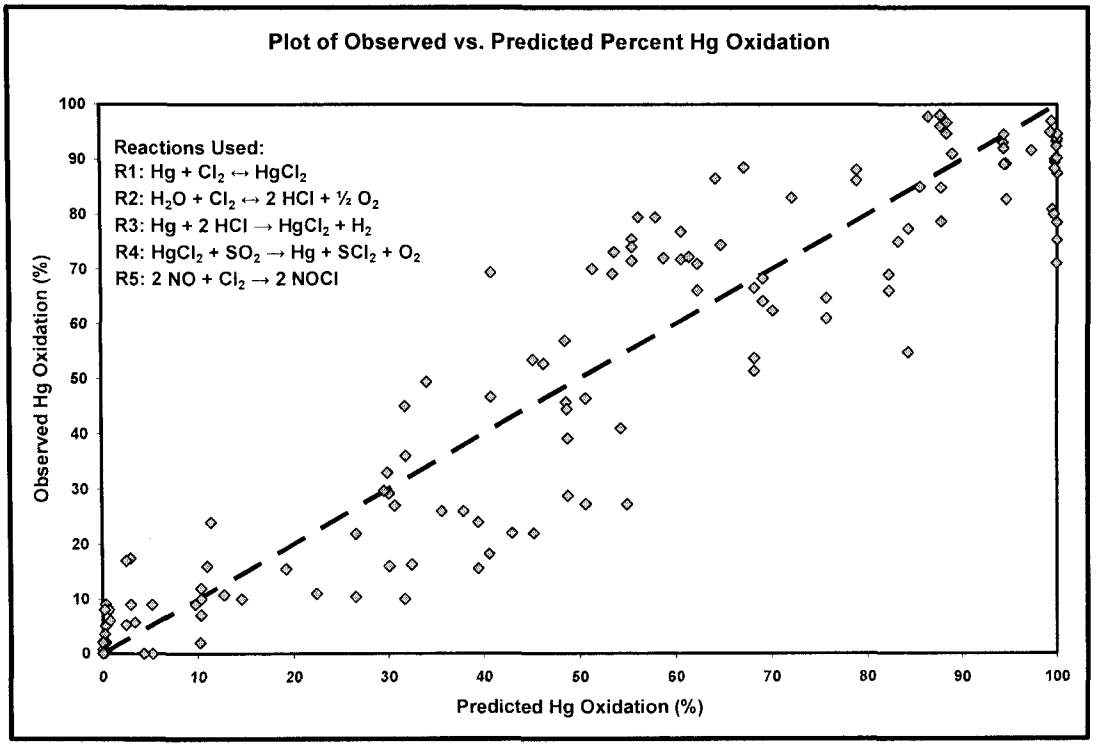

Figure 6.5-5: Plot of Observed Hg oxidation versus Predicted Hg Oxidation, using Reaction 1, 2, 3, 4 and 5.

Figure 6.5-6 shows the breakdown of the predictions versus observed values for the experimental data collected by the individual researchers used to validate the model proposed in this chapter. As seen, some data fits better than others, and this is expected. However, the difference between the percent Hg oxidation predictions and the observed percent Hg oxidation does not exceed 30 percent for any of the data points. This is very good, considering the large range of experiments included in the validation.

Reproduced with permission of the copyright owner. Further reproduction prohibited without permission.

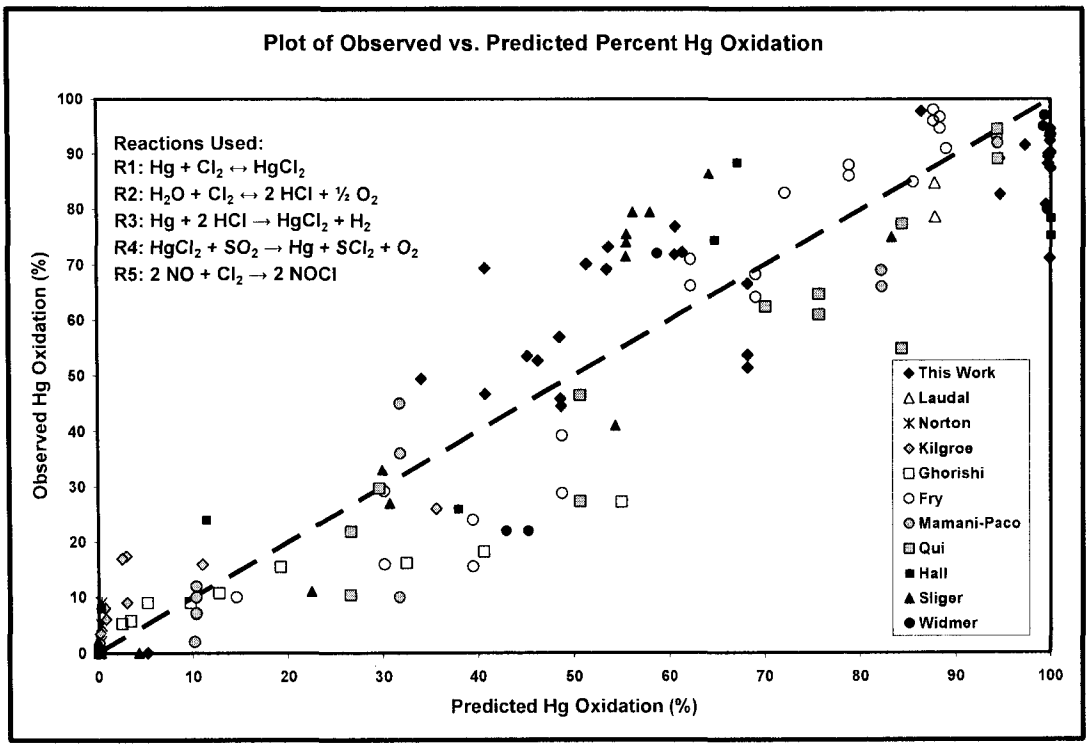

Figure 6.5-6: Plot of Observed Hg oxidation versus Predicted Hg Oxidation, using Reactions 1, 2, 3, 4 and 5. The plot shows the distribution of individual researcher's data.

Reproduced with permission of the copyright owner. Further reproduction prohibited without permission.

6.6 Conclusions

A global kinetic model was developed to predict Hg oxidation by chlorine species. Five reactions were proposed to predict experimental data produced using simulated flue gas containing Hg and the majority of the experimental data published in the literature. Two of the five reactions are reversible, while the remaining three were irreversible. Eleven independent researchers' data are used to validate the model, considering a number of variables. This contributes to the robustness of the model. The following features can be obtained from the model:

- the oxidation of Hg by Cl_2 – where the concentration of Cl_2 ranges from 1 to 500 ppm_v (Qui et al.'s work).
- the oxidation of Hg by HCl – where the concentration of HCl ranges from 50 in Laudal et al.'s work to 3000 ppm_v in Widmer et al.'s work.
- the effect of a wide range of temperatures – from a constant temperature of 175°C in Laudal et al.'s experimental apparatus to over 1100°C in Fry et al.'s apparatus.
- the effect of a wide range of residence times – ranging from 0.70 seconds in Widmer et al.'s experimental apparatus to 6.2 seconds in Mamani-Paco and Helble's experimental apparatus.
- the inhibitory effect of SO_2 on Hg oxidation by a chlorine species – where the concentration of SO_2 ranged from 100 ppm_v in Qiu et al.'s work to 1600 ppm_v in Norton et al.'s work.
- the use of different reactor types – Teflon was used by Laudal et al., Quartz was used by Kilgroe et al., Fry et al. and Qiu et al., a furnace lined with refractory material was used by Sliger et al., and stainless steel was used by Hall et al. and Agarwal et al..
- the use of different methods of measuring the mercury species – the most commonly used methods were the Ontario-Hydro Method and a Continuous Emissions Monitoring (CEM) device. The EPA Method 29 and cold vapor atomic adsorption spectroscopy (CVAAS) were also used.

Reproduced with permission of the copyright owner. Further reproduction prohibited without permission.

The global scheme was able to predict the data from up to eleven experimental data sources. Approximately 70% of the data obtained in the experimental rig presented in this work were accurately predicted. Of the eleven data sources, 146 data points were used to validate the global scheme, and nearly 90% of these data points were accurately predicted.

Reproduced with permission of the copyright owner. Further reproduction prohibited without permission.

CHAPTER 7

Conclusions

7.1 Introduction

This research project accomplished several purposes:

1. The construction of a unique experimental apparatus that has the ability to simulate a power plant temperature and residence time profile. This apparatus also had the ability to test both homogeneous Hg oxidation and heterogeneous Hg oxidation by means of injecting sorbents.
2. The ability to perform experimental work involving the injection of Cl_2 into a heated gas blend that simulated the flue gas obtained by combusting PRB coal. Experimental work focused on varying the temperature profile of the apparatus, varying the concentration of Cl_2, and observing the effects of all flue gas components on the oxidation of Hg^0.
3. The development of a global kinetic model that was based on the data collected in the experimental apparatus. Five reactions were proposed, where two are reversible reactions, and three are irreversible reactions.
4. The use of the global kinetic model to predict experimental data from eleven independent sources from literature, and in the process show the robustness of this model in its predictive ability.

7.2 Summary of the Experimental Apparatus Constructed.

The experimental apparatus was built to serve two purposes. The first was to perform experimental work involving the oxidation of elemental Hg by a chlorine species. The second was to perform heterogeneous oxidation of elemental Hg by the injection of activated carbon or sorbents. The focus of this dissertation was on the oxidation of Hg^0 by a chlorine species.

Reproduced with permission of the copyright owner. Further reproduction prohibited without permission.

The flue gas was created by blending gases and heating the blend to the desired temperature. Chlorine gas was injected at the exit of the Final Pre-heater (R1) and a sample of gas was continuously collected and measured for Hg concentration. A continuous emissions monitor (CEM) was used to measure the concentration of Hg in the sample gas stream.

7.3 Summary of the Experimental Work

It was found that Cl_2 oxidizes elemental Hg to Hg^{2+} very effectively. In the absence of all flue gas components, only 1 ppmv Cl_2 was required to give over 70% Hg oxidation. Temperature also played an important role in this work. At temperatures above 320°C, 1 ppmv Cl2 resulted in less than 55% Hg oxidation. At temperatures below 320°C, 1 ppmv Cl2 resulted in over 70% Hg oxidation. This shows that the effectiveness of Cl2 as an oxidizing agent increases as the temperature decreases.

The various flue gas components also impacted the percent Hg oxidation. SO_2 and H_2O severely inhibited the oxidation of Hg by Cl_2. NO also seemed to inhibit the process, but to a lesser degree. The other flue gas components, N_2, O_2, CO_2 and CO did not affect the oxidation in any way.

7.4 Creating a Global Kinetic Mechanism

In order to accurately predict the data collected from the experimental apparatus presented in this thesis, a global kinetic mechanism was developed. Five reactions were proposed as crucial to predict this data:

$$Hg(g) + Cl_2(g) \xleftrightarrow{k_1} HgCl_2(g) \quad (1)$$

$$H_2O(g) + Cl_2(g) \xleftrightarrow{k_2} 2HCl(g) + \tfrac{1}{2}O_2(g) \quad (2)$$

$$Hg(g) + 2HCl(g) \xrightarrow{k_3} HgCl_2(g) + H_2(g) \quad (3)$$

$$HgCl_2(g) + SO_2(g) \xrightarrow{k_4} Hg(g) + SCl_2(s,g) + O_2(g) \quad (4)$$

$$2NO(g) + Cl_2(g) \xrightarrow{k_5} 2NOCl(g) \quad (5)$$

Reactions 1 and 2 are reversible reactions, while the remaining three reactions are irreversible. The reaction rate constants follow the Arrhenius expression. A Matlab routine was

Reproduced with permission of the copyright owner. Further reproduction prohibited without permission.

written to find the least square fit for the data presented in this paper in order to find the values for the five pre-exponential factors and the five activation energies for the reactions. It was found that the predictions corresponded very well with the observed experimental values.

7.5 Validating the Global Kinetic Mechanism

Once the global kinetic mechanism was developed, eleven independent researchers' data was used to validate the model. The data encompassed a wide variety of variables, such as the use of Cl_2 or HCl as the oxidizing agent, temperature profiles, quenching rates, the effects of flue gas components and the respective concentrations, the inhibitory effects of SO2 and H2O on Hg oxidation, the use of different reactor types (ranging from Teflon to stainless steel pipes), and a variety of measurement techniques (from CEM to the EPA Method 29). Altogether, 146 data points were used to validate the model and show its robustness, and nearly 90% of these data points were accurately predicted by the model.

Reproduced with permission of the copyright owner. Further reproduction prohibited without permission.

References

1. Physical Properties of Hg: http://www.lenntech.com/Periodic-chart-elements/Hg-en.htm (Accessed on May 29, 2006)
2. Otani, Y.; Emi, H.; Kanaoka, C.; Matsul, S. "Behavior of Metal Mercury in Gases", *Environ. Sci. Technol.*, (**1984**), *18*, 793-796.
3. U.S. Department of Labor: Occupational Safety & Health Administration http://www.osha.gov/dts/chemicalsampling/data/CH_250510.html (Accessed May 29, 2006)
4. Brechignac, C.; Broyer, M.; Cahuzac, P.; Delacretaz, G.; Labastie, P.; Wolf, J. P.; Woeste, L. "Probing the transition from van der Waals to metallic mercury clusters." *Physical Review Letters* (**1988**), *60(4)*, 275-8.
5. Uchtmann, H.; Rademann, K.; Hensel, F. "Metal-nonmetal transition and homogeneous nucleation of mercury vapor." *Annalen der Physik*, (**1991**), *48(1-3)*, 207-14.
6. Haberland, H., B. von Issendorff, J. Yufeng, T. Kolar, and G. Z. Thanner, "Ground State and Response Properties of Mercury Clusters," *J. Phys. D.*, (**1993**), *26*, 8.
7. Wikipedia http://en.wikipedia.org/wiki/Isoelectronic (Accessed May 29, 2006)
8. Hall, B.; Schager, P.; Lindqvist, O. "Chemical Reactions of Mercury in Combustion Flue gases". *Water, Air, Soil Pollut.* (**1991**), *56*, 3-14.
9. Haberland, H., B. von Issendorff, J. Yufeng, T. Kolar, and G. Z. Thanner, "Ground State and Response Properties of Mercury Clusters," *J. Phys. D.*, (**1993**), *26*, 8.
10. Davidson, P. W.; Myers, G. J.; Weiss, B. "Mercury Exposure and Child Development Outcomes." *Pediatrics* (**2004**), *113*, 1023-1029.
11. Sondreal, E. A.; Benson, S. A.; Pavlish, J. H. "Status of research on air quality: mercury, trace elements, and particulate matter." *Fuel Proc. Technol.*, (**2000**), *65-66*, 5-19.
12. Clarkson, T.W.; Magos, L.; Greenwood, M.R.; "The Transport of Elemental Mercury into Fetal Tissues" *Biological Neonate*, (**1972**), *21*, 239-244.

Reproduced with permission of the copyright owner. Further reproduction prohibited without permission.

13. Material Safety Data Sheet: http://www.jtbaker.com/msds/englishhtml/M1599.htm (Accessed on May 29, 2006)
14. Carpi, A. and Chen, Y.F. "Gaseous elemental mercury as an indoor air pollutant." *Environ. Sci. Technol.*, (**2001**), *35*, 4170-4173.
15. U.S. Environmental Protection Agency http://www.epa.gov/iris/subst/0370.htm (Accessed May 29, 2006)
16. U.S. Environmental Protection Agency http://www.epa.gov/ttnatw01/hlthef/hapglossaryrev.html (Accessed May 29, 2006)
17. Wikipedia http://en.wikipedia.org/wiki/LD50 (Accessed May 29, 2006)
18. Von Burg. R. "Toxicology update: inorganic mercury." *J. Appl. Toxicol.* (**1995**), 15, 483-493.
19. The Risk Assessment Information System http://risk.lsd.ornl.gov/tox/profiles/mercury_f_V1.shtml (Assessed May 29, 2006)
20. "Toxicological profile for Mercury", U.S. Department of Health and Human Services, Public Health Service, Agency for Toxic Substances and Disease Registry (ATSDR), March **1999**. Available at http://www.atsdr.cdc.gov/toxprofiles/tp46.html (Accessed May 29, 2006)
21. Halbach, S. and T. W. Clarkson. "Enzymatic oxidation of mercury vapor by erythrocytes." *Biochem. Biophys. Acta* (**1978**), *523*, 522-531.
22. Magos, L., T. W. Clarkson, and M. R. Greenwood. "The depression of pulmonary retention of mercury vapor by ethanol; identification of the site of action." *Toxicol. Appl. Pharmacol.* (**1973**), 26, 1-4.
23. Hursh, J. D, M. R. Greenwood, T. W. Clarkson, et al. "The effect of ethanol on the fate of mercury vapor inhaled by man." *J. Pharmacol. Exp. Ther.* (**1980**), *214*, 520-527.
24. U.S. Environmental Protection Agency http://www.epa.gov/ttnatw01/hlthef/mercury.html (Accessed May 29, 2006)

Reproduced with permission of the copyright owner. Further reproduction prohibited without permission.

25. Agocs, M. M.; Etzel, R. A.; Parrish, R. G.; Paschal, D. C.; Campagna, P. R.; Cohen, D. S.; Kilbourne, E. M.; Hesse, J. L. "Mercury exposure from interior latex paint." *New England journal of medicine*, (**1990**), *323(16)*, 1096-1101.

26. Swensson, A. and Ulfvarson, U. "Toxicology of Organic Mercury Compounts used as Fungicides." *Occupational health review*, (**1963**), *15*, 5-11.

27. Spedding, D. J. and Hamilton, R. B. "Adsorption of mercury vapor by indoor surfaces." *Environmental research*, (**1982**), *29(1)*, 30-41.

28. USEPA: Characterization of Products Containing Mercury in Municipal Solid Waste in the United States, 1970 to 2000, April 1992, EPA530-R-92-013.

29. The Massachusetts Department of Environmental Protection http://www.mass.gov/dep/files/mercury/hgch3a.htm (Accessed May 29, 2006)

30. Energy Citations Database http://www.osti.gov/energycitations/product.biblio.jsp?osti_id=6505014 (Accessed May 29, 2006)

31. Boening, D. W. "Ecological effects, transport, and fate of mercury: a general review." *Chemosphere*, (**2000**), *40(12)*, 1335-51.

32. U.S. Environmental Protection Agency. Summary Review of Health Effects Associated with Mercuric Chloride: Health Issue Assessment. EPA/600/R-92/199. Office of Health and Environmental Assessment, Washington, DC. **1994**.

33. Qian, S. S.; Warren-Hicks, W.; Keating, J.; Moore, D. R.; Teed, R. S. "A predictive model of mercury fish tissue concentrations for the southeastern United States." *Environ. Sci. Technol*, (**2001**), *35(5)*, 941-7.

34. Patra, M. and Sharma, A. "Mercury Toxicity In Plants." *Botanical Rev.* (**2000**), *66*, 379-422.

35. Wilcox, J.; Robles, J.; Marsden, D.C.J.; Blowers, P. "Theoretically Predicted Rate Constants for Mercury Oxidation by Hydrogen Chloride in Coal Combustion Flue Gases." *Environ. Sci. Technol.* (**2003**), *37*, 4199-4204.

Reproduced with permission of the copyright owner. Further reproduction prohibited without permission.

36. U. S. Environmental Protection Agency http://www.epa.gov/mercury/exposure.htm (Accessed on May 29, 2006)

37. USEPA: Database: National Survey of Mercury Concentrations in Fish (1990-1995) - http://www.epa.gov/waterscience/fish/mercurydata.html (Accessed May 29, 2006)

38. Martinelli, L.A., J.R. Ferreira, B.R. Forsberg, R.L. Victoria. "Mercury contamination in the Amazon: A gold rush consequence." *Ambio*, (**1988**), *17 (4)*, 252-254.

39. Slemr, F.; Schuster, G.; Seiler, W. "Distribution, speciation, and budget of atmospheric mercury." *Journal of Atmospheric Chemistry*. (**1985**), *3(4)*, 407-434.

40. Slemr, F., Seiler, W., and Schuster, G. "Latitudinal distribution of mercury over the atlantic ocean", *J. Geophys. Res.*, (**1981**), *86*, 1159-1166.

41. Lindqvist, O.; Johansson, K.; Aastrup, M.; Andersson, A.; Bringmark, L.; Hovsenius, G.; Haakanson, L.; Iverfeldt, A.; Meili, M.; Timm, B. "Mercury in the Swedish environment - recent research on causes, consequences and corrective methods." *Water, Air, and Soil Pollution*. (**1991**), *55(1-2)*, 1-261.

42. Hall, B. "The gas phase oxidation of elemental mercury by ozone." *Water, Air, and Soil Pollution*. (**1995**), *80(1-4)*, 301-315.

43. Kilgroe, J.D.; Sedman, C.B.; Srivastava, R.K.; Ryan, J.V.; Lee, C.W.; Thorneloe, S.A. "Control of Mercury Emissions from Coal Fired Electric Utility Boilers." Interim Report, No. EPA-600/R-01-109, U.S. Environmental Protection Agency, Washington, DC, December **2001**.

44. Galbreath, K.C. and Zygarlicke,C.J. "Mercury speciation in Coal Combustion and gasification flue gases". *Environ. Sci. Technol.* (**1996**), *30*, 2421-2426.

45. Wang, J.; Cobb, J. T., Jr.; Elder, W. W., III. "Study of mercury oxidation in the post-combustion zones of coal-fired boilers." *Preprints of Symposia - American Chemical Society, Division of Fuel Chemistry*, (**2001**), *46(2)*, 711-712.

46. Brown, T.D.; Smith, D.N.; Hargis, R.A. Jr; O'dowd, W.J. "What We Know, Have Learned, and Need to Further Investigate." *J. Air and Waste Management Assoc.* (**1999**), 1-97.

Reproduced with permission of the copyright owner. Further reproduction prohibited without permission.

47. Agency for Toxic Substances and Disease Registry: http://www.atsdr.cdc.gov/tfacts46.html (Accessed on May 29, 2006)

48. Wren, C.D.; Stokes, P.M. "Depressed Mercury Levels in Biota from Acid and Metal Stressed Lakes Near Sudbury, Ontario", *Ambio*, (**1988**), *17 (1)*.

49. Wren, C.D. "Distribution of Metals in Tissues of Beaver, Raccoon and Otter from Ontario, Canada", *The Science of the Total Environment*, (**1984**), *34*, 177-184.

50. Richman, L.A.; Wren C.D.; Stokes, P.M. "Facts and Fallacies concerning Mercury uptake by Fish in Acid Stressed Lakes", *Water, Air, Soil Pollution*, (**1988**), *37*, 467-473.

51. Lindberg, S.E.; Southworth, G.R.; Bogle, M.A.; Blasing, T.J.; Owens, J.; Roy, K.; Zhang, H.; Kuiken, T.; Price, J.; Reinhart, D.; Sfeir, H. "Airborne Emissions of Mercury from Municipal Solid Waste. I: New Measurements from Six Operating Landfills in Florida", *Journal of Air and Waste Management Association,* (**2005**), 55, 859-869.

52. Mercury Study Report to Congress, Volume I: Executive Summary, Report No. EPA-452/R-97-003, U.S. Environmental Protection Agency, Office of Air Quality Planning and Standards and Office of Research and Development, Washington, DC, **1997**.

53. U.S. Department of Energy, Energy Information Administration. U.S. Coal Reserves: 1997 Update. DOE/EIA-0529(97). Office of Coal, Nuclear, Electric and Alternate Fuels, Office of Integrated Analysis and Forecasting, Washington, DC. February **1999**. Available at: < http://www.eia.doe.gov/cneaf/coal/reserves/front-1.html >.

54. U.S. EPA, "A study of hazardous air pollutant emissions from electric utility steam generating units: Final Report to Congress". EPA-453/R-98-004a; U.S. EPA Office of Air Quality Planning and Standards, U.S. Government Printing Office: Washington, DC, February **1998**.

55. Galbreath, K. C. and Zygarlicke, C. J. "Mercury transformations in coal combustion flue gas." *Fuel Proc. Technol.* (**2000**), *65-66*, 289-310.

Reproduced with permission of the copyright owner. Further reproduction prohibited without permission.

56. Center for Applied Research in Digital Government Information Systems. http://www1.cs.columbia.edu/nlp/flkb/eia_web/output_none.html (Accessed May 29, 2006)
57. Meij, R.; Vredenbregt, H.J.; Winkel H.T "The fate and behavior of mercury in coal-fired power plants", *Journal of Air and Waste Management Association,* (**2002**), *52*, 912-917.
58. BioSpace: http://biospace.intota.com/multisearch.asp?strsearchtype=all&strquery=flue%20gas (Accessed May 29, 2006)
59. Center for Applied Research in Digital Government Information Systems. http://www1.cs.columbia.edu/nlp/flkb/eia_web/output_none.html (Accessed May 29, 2006)
60. Fording: Canadian Coal Trust: http://www.fording.ca/cache/page_238-469.html (Accessed May 29, 2006)
61. Chen, B. I. T. "Workshop: Mercury Emissions Measurements and Control" Lehigh University Energy Research Center, Annual Meeting (**2005**).
62. U.S. Environmental Protection Agency: Clean Air Interstate Rule: http://www.epa.gov/cair/ (Accessed May 29, 2006)
63. U.S. Environmental Protection Agency: Clean Air Mercury Rule: http://www.epa.gov/mercuryrule/ (Accessed May 29, 2006)
64. Sale, J. "Overview of Mercury Regulations and Economic Modeling of Control Alternatives." Workshop on Hg emissions and controls" Lehigh University Energy Research Center, (**2005**).
65. Concise International Chemical Assessment Document 50 http://www.inchem.org/documents/cicads/cicads/cicad50.htm#2.2 (Accessed May 29, 2006)

Reproduced with permission of the copyright owner. Further reproduction prohibited without permission.

66. Material Safety Data Sheet http://www.conncoll.edu/offices/envhealth/MSDS/botany/M/Mercuric-chloride.html (Accessed May 29, 2006)

67. Answers: http://www.answers.com/main/ntquery;jsessionid=fll5teq3425hi?method=4&dsid=2222&dekey=Mercury%28II%29+chloride&gwp=8&curtab=2222_1&sbid=lc04b (Accessed May 29, 2006)

68. Answers: http://www.answers.com/main/ntquery;jsessionid=fll5teq3425hi?method=4&dsid=2222&dekey=Cinnabar&gwp=8&curtab=2222_1&sbid=lc04b (Accessed May 29, 2006)

69. InChem: http://www.inchem.org/documents/icsc/icsc/eics0982.htm (Accessed May 29, 2006)

70. Perry R. H. and Green D. W. "Perry's Chemical Engineers' HandBook", 7th Edition, McGraw Hill Professional, **1997**.

71. InChem: http://www.inchem.org/documents/icsc/icsc/eics0981.htm (Accessed May 29, 2006)

72. Hilgen, H.; Rekers; Casper, J.N.; "Process for recovering mercury from a gas containing mercury vapor". USPTO #3849267, November 19, **1974**.

73. Wilhelm, K. and Guenter H. "Process and apparatus for recovering mercury or mercury(ii) chloride from catalysts containing mercury"; Patent #: GB1121845; November 25, **1965**. http://v3..cespacenetom/textdoc?DB=EPODOC&IDX=DE 5705&F=8 (Accessed May 29, 2006)

74. Birke, L.G.; Oslo, R.; Jebems, A.; Hosle; Eystein, I.; Dyvik, F. "Process for the removal of mercury from gases". USPTO # 3838190, September 24, **1974**.

75. Liu, K.; Gao, Y.; Riley, J. T.; Pan, W-P.; Metha, A. K.; Ho, K. K.; Smith, S. R. "An investigation of mercury emissions from FBC systems fired with High chlorine coals." *Energy and Fuels* (**2001**), *15*, 1173-1180.

Reproduced with permission of the copyright owner. Further reproduction prohibited without permission.

76. Laudal, D. L.; Brown, T. D.; Nott, B. R. "Effects of Flue Gas Constituents on Mercury Speciation". *Fuel Process. Technol.* **2000**, *65-66*, 157-165.

77. Norton, G. A.; Yang, H.; Brown, R. C.; Laudal, D.; Dunham, G. E.; Eryavec, J. "Heterogeneous Oxidation of Mercury in Simulated Post Combustion Conditions". *Fuel* (**2002**), *82*, 107-116.

78. Wang, J.; Clements, B.; Zanganesh, K. "An Interpretation of Flue-Gas Mercury Speciation Data from a Kinetic Point of View". *Fuel* (**2003**), *82*, 1009-1011.

79. Fujiwara, N.; Fujita, Y.; Tomura, K.; Moritomi, H.; Tuji, T.; Takasu, S.; Niksa, S. "Mercury Transformations in the Exhausts from Lab-Scale Coal Flames". *Fuel* (**2002**), *81*, 2045-2052.

80. Xu, M.; Qiao, Y.; Zheng, C.; Li, L.; Liu, J. "Modeling of Homogeneous Mercury Speciation using Detailed Chemical Kinetics". *Combust. Flame* (**2003**), *132*, 208-218.

81. Senior, C. L.; Sarofim, A. F.; Zeng, T.; Helble, J. J.; Ruben, M. "Gas-Phase Transformations of Mercury in Coal-Fired Power Plants". *Fuel Process. Technol.* (**2000**), *63*, 197-213.

82. Sliger, R. N.; Kramlich, J. C.; Marinov, N. M. "Towards the Development of a Chemical Kinetic Model for the Homogenous Oxidation of Mercury by Chlorine Species ". *Fuel Process. Technol.* (**2000**), *65-66*, 423-438.

83. Nishitani, T.; Fukunaga, I.; Itoh, H.; Nomua, T. "The Relationship between HCl and Mercury Speciation in Flue Gas from Municipal Solid Waste Incinerators". *Chemosphere* (**1999**), *39 (1)*, 1-9.

84. Niksa, S.; Helble, J. J.; Fujiwara, N. "Kinetic Modeling of Homongeneous Mercury Oxidation: The Importance of NO and H2O in Predicting Oxidation in Coal-Derived Systems". *Environ. Sci. Technol.* (**2001**), *35*, 3701-3706.

85. Cao, Y.; Duan, Y.; Kellie, S.; Li, L.; Xu, W.; Riley, J.T.; Pan, W-P.; Chu, P.; Metha, A. K.; Carty, R. "Impact of Coal chlorine on mercury speciation and emission from a 100-MW

Reproduced with permission of the copyright owner. Further reproduction prohibited without permission.

utility boiler with cold side electrostatic precipitators and low-NOx burners". *Energy and Fuels.* (**2005**), *19*, 842-854.

86. Shao, D.; Hutchinson, E. J.; Cao, H.; Pan, W. "Behavior of Chlorine During Coal Pyrolysis." *Energy Fuels* (**1994**), *8 (2)*, 399-401.
87. Liu, K.; Gao, Y.; Kellie, S.; Xie, W.; Pan, W.-P.; Riley, J.T.A. "Study of Mercury Removal in FBC System Fired with High Chlorine Coals". *Combustion Science Technology.* (**2001**), *164*, 145-162.
88. Edwards, J.R.; Srivastava, R.K.; Kilgroe, J.D. "A Study of Gas Phase Mercury Speciation Using Detailed Chemical Kinetics." *Journal of Air and Waste Management Association.* (**2001**), *51*, 869-877.
89. Kellie, S.; Cao, Y.; Duan, Y.; Li, L.; Chu, P.; Mehta, A.; Carty, R.; Riley, J.T.; Pan, W.-P. "Factors Affecting Mercury speciation in a 100-MW Coal Fired Boiler with Low Nox Burners". *Energy and Fuels.* (**2005**). *19*, 800-806.
90. Frandsen, F.; Dam-Johansen, K.; Rasmussen, P. *Prog. Energy Combust. Sci.* (**1994**), *20*, 115-138.
91. Lindbauer, R.L.; Wurst, F.; Prey, T. "Combustion Dioxin suppression in municipal solid waste incineration with sulphur additives". *Chemosphere.* (**1992**), *25 (7-10)*, 1409-1414.
92. Griffin, R.D. "A new theory of dioxin formation in municipal solid waste combustion". *Chemosphere.* (**1986**), *15 (9-12)*, 1987-1990.
93. Xie, W.; Pan, W-P.; Riley, J.T. "Behavior of Chloride during coal combustion in an AFBC System". *Energy Fuels.* (**1999**), *13*, 585-591.
94. Flagan, R.C. and J.H. Seinfeld, "Fundamentals of Air Pollution Engineering." Prentice Hall, Englewood Cliffs, New Jersey, **1988**, pp. 217-219.
95. Barrett, R.E., Hummell, J.D., and Reid, W.T. "Formation of SO3 in a Noncatalytic combustor," *J. Eng. Power Trans. ASME, A88,* (**1966**), 165-172.
96. Westenberg, A.A., and De Haas, H. "Rate of the Reactor O + SO2 + M → SO3 + M*," *J. Chem. Phys.,* (**1975**), *63*, 5411-5415.

Reproduced with permission of the copyright owner. Further reproduction prohibited without permission.

97. Romero, C.E.; Bilirgen, H.; Li, Y. "Development of a gas phase mercury oxidation kinetic model for coal fired power plant flue gas", November **2002**. Energy Research Center, Lehigh Univeristy, Report No. 02-400-20-25.

98. Deacon, H., USPTO 118209, August **1871**.

99. Deacon, H., USPTO 165802, July **1875**.

100. Deacon, H., USPTO 85370, December **1868**.

101. Deacon, H., USPTO 141333, July **1875**.

102. Pan, H.Y.; Minet, R.G.; Benson, S.W.; Tsotsis, T.T. "Process for Converting Hydrogen Chloride to Chlorine." *Industrial & Engineering Chemistry Research*, (**1994**), *34(12)*, 2996-3003.

103. van der Vaart, R.; Akkerhuis, J.; Feron, P.; Jansen, B. "Removal of mercury from gas streams by oxidative membrane gas adsorption", *Journal of Membrane Science.* (**2001**), *187*, 151-157.

104. Korpiel, J.A. and Vidic, R.D. "Effect of sulfur impregnation method on activated carbon uptake of gas phase mercury". *Environ. Sci. Technol.* (**1997**), *31*, 2319-2325.

105. Li,Y.H.; Serre, S.D.; Lee, C.W.; Gullett, B.K. "Elemental Mercury Adsorption by activated carbon treated with sulfuric acid". U.S. EPA/DOE/EPRI, The Mega Symposium and Fate, Effects and Control on Hg emissions, Chicago, IL. August 20-23, **2001**.

106. Prestbo, E.M.; Bloom, N.S. "Mercury speciation adsorption (MESA) method for combustion flue gas: methodology, artifacts, intercomparison, and atmospheric implications", *Water, Air, Soil Pollution*, (**1995**), *80*, 145-158.

107. Fahlke, J.; Bursik, A. "Impact of the state of the art flue gas cleaning on mercury species emissions from coal-fired steam generators", *Water, Air, Soil Pollution*, (**1995**), *80*, 209-215.

108. Meij, R.; Vredenbregt, H.J.; Winkel H.T "The fate and behavior of mercury in coal-fired power plants", *Journal of Air and Waste Management Association,* (**2002**), *52*, 912-917.

Reproduced with permission of the copyright owner. Further reproduction prohibited without permission.

109. deJong; Geert J.; Vos; Hendrick,J. USPTO 4,196,173. April 1, **1980**.

110. Felsvang, K. S.; Nielsen, K. K.; Ove, B. C. USPTO 5,435,980. July 25, **1995**.

111. McIntyre, B. W. and Biggar J.W. USPTO 4,619,608. October 28, **1986**.

112. Caldwell, D.; Biggar, J. W.; McIntyre, B.W. USPTO: 6,447,740. September 10, **2002**.

113. Wiklund, J. E. USPTO 4,443, 417. April 17, **1984**.

114. Nolan, P. S.; Bailey, R.T.; Downs, W. USPTO 20020068030, June 6, **2002**.

115. Lissianski, V. V.; Zamansky, V.M.; Maly, P.M.; Seeker, W.R.; USPTO: 20050036926. February 17, **2005**.

116. Ide; Akira; Shigenaka; Tsutomu; Kokado; Masayuki; Kondo; Shigeru. USPTO: 4,729,882. March 8, **1988**.

117. Breen, B. P. and Gabrielson, J.E. USPTO 20030147793. August 7, **2003**.

118. Meischen, S. J. and Van Pelt; V. J. USPTO: 6,136,281. October 24, **2000**.

119. Biswas, P. and Wu, C-Y. USPTO: 6,248,217. June 19, **2001**.

120. Mendelsohn, M.H. and Huang, H-S. USPTO: 5,900,042. May 4, **1999**.

121. Oehr, K.H. USPTO: 20030161771. August 28, **2003**.

122. Vosteen, B; Beyer, J.; Bonkhofer, T-G.; Fleth, O.; Wieland, A.; Pohontsch, A.; Rico, K.; Standau, E.; Mueller, C.; Nolte, M.; Koeser, H. USPTO: 20040086439. May 6, **2004**.

123. Nikolai B. and Peterson, K.A. "Mercury and Reactive Halogens: The thermochemistry of Hg + {Cl_2, Br_2, BrCl, ClO and BrO}. *J. Phys. Chem. A.* (**2003**), *107*, 7465-7470.

124. Behra, P.; Bonnissel-Gissinger, P.; Alnot, M.; Revel, R.; Ehrhardt, J. "XPS and XAS Study of the Sorption of Hg0 onto Pyrite". *Langmuir* (**2001**), *17*, 3970-3979.

125. Rio, S.; Delebarre, A. "Removal of Mercury in Aqueous Solution by Fluidized Bed Plant Fly Ash". *Fuel* (**2003**), *82*, 153-159.

Reproduced with permission of the copyright owner. Further reproduction prohibited without permission.

126. Serre, S. and Silcox, G. "Adsorption of Elemental Mercury on the Residual Carbon in Coal Fly Ash". *Ind. Eng. Chem. Res.* (**2000**), 39, 1723-1730.

127. Gibb, W.H.; Clarke, F.; Metha, A.K. "The fate of coal mercury during combustion". *Fuel Processing Technology*. (**2000**), *65-66*, 365-377.

128. Huang, H. S., J. M. Wu, and C. D. Livengood, "Development of Dry Control Technology for Emissions of Mercury in Flue Gas," *Hazard. Waste & Hazard. Materials*, (**1996**), *13*, 107.

129. Vidic, R. D. and McLaughlin, J.B. "Uptake of Elemental Mercury Vapors by Activated Carbons," *J. Air Waste Mgmnt. Assocn.*, (**1996**), *46*, 241.

130. Biswas, P. and Wu, C.Y. "Control of Toxic Metal Emission from Combustors using Sorbents: A Review," *J. Air Waste Mgmnt. Assocn.*, (**1998**), *48*, 113.

131. Liu, W.; Vidic, R.D.; Brown, T.D. "Optimization of Sulfur Impregnation Protocol for Fixed Bed Application of Activated Carbon-Based Sorbents for Gas-Phase Mercury Removal," *Environ. Sci. Technol.*, (**1998**), *32*, 531.

132. Sinha, R. K. and P. L. Walker, "Removal of Mercury by Sulfurized Carbons," *Carbon*, (**1972**), *10*, 754.

133. Otani, Y.; C. Kanaoka; C. Usul; S. Matsui; H. Emi. "Adsorption of Mercury Vapor on Particles," *Environ. Sci. & Technol.*, (**1986**), *20*, 735.

134. Krishnan, S. V., B. K. Gullett, W. Jozewicz, "Sorption of Elemental Mercury by Activated Carbons," *Environ. Sci. Technol.*, (**1994**), 28, 1506.

135. Karatza, D., A. Lancia, D. Musmarra, F. Pepe, and G. Volpicelli, "Removal of Mercuric Chloride from Flue Gas by Sulfur Impregnated Activated Carbon," *Hazard. Waste & Hazard. Materials*, (**1996**), 13, 95.

136. Korpiel, J. A. and R. D. Vidic, "Effect of Sulfur Impregnation Method on Activated Carbon Uptake of Gas-Phase Mercury," *Environ. Sci. Technol.*, (**1997**), 31, 2319.

Reproduced with permission of the copyright owner. Further reproduction prohibited without permission.

137. Vidic, R. D. and M. T. Chang, "Kinetics of Vapor-Phase Mercury Uptake by Virgin and Sulfur-Impregnated Activated Carbons," *J. Air Waste Mgmnt. Assocn.*, (**1998**), 48, 247.

138. Tai-Gyu "Teddy" Lee. "Study of Mercury Kinetics and Control Methodologies in Simulated Combustion Flue Gases", Doctoral Dissertation. Division of Research and Advanced Studies of the University of Cincinnati, **1999**.

139. Material Safety Data Sheet http://www.jtbaker.com/msds/englishhtml/m1547.htm (Accessed May 29, 2006)

140. Romero, C. E. "Combustion tuning for Mercury emissions control", Energy Research Center Planning Workshop, November 19-20, **2003**.

141. Roberts, D.L.; Broderick, T.; Stewart R.; Albiston, J.; Greenwell C.; "Novel Process for removal and recovery of vapor phase mercury", *Advanced coal based power and environmental systems 1997 Conference,* Federal Energy Technology Center, Pittsburgh, PA, July 22-24, **1997**.

142. Baldrey, K; Comer, J.; Johnson, S. "Control of PRB Flyash Cementing Properties", *Presented at The Thirteenth International Symposium on Management and Use of Coal Combustion Products"*, January 11, **1999**, ADA-ES Publication 99007.

143. Durham, M.; Bustard, J.; Starns, T.; Sjostrom, S.; Lindsey, C.; Martin, C.; Schlager, R., Renninger, S.; Chang, R.; Afonso, R.; "Full-scale Evaluation of Mercury Control by injecting Activated Carbon Upstream of ESPS", *Air Quality IV: Mercury, Trace Elements, and Particulate Matter.* September 22-24, **2003**, Arlington, VA.

144. Durham, M.D.; Schlager, R.J.; Sappey, A.D.; Sagan F.J.; Marmaro, R.W.; Wilson, K.G. USPTO # 5,679,957. October 21, **1997**.

145. Durham, M.D.; Hyatt, D.E.; Stewart, R.M.; Schlager, R.J. USPTO # 5,409,522. April 25, **1995**.

Reproduced with permission of the copyright owner. Further reproduction prohibited without permission.

146. "Field Testing of Mercury Control Technologies for Coal-Fired Power Plants", DOE/NETL Mercury R&D Program Review, May **2005**.

147. Licata, A.; Fey, W. "Advanced Technology to control mercury emissions", *The U.S. EPA/DOE/EPRI Combined Power Plant Air Pollutant Control Symposium: "The Mega Symposium"* August 20-23, **2001**, Chicago, Illinois, U.S.A.

148. Licata, A.; Schuttenhelm, W.; Klein, M. "Mercury control for MWCs using the sodium tetrasulfide process", *8th Annual North American Waste-to-Energy Conference,* May 22-24, **2000**, Nashville, Tennessee, U.S.A.

149. Licata, A.; Beittel, R.; Ake, T.; "Multi-pollutant emissions control and strategies – coal fired power plant mercury control by injecting sodium tetrasulfide", *ICAC FORUM 2003*, October 14-15, **2003**, Nashville, Tennessee, U.S.A.

150. Nolan, P.S.; Farthing, G.A. "Development of Mercury Emissions Control Technologies for the Power Industry", *EPRI-DOE-EPA Combined Utility Air Pollution Control Symposium*, August 16-20, **1999**, Atlanta, Georgia, U.S.A.

151. Renninger, S.A.; Farthing, G.A.; Ghorishi, S.B.; Teets, C.; Neureuter, J.A. "Effects of SCR Catalyst, Ammonia Injection and Sodium Hydrosulfide on Speciation and Removal of Mercury within a Forced-Oxidized Limestone Scrubber", *EPRI-DOE-EPA Combined Utility Air Pollution Control Symposium*, August 30-September 2, **2004**, Washington DC, U.S.A.

152. Milobowski, M.G.; Amrhein, G.T.; Kudlac, G.A.; Yurchison, D.M. "Wet FGD Enhanced Mercury Control for coal fired utility boilers", *The U.S. EPA/DOE/EPRI Combined Power Plant Air Pollutant Control Symposium: "The Mega Symposium"* August 20-23, **2001**, Chicago, Illinois, U.S.A.

153. Bielawski, G.T.; Rogan, J.B.; McDonald, D.K.; "How Low can we go? Controlling Emissions in New Coal fired power plants", *The U.S. EPA/DOE/EPRI Combined Power Plant Air Pollutant Control Symposium: "The Mega Symposium"* August 20-23, **2001**, Chicago, Illinois, U.S.A.

Reproduced with permission of the copyright owner. Further reproduction prohibited without permission.

154. "Full-scale testing of enhanced mercury control technologies for wet FGD systems" Presented by McDermott Technologies, Inc. at the 27th International Technical Conference on Coal Utilization and Fuel Systems in Clearwater, Florida March 4-7, **2002**. http://www.netl.doe.gov/coal/E&WR/mercury/control-tech/test-wet-fgd.html (Accessed June 30, 2005)

155. Excerpt from "Federal Technology Transfer 2005." http://www.powerspancorp.com/technology/pco_overview.shtml (Accessed May 29, 2006)

156. Excerpt from "2005 FLC Awards Program Book." http://www.powerspancorp.com/technology/pco_overview.shtml (Accessed May 29, 2006)

157. "Evaluations of a Novel Sample Conditioning System for Real-Time Monitoring of Mercury in Coal Combustion Flue Gas", Poster presented at the AWMA Mega Symposium, **2004**. http://www.apogee-sci.com/page7.html (Accessed June 30, 2005)

158. "Large Scale Demonstration of the MERCAPTM Technology for Mercury Control", Presented at the AWMA Mega Symposium, **2004**. http://www.apogee-sci.com/page7.html (Accessed June 30, 2005)

159. "Assessment of Low-Cost Novel Sorbents for Coal-fired Power Plant Mercury Control": Presented at the AWMA Mega Symposium, **2004**. http://www.apogee-sci.com/page7.html (Accessed June 30, 2005)

160. "Evaluation of Gold MerCAP - Process for Flue Gas Mercury Removal – Program Review" http://ww.netl.doe.gov/publications/proceedings/04/HgReview/Ebner.MerCAP%20Program%20Review%20presentation%2007.pdf (Accessed June 30, 2005)

161. "Evaluation of Gold MerCAP - Process for Flue Gas Mercury Removal – Kick off meeting presentation" http://ww.netl.doe.gov/coal/E&WR/mercury/control-

Reproduced with permission of the copyright owner. Further reproduction prohibited without permission.

tech/pubs/MerCAP%20kickoff%20mtg%20presentation-public.pdf (Accessed June 30, 2005)

162. "Evaluation and comparison of novel, Low-cost sorbents for mercury control." http://ww.netl.doe.gov/coal/E&WR/mercury/control-tech/pubs/A5-B1.pdf (Accessed June 30, 2005)

163. "Assessment of Low-Cost Novel Sorbents for Coal Fired Power Plant Mercury Control" http://www.netl.doe.gov/publications/proceedings/04/HgReview/hg-review04.html#Papers (Accessed June 30, 2005)

164. "Full Scale Evaluation of Mercury Control at Great River Energy's Stanton Generating Station using Injected Sorbents and a Spray Dryer/Baghouse" *Air Quality III.* September 12, **2002**.

165. "Pipe Dimensions" http://home.mchsi.com/~gweidner/pipe-dimensions.pdf (Accessed May 29, 2006)

166. "The A to Z of materials" http://www.azom.com/details.asp?ArticleID=966 (Accessed May 29, 2006)

167. "Honeywell" http://www.honeywell.com/sites/honeywell/ (Accessed May 29, 2006)

168. Thermcraft Manufactures Laboratory and Industrial Furnaces http://www.thermcraftinc.com/home.html/ (Accessed May 29, 2006)

169. "McMaster Carr Supply Company" http://www.mcmastercarr.com/ (Accessed May 29, 2006)

170. "VWR" http://www.vwrsp.com/ (Accessed May 29, 2006)

171. "Omega Engineering, Inc." http://www.omega.com/ (Accessed May 29, 2006)

172. "Swagelok – Fluid Systems Technologies" http://www.swagelok.com/ (Accessed May 29, 2006)

173. "Magellan – Worldwide Suppliers of Specialty Metals" http://www.magellanmetals.com/inconel_625.htm (Accessed May 29, 2006)

Reproduced with permission of the copyright owner. Further reproduction prohibited without permission.

174. "The Flexitallic Group" http://www.flexitallic.com/home.htm (Accessed May 29, 2006)

175. "Apex Instruments" http://www.apexinst.com/products/hsrl.htm (Accessed May 29, 2006)

176. "Cole-Parmer" http://www.coleparmer.com/ (Accessed May 29, 2006)

177. "AirGas" http://www.airgas.com/ (Accessed May 29, 2006)

178. "PSA" http://www.psanalytical.com/ (Accessed May 29, 2006)

179. "Tekran Instruments Corporation" http://www.tekran.com/ (Accessed May 29, 2006)

180. "ADA Technologies, Inc." http://www.adatech.com/ (Accessed May 29, 2006)

181. "AGS Scientific" http://www.agssci.com/ (Accessed May 29, 2006)

182. "Ohio Lumex" http://www.ohiolumex.com/ (Accessed May 29, 2006)

183. Ghorishi, S. B. "Fundamentals of Mercury Speciation and Control in Coal-Fired Boilers", Report EPA-600/R-98-014, U.S. Environemntal Protection Agency, Washington, DC, February **1998**.

184. Sliger, R. N. "Development of a Chemical Kinetic Model for the Homogeneous Oxidation of Mercury by Chlorine Species: A tool for Mercury Emissions Control", Doctoral Dissertation, University of Washington, 2001.

185. Widmer, N. C.; Cole, J. A.; Seeker, W. R.; Gaspar, J. A. "Practical Limitation of Mercury Speciation in Simulated Municipal Waste Incinerator Flue Gas", *Combustion Science and Technology*. (**1998**), *134*, 315-326.

186. Agarwal, H.; Stenger, H. G.; Wu, S.; Fan, Z. "The Effects of H_2O, SO_2 and NO on Homogeneous Hg oxidation by Cl_2." *Energy and Fuel.* (**2006**), in press.

187. Mamani-Paco, R. M. and Helble, J. J. "Bench-Scale Examination of Mercury oxidation under non-isothermal conditions," *Proc. A&WMA Annual Conference*, Salt Lake City, June, **2000**.

Reproduced with permission of the copyright owner. Further reproduction prohibited without permission.

188. Agarwal, H. and Stenger, H. G. "Development of a Predictive Kinetic Model for Homogeneous Hg Oxidation Data." *Mathematical and Computer Modeling.* 2006, in press.

189. Qiu, J.; Sterling, R. O.; Helble, J. J. "Development of an Improved Model for Determining the Effects of SO2 on Homogeneous Mercury Oxidation", *Clear water conference*, (**2003**).

190. Agarwal, H.; Romero, C. E.; Stenger, H. G. "Comparing and Interpreting laboratory results of Homogeneous Hg Oxidation by a Chlorine Species" – in preparation.

191. Widmer, N. C.; West, J.; Cole, J. A. "Thermochemical Study of Mercury Oxidation in Utility Boiler Flue Gases", *Proceedings of the Air and Waste Management Association's 93rd Annual Meeting*, Salt Lake City, Utah, June, (**2000**).

192. Levenspiel, O. "Chemical Reaction Engineering", pp. 27, John Wiley & Sons, New York (1999).

193. http://www.mathworks.com/access/helpdesk/help/techdoc/ref/fminsearch.html (Accessed March 18, 2006)

194. http://www.mathworks.com/access/helpdesk/help/toolbox/simbio/ug/bqatp4l.html (Accessed March 18, 2006)

195. Fry, A.; Lighty, J. S.; Silcox, G. D.; Cauch, B.; Senior, C. L. "Detailed Kinetic Modeling of Homogeneous Mercury Oxidation Reactions in a 1000 Btu/hr Quartz Furnace", *22nd International Pittsburgh Coal Conference*, Pittsburgh, PA, **2005**.

Reproduced with permission of the copyright owner. Further reproduction prohibited without permission.

APPENDIX

Ph.D. DEFENSE PRESENTATION

Reproduced with permission of the copyright owner. Further reproduction prohibited without permission.

A Study of Mercury Oxidation and the Development of a Global Predictive Kinetic Model

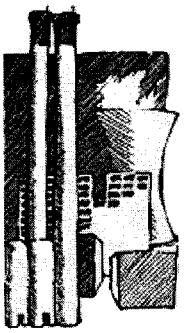

Hans Agarwal
June 28, 2006

Academic Advisor:
Professor Harvey G. Stenger

LEHIGH UNIVERSITY

OUTLINE OF PRESENTATION

- Background
  - Mercury in Coal and in the Environment
  - Literature Review – A brief Summary
- Current Work
  - The Testing Facility and Mercury Analyzer
  - Experiments and Results
- Development of Predictive Kinetic Model
  - Reactions and corresponding equations used
  - Modeling results
- Conclusions and Further Work

Reproduced with permission of the copyright owner. Further reproduction prohibited without permission.

BACKGROUND: Hg in Coal

- Coal is a major source of energy supply
- ~ 1.5 x 10^{12} tons used per year (1999)
- Contains: C, H, O, S, N, Cl, Hg
- S, N, Cl, Hg are pollutants to the environment
- Hg concentrations average ~ 3 – 20 μg/m^3 of Flue Gas
  - Depends on coal rank
  - Lignite, sub-bituminous, bituminous and anthracite

3

BACKGROUND: Hg in the Environment

- 72 – 158 tons (1999) released into atmosphere
- Exists in 3 states
  - Hg^0 – elemental mercury, most abundant
  - Hg^{2+} – oxidized mercury
  - Hg^p – particulate mercury
- Accumulation in atmosphere: 0.5 – 2 years residence time
- Trace amounts dissolved in water on land
- Bio-accumulation – fat soluble, a health hazard
- Bacteria forms Methyl-mercury (CH_3Hg): most toxic

4

Reproduced with permission of the copyright owner. Further reproduction prohibited without permission.

SOME PROPERTIES

- Hg^0
  - Inert – volatile at high temperatures
  - Not soluble in water
  - Difficult to capture – by adsorption or scrubbing
- Hg^{2+}
  - Very water soluble
  - Adsorbs onto particulate matter or other surfaces easily
- Hg^p
  - Mercury entrained in particulate matter such as fly ash
  - Easily removed in ESP or Bag-house
- Ideally: Convert Hg^0 to Hg^{2+} or Hg^p for efficient removal

5

LITERATURE REVIEW – A Summary

- Flue Gas components effect Hg speciation differently
- Temperature profiles effect Hg speciation
- Nine unique researchers
  - Different oxidants – Cl_2 or HCl
  - Different reactors – Quartz, Stainless Steel, Teflon
  - Different Hg analyzers – OHM or CEM
  - Different temperature profiles – 175°C to over 1000°C
  - Different residence times – 0.7 to 6 seconds
- SO_2 and H_2O – inhibit Hg oxidation
- Thermodynamic equilibrium calculations:
  - $Hg + Cl_2 \leftrightarrow HgCl_2$
  - $H_2O + Cl_2 \leftrightarrow 2HCl + ½ O_2$

6

Reproduced with permission of the copyright owner. Further reproduction prohibited without permission.

LITERATURE REVIEW – A Summary

- Thermodynamic equilibrium calculations
- $[O_2] = 0.35$; $[H_2O] = 0.13$; $[Hg] = 1.1x10^{-9}$; $[Cl_2] = 2.5x10^{-5}$

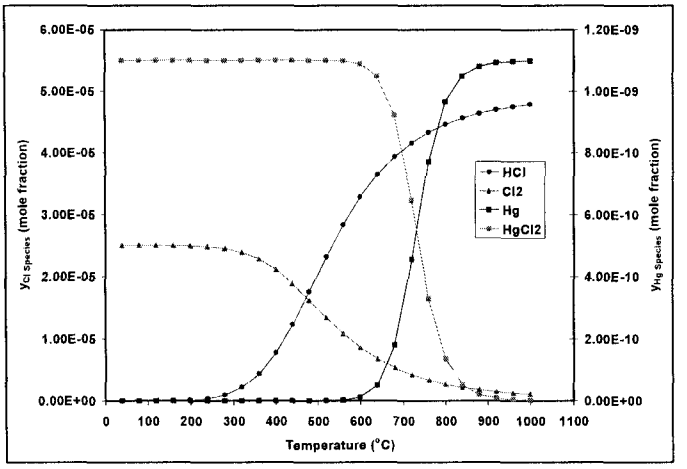

- $[Cl_2] > [HCl]$ at $T < 480°C$; $[Cl_2] < [HCl]$ at $T > 480°C$;

7

OBJECTIVE OF PROJECT

- Experimental work on PRB derived Flue Gas
  - Convert Hg^0 to Hg^{2+} – for easy removal
  - Test the effects of flue gas components on Hg oxidation
- Temperature range between 160°C and 540°C
- Build a unique experimental apparatus
  - Capable of oxidant and sorbent testing
  - Follows power plant temperature vs. residence time profile
- Develop a robust kinetic predictive model to predict a maximum amount of literature data

8

Reproduced with permission of the copyright owner. Further reproduction prohibited without permission.

TESTING FACILITY

9

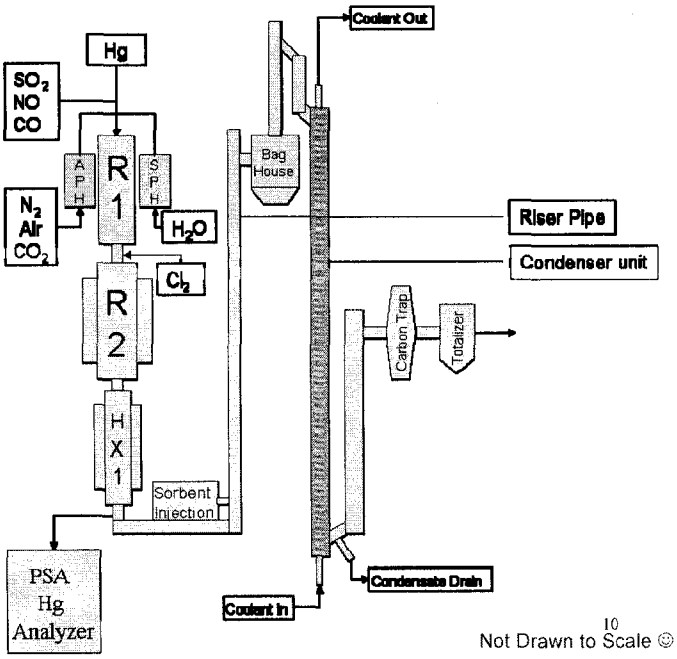

10

Not Drawn to Scale ☺

Reproduced with permission of the copyright owner. Further reproduction prohibited without permission.

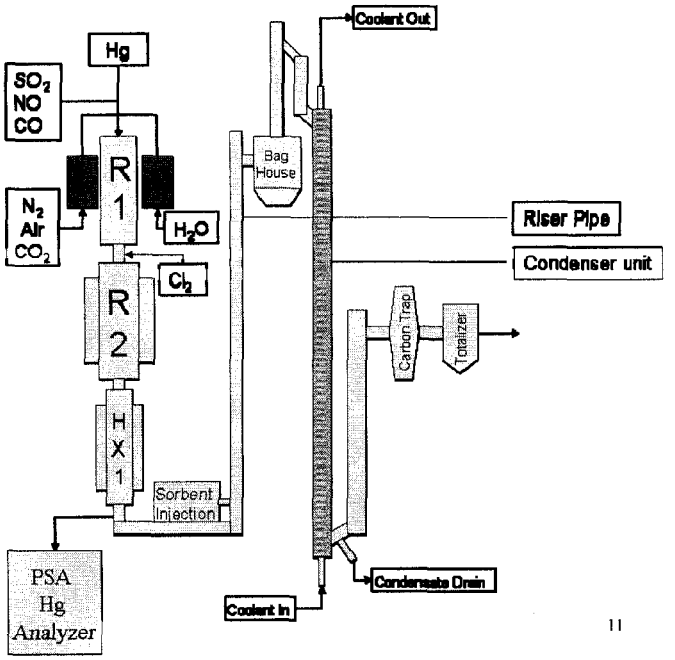

11

DETAILS OF RIG

- Air and Steam Pre-Heater (APH and SPH)
  - Material: SS316
  - Length: 15 inches
  - ID: 0.935 inches
  - Packing Material: 7/16" SS304 Nuts
  - Exit Temperature: ~ 120°C to 300°C

12

Reproduced with permission of the copyright owner. Further reproduction prohibited without permission.

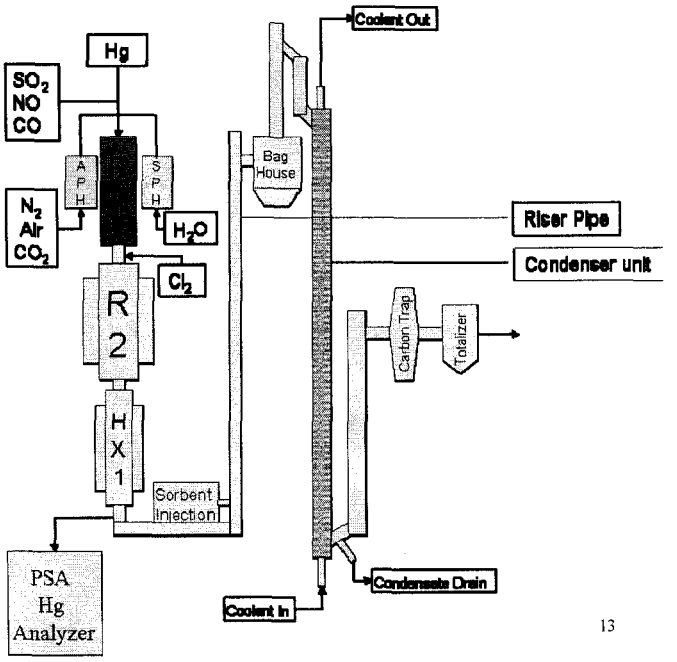

13

DETAILS OF RIG

- Air and Steam Pre-Heater (APH and SPH)
  - Material: SS316
  - Length: 15 inches
  - ID: 0.935 inches
  - Packing Material: 7/16" SS304 Nuts
  - Exit Temperature: ~ 120°C to 300°C
- R1
  - Material: SS310
  - Length: 45 inches
  - ID: 1.6 inches
  - Packing material: 7/16" SS304 Nuts
  - Temperature readings taken at several spots
  - All gases enter from ports on top flange
  - Exit Temperature: up to ~ 860°C

14

Reproduced with permission of the copyright owner. Further reproduction prohibited without permission.

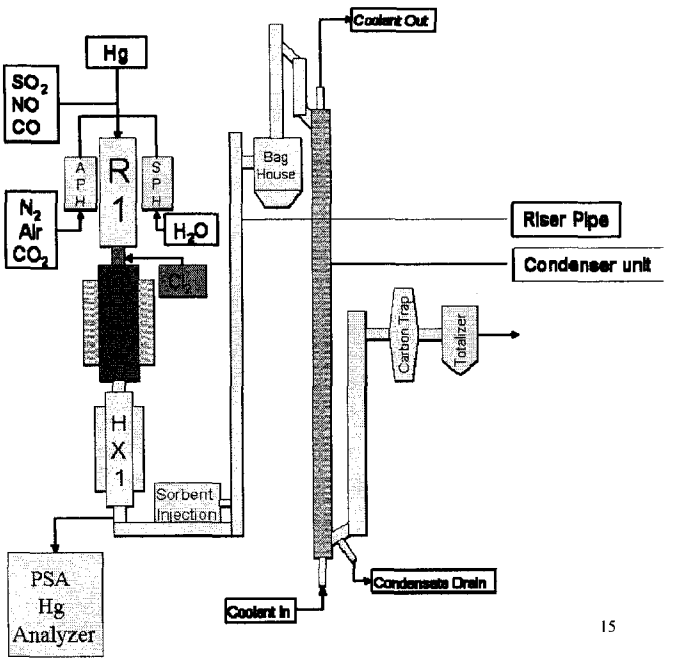

15

DETAILS OF RIG

- R2
  - Material: Inconel
  - Length: 36 inches; ID: 4 inches
  - Built-in Heat Exchanger
  - 4 Sample / Injection / Thermocouple Ports
  - Exit Temperature: up to ~ 540°C
  - Residence time: ~ 2 seconds

16

Reproduced with permission of the copyright owner. Further reproduction prohibited without permission.

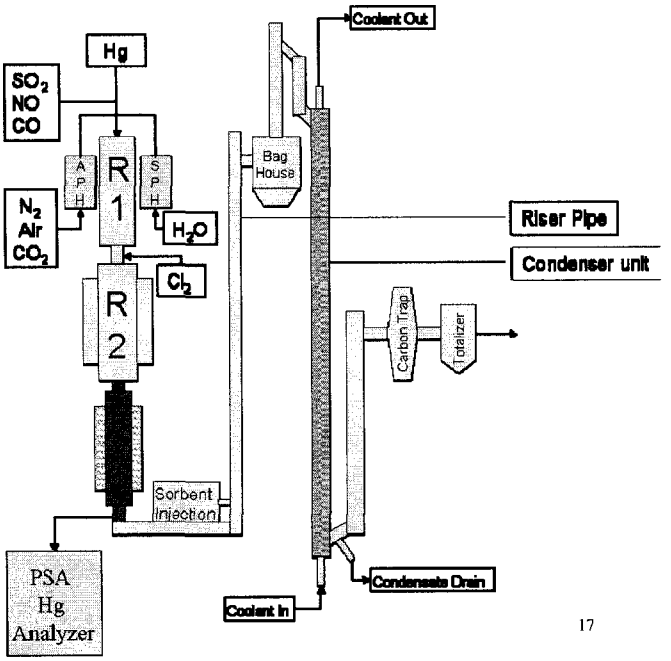

17

DETAILS OF RIG

- R2
  - Material: Inconel
  - Length: 36 inches; ID: 4 inches
  - Built-in Heat Exchanger
  - 4 Sample / Injection / Thermocouple Ports
  - Exit Temperature: up to ~ 540°C
  - Residence time: ~ 2 seconds
- HX1
  - Material: Inconel
  - Length: 24 inches; ID: 1.6 inches
  - Built-in Heat Exchanger
  - 2 Sample / Injection / Thermocouple Ports
  - Exit Temperature: up to ~ 300°C
  - Residence time: ~ 0.3 seconds

18

Reproduced with permission of the copyright owner. Further reproduction prohibited without permission.

DETAILS OF RIG

- Riser and Bag-house section
  - Gives additional residence time where needed
  - Allows for testing of sorbents

- Sample Line
  - Material: Teflon
  - Length: 6 feet; ID: ¼ inch
  - Heat traced – constant temperature at 120°C
  - Residence time: < 0.1 seconds

19

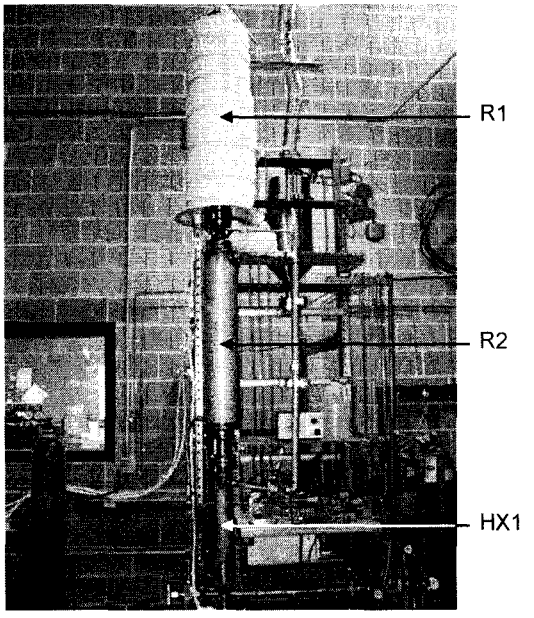

20

Reproduced with permission of the copyright owner. Further reproduction prohibited without permission.

TEMPERATURE vs. RESIDENCE TIME

- Total flow rate of 87 lpm flue gas to get profile
- Determined by Foster Wheeler North America Corp.
- Apparatus profile similar to power plant profile

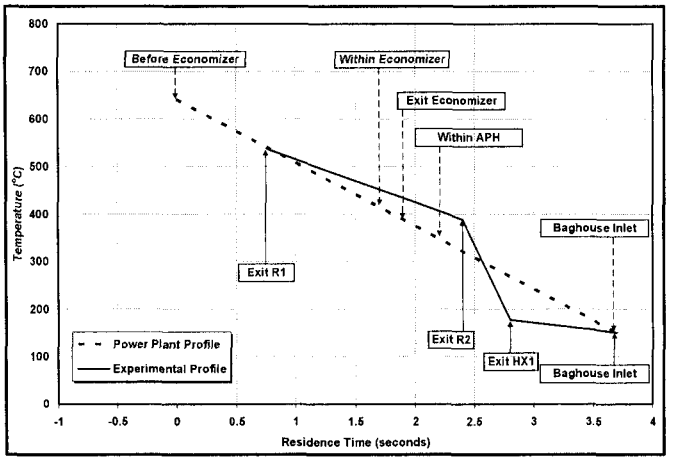

21

TEMPERATURE vs. RESIDENCE TIME

- Economizer: Re-heats steam leaving the turbine
- APH: Pre-heats air entering boiler
- Baghouse: Traps all particulate matter, e.g. fly ash

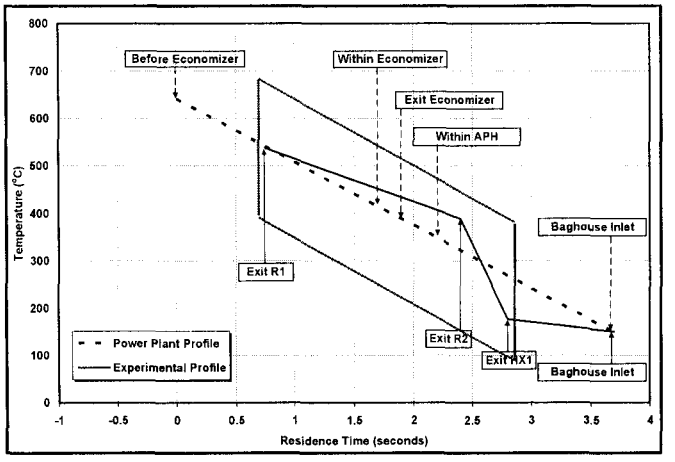

22

Reproduced with permission of the copyright owner. Further reproduction prohibited without permission.

PSA MERCURY ANALYZER

- Based on Atomic Fluorescence
- Sample stream passes though conditioning unit
  - Hot Box – splits stream into two
  - Impingers
    - 2% $SnCl_2$ / 20% NaOH – reduces Hg^{2+} to Hg^0
    - 10% KCl / 10% NaOH – removes Hg^{2+}
  - Chiller Unit – condenses water
- Stream Selector Box switches between streams
- Gold trap forms amalgam with Hg – fluorescence released by amalgam is detected by photo detector
  - Calibration determines Hg concentration
- Tough to maintain – constant plugging and cleaning

23

SIMULATED FLUE GAS

- Composition derived from Powder River Basin (PRB) Coal combustion
- Difficult composition to work with
  - H_2O, SO_2 and Cl concentration
  - H_2O – forms HCl (less effective at low temperatures)
  - SO_2 and H_2O – inhibit Hg oxidation
  - Very low Hg concentrations

Component	N_2	O_2	CO_2	H_2O	SO_2	NO	CO	Cl	Hg
Composition	70%	3.5%	13.5%	13%	370ppm	160ppm	300ppm	100ppm	10µg/m³

24

Reproduced with permission of the copyright owner. Further reproduction prohibited without permission.

EXPERIMENTAL WORK

25

OVERVIEW

- Determine the effects of:
  - Cl_2 on Hg oxidation – 0 ppm to 52.5 ppm Cl_2
  - Flue Gas Components on Hg oxidation
    - SO_2 – 0 ppm to 370 ppm
    - NO – 0 ppm to 160 ppm
    - CO – 0 ppm to 300 ppm
    - H_2O – 0% to 13%
  - Temperature / Residence Time profile (Total flow of 87 lpm)

	Temperature Range (°C)	Residence Time (seconds)
TP1	166°C - 121°C	2.5
TP2	232°C - 121°C	2.4
TP3	320°C - 163°C	2.2
TP4	430°C - 163°C	2.1
TP5	540°C - 177°C	1.9

26

Reproduced with permission of the copyright owner. Further reproduction prohibited without permission.

MERCURY MATERIAL BALANCE

- Important to maintain Hg material balance
- Tough to get Hg concentration of 10μg/m^3
- Material Balance depends on:
  - Accurate flows of individual gas components
  - No leaks in the apparatus and analyzer
  - Keeping apparatus clean – main rig and mercury analyzer
  - Good sampling techniques – constant heated sample line
- Best way to check material balance:
  - Plug up entire rig
  - Inject 10μg/m^3
  - Sample entire stream at exit of HX1
- Successful in closing material balance.

27

EXPERIMENT 1 – Cl_2 effects

- Gas Composition: 100% N_2 and 10μg/m^3 Hg
- Gas flow rate: 87 lpm
- 1 ppmv Cl_2 used at different Temperature profiles

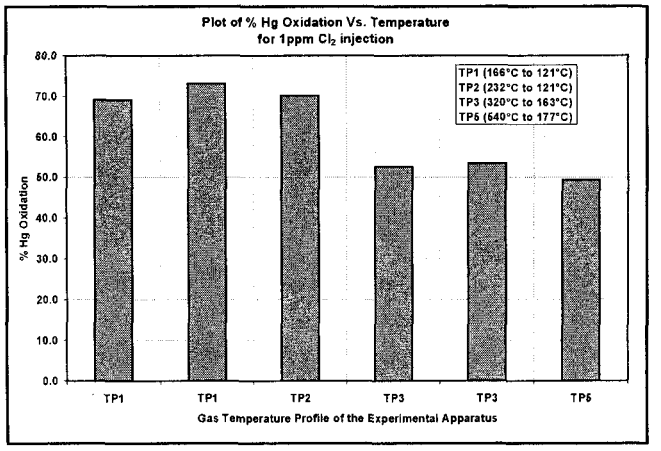

28

Reproduced with permission of the copyright owner. Further reproduction prohibited without permission.

EXPERIMENT 1 – Cl_2 effects

- As temperature profile increases, the effectiveness of Cl_2 as an oxidant decreases
- Without any inhibitory components, and at temperatures below 500°C, 1ppmv Cl_2 is sufficient to cause above 70% oxidation

29

EXPERIMENT 2 - Component Effects

- Full flue gas composition – injected 2ppmv Cl_2
- Exit R1 temp. of 540°C (Temperature profile TP5 used)
- TP5: 540°C to 177°C
- Residence time: ~1.9 seconds
- Gas flow rate: 87 lpm

Components in Flue Gas Stream									
Hg^0	N_2	O_2	CO_2	SO_2	NO	CO	H_2O	Cl_2	Hg Oxidation
($\mu g/m^3$)	(%)	(%)	(%)	(ppmv)	(ppmv)	(ppmv)	(%)	(ppmv)	(%)
11.6	96.5	3.5	--	--	--	--	--	2.0	71.7
13.4	83.5	3.5	13.5	--	--	--	--	2.0	76.9
14.9	83.5	3.5	13.5	370	--	--	--	2.0	52.3
12.7	83.5	3.5	13.5	370	170	--	--	2.0	45.7
11.7	83.5	3.5	13.5	370	170	300	--	2.0	47.0
10.0	70.0	3.5	13.5	370	170	300	13	2.0	0.0

30

Reproduced with permission of the copyright owner. Further reproduction prohibited without permission.

EXPERIMENT 2 - Component Effects

- Each component is added in sequence
  - N_2 and O_2, CO_2, SO_2, NO, CO, H_2O
- Cl_2 is injected at 2ppm, at exit R1
- SO_2 – inhibits Hg oxidation
- H_2O – inhibits Hg oxidation
- NO – inhibits Hg oxidation slightly
- Need to find Cl_2 concentration to overcome H_2O effects

31

EXPERIMENT 3 - Water Effects

- Exit R1 temp. of 540°C (Temperature profile TP5 used)
- Residence time: ~1.9 seconds
- Gas flow rate: 87 lpm

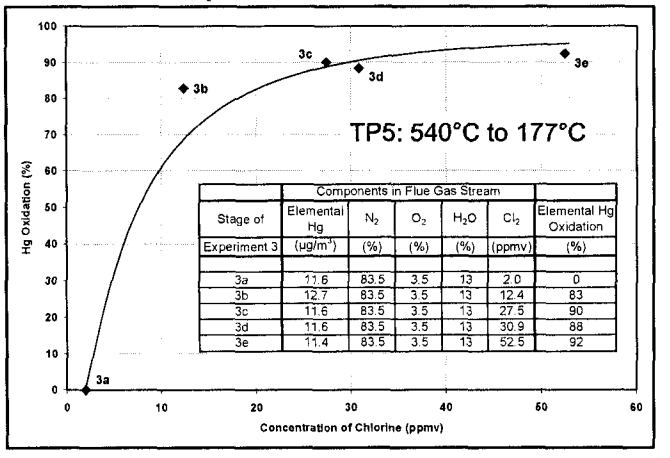

	Components in Flue Gas Stream					
Stage of Experiment 3	Elemental Hg ($\mu g/m^3$)	N_2 (%)	O_2 (%)	H_2O (%)	Cl_2 (ppmv)	Elemental Hg Oxidation (%)
3a	11.6	83.5	3.5	13	2.0	0
3b	12.7	83.5	3.5	13	12.4	83
3c	11.6	83.5	3.5	13	27.5	90
3d	11.6	83.5	3.5	13	30.9	88
3e	11.4	83.5	3.5	13	52.5	92

32

Reproduced with permission of the copyright owner. Further reproduction prohibited without permission.

EXPERIMENT 3 - Water Effects

- Minimum Cl_2 concentration required to show appreciable Hg oxidation is ~27.5 ppmv
- Higher Cl_2 concentration does not effect Hg oxidation significantly
- Repeat Experiment 2
  - With 27.5ppmv Cl_2
  - With H_2O continuously in system

33

EXPERIMENT 4 - Component Effects

- Full flue gas composition – injected 27.5 ppmv Cl_2
- Exit R1 temp. of 540°C (Temperature profile TP5 used)
- TP5: 540°C to 177°C
- Residence time: ~1.9 seconds
- Gas flow rate: 87 lpm

Components in Flue Gas Stream									
Elemental Hg	N_2	O_2	CO_2	SO_2	NO	CO	H_2O	Cl_2	Elemental Hg Oxidation
($\mu g/m^3$)	(%)	(%)	(%)	(ppmv)	(ppmv)	(ppmv)	(%)	(ppmv)	(%)
10.5	83.5	3.5	--	--	--	--	13	27.5	90
10.6	70.0	3.5	13.5	--	--	--	13	27.5	90
10.3	70.0	3.5	13.5	370	--	--	13	27.5	57
10.6	70.0	3.5	13.5	370	170	--	13	27.5	46
10.8	70.0	3.5	13.5	370	170	300	13	27.5	45

34

Reproduced with permission of the copyright owner. Further reproduction prohibited without permission.

EXPERIMENT 4 - Component Effects

- Similar to Experiment 2 – H_2O is continuously in system
- Each component is added in sequence
  - (N_2 + O_2 + H_2O), CO_2, SO_2, NO, CO
- Cl_2 is injected at 27.5ppm, at exit R1
- SO_2 – inhibits Hg oxidation
- NO – inhibits Hg oxidation slightly

35

SUMMARY

- Cl_2 is an effective oxidant at temperatures below 540°C
- Only 27.5 ppmv Cl_2 (or 55 ppmv HCl equivalent) needed to oxidize Hg effectively
- SO_2 and H_2O strongly inhibit Hg oxidation
- NO slightly inhibits Hg oxidation
- Develop a kinetic model to predict this data

36

Reproduced with permission of the copyright owner. Further reproduction prohibited without permission.

A GLOBAL PREDICTIVE KINETIC MODEL

37

EQUATIONS USED

- **Consists of 5 reactions – 2 reversible, 3 irreversible**

R1 $Hg(g) + Cl_2(g) \xleftrightarrow{k_1} HgCl_2(g)$

R2 $H_2O(g) + Cl_2(g) \xleftrightarrow{k_2} 2HCl(g) + \frac{1}{2}O_2(g)$

R3 $Hg(g) + 2HCl(g) \xrightarrow{k_3} HgCl_2(g) + H_2(g)$

R4 $HgCl_2(g) + SO_2(g) \xrightarrow{k_4} Hg(g) + SCl_2(s,g) + O_2(g)$

R5 $2NO(g) + Cl_2(g) \xrightarrow{k_5} 2NOCl(g)$

- **'k' defined by Arrhenius Equation** $k = A \cdot \exp[\frac{-E}{R \cdot T}]$
- **Rate constants of reversible reactions use Keq as a function of temperature**
- **Keq found from equilibrium calculations using RGIBBS block in ASPEN**

38

Reproduced with permission of the copyright owner. Further reproduction prohibited without permission.

REACTION RATES

- Reaction rates for the individual reactions (R1 to R5)
- 'y' is the mole fraction of the species in the gas phase

$$k = A \cdot \exp[\frac{-E}{R \cdot T}]$$

$$r_1 = k_1 \cdot \left(y_{Hg} \cdot y_{Cl_2} - \frac{y_{HgCl_2}}{Keq_1} \right)$$

$$r_2 = k_2 \cdot \left(y_{H_2O} \cdot y_{Cl_2} - \frac{y_{HCl}^{\,2} \cdot y_{O_2}^{\,1/2}}{Keq_2} \right)$$

$$r_3 = k_3 \cdot \left(y_{Hg} \cdot y_{HCl}^{\,2} \right)$$

$$r_4 = k_4 \cdot \left(y_{HgCl_2} \cdot y_{SO_2} \right)$$

$$r_5 = k_5 \cdot \left(y_{Cl_2} \cdot y_{NO}^{\,2} \right)$$

39

DIFFERENTIAL EQUATIONS

- Solve differential equations simultaneously for the concentrations of Hg, $HgCl_2$, Cl_2 and HCl
- Assumptions:
  - $[H_2O]$ and $[O_2]$ are orders of magnitude higher – unchanged w.r.t. time
  - $[SCl_2]$ and $[H_2]$ are smaller than Hg – produced in very small amounts

$$R_{Hg} = \frac{d[Hg]}{dt} = r_4 - r_1 - r_3$$

$$R_{HgCl_2} = \frac{d[HgCl_2]}{dt} = r_1 + r_3 - r_4$$

$$R_{Cl_2} = \frac{d[Cl_2]}{dt} = -r_1 - r_2 - r_5$$

$$R_{HCl} = \frac{d[HCl]}{dt} = 2 \cdot r_2 - 2 \cdot r_3$$

$$R_{SO_2} = \frac{d[SO_2]}{dt} = -r_4$$

$$R_{NO} = \frac{d[NO]}{dt} = -2 \cdot r_5$$

40

Reproduced with permission of the copyright owner. Further reproduction prohibited without permission.

KINETIC MODEL

- Written in MATLAB
- Makes use of fourth order Runge Kutta routine (ODE45)
- Minimize the function:

$$ERROR = \sum_{i=1}^{N} (x_{Hg,\text{model}} - x_{Hg,\text{data}})_i^2$$

- '*x*' is the conversion of Hg
- Program solved for A and E of all rate constants

- Compare experimental to predicted values via parity plot

- Use data available in literature to test for model robustness

41

LITERATURE DATA

- Data taken from 11 sources – includes current work

Name	Location	Rig Material	Hg Analyzer	Focus of Study	Publication
Laudal	EERC, North Dakota	Teflon	OHM	Cl_2, HCl and Flue Gas components	Fuel Proc. Tech. (2000)
Norton	Iowa State U.	Stainless Steel	OHM	Effects of NO	Fuel (2003)
Kilgroe	EPA	Quartz	CEM	Effects of H_2O and SO_2	EPA-600/R-01-109 (2001)
Ghorishi	EPA	Quartz	CEM	Effects of H_2O, SO_2 and temperature	EPA-600/R-98-014 (1998)
Fry	U. Utah	Quartz	CEM: Tekran	High Temperature quenching effects	22nd International Pittsburgh Coal Conference (2005)
Mamani-Paco	U. Connecticut	Stainless Steel	CVAAS	Effects of HCl and Cl_2 at high temperatures	Proc. A&WMA Annual Conference (2000)
Qui	U. Connecticut	Stainless Steel	CVAAS	Effects of SO_2 at high temepratures	Clear water conference (2003)
Hall	U. Goteborg, Sweden	Stainless Steel	CVAAS	HCl and temperature effects on Hg ox.	Water, Air, Soil Pollut. (1991)
Sliger	U. Washington	Refractory Material and Quartz	EPA Method 29	HCl and H_2O effects	Fuel Proc. Tech. (2000, 2001)
Widmer	EERC, California	Quartz	EPA Method 29	Effects of HCl at various temperatures	Comb. Sci. and Tech. (1998)
Agarwal	Lehigh University	Stainless Steel	CEM: PSA	Cl_2, Flue gas components and temperature effects	Energy and Fuel (2005, 2006) Fuel Proc. Tech. (2006)

42

Reproduced with permission of the copyright owner. Further reproduction prohibited without permission.

KINETIC MODEL - RESULTS

RXN	A (s⁻¹)	E (x10³) (cal/mole)
R1	0.24	0.13

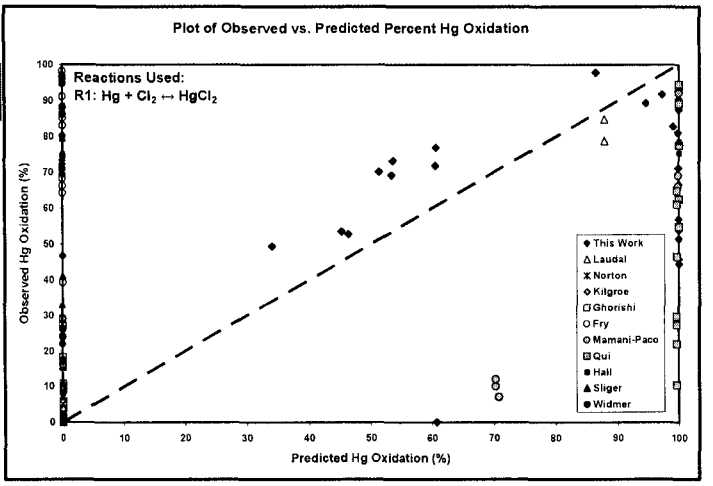

- Model Predictions using R1 for 146 Data points (10 sources)
- Average Error between Predicted and Observed Hg oxidation: ± 34%

43

KINETIC MODEL - RESULTS

RXN	A (s⁻¹)	E (x10³) (cal/mole)
R1	0.24	0.13
R2	80.55	12.10

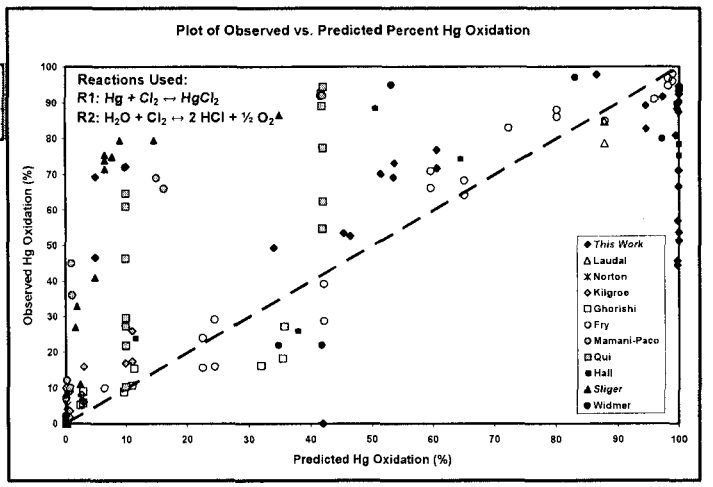

- Model Predictions using R1, R2 for 146 Data points (10 sources)
- Average Error between Predicted and Observed Hg oxidation : ± 18%

44

Reproduced with permission of the copyright owner. Further reproduction prohibited without permission.

KINETIC MODEL - RESULTS

RXN	A	E (x10³) (cal/mole)
R1	0.24	0.13
R2	80.55	12.10
R3	32.65	29.99

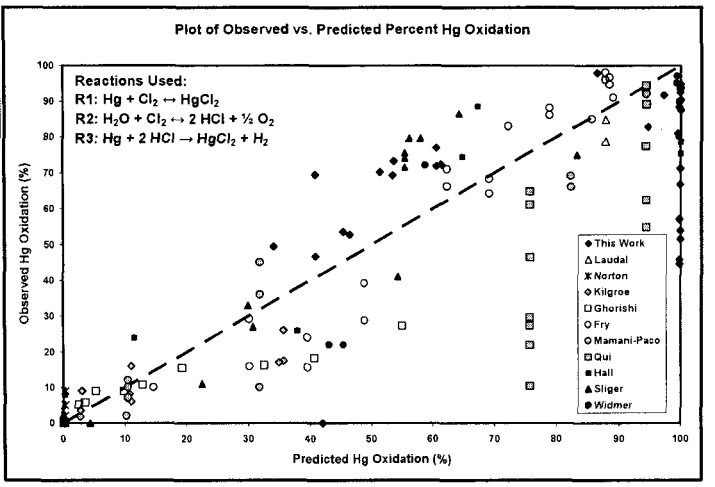

- Model Predictions using R1, R2, R3 for 146 Data points (10 sources)
- Average Error between Predicted and Observed Hg oxidation : ± 13%

45

KINETIC MODEL - RESULTS

RXN	A	E (x10³) (cal/mole)
R1	0.24	0.13
R2	80.55	12.10
R3	32.65	29.99
R4	129.86	13.32

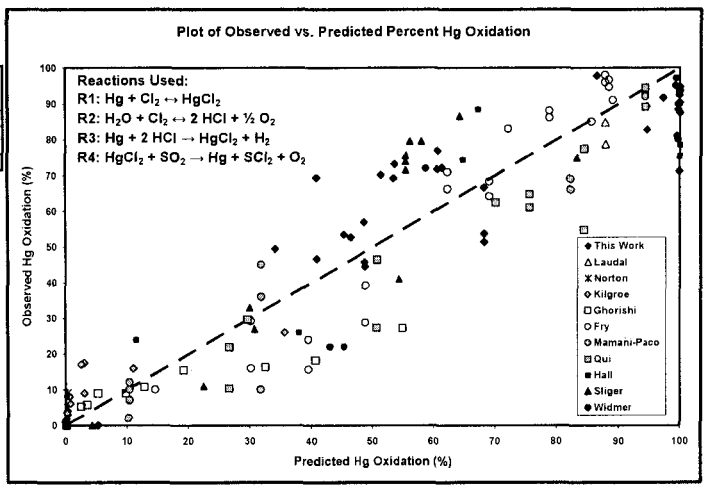

- Model Predictions using R1, R2, R3, R4 for 146 Data points (10 sources)
- Average Error between Predicted and Observed Hg oxidation : ± 9.2%

46

Reproduced with permission of the copyright owner. Further reproduction prohibited without permission.

KINETIC MODEL - RESULTS

RXN	A (s^{-1})	E (x10^3) (cal/mole)
R1	0.24	0.13
R2	80.55	12.10
R3	32.65	29.99
R4	129.86	13.32
R5	9.64	249.76

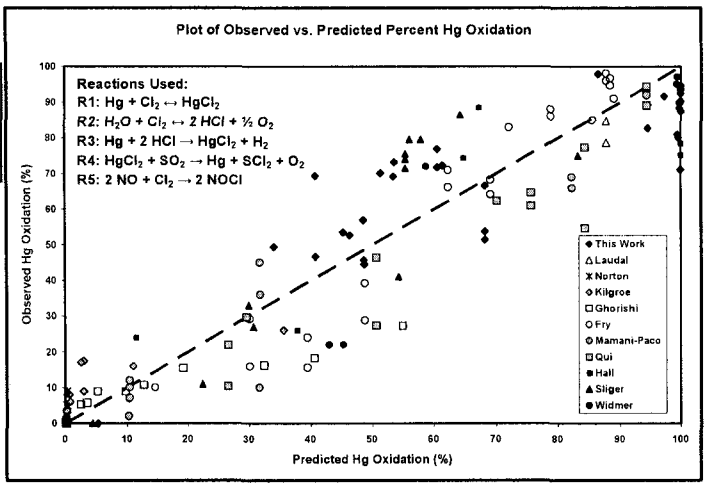

- Plot shows distribution of researchers data based on predictions
- Average Error between Predicted and Observed Hg oxidation : ± 9.2%

47

KINETIC MODEL - RESULTS

	Reaction	A	E (x10^3) (cal/mole)	$k = A \cdot \exp[\frac{-E}{R \cdot T}]$ (s^{-1})
1	$Hg(g) + Cl_2(g) \xleftrightarrow{k_1} HgCl_2(g)$	0.24	0.13	$k_1 = 0.24 \cdot \exp[\frac{-0.13 \cdot 10^3}{1.987 \cdot T}]$
2	$H_2O(g) + Cl_2(g) \xleftrightarrow{k_2} 2HCl(g) + \frac{1}{2}O_2(g)$	80.55	12.10	$k_2 = 80.55 \cdot \exp[\frac{-12.10 \cdot 10^3}{1.987 \cdot T}]$
3	$Hg(g) + 2HCl(g) \xrightarrow{k_3} HgCl_2(g) + H_2(g)$	32.65	29.99	$k_3 = 32.65 \cdot \exp[\frac{-29.99 \cdot 10^3}{1.987 \cdot T}]$
4	$HgCl_2(g) + SO_2(g) \xrightarrow{k_4} Hg(g) + SCl_2(g,g) + O_2(g)$	129.86	13.32	$k_4 = 129.86 \cdot \exp[\frac{-13.32 \cdot 10^3}{1.987 \cdot T}]$
5	$2NO(g) + Cl_2(g) \xrightarrow{k_5} 2NOCl(g)$	9.64	249.76	$k_5 = 9.64 \cdot \exp[\frac{-249.76 \cdot 10^3}{1.987 \cdot T}]$

48

Reproduced with permission of the copyright owner. Further reproduction prohibited without permission.

SUMMARY

Experimental

- A unique testing facility was built to perform experimental work
- Cl_2 oxidized Hg very effectively
- SO_2 and H_2O strongly inhibited Hg oxidation
- NO weakly inhibited Hg oxidation

Simulation

- A 5 reaction model was developed to predict experimental data
- Over 140 unique data points were used to test for model robustness
- Average error between predicted and observed Hg oxidation less than 10%

49

FURTHER WORK - EXPERIMENTAL

- Test Hg oxidation with other halogen compounds
  - HCl, Br_2, I_2, HBr, HI
- Test Hg oxidation with a range of flue gas component concentrations
  - Example: SO_2 – from 300 to 2000 ppmv
  - Example: H_2O – from 1% to 15%
  - Example: NO – from 100 to 500 ppmv

50

Reproduced with permission of the copyright owner. Further reproduction prohibited without permission.

FURTHER WORK – SIMULATION

- **Use full Arrhenius Equation** $k = A \cdot T^{n} \cdot \exp[\frac{-E}{R \cdot T}]$
- **Determine if 'T^{n}' has any effect**

- **Perform a sensitivity analysis on kinetic model**
  - Additional check for robustness of model
  - Presents trends and effects of all flue gas components

- **Simple method:**
  - Use current A and E values
  - Fix concentrations based on PRB Flue Gas composition
  - Vary concentrations of components to observe Hg oxidation

- **Compare predictions with industry data**

51

PRELIMINARY ANALYSIS on Cl_2

- **Flow: 87 lpm; Gas composition same as PRB flue gas**
- **Temperature profile TP5: 540°C to 177°C**
- **Residence time: ~1.9 seconds**
- **Cl_2 concentration ranged from 0 to 200 ppm**

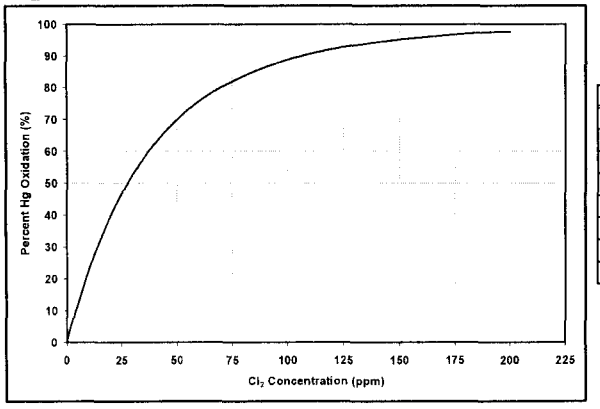

Component	Composition
Nitrogen (N_2)	70.0%
Oxygen (O_2)	3.5%
Carbon Dioxide (CO_2)	13.5%
Water (H_2O)	13%
Sulfur Dioxide (SO_2)	370 ppm
Nitric Oxide (NO)	170 ppm
Carbon Monoxide (CO)	300 ppm
Elemental Mercury (Hg)	10 $\mu g/m^3$

52

Reproduced with permission of the copyright owner. Further reproduction prohibited without permission.

PRELIMINARY ANALYSIS on H_2O

- Flow: 87 lpm; Gas composition same as PRB flue gas
- Temperature profile TP5: 540°C to 177°C
- Residence time: ~1.9 seconds
- H_2O concentration ranged from 0 to 0.2 (mole fraction)

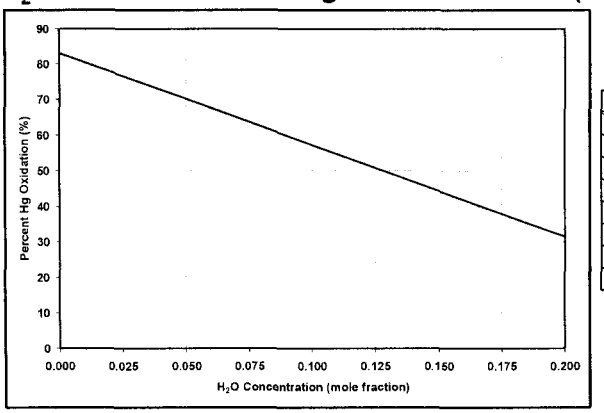

Component	Composition
Nitrogen (N_2)	70.0%
Oxygen (O_2)	3.5%
Carbon Dioxide (CO_2)	13.5%
Chlorine (Cl_2)	27.5 ppm
Sulfur Dioxide (SO_2)	370 ppm
Nitric Oxide (NO)	170 ppm
Carbon Monoxide (CO)	300 ppm
Elemental Mercury (Hg)	10 $\mu g/m^3$

53

ACKNOWLEDGEMENTS

Professor Harvey G. Stenger
Dr. Carlos E. Romero
Sandhya Eswaran

Lehigh University

Department of Chemical Engineering

Energy Research Center

Foster Wheeler North America Corp.

54

Reproduced with permission of the copyright owner. Further reproduction prohibited without permission.

THANK YOU FOR YOUR ATTENTION

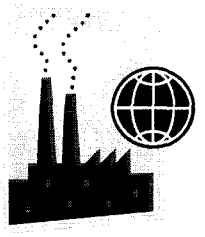

55

BLANK

Reproduced with permission of the copyright owner. Further reproduction prohibited without permission.

LITERATURE REVIEW

- Flue Gas components effect Hg speciation differently

- Hall et al. (1991)
  - Experiments between 300-900°C
  - Residence time of 1.4-2 s
  - HCl oxidizes better at higher temperatures
  - Cl_2 better at lower temperatures
- Widmer et al. (1998)
  - Experiments between 423-876°C
  - Residence time between 0.7-1 s
  - HCl oxidizes better at higher temperatures
- Ghorishi (1998)
  - Experiments between 515-754°C
  - Residence time between 1.22-0.97s
  - HCl oxidizes Hg^0 better at higher temperatures

57

LITERATURE REVIEW

- Sliger (2000)
  - Experiments between 922-1071°C
  - Residence time between 1.4s
  - HCl oxidizes Hg^0; H_2O inhibits oxidation
- Laudal et al. (2000)
  - Experiments at 175°C
  - Residence time of 1 s
  - Cl_2 oxidizes Hg^0; SO_2 inhibits oxidation; HCl has no effect
- Kilgroe et al. (2001)
  - Experiments at 754°C
  - Residence time of 0.97 s
  - HCl oxidizes Hg^0; SO_2 and H_2O inhibit oxidation
- Norton et al. (2002)
  - Experiments at 180°C
  - Residence time of 1 s
  - HCl has no effect; SO_2 and NO inhibit oxidation

58

Reproduced with permission of the copyright owner. Further reproduction prohibited without permission.

LITERATURE REVIEW

- Qiu et al.(2003)
  - Experiments at 1080°C
  - Residence time between 1.4-6.2 s
  - Cl_2 oxidizes Hg^0; SO_2 inhibits oxidation
- Fry (2005)
  - Experiments at 1130°C
  - Residence time of 6 s; 2 quench rates
  - HCl oxidizes Hg^0; higher quench rate = higher rate and % Hg oxidation

59

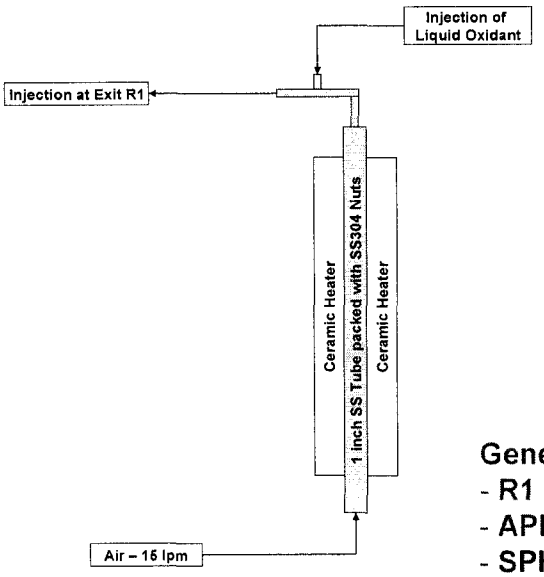

General Setup for
- R1
- APH
- SPH
- Liquid Oxidant injection

60

Reproduced with permission of the copyright owner. Further reproduction prohibited without permission.

DETAILS OF RIG

- Riser: ~1-3 s residence time for sorbent contacting
- Bag house: trap and remove sorbents
- 30" extension: measure linear flow rate
- Condenser system: removes water in gas stream
- Carbon Trap: removes excess water and trace gases
- Totalizer: measures overall volumetric flow
- Sample Line: Custom built vs. Apex Instruments

61

Location vs. Temp / Residence Time

Location		Temperature	Residence Time
Experimental Rig	Power Plant	(F)	(seconds)
Exit R1	Before Economizer	1186	0
Exit R2	Within Economizer	870	1.7
Exit HX1	Exit Economizer	727	1.9
Sorbent Injection Port	Within APH	550	2.2
Baghouse Inlet	Baghouse Inlet	300	3.7

62

Reproduced with permission of the copyright owner. Further reproduction prohibited without permission.

EXPERIMENT 2 - Component Effects

- Full flue gas composition – injected 2ppmv Cl_2
- Exit R1 temperature: 540°C

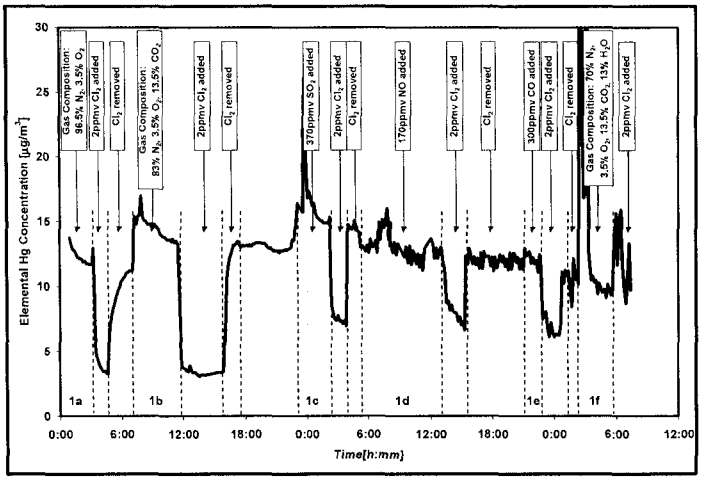

63

Comparing Experiment 2 and 4

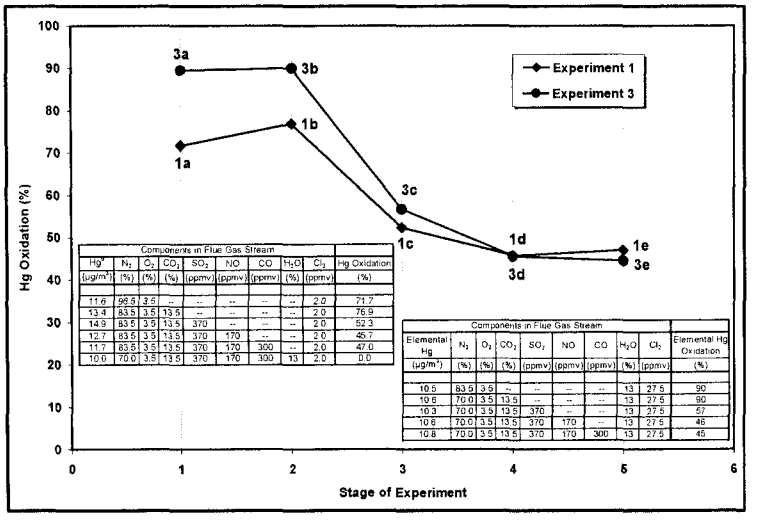

Components in Flue Gas Stream									
Hg^0	N_2	O_2	CO_2	SO_2	NO	CO	H_2O	Cl_2	Hg Oxidation
(µg/m³)	(%)	(%)	(%)	(ppmv)	(ppmv)	(ppmv)	(%)	(ppmv)	(%)
11.6	96.5	3.5	--	--	--	--	--	2.0	71.7
13.4	83.5	3.5	13.5	--	--	--	--	2.0	76.9
14.9	83.5	3.5	13.5	370	--	--	--	2.0	52.3
12.7	83.5	3.5	13.5	370	170	--	--	2.0	45.7
11.7	83.5	3.5	13.5	370	170	300	--	2.0	47.0
10.0	70.0	3.5	13.5	370	170	300	13	2.0	0.0

Components in Flue Gas Stream									
Elemental Hg	N_2	O_2	CO_2	SO_2	NO	CO	H_2O	Cl_2	Elemental Hg Oxidation
(µg/m³)	(%)	(%)	(%)	(ppmv)	(ppmv)	(ppmv)	(%)	(ppmv)	(%)
10.5	83.5	3.5	--	--	--	--	13	27.5	90
10.6	70.0	3.5	13.5	--	--	--	13	27.5	90
10.3	70.0	3.5	13.5	370	--	--	13	27.5	57
10.6	70.0	3.5	13.5	370	170	--	13	27.5	46
10.8	70.0	3.5	13.5	370	170	300	13	27.5	45

64

Reproduced with permission of the copyright owner. Further reproduction prohibited without permission.

RESIDENCE TIME vs. TEMPERATURE

- Different profiles have different residence times
- Plot shows 5 profiles with respect to apparatus location

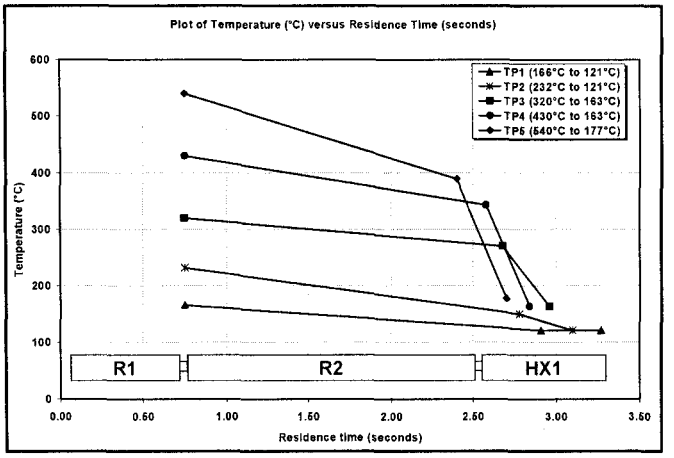

65

REACTION RATES

$$r_1 = k_1 \cdot \left(y_{Hg} \cdot y_{Cl_2} - \frac{y_{HgCl_2}}{Keq_1} \right)$$

$$r_2 = k_2 \cdot \left(y_{H_2O} \cdot y_{Cl_2} - \frac{y_{HCl}^{\,2} \cdot y_{O_2}^{\,1/2}}{Keq_2} \right)$$

$$r_3 = k_3 \cdot \left(y_{Hg} \cdot y_{HCl}^{\,2} \right)$$

$$r_4 = k_4 \cdot \left(y_{HgCl_2} \cdot y_{SO_2} \right)$$

$$r_5 = k_5 \cdot \left(y_{Cl_2} \cdot y_{NO}^{\,2} \right)$$

$$r_1 = A_1 \cdot \exp\left[\frac{-E_1}{R \cdot T}\right] \cdot \left([Hg] \cdot [Cl_2] - \frac{[HgCl_2]}{\exp\left[-17.833 + \frac{17133.1}{T}\right]} \right)$$

$$r_2 = A_2 \cdot \exp\left[\frac{-E_2}{R \cdot T}\right] \cdot \left([H_2O] \cdot [Cl_2] - \frac{[HCl]^2 \cdot [O_2]^{1/2}}{\exp\left[13.707 - \frac{4769.2}{T}\right]} \right)$$

$$r_3 = A_3 \cdot \exp\left[\frac{-E_3}{R \cdot T}\right] \cdot [Hg] \cdot [HCl]^2$$

$$r_4 = A_4 \cdot \exp\left[\frac{-E_4}{R \cdot T}\right] \cdot [HgCl_2] \cdot [SO_2]$$

$$r_5 = A_5 \cdot \exp\left[\frac{-E_5}{R \cdot T}\right] \cdot [NO]^2 \cdot [Cl_2]$$

66

Reproduced with permission of the copyright owner. Further reproduction prohibited without permission.

POWER PLANT PICTURE

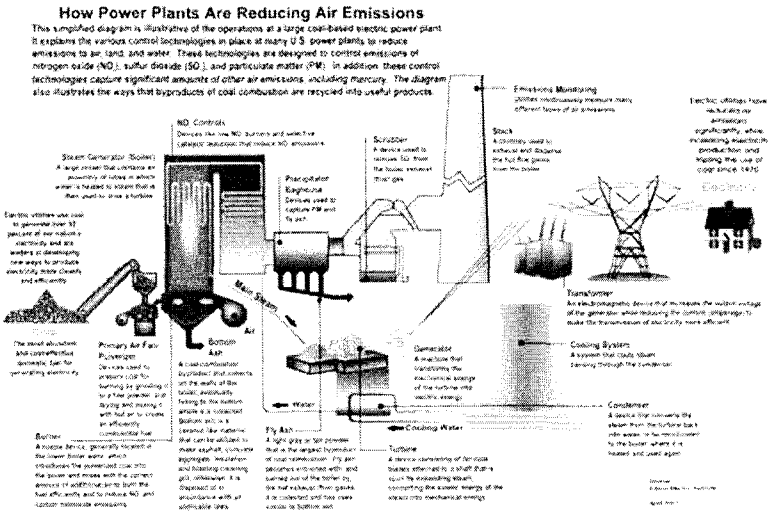

67

Reproduced with permission of the copyright owner. Further reproduction prohibited without permission.

CURRICULUM VITAE

Name: Hans Agarwal

Date of Birth: May 15, 1980

Place of Birth: Munich, Germany

Parents: Ravi P. Agarwal and Sadhna Agarwal

EDUCATION

Lehigh University, Bethlehem, PA, expected, August 2006
Ph.D. in Chemical Engineering
Thesis: A Study of Homogenous Mercury Oxidation and the Development of a Global Predictive Kinetic Model
Advisor: Harvey G. Stenger

Lehigh University, Bethlehem, PA, May 2004
M.S. in Chemical Engineering
Thesis: Removal of Gas Phase Mercury from Power Plant Flue Gases
Advisor: Harvey G. Stenger

University of Delaware, Newark, DE, May 2001
B.S. in Chemical Engineering

PROFESSIONAL / RESEARCH EXPERIENCE

Teaching Assistant for Chemistry Academic Course – Lehigh University (01/16/06 – 05/20/06)
Handled several aspects of laboratory experiments for two laboratory sections of an undergraduate general chemistry class for first-year students; including grading and office hours.

Research Engineer and Scientist – Energy Research Center, Lehigh University
October 9-14, 2005 at the Detroit Edison Power Plant, St. Clair, MI
Assisted Drs. Carlos Romero and Harun Bilirgen in performing mercury capture experimentation, followed by data processing and validation.

Research Assistant – Energy Research Center, Lehigh University (09/01/05 – 01/15/06)
Assisted Dr. Carlos Romero and the Energy Research Center in performing required experimental work, including consultation projects.

Research Engineer and Scientist – Energy Research Center, Lehigh University
September 20-30, 2004 at the Brayton Point Station, Stoughton, MA
Assisted Drs. Carlos Romero and Nenad Sarunac. Supervised mercury capture experiment performed by Western Kentucky University and ADA Technologies. Coordinated scheduled experiments, sample collection, and data collection and analysis.

Graduate Research Assistant, Foster Wheeler Scholar – Lehigh University (01/02 – current)
Team member for research sponsored by the Foster Wheeler Inc., focused on the homogeneous oxidation of elemental mercury in a simulated coal combustion power plant flue gas system.

Reproduced with permission of the copyright owner. Further reproduction prohibited without permission.

Teaching Assistant for Chemical Engineering Academic Course – Lehigh University (Fall 2001)
Handled grading for a Chemical Engineering undergraduate Heat Transfer academic class.

Undergraduate Research Assistant – University of Delaware (06/99 – 05/01)
Honor research sponsored by Undergraduate Research Department. Developed a filtration system for separating protein from water.

Grader for Chemical Engineering Academic Course – Lehigh University (Fall 2003; Spring 2005)
Handled grading for an introductory Chemical Engineering undergraduate academic class.

Experimental Assistant – University of Delaware (Summer 2001)
Worked as an experimentalist, executed chemistry experiments for validation purposes and helped re-write several of the standard operating procedures.

Teaching Assistant and Laboratory Coordinator – University of Delaware (Summer 2001)
Handled all aspects of laboratory experiments for an undergraduate general chemistry class.

US PATENT

US Patent and Trademark Office - USPTO #6,719,147 (2002)
"Supported Mesoporous Carbon Ultrafiltration Membrane and Process for Making the Same"
Authors: Michael S. Strano, Hans Agarwal and Henry C. Foley

JOURNAL PUBLICATIONS

Energy and Fuel
"A Global Kinetic Mechanism for the Prediction of Hg Oxidation by a Chlorine Species"
Submitted: June 2006
Authors: Hans Agarwal, Carlos E. Romero and Harvey G. Stenger.

Fuel Processing Technology
"Comparing and Interpreting laboratory results of Hg Oxidation by a Chlorine species"
Submitted: June 2006
Authors: Hans Agarwal, Carlos E. Romero and Harvey G. Stenger.

Mathematical and Computer Modeling
"Development of a Predictive Kinetic Model for Homogeneous Hg Oxidation Data"
Submitted: March 13, 2006; Revised: March 20, 2006; Accepted: April 24, 2006
Authors: Hans Agarwal and Harvey G. Stenger.

Chemical Engineering Communications
"Comparison and Validation of OHM and SCEM Measurements for a Full-Scale Coal-Fired Power Plant"
Submitted: May 2006
Authors: Boshu He, Yan Cao, Carlos E. Romero, Harum Bilirgen, Nenad Sarunac, Hans Agarwal, Wei-Ping Pan.

Reproduced with permission of the copyright owner. Further reproduction prohibited without permission.

Energy and Fuel
"The Effects of H2O, SO2 and NO on Homogeneous Hg oxidation by Cl2"
Submitted: November 2005; Accepted: February 2006
Authors: Hans Agarwal, Harvey G. Stenger, Wu Song and Zhen Fan.

Computers and Mathematics with Applications (2006), 51, 1021-1046.
"Interpolation for Nonlinear BVP in Circular Membrane with Known Upper and Lower Solutions"
Authors: Syamal K Sen, Hans Agarwal and T. Samanta

Mathematical and Computer Modeling (2006), 43, 658-672.
"2^n in scientific computation and beyond."
Authors: Syamal K Sen and Hans Agarwal

Computers and Mathematics with Applications (2005), 49, 1499-1514.
"Mean Value Theorem for Boundary Value Problems with Given Upper and Lower Solutions."
Authors: Syamal K Sen and Hans Agarwal

Carbon (2003), 41, 2501-2508.
"Templated pyrolytic carbon: the effect of poly(ethylene glycol) molecular weight on the pore size distribution of poly(furfuryl alcohol)-derived carbon"
Authors: Michael S Strano, Hans Agarwal, John Pedrick, Dennis Redman and Henry C. Foley.

Journal of Membrane Science (2002), 198, 173-186.
"Ultrafiltration Membrane Synthesis by Nanoscale Templating of Porous Carbon"
Authors: Michael S. Strano, Andrew L. Zydney, Howard Barth, Gilber Wooler, Hans Agarwal and Henry C. Foley

CONFERENCE PRESENTATIONS / POSTERS

AICHE Annual Conference: October 30 - November 4, 2005
Advances in Environmental Technology (09011)
"The Effects of H2O, SO2 and NO on Homogeneous Hg oxidation by Cl2"
Authors: Hans Agarwal and Professor Harvey G. Stenger

Conference on Differential and Difference Equations: August 1-5, 2005
"Fitting Laboratory Scale Data to a Non-Linear Reaction System"
Author and Presenter: Hans Agarwal
Florida Institute of Technology, Melbourne, FL.

Energy Liaison Program Annual Meeting: June 7-8, 2004
"Mercury Oxidation Studies"
Authors: Prof. Harvey Stenger, Hans Agarwal, Sandhya Eswaran
Energy Research Center, Lehigh University, Bethlehem, PA.

Energy Liaison Program Annual Meeting: June 7-8, 2004
"Mercury Capture – Selective Catalytic Reduction, Fly Ash and Activated Carbon"
Authors: Prof. Harvey Stenger, Hans Agarwal, Sandhya Eswaran, Faaiza Rasheed, John McMullen
Energy Research Center, Lehigh University, Bethlehem, PA.

Energy Liaison Program Annual Meeting: June 3-4, 2003
"Mercury Control Technologies – Recent Laboratory Results"
Authors: Prof. Harvey Stenger, Hans Agarwal, Sandhya Eswaran

Reproduced with permission of the copyright owner. Further reproduction prohibited without permission.

Energy Research Center, Lehigh University, Bethlehem, PA.

AICHE Annual Conference: November 11-18, 2000
- National Student Poster Session, "Porous Carbon Membranes for Macromolecular Separation"
- Coauthor, "Porous Carbon Membranes for Macromolecular Separation" – Talk by Dr. Michael Strano
- Coauthor, "Modeling Transport and Reaction in Catalytic Nanoporous Carbon Membranes"

Poster Session: Honors Presentation – April 28, 2000
"Ultrafiltration Using a Nanoporous Carbon Membrane" – University of Delaware, Newark, DE.

Poster Session: 16th Annual Undergraduate Research Symposium – May 5, 2001
"Porous Carbon Membranes for Macromolecular Separation" – University of Delaware, Newark, DE.

Report: December 2005. Document # 05-400-08-10
"An Investigation of Boiler Operation Modifications for Mercury Emissions Control at DTE Energy's St. Clair Station Unit 4."
Authors: Carlos Romero, Harun Bilirgen, Nenad Sarunac, Hans Agarwal.

Report: February 2005. Document #05-400-02-03
"Mercury Emissions Control at Brayton Point Station – Activated Carbon Injection".
Authors: Carlos Romero, Harun Bilirgen, Nenad Sarunac, Hans Agarwal, Sandhya Eswaran.

Report: May 2002. Document #02-500-05-22
"Lehigh / Foster Wheeler Mercury Removal Project Quarterly Report #1"
Authors: Hans Agarwal, Sandhya Eswaran, and Prof. Harvey Stenger.

Reproduced with permission of the copyright owner. Further reproduction prohibited without permission.